ATMOSPHERIC DYNAMICS OF THE PLANETS

(Volume One - Venus UV Cloud Motions)

V. E. Suomi
R. J. Krauss
S. L. Limaye
D. Phillips

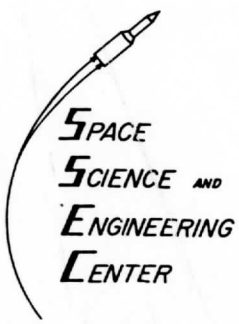

The University of Wisconsin - Madison

This work was funded by JPL Contract 953034 and NASA Grant NGR-50-002-189

COVER PICTURES

CENTER - A "normalized" view of Venus showing true cloud albedo, with the image data corrected for variations in illumination and viewing angles.

UPPER LEFT - Vortex-like velocity profile of zonal winds in the stratosphere of Venus.

UPPER RIGHT - Calculated vertical temperature profile shows tropopause near 50km altitude and the need for considerably more nitrogen than has been so far been measured in order to explain the observed lapse rate.

LOWER LEFT - Venus appears to have a 4 1/2 day wave influencing the dynamics of its upper atmosphere.

LOWER RIGHT - Momentum is transported from the equator to higher latitudes by eddy motions as well as by the mean flow.

FOREWORD

This is the first in a series of reports to be published at one to two year intervals detailing work done at the University of Wisconsin Space Science and Engineering Center on the atmospheric dynamics of the planets. The work presented is based on our participation in planetary probes and flybys sponsored by the National Aeronautics and Space Administration through a grant from the Office of Planetary Studies and a contract with the Jet Propulsion Lab. This first volume deals exclusively with the planet Venus, but other planets with atmospheres will eventually be added as time progresses.

The planets of our Solar System form a unique collection of "laboratories in space" where nature has given us a variety of conditions within which to observe how the laws of fluid dynamics govern atmospheric motions. The knowledge we derive from such studies can help us to better understand key problems such as global energy balance, climate, and weather prediction. Venus is especially helpful because it has an atmosphere which appears to be structurally and dynamically simpler than the Earth's. The study of Venus is not complicated by seasons, oceans, generous amounts of water vapor, and varied cloud cover--conditions which make weather on Earth difficult to predict as well as difficult to study.

The Mariner 10 pictures of Venus are a very important data set. They are the first closeup views of Venus ever obtained. They also cover a wide range of time and space scales, needed to understand the various scales of dynamic interactions. Most important, they contain a tremendous amount of structural and dynamic detail--very much more than we expected to find when the mission was planned. This mass of data will remain unique and useful for many years to come. We can consider outselves fortunate that nature chose to reveal Venus to so great an extent in these first pictures. Even though much hard work will be needed before we can unravel all the complexities we see, the promise of gaining more understanding leaves us eagerly looking forward to the future.

I would like to thank the people who have contributed to this volume: Robert Krauss, our program manager--whose primary responsibility has been getting the data organized and getting the winds measured; Sanjay Limaye, who is writing his Meteorology Ph.D. thesis on Venus--and who, hopefully, will be able to bring some order to our understanding of the wind field dynamics; Dennis Phillips, the applied mathematician who developed much of the navigation and measurement software used on McIDAS; and the numerous others at SSEC who gave of themselves in a variety of tasks which would take too long to mention: Ralph Dedecker, Gary Chatters, J.T. Young, John Benson, Bruce Sawyer, Eric Smith, Nancy Haack, Bruce Knaack, Linda Kluck, Barbara Mueller, and Rosanne Koehler.

Special thanks should also go to the many people at the Jet Propulsion Lab who assisted us during the Mariner 10 mission and the data analysis period thereafter, particularly Ed Danielson, Ken Klaasen, Patsy Conklin, Jim Soha, Don Lynn, and Joel Mosher. The support provided by JPL has been truly outstanding, and we look forward with pleasure to continued association with them in future programs.

April, 1976

Verner E. Suomi
Director, SSEC

TABLE OF CONTENTS

Summary of Program Activities

Robert J. Krauss

During the Venus flyby of Mariner 10 in February, 1974, and for several months thereafter, Verner Suomi and Robert Krauss were in residence at the Jet Propulsion Lab, examining over 5000 TV images which were obtained, and organizing the data for shipment to the Space Science and Engineering Center of the University of Wisconsin. Close to 600 digital tapes now reside in the Venus data library at SSEC. This collection of digital tapes is the only one in existence outside of JPL and contains the complete set of Venus flyby images for use in future analysis. This taped data base is likely to remain unique for the next 10-15 years, for it contains a range of atmospheric motions from scale height resolution images taken seconds apart, to full disk images of large scale features taken hours or days apart.

Previous experience in measuring winds was gained at SSEC through long association with Earth oriented spin scan imaging missions that began with the launch of ATS-1 in 1967. Thus, when the data tapes began arriving at our institution for analysis, the cloud tracking techniques were already well refined, and complex and sophisticated instrumentation--the Man-Computer Interactive Data Access System (McIDAS) - had been developed to process satellite imagery and obtain wind fields.

The Mariner images were new to us, however. They were generated by a vidicon mounted on a 3-axis stabilized vehicle, instead of being formed by a line scanner on a spinning platform. This required that a completely new analytic "navigation" approach be developed to permit accurate transformation from line-element coordinates in the image to latitude-longitude coordinates on the planet.

The camera-spacecraft-planet-sun geometry is an extremely difficult and complex concept to grasp, with a large amount of "bookkeeping" required to correctly handle the camera calibration, spacecraft attitude and orbit data, and telescope pointing information to generate a proper set of transform matrices. It is a tribute to Dennis Phillips and his experience gained on other missions, that he did the job in less than six months and moreover, got it to work well using his initially proposed concept of navigating on the bright limb of the planet. We had taken the precaution of imaging the Earth simultaneously with both Mariner 10 and ATS-3 at the time of launch, so that we would have a calibrated comparison of cloud motions in the event we ran into trouble. We never had to use the Earth images. Tests have shown that the Mariner 10 image alignment on McIDAS permits us to get absolute velocity accuracies under 5 m/s on Venus. That is 3 times better than we had expected to be able to do, and it has opened up a whole new vista of second order motions and perturbations in the global velocity field which we should now be able to detect.

The first article is a reprint of Suomi's initial report on the cloud motions, presented at the GISS Conference on Venus in October 1974, and later published (1975) in the proceedings of that conference ("The Atmosphere of Venus", NASA SP-382). In this report, based on the first six months of image analysis, Suomi identifies the key features of the motion field. This identification of the basic velocity field structure provided concepts that set the stage for the following work at SSEC in 1975. Suomi first identifies a zonal wind maximum near 45 degrees latitude. A region of solid rotation (constant angular velocity) exists on the poleward side of the mid-latitude velocity transition zone. At low latitudes is found a tendency to conserve angular momentum, thereby implying meridional motion from equator to poles. Suomi sees the velocity profiles as being those of a vortex, and he suggests cyclostrophic balance as a means of stablilizing the slow meridional flow against pressure gradients introduced by solar heating. The basic view is that of a slowly overturning Hadley cell modified by the swift zonal motions. He then further suggests that the spiral streak features on Venus could be due to horizontal shear in the vortex motion field. These speculations were presented in talks to a number of scientific groups in Europe and the U.S. in the winter of 1974-75. Additional evidence obtained by us from study of the Mariner 10 images during the following year has supported every one of these initial speculations.

The second article by Krauss reports on the complete analysis of the first 4-picture data set. Much of this work was done following the GISS conference, and in the early months of 1975. The number of measurements were doubled to improve statistics, and a determined effort was made to find out the cause of the observed measurement scatter and thereby determine the true accuracy of the measurements. Existing observational evidence is first reviewed from the viewpoint of atmospheric dynamics to provide a context in which to interpret the measurements. The cloud features are estimated to lie within a 60 to 70 km altitude range and within narrow limits of temperature and pressure. Then, considerable space is devoted to explaining how the Mariner 10 pictures are processed and aligned, and Krauss describes the techniques and hardware associated with how the cloud motions are measured. Results of an error analysis are presented to show that absolute velocity accuracies near 5 m/s are attainable using the McIDAS system.

The wind field measurements presented by Krauss are more detailed than the summary presented earlier by Suomi on the basis of preliminary analysis of the same data set. Especially important is the confirmation of a small but definite meridional flow from equator to poles. Careful study shows that additional fine structure is also present in the cloud motion measurements, however. The large amount of scatter in the u-component vectors is most likely due to vertical wind shear, which can even be directly seen in a few cases. The presence of such shear supports the assumption of a global cyclostrophic balance. In addition, the zonal motions are seen to accelerate slightly as they are measured closer toward the evening terminator. The implication is that there is some direct sun related feature driving the zonal flow. This effect had been seen by others as well. It must be noted, however, that in the following day's data, as reported later in this volume, slower motions were found at the evening terminator, so the present picture is still somewhat unclear.

One unusual aspect of the data is the evidence that some kind (or kinds) of large scale wave motion in the stratosphere may be present. A few undistinguished looking cloud features, measured using a tracking technique sensitive to cloud edges, appear to move at constant angular velocity in some organized way. The vortex flow, with associated horizontal wind shear in low latitudes, is the predominant mass motion field defined by the great majority of clouds. A few measurements, however, show a second type of organization apparently not related to the main mass flow, exhibiting no horizontal shear at all. Further evidence, presented in a later article, shows that the zonal flow fluctuates in time with hints of a periodic nature.

The third article, by Dennis Phillips and Sanjay Limaye, gives mathematical details of the image alignment technique which forms the foundation of the Venus cloud motion determinations. The transforms used to convert from Mariner 10 image coordinates to cloud velocities are described. The technique is based on finding a simple least squares solution to the bright limb of the planet, thereby defining both the planet center and the scale of the latitude-longitude grid. The sun-planet-spacecraft geometry then defines image tilt, and permits definition of the orientation of the grid on the planet. This first paper on the navigation process serves as an introduction to a complex but highly necessary part of measuring cloud motions.

Dennis spent much of the winter and spring of 1975-76 on leave from SSEC while he worked on completion of his Ph.D. thesis in applied mathematics. Before he left, he developed plans to extend the bright limb navigation to the high resolution mosaics of Venus. This is much more complicated, for the least squares fit to the bright limb breaks down if there is insufficient arc length to specify the planet center uniquely. To deal with the mosaics, one must identify both the limb, where it appears, and points of overlap in successive pictures, then correct for the effect of large scale atmospheric motions during the time interval between the pictures, and then iterate to get a best fit for the entire set of frames in the mosaic. When this navigational scheme is operating in late 1976, the first 36 hours worth of Mariner data taken immediately after the Venus encounter will become available to us. This data is extremely crucial for detecting fluctuations in the motion field with periods longer than 2 days.

During the last half of 1975, work was begun on the analysis of additional images. In the fourth article, Krauss extends the cloud motion measurements to three additional data sets covering a period of 12-36 hours following the data analyzed in the initial reports. The findings are generally in agreement with the motion field from a day earlier. There is a small component of meridional motion toward the poles, slightly larger this time. The increase in zonal velocity from equator to mid-latitudes is still seen. Two new features in the data were observed. A small amount of eddy transport of momentum toward the poles is present in the measurements. This component is at least one order of magnitude less than the transport by the vortex, which still appears to be the predominent dynamic feature of the stratospheric motion field on Venus, but the simple presence of an eddy component strengthens the arguments for a large scale wave being present.

The most significant information is probably the fact that the trend of the zonal velocity gradient indicates that there are occasionally smaller velocities at the evening terminator. This throws some doubt on the validity of assuming a direct sun-locked driving mechanism for the zonal winds on Venus.

The fifth article presents work by Sanjay Limaye, a graduate student in meteorology, who became associated with our program shortly after the Mariner 10 data was shipped from JPL to Wisconsin. Limaye has extended the Mariner 10 navigation model developed by Phillips to remove the effect of lighting conditions (sun zenith angle) and viewing conditions (emission angle) in the Venus images. A photometric function based on Chandrasekhar's H-functions can be applied to the image data which will change the brightness level of every cloud element to that which it would have if it were on a plane, illuminated by plane parallel light, and then viewed from infinitely far away. This permits the Venus clouds in any Mariner 10 image to be corrected so they have a brightness directly proportional to the true albedo, which is closely dependent on optical depth, or thickness. The clouds can then be analyzed to study growth rates and changes, or one can measure divergence or eddy transport independent of the effects of geometry or phase angle. The technique will be used primarily to infer vertical motions in the equatorial regions of Venus and to investigate cloud thickness or any other properties which may be masked or altered by lighting conditions and geometry. A relation may exist between absolute cloud brightness and altitude, for example, which could be used to stratify the cloud motion fields in the vertical.

Krauss presents a shear model for the spiral streaks in the Venus clouds. He shows how the shape of the streaks can be generated using the vortex velocity field from cloud motion measurements. The process can be inverted to infer cloud motions from the shape of the streaks, and in so doing, a 4 1/2 day periodicity is noted, which correlates with the meridional motion of the bright polar band and with the appearance of the large "Y" albedo feature often seen from Earth. The indication is that a global scale wave with a 4 1/2 day period is superimposed on the vortex. This wave appears to affect not only the cloud velocities (being about a 10% effect on the motion field), but also shows correlations with albedo features and the shift in latitude of the polar band. By combining these and other facts that have been discovered, (such as the presence of vertical shear) Krauss speculates what the upper atmosphere circulation of Venus might be like if the observed facts were put together in a physically consistent model. He suggests that the vortex is the predominant dynamic feature of the stratospheric motions, and that cyclostrophic balance is also present. The global wave becomes a necessary part of the dynamic system by deriving energy from the sun and pumping momentum up from the surface of the planet to maintain the vortex.

In the last paper, Limaye has generated a set of adiabatic lapse rate diagrams based on examination of the Venera 8 temperature profile and the Mariner 10 radio occultation data. The motivation for this work was the fact, first mentioned in 1972 by Marov, and since confirmed by several subsequent measurements, that Venus appears to have a slightly superadiabatic lapse rate in the lowest portions of its atmosphere. What this implies is that the whole equatorial region of Venus would have to be in forced convection, a somewhat improbable condition. A deep convective region goes against our Earthlike experience, which says that an atmosphere should be more stratified. Moreover, the Venera and Mariner observations indicate presence of vertical structure and not simply a well mixed atmosphere, as the adiabatic assumption would imply.

Up to now, the lapse rate problem has been virtually ignored. Either the observations are assumed a bit faulty, or else the data reduction is assumed slightly in error because a composition of 100% CO_2 was used. Limaye performs an iterative calculation using the real gas equation and the most accurate available data on CO_2. He reaches the conclusion that a considerably lower concentration of CO_2 must be used in order to explain the vertical lapse rate measurements. Better than 12% nitrogen must be included to make the measured lapse rate adiabatic. Such a large nitrogen content has not been measured on Venus, so as a result it may be necessary to include dynamic effects or another heavy gas to get all the observations to agree. Observations which have depended on the assumption of 100% CO_2 in their data reduction may be incorrectly interpreted, or at best very naive.

Work is now proceeding to get the mosaic navigation operational and to extend the cloud motion measurements to other time periods in the Mariner flyby data. This will complete our survey of the global scale wind field. Many of the second order effects, such as gravity waves, local convection, eddy motions, and vertical shear, remain to be looked at in quantitative terms. The high resolution mosaics of Venus, recently completed at JPL by USGS workers, show a large variety of smaller scale dynamical features. In addition, large scale organization slightly different from previously studied pictures also seems evident. The subsolar convection zone, seen near the equator at later times in the mission, appears slightly shifted into the northern hemisphere in the early high resolution mosaics. Small gravity waves also now show up on the equator where they were not visible before. We should be able to measure the relation of such small features to the large scale motion field very accurately. Finally, we also have the large scale wave features to analyze. What produces the bowlike waves, and why do they tend to show up in pairs? What does the circumequatorial belt represent? What causes the motion of a few clouds to substantially differ from the surrounding mass flow? Some of the answers lie in the image data remaining to be analyzed.

UV Cloud Motions on Venus from Mariner 10 Images

Robert J. Krauss

ABSTRACT

A synoptic scale wind field has been measured in the stratosphere of Venus by observation of the motion of 100-300 km size UV cloud features in four Mariner 10 TV images. The cloud features are estimated to lie primarily in the 60-70 km altitude range. The UV images have an effective wavelength of 355 nm, cover a time interval of 3 1/2 hours, and were made about 2 1/2 days after Venus encounter. Major features of the wind field include: a) a vortex structure in each hemisphere with probable widespread upwelling at low latitudes and convergence at the poles; b) an equatorial zonal velocity of - 92 $\pm$ 7 m/s increasing to - 120 $\pm$ 10 m/s near 45° latitude; c) a mean meridional velocity gradient of 0.12 m/s/deg; d) a widespread longitudinal velocity gradient comparable to the meridional gradient in magnitude and observed at all latitudes below 60°; e) vertical wind shear in the zonal flow at low latitudes, with a mean value of 10-15 m/s rms. Considerable space is devoted to summarizing previous data in a dynamical context, and to explaining the measuring process and analysis techniques before full details of the measurements are presented.

CONTENTS

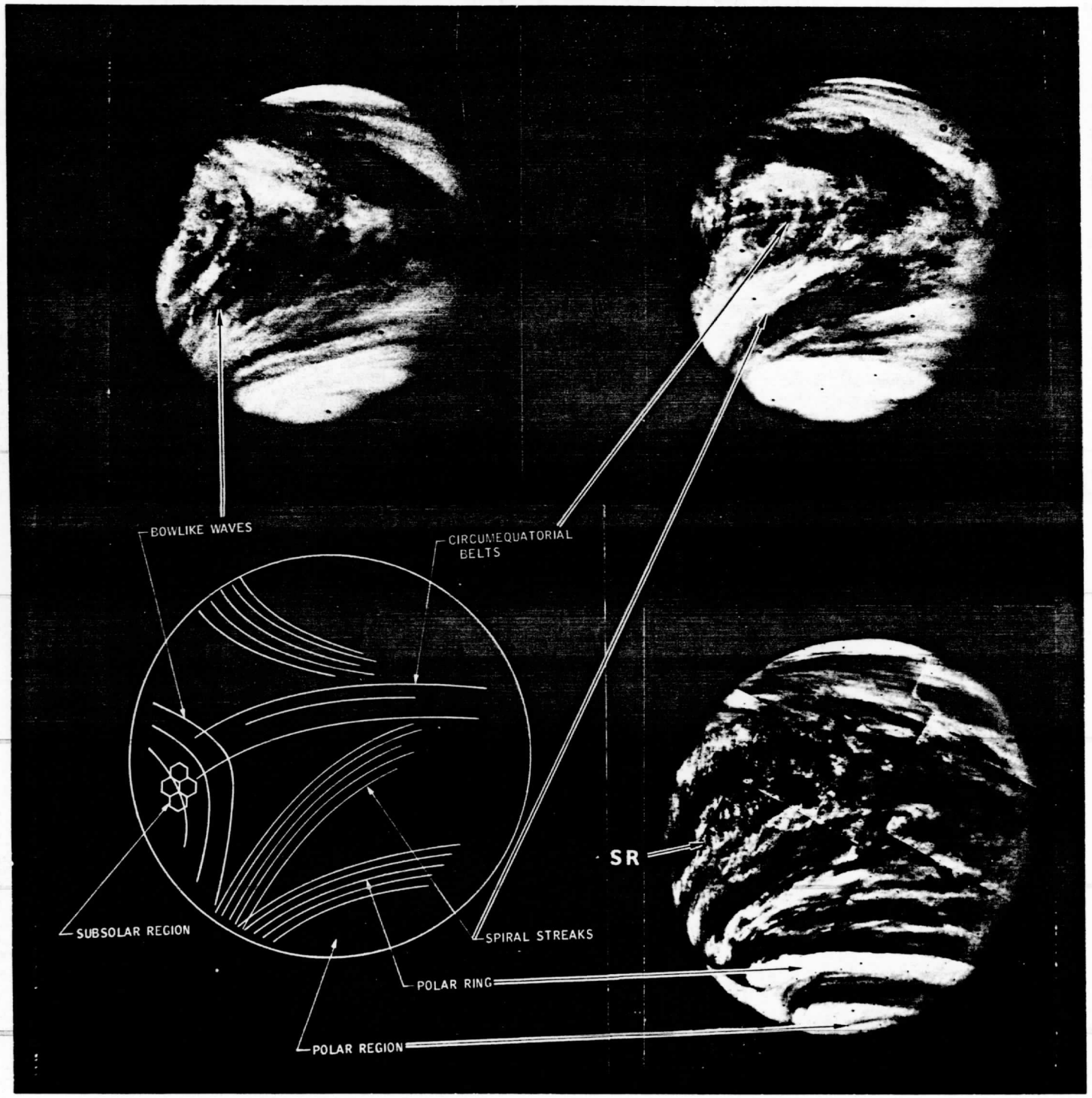

Figure 1. Venus, seen by Mariner 10 at approximately 4 days (upper left), 3 days (upper right), and 1 day (lower right) after encounter. While there is some definite loss of high resolution detail in the images as the spacecraft moves further away, note how different large scale features show up only at certain times, and how the polar ring changes latitude.

I. INTRODUCTION

A planetary atmosphere radiatively heated at the equator and cooled at the poles must transport heat poleward to maintain its global energy balance and relieve sun induced pressure gradients. A stringent dynamical contraint is also imposed on the resulting mass flow. There will be a need to conserve angular momentum. In addition, pressure induced motions will be distributed zonally, meridionally, and vertically by friction and dynamically induced shear. Thus, any physically complete atmospheric model must be a three dimensional system with a dynamic balance of mass, energy, and momentum. Even though these conditions strongly limit the range of possibilities for models of the circulation, any planetary atmosphere is structurally complex enough, to have many unknown quantities remaining. Observations of atmospheric motions on a global scale provide a useful additional constraint on such models. Motions of the UV markings measured in the Mariner 10 flyby images of Venus were first reported by Murray, et.al. (1974). Figure 1 (from the report) illustrates the major global scale features on Venus and nomenclature. Additional observations using the Mariner 10 images are reported here, based on tracking edge detail and light and dark features of 100-300 km scale size in four Mariner 10 TV images with 15 km/pixel resolution. The total time interval was about 3 1/2 hours.

Before the techniques and measurements are presented, however, it should be made clear just what is being measured. The subject of the Venus clouds has been a long standing and many-sided controversy, often surrounded by confusion. Full understanding of the data requires the proper conceptual framework, which is lacking at the present time. It is unlikely that all the data assembled to date can be properly interpreted until we gain better understanding of vertical structure, atmospheric chemistry, and the general circulation. Such knowledge can be gained from atmospheric probes and from long time base observations of the cloud motions. The Pioneer Venus mission in 1978 will help greatly in this regard. There have, however, been a few commonly accepted pieces of evidence which are well established. Coupled with new observations from Mariner 10, those established facts can be used as a basis to interpret the motions of the UV markings and to provide fresh insight, if not full understanding. So we will first review some of the evidence, with emphasis on dynamical features of the atmosphere and how they might be related to the UV markings.

The solid surface of Venus has never been reliably seen, and its high albedo led many astronomers to conclude that Venus was completely cloud covered. The Mariner 10 pictures have shown this to be true. Through the orange filter, Venus appears to be a diffuse and featureless ball of fog, though very faint large scale contrasts can occasionally be seen (Murray, et.al. 1974) which generally correlate with the more distinct large scale UV contrasts (Hapke, 1975). In blue light, the same large scale features have slightly greater contrast than in orange but there is a more definite threshold near 400 nm (Coffeen, 1971). Many additional small scale details ~100 km, begin to show up in the Mariner 10 UV images with contrasts of 5-10%. This contrast threshold in the UV has led many observers to conclude that the Venus clouds contain a UV absorber, since it is difficult to explain such a sharp contrast change in terms of physical cloud structure alone.

Travis (1975) and Hapke (1975) review the cloud contrast problem in terms of recent evidence and discuss various models.

The diffuse haze structure of the clouds seems well established, however. Hapke (1975) and Deveaux (1974) find that at all wavelengths of the Mariner 10 images the clouds act like isotropic scatterers characteristic of a deep homogeneous scattering medium. Detailed analysis of earth based polarization measurements (Hansen and Hovenier, 1974) supports this structural picture and places some hard quantitative limits on: (a) particle shape - spherical and therefore probably liquid; (b) effective radius 1.05 $\pm$ 0.10 μm with a narrow size distribution of 0.07 $\pm$ 0.02 μm effective variance; and, (c) visual refractive index 1.44 $\pm$ 0.015 with a normal dispersion curve. A strong electrolyte solution could form such a fine liquid aerosol at the existing temperatures and vapor pressures. Only one - sulfuric acid - has the proper refractive index and satisfies other observational evidence (Young, 1973, 1975, Pollack et.al., 1975).

The mean pressure at which scattered light is observed in the polarization observations is ~50 mb (Hansen and Hovenier, 1974), and corresponds to approximately the $\tau = 1$ optical depth and about 65-70 km altitude when looking vertically into this aerosol haze. Estimates of particle density yield 30-40 droplets per cubic centimeter (from observed mixing ratios), so visibility at this altitude is more like a hazy day in Los Angeles. We are not observing a dense fog or Earthlike cumulus type clouds.

O'Leary (1975) measured the limb haze layer in the Mariner 10 images at approximately 80 km altitude (~5 mb) and found a scale height of 1.5 km, whereas he got a scale height for the underlying haze of 2.5-3 km. Neither O'Leary nor Murray, et.al. (1974) saw any horizontal variation of the 5 mb haze in the Mariner 10 pictures on the scale of the UV marking details we have measured. The 5 mb haze layer seems horizontally uniform on a scale of 1000 km or more, while we report here on tracking of cloud elements of 100-300 km which are clearly contrasted with their surroundings. If the 5 mb haze contained the UV markings, the markings ought to have been visible in the Mariner 10 limb pictures. The UV markings must therefore be lower than 5 mb (80 km). If one assumes that the UV absorber is vertically distributed rather than concentrated in a thin horizontal layer, that is, if the absorber is subject to the same transport conditions as the rest of the surrounding atmosphere, then it is likely the UV markings are substantially lower than 80 km. They would be below 70 km, for it would not be possible to produce the observed 5-10% contrast variations at 75 km ($\tau \approx 2$) without getting variations as well from still visible portions of the atmosphere near 60-65 km, ($\tau \approx 3$-4) for example. If the markings are restricted to a very thin altitude layer, however, we can only say that they are above 60 km, the lower limit of visibility in the haze.

Spectroscopic studies of absorption on Venus in the near IR (Young, 1972) provide valuable information on gas concentration, temperature and pressure. Such absorption lines are formed lower in the atmosphere, around 100-200 mb (60-65 km), since the effective reflecting layer for longer wavelengths is lower in the hazy atmosphere. Surprisingly, the amount of CO_2 above this reflecting layer varies by as much a factor of 2 from day to day, corresponding to a large scale organized vertical motion of ~3 km in the reflecting layer or a change of 50-100% in the gas concentration above the reflecting layer

if the layer remains at constant altitude.

Water vapor, on the other hand, has been observed to vary locally across the disk of Venus, and in concentrations ranging over 2 orders of magnitude (Young, 1975; Barker, 1975). While the haze cannot be water drops or ice, it is possible that the water vapor is somehow related to small scale atmospheric activity such as the observed convective cells (Murray, et.al., 1974), while the CO_2 variations are related to global scale mass motions or waves. The important fact is that there is temporally varying activity between 100-200 mb on the same spatial scales as we see details in the Venus UV clouds. The scattered effective temperatures clustering around 250° $\pm$ 10°K are also consistent with some vertical and horizontal inhomogeneity at these altitudes.

Traub and Carlton (1975), have investigated Doppler shifts in the near IR spectral features and find a mean retrograde mass motion of 83 $\pm$ 10 m/s at the equator, with a tendency for higher velocities at the evening terminator. Meridional motion, if it exists, is smaller, and the direction somewhat less conclusive. Since the velocities were measured at widely varying times, much of the scatter might be real; and since these are absorption lines, it is hard to ascribe the Doppler shifts to anything but mass motion of CO_2. Traub and Carlton review ground based measurements of the large scale UV markings, which also show ~100 m/s zonal motion and a tendency to accelerate from morning to evening. The total picture of the spectroscopic studies indicates that the UV features in the Mariner 10 images are embedded in a fast zonal mass flow exhibiting dynamic variations over a wide variety of time and space scales.

Going still lower in the atmosphere, we note that the minimum observable contrast the Mariner 10 TV cameras can resolve is ~1/2%, so that even if the UV markings had 100% contrast and were buried deep in the haze, we could not see them below $\tau = 5$. For moderate contrasts, it seems unlikely, with a haze scale height of 2.5-4 km, that we are looking at cloud features below 60 km altitude, although the possibility of holes in the clouds remains.

Lacis (1975) has placed a number of the upper atmosphere observations on a convenient diagram (Figure 2), showing that there is probably a discontinuity in aerosol scale height above 50 mb, in agreement with the findings of O'Leary (1975). This transition may conceivably vary in height from time to time, but its presence could well indicate a change in the dynamics of the atmosphere as well as a structural change. It is likely that above the transition, vertical eddy transport is no longer as effective in supporting the haze and we see a vertical haze distribution closer to the natural fallout time. Hapke (1975) sees correlation of bright clouds with polarization, indicating that at least the tops of the UV markings must reach near 70 km, since multiple scattering at 65 km and below would destroy polarization effects.

One result of the observations so far discussed is that it is possible to put limits on what we see in the Mariner 10 UV images. The evidence points to variable atmospheric activity on both large and small scales within the limits $h = 65 \pm 5$ km, $P = 150 \pm 100$ mb, $T = 250 \pm 10$°K. Whatever motions we

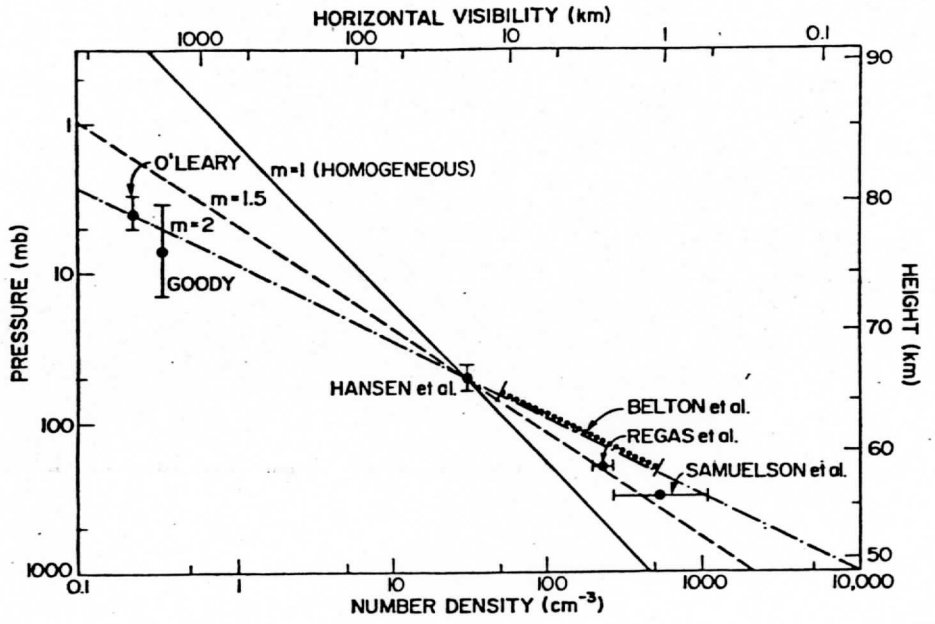

Figure 2. Cloud particle distribution in the upper atmosphere of Venus (from Lacis, 1975). The number m is the ratio of gas scale height to particle scale height. The data points are for measurements of various types: limb haze and star transit on the left, polarization in the center, and CO_2 absorption on the right. The number density and horizontal visibility scales assume 1.05 μm particles and m = 1 and should be linearly scaled for other values of m. The ratio of scale heights shows a tendency to change around 50 mb. Assuming the gas scale height is constant, the particle scale height is about 50% less above 70 km.

measure must lie primarily within these limits, and whatever structure we see is probably correlated with dynamical processes on Venus and limited to vary within the narrow limits just mentioned. It is highly unlikely that all visible phenomena in a 10 km thick slice of atmosphere will be decoupled. Determining what the clouds really are, and what mechanisms affect their form and evolution may be difficult, however,

The lapse rate between 60 and 70 km altitude is no greater than 3°K/km (Marov, 1972, Howard, et.al., 1974), which is strongly sub-adiabatic and would tend to inhibit convection and vertical mixing. The size of the convective cells seen by Murray, et.al. (1974) (~200 km) compared with the vertical structure observed (3-4 km scale height, ~10 km visible thickness) tends to support widespread and somewhat shallow solar heating as a more reasonable explanation for the convection than localized release of latent heat. The >20:1 ratio of width to height is also more representative of Benard cells than convective storm towers on Earth. Murray, et.al. (1974) ascribe the quickly varying temporal behavior of the markings to a condensate rather than to dust, but can reach no conclusion as to whether the clouds are bright features in a dark absorbing medium, or dark features in a bright scattering medium. A serous problem is that no suitable condensate has ever been proposed for the clouds of Venus which could fit all the evidence.

Even sulfuric acid droplets, once formed, may change size or H_2O content a few percent, depending on local heating or vapor pressure but will not completely evaporate again unless subjected to much higher temperatures (Young, 1975, Prinn, 1975). Such droplets can exist in equilibrium with little physical change over a range of two orders of magnitude in water vapor concentration and over a wide range of altitudes and temperatures on Venus. The cloud haze on Venus forms small scale features and dissipates them as well over times as short as a few hours. Thus, the UV markings are as unlikely to consist simply of evaporating acid aerosol as they are to consist of dust.

The stable lapse rate virtually guarantees the presence of waves between 60 and 70 km. At the very least one can predict a solar thermal tide. The subsolar convection zone is a possible mechanism to excite such waves. Therefore, the question should not be whether there are waves on Venus, but what kind? What are the dominant modes of oscillation and how are they excited and coupled to each other? Murray, et.al. (1974) report: (a) bowlike waves - moving at a slightly slower speed than the mean zonal equatorial flow and intensifying as they move toward the evening terminator; (b) circumequatorial belts - drifting across the equator from north to south; (c) Y features - appearing to be formed in part by the spiral streak patterns and having a 4 day periodicity. Belton, et.al. (1976) have found that the intensity of the Y feature is also modulated with a 4 day period. In light of the observed differential zonal motion of the small scale features, they conclude that the contrast variation is wave related since it moves with the 4 day equatorial features but against the faster mid latitude features.

One can observe in Figure 1 that the polar ring oscillates in latitude. There could therefore be a meridional motion oscillation related to the Y feature and its intensity variation. The variable CO_2 concentration hints at vertical oscillations on a large scale, while the wide spread of measured zonal velocities hints at variations in the zonal flow. It may be impossible

to determine the "mean" state without a continuous series of observations over a long time. This must be kept in mind in interpreting any results from a limited series of Mariner 10 images, although we can say that the appearance of Venus during the flyby would seem to be its most usual appearance.

The fact that a number of wavelike phenomena are visible at all in the UV images is remarkable. Surely, as we have indicated, one ought to expect waves. One should not, however, given the appalling lack of reasonable condensates, expect to see all of these waves. The fact that we see so much wavelike detail indicates that the UV absorber is modulated by very subtle changes in the balance of pressure, temperature, and altitude within the previously stated limits ($T = 250 \pm 10^{\circ}K$, $h = 65 \pm 5$ km, $P = 150 \pm 100$ mb). It is hard to ascribe this to anything but a phase change. Sulfuric acid freezes within these limits, and it is possible that scattering off the solid aerosol surface could modify the effect of UV absorption inside the droplets or in the surrounding medium. The presence of HCl and HF as impurities in the $H_2O - H_2SO_4$ system makes the physical chemistry very difficult to specify, however, and too corrosive to do exacting laboratory tests needed to determine phase diagrams.

It is apparent that while there are numerous established facts, there is as yet no clear interpretation of them. What must be kept in mind is that regardless of what the clouds of Venus consist of, or what color they are, or what causes them to evolve the way they do, we can confidently say that they move in a certain way on a global scale. The implications which derive from such motions are significant for understanding the general circulation of Venus, for they will permit us to separate wavelike motions from mass motions, to understand the physical scales at which dynamical phenomena of a given type are occurring, and to bound the range of dynamic models which can explain the general circulation.

II. IMAGE GEOMETRY AND NAVIGATION

The Space Science and Engineering Center at the University of Wisconsin has a large number of Experimenter Data Record (EDR) tapes copied from the original set at the Jet Propulsion Lab. These raw image tapes will form the bulk of our future wind analysis program. To minimize the amount of preparation and programming time necessary to use the image data, a small subset of 18 images of Venus was preprocessed at the Image Processing Laboratory (IPL) at Jet Propulsion Lab using the well known programs FICOR and GEOM, originally developed for the Mariner 9 Mars Orbiter mission and adapted for Mariner 10 (Soha, et.al., 1975). Relative photometry of a few percent and geometric accuracy of ~1 pixel is obtainable throughout most of a TV frame. The pictures were photometrically decalibrated, and then geometrically rectified (remapped to object space) with a scale factor such that the planet disk is the same apparent diameter in each picture and free of gross distortions.

Two time lapse sequences were generated from the decalibrated images, one with 25 km/pixel ground (cloud) resolution, and the other with 15 km/pixel resolution. The higher resolution sequence, containing 4 images spanning a 3 1/2 hour time period, was chosen to provide the initial cloud velocity profile. The lower resolution pictures form a longer time sequence covering 16 hours. This series more clearly shows the large scale UV markings and bowlike waves, but has not yet been extensively analyzed. We intend to eventually measure several sets of full disk images to improve statistics and determine if there are measureable changes in the global velocity distribution from day to day.

A. The Man-computer Interactive Data Access System (McIDAS)

The image alignment, time lapse display, and motion measurement is done using the Man-computer Interactive Data Access System (McIDAS) developed at the University of Wisconsin Space Science and Engineering Center.

McIDAS is designed to optimize the mixture of analog processes, digital processes, and human processes used in image analysis. The system is designed around a Datacraft 6024/5 mini-computer control system with 24 bit 64 K word memory. The computer has four basic functions:

1. Control of bulk data input/output processes (analog and digital)
2. Computational tasks
3. Control and coordination of a video display system
4. Interactive communication and response in real-time with scientists, graduate students, or operations personnel.

The basic operational approach for the McIDAS system has the operator in front of a color TV monitor. He has a keyboard and a joystick, which allows him to interact simply and effectively with the computer in a mechanical and verbal command "language". With these controls, the operator tells the computer the type of data to display, the scale and format he wants to see, and

the type of enhancement and image blending or pixel interlace he wants to use. The computer translates his requests into specific commands and sequences of commands which are transmitted to the peripheral display system hardware, which in turn presents the requested display to a color monitor. The operator then examines the display, performs judgement, selection, or decision functions, and directs the computer to perform measurement or analysis functions on the specific data sample selected. The computer recovers the required data sample from the original digital data in the archive, processes the data to the condition selected by the operator, performs the measurement or analysis function and presents the results. Usually the results will be in the form of another display on the color monitor, or a few lines of printout on a CRT display. The entire set-up is geared to let McIDAS do the data transfer, editing, and quantitative manipulations while the operator provides the selection and judgement functions.

The Mariner 10 images, photometrically and geometrically decalibrated to maximum possible precision, are thus input to a measurement and display system which allows none of the original image precision to be lost in measurement, yet permits highly complicated interaction of a guiding scientist with both the data and the data processing in near real-time. Most display systems lack intelligence and precision. Most measuring systems lack intelligence and speed. McIDAS combines speed, precision, and the operator's intelligence in a truly "interactive" system, using an optimized combination of analog, digital, and human capabilities.

B. Image Navigation

The motion of the clouds on Venus is measured in the Mariner 10 TV images in image coordinates. To get velocities, the motion must be determined in a Venus reference system. Thus, we need to define a transform which converts from line-element or pixel coordinates to latitude-longitude or Venus coordinates. We call the definition and use of this transform "Image Navigation". Once done properly, it is possible to tell where on the planet each pixel in the TV image lies, or inversely, which pixel corresponds to a given latitude and longitude.

Two approaches can be used. The first approach is to apply the navigation transform directly to the image data before measuring cloud motions. Computer programs have been developed at JPL which map a geometrically rectified TV image into any number of standard cartographic projections. These have been used to produce maps of the moon, Mars, and now Mercury. The programs require input from the Supplementary Experimenter Data Record (SEDR) which converts engineering data on spacecraft attitude, spacecraft mass distribution, drift rates, trajectory position, scan platform backlash, camera mounting angles, etc. into a best estimate of where the TV camera optic axis intersects the planet. This information is useful as a first estimate, but the error in determining absolute pointing angles from engineering data (0.1°) would have been larger than many of the cloud displacements we were attempting to measure.

IMAGE NAVIGATION

a) BEST FIT TO A SPHERE:

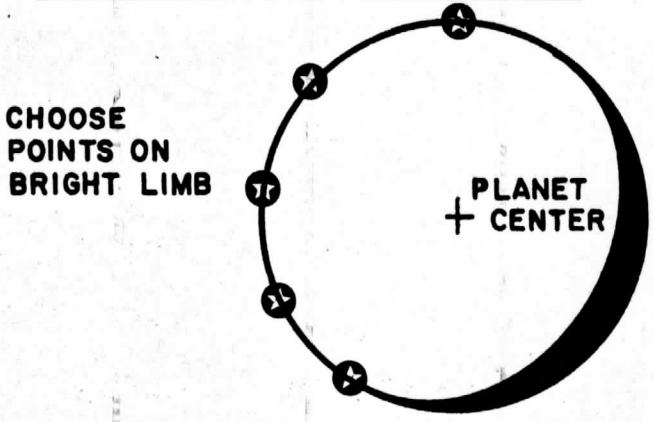

b) PLANET GRID DEFINITION:

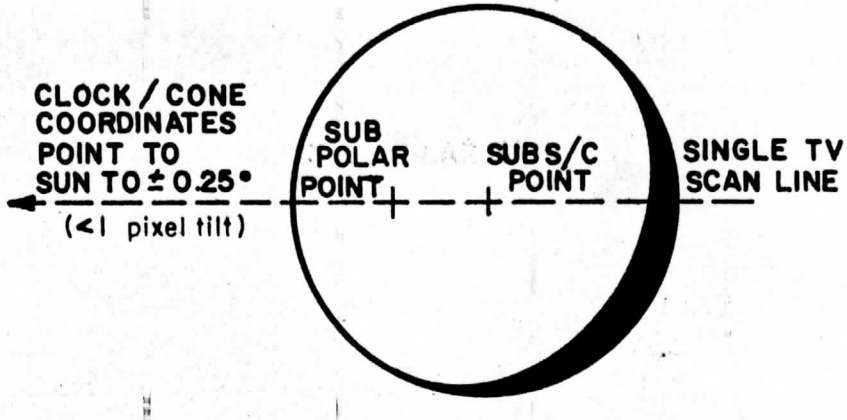

INPUTS

- LIMB POINT COORDINATES
- LINES PER FRAME
- ELEMENTS PER FRAME
- HEIGHT OF FRAME (deg)
- WIDTH OF FRAME (deg)
- DISTANCE TO VENUS SURFACE

- LATITUDE OF S/C SUB POINT
- LONGITUDE OF S/C SUB POINT
- LATITUDE OF SUB SOLAR POINT
- LONGITUDE OF SUB SOLAR POINT

Figure 3. Image navigation occurs in two parts. Part (a) shows the best fit to a sphere using the image data, viewing geometry, and camera calibration. This determines the scale of the planet navigation model. Part (b) shows how the epoch and trajectory information from Mariner 10 is used to place a latitude-longitude grid on the navigation model with the proper orientation.

The second approach is to make measurements of cloud displacements in TV image coordinates and then apply the navigation transform derived from the images themselves to the displacement vector. Provided the spacecraft is far enough from the planet to see the bright limb, there is enough information in the original images to uniquely determine camera pointing angles with respect to Venus. The use of the images themselves theoretically permits determining camera pointing angles to the order of a pixel (9.4 μr) rather than 0.1 degrees. We chose, therefore, to initially measure cloud motions in images where a substantial portion of bright limb was visible (~150 degrees of arc).

The navigation model used consists of two parts (Figure 3a and b). Part one is the best fit to a sphere. Five to ten points are chosen at a DN threshold on the bright limb and a least squares fit is made to determine the center of the planet. The residuals of the five points must be within one resolution element (pixel) of the assigned radius of the planet plus cloud deck. Using data supplied by O'Leary (private communication) we chose to define the limb radius at 6131 km for a brightness threshold of 35-40 DN. This is approximately the $\tau = 1$ slant optical depth for the UV images.

The value of the radius is not crucial since it only affects the scale of the navigation model. Provided we stay away from the limb when measuring (to avoid foreshortening) an error of 60 km in assigned radius would be only a 1% error in the scale of the displacement vectors (~1 m/s). What is very important, however, is that the radius and brightness threshold be consistently chosen, for if the planet centers are inconsistently found, the absolute displacement error from one frame to the next transfers directly to the measured cloud displacements. For example, a 60 km error in determining or aligning planet centers in successive frames could yield a 16 m/s velocity error over a one hour time interval between pictures.

The required inputs to obtain the best fit to a sphere are:

1. Coordinates of 5 limb points
2. Lines per TV frame
3. Elements per TV frame
4. Angular height of frame
5. Angular width of frame
6. Distance to Venus surface (altitude)

The angular size of the TV frame is accurately known from camera calibration. The black mask framing the vidicon and the focal length of the telescope precisely define these parameters. The angular distance between reseau marks is also well known from the camera calibration. Thus, by choosing reseau pairs and measuring the distance between them in lines or elements, one can determine the lines and elements per frame as well as the magnification factor applied during the geometric decalibration. Calculation of the aspect ratio (element to line ratio between reseaus) allows a double check on the consistency of the measurements. The altitude of the spacecraft is well known from trajectory data. Table I shows the results of the image geometry determination.

The next step is to verify that using the geometrically decalibrated and scaled images, we can get the navigation models to properly align with each

TABLE I

IMAGE GEOMETRY

From Resau Measurements
on Rectified Venus Frames

MVM '73 A CAMERA: FOCAL LENGTH 1495.66 mm

FRAME HEIGHT 0.3663 deg

FRAME WIDTH 0.4723 deg

FDS	SHUTTER TIME GMT		# RESEAU PAIRS MEASURED HORIZ.	VERT.	MEAS. FRAME SIZE LINES	ELEMENTS	ASPECT RATIO	MAG. FACTOR
62693	039	020656	12	9	799.932	965.366	1.206	1.099
62839	039	034908	6	7	824.386	993.344	1.205	1.132
62857	039	040144	11	9	828.075	997.616	1.205	1.137
62987	039	053244	12	9	849.175	1024.543	1.206	1.167

TABLE II

IMAGE NAVIGATION

(For 5 Point Fit)

MVM '73 A FRAME: .3663 x .4723 deg.

35-40 DN THRESHOLD AT 6131 km

FDS	HEIGHT (km)	FRAME SIZE FROM RESEAUS LINES	FRAME SIZE FROM RESEAUS ELEMENTS	BEST FIT FRAME SIZE (NAVIGATION MODEL) LINES	BEST FIT FRAME SIZE (NAVIGATION MODEL) ELEMENTS	RMS RESIDUALS AT LIMB (km)	NAVIGATION MODEL PLANET CENTER LINES	NAVIGATION MODEL PLANET CENTER ELEMENTS
62693	1694932	800	965	802	968	14	447	597
62839	1745295	824	993	828	994	0	447	596
62857	1751505	828	998	830	998	11	446	597
62987	1796354	849	1025	849	1024	5	447	597

GROUND RESOLUTION ~15 km/PIXEL AT

SPACECRAFT SUB POINT

other from image to image. Table II shows those results. The frame size of FDS 62693 required a change of 2-3 pixels (with the angular size fixed) to obtain the best fit, indicating that either the altitude or chosen magnification factor for remapping the image was probably incorrect by 0.2 - 0.3% for that frame. However, since we are directly using the image data to navigate, no scale factor error is introduced. The planet centers and limbs all agree and align with each other to 1 pixel or less.

The second part of the navigation procedure, once one has obtained the best fit to a sphere, is to put the latitude longitude grid on the planet. The basic inputs are:

1. Latitude of sub-spacecraft point
2. Longitude of sub-spacecraft point
3. Latitude of subsolar point
4. Longitude of subsolar point

The sub-spacecraft point is known extremely well from trajectory data which had to be reduced early in order to make course corrections to get to Mercury. This point is identical with the planet center in the images. The latitude and longitude of the subsolar point is also well known from celestial mechanics and radar. The 3 axis stabilized spacecraft was held to its attitude within a limit cycle of ± 0.25 degree in each axis. Since the camera was mounted on the scan platform in a clock-cone coordinate system, every scan line in the TV image points to the sun to approximately ± 0.25 degree, and the subsolar point and sub-spacecraft point must therefore both lie on a single scan line. With the best fit to a sphere defining the planet scale, and with the sub-spacecraft point used as an anchor point; the latitude-longitude grid is rotated until the given subsolar point lies on the same scan line as the planet center. This completes the definition of the navigation geometry.

The maximum deviations from picture to picture in pitch, yaw, and roll (determined from the Mariner 10 engineering data tapes) were: pitch, 0.108°; yaw, 0.237°; and roll 0.144°. Thus, the maximum scan line tilt of the camera between any picture pair is less than 0.3°. A 0.3° tilt of a scan line corresponds to <1 pixel error in attitude for subsolar and sub-spacecraft points ~175 pixels apart. There is also ~1/2 pixel error in roundoff and truncation possible in the navigation model because integer pixel coordinates are used. As a result, the total RMS error in navigation (including image rectification) is ~2 pixels (Table III). As we shall see later, the correlation methods used in measuring cloud displacement interpolate to better than 0.1 pixel, so measurement error by the computer is negligible. When the McIDAS operator uses single point tracking so that he measures the displacement himself by positioning the cursor on a point, one has to increase the RMS error. There is a 1 pixel granularity in cursor position plus up to several pixels for operator accuracy, so the anticipated RMS error for operator measured cloud displacements is 4-5 pixels. That is about double the error for the computer measurements, where the operator merely selects a cloud target with the computer doing the measuring. As a result, we must treat single point tracking measurements separately in the motion analysis since they can be expected to have larger scatter.

TABLE III

ERROR SOURCES

GEOMETRIC RECTIFICATION	~1 pixel
NAVIGATION MODEL FIT	~1 pixel
LAT-LON GRID DEFINITION	~1 pixel
ROUNDOFF & TRUNCATION	~1/2 pixel
RMS ERROR	~2 pixels

SP TRACKING ADDS 1 PIXEL GRANULARITY IN MEASURING PLUS UP TO SEVERAL PIXELS FOR OPERATOR ACCURACY, THUS THE RMS ERROR IS ~4-5 PIXELS

TABLE IV

VELOCITY ERROR

(15 km/pixel Resolution)

PIXELS SHIFTED	km SHIFT	VELOCITY INCREMENT FOR A GIVEN TIME INTERVAL(m/s) 15 MIN.	30 MIN.	1 HR.	1-1/2 HR.	3 HR.
1	15 km	16 m/s	8 m/s	4 m/s	3 m/s	1.5 m/s
2	30	32	16	8	6	3
4	60	67	33	16	10	5
6	90	100	50	25	18	9

Knowing the expected errors in alignment and measuring, we can predict the velocity errors we should expect. Table IV shows the situation for the 15 km/pixel resolution data. For a 2 pixel error, any time interval greater than 1 hour between frames will give <10 m/s uncertainty in the measurements. For a 4 pixel error, we need a time interval over 1-1/2 hours to do as well. For 5 m/s accuracy, we need time intervals of 2-3 hours at this resolution.

One pair of frames (Table I) had a 13 minute time interval. True to expectations, we found scatter in the measurement as high as 70-80 m/s, so this short time interval, T_2-T_3, was not used for velocity determinations. Five other time intervals formed from the four 15 km/pixel resolution images were found acceptable: T_1-T_2, T_1-T_3, T_1-T_4, T_2-T_4, T_3-T_4. These time intervals formed the basis for the initial measurement of the global velocity field on Venus reported here.

III. CLOUD MOTION MEASUREMENT

In addition to image navigation, it is important to understand the measuring process in order to judge the significance of the results. The entire 8 days of Mariner images of Venus exhibit characteristics similar to the most common ground based observations, e.g. the 4-day rotation, reversed "C" features, "Y" features, and two bright polar rings or caps. It is reasonable, therefore, to assume that the Mariner 10 observations are representative of Venus as it usually is. If the meridional motion and the zonal motion, as measured, are both representative of the mean state of the upper atmosphere, it then becomes possible to set some boundary conditions on the general circulation.

A very important consideration to keep in mind is the confidence one can place in deviations from the velocity structure we see. Provided one believes in the accuracy of the navigation and the measurements, the scatter in the u-component is significantly larger than it should be. We also observe a small number of deviant measurements, again significantly more deviant than should be expected. This has made us look more closely at the possibilities of additional structure superimposed on the vortex and at vertical shear and varied kinds of wave perturbations on the steady state. Evidence for these phenomena can be found in the images, but the best quantitative measures we have to date rest in the "significant deviations" mentioned above. Study of such second order effects in the data may be a major part of future analysis.

A. Motion Measurement Techniques

Large scale features can be easily traced across the full disk of Venus, but smaller features <200 km across are harder to track. They have low contrast, they may appear and disappear either by changing shape or brightness substantially so as to become unrecognizable over periods of a few hours, or they may just fade away into a background of pulsating light and dark features. It should be noted here that by pulsating brightness, we are talking about relative contrast variations of a percent or two. The images must be contrast stretched to a high degree to see anything at all, and it is not unreasonable to expect that some of the variation is due to quantization roundoff in the cameras. In general, one can say that the longer the time interval, the harder it is to follow a feature. The shorter the time interval of observation, however, the less accurate the velocity determination. We initially tried several techniques to ascertain the differences between them and their relative accuracies on the same or similar cloud targets.

Measurement of cloud motions is done in the TV images of Venus in two ways. The first method is called "single point tracking." The McIDAS operator, using a joystick, superimposes a cross cursor on the TV screen over the Venus image played back from a track on an analog disk. Since the cursor is electronically generated on the TV screen, there is no parallax. The operator chooses a cloud feature, moves the cursor to coincide with the feature, and presses a key on his communication console. The computer inquires of the cursor electronics where the cursor is positioned in the TV image relative to the analog disk timing track and receives a line-element image coordinate accurate to ~1/2 pixel.

The analog disk head is advanced automatically to the next TV frame in the time sequence being analyzed and the operator moves the cursor to the new position of the cloud he is tracking and again presses the key. The computer records the second set of coordinates and calculates a displacement from the first position in lines per hour and elements per hour. The Venus navigation model can then be applied to transform the vector magnitude and direction to planet centered U and V components and meters per second.

The second method of measuring motions utilizes the computer to do objective image matching rather than the operator. The operator chooses a cursor size and shape in the form of a k by ℓ pixel box. The cursor box is then positioned over a cloud or cloud feature to define an image target grid A (Figure 4). A lag size s is defined such that when the operator pushes the key on his console the digital data in image grid A is moved from digital disk to core, and the cursor is enlarged to a m by n box where $m = k + s$ and $n = \ell + s$. The frame is advanced and the operator places the enlarged cursor over the same cloud target at the new time and position and then presses the key to define the image search grid B. The grids A and B are then compared over all the different possible lag positions (p, q) and a match coefficient matrix generated (Fig. 4b, 4c, 4d).

The image match coefficients are constructed as vector products using varied norms. The Cross Correlation Norm (CC) is simply a direct product of the elements in A and B, the "angle" between the two "vectors". The Euclidean Norm (EN) is the "distance" between the grid vectors, the square root of the sum of the squares of the products. Any LP Norm can be generated as well. The difference between the norms is that the lower power norms are more sensitive to edges and image details. The higher power norms are more sensitive to light and dark patches. The Euclidean Norm seems to be more sensitive to image detail in general, emphasizing neither edges nor area contrast. Because the target clouds varied in structure and were diffuse and changeable with time, we chose to measure each target with single point tracking (SP) and the norms CC, EN, and LP5. We expected to find differences between edge and patch tracking because of the observed variability of the clouds with position on the planet.

At each lag position the match coefficient matrix is searched to find the particular lag position at which the best match occurs (usually the greatest relative maximum). The lag position corresponds to the displacement of the cloud in grid A over the T_1-T_2 interval. The peak of the image match

Figure 4. (a) Computer image matching is done by moving the data in Target grid A around in Search grid B until maximum correlation is achieved.

(b) Image match coefficient matrix for an image correlated against itself, a perfect match.

(c) Image match coefficient matrix for a good correlation in the Venus images.

(d) Image match coefficient matrix for a correlation failure. Note the broader peak and lack of a well defined maximum within the matrix boundaries.

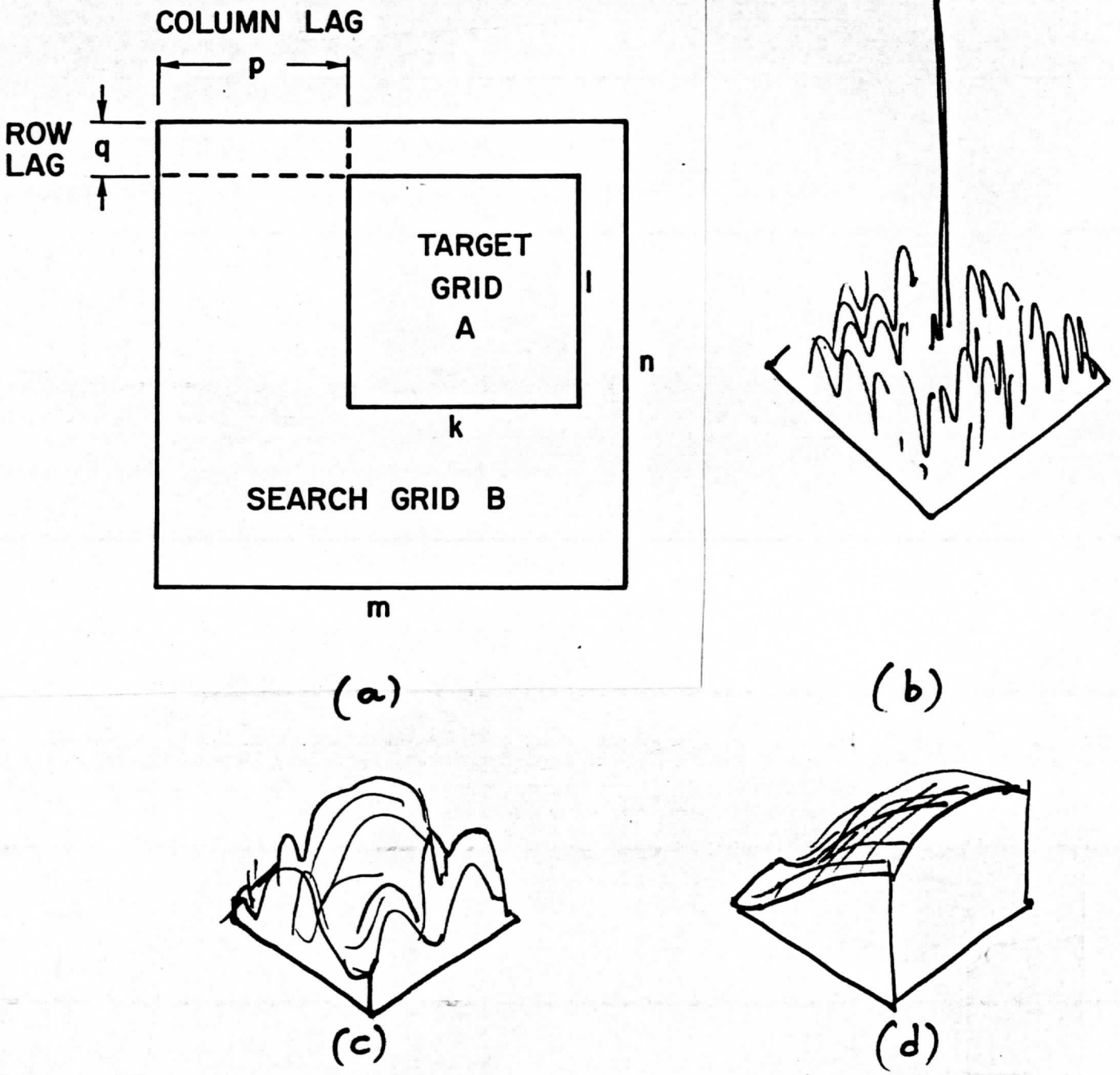

FIGURE 4 a) Computer image matching is done by moving the data in Target grid A around in Search grid B until maximum correlation is achieved.

b) Image match coefficient matrix for an image correlated against itself, a perfect match.

c) Image match coefficient matrix for a good correlation in the Venus images.

d) Image match coefficient matrix for a correlation failure. Note the broader peak and lack of a well defined

coefficient matrix represents the best match of the target grid with the search grid. The difference between the (0,0) lag coefficient coordinate and the best match coefficient coordinate is determined by quadratic interpolation in 2 dimensions in the image match coefficient matrix. The cloud motion displacement vector is determined in image coordinates. Transforming the lag displacement vector end points to Venus coordinates results in the wind estimate.

Because of the cofficient matrix interpolation there is no granularity in the computer displacement measurements as there is in single point tracking by the operator. With Earth clouds, we have determined the interpolation to be accurate to <0.1 pixel. The Venus cloud data is much more diffuse and less contrasty, however, with a significant lack of detail. As a result, many of the correlation peaks, especially away from the Venus equator, were quite broad. If the correlation surfaces or image match coefficient matrices did not have a well defined relative maximum, they were rejected by the computer as correlation failures.

The failures were in large part due to the fact that a cloud feature had evolved so much as to become unrecognizeable to the computer. In most cases, single point tracking was still possible since the operator has the advantage of seeing coherence of the feature in time and can move forward and backward in the multi-picture loop until he has the target clearly recognized. The computer only has two image grids to compare and can utilize no other information. The computer is more precise, but inherently subject to more confusion. This points out the need for consistency checks on the computer measurements. If the same velocity is not measured over successive time intervals for the same cloud target, the computer may have lost the target or latched on to a nearby cloud which was similarly shaped. A target giving vastly different velocities when measured over different time intervals and with different norms must be suspect as not passive enough to be a good wind tracer and must be rejected. Unfortunately, the scatter in individual measurements in the Venus data was too great to use such a quality control criterion. A statistical approach to analysis was used instead.

B. Velocity Measurements on the Mariner 10 Venus Images

Targets were chosen in the four 15 km/pixel images on the basis of their discriminability and ease of tracking. The cloud features were generally of too low contrast to be clearly discernable in the raw images. Most of the time the image on the McIDAS TV screen had to be contrast enhanced or occasionally even high pass filtered to aid discrimination of features by the operator. Thus, SP tracking could possibly be biased by artifacts introduced in the enhancement or filtering process. To provide a control on such a possibility, the computer is required to do correlation and image matching only on the "raw" unenhanced data for the EN, CC and LP5 norms. "Raw" data has only been subject to noise spike removal, photometric correction for removal of vidicon shading, and geometric rectification for removal of distortion in the camera deflection system. Such images are as close to the true scene information as possible and free of processing artifacts introduced by computer filtering. Thus, different measurement techniques operating in parallel can be used as a trap

to catch biases or as an indicator of subtle differences in cloud characteristics not readily apparent to the operator.

SP tracking involves only the designation of a line element coordinate for each target. There is no image matching surface to examine. The acceptance rate for such measurements is therefore 100%. The "objective" computer tracking algorithms were applied by placing the center of the joystick operated cursor at the center of the cloud target, making the rectangular cursor box large enough to contain the target. All 6 image pair combinations were tried with each of the four norms. With the 3 computer norms, however, the computer had to examine each resulting image match surface to find a well defined maximum correlation peak within the bounds of the surface. No peak, or a maximum at the outer edge of the surface caused the computer to label the correlation a failure. More than 20-25% failures on a target would indicate that the computer was having difficulty. In such cases, the target was rejected by the operator and a new target chosen for measurement. A final measurement set of 47 targets and 1067 vectors was produced.

It is instructive to examine characteristics of the target tracking techniques in operation. Some cloud targets change substantially in size and shape over the longer time intervals of 2-3 hours. As a result, more operator indecision over the exact position of the target was noted, and the computer had a lower success rate in making image comparisons in the raw data. On the other hand, there was no difficulty encountered following features in the 13 minute time interval for either the operator or the computer, but the velocity measurement errors were proportionately larger. The short time interval was found especially useful in identifying vertical wind shear, but did not provide very accurate measurements.

We conclude that the optimum observation appears to be 15-20 minute time resolution over a time interval of at least 4 hours, a sequence of roughly 10 time lapse images. The high time resolution provides continuity for tracking purposes while the longer time interval provides greater accuracy in the velocity measurements. The lack of observed cloud features on Venus at resolution better than 10 km would seem to eliminate the need for higher time and space resolution. If one has poorer ground resolution than 15 km, the time intervals become proportionately larger, and the ability to resolve small velocity increments is reduced. These facts should be kept in mind when designing an optimum imaging system to study atmospheric dynamics from the next generation Venus orbiters.

The performance of the three computer cloud tracking techniques surprisingly yielded no discernable differences in accuracy. If a correlation was possible, the EN, CC, and LP5 determined velocities averaged out with nearly the same target means and the same amount of scatter to within 1-2 m/s. Given velocity profiles determined by the three different techniques, it would be impossible to distinguish which velocity profile was made with which technique. For that reason, we will treat all the computer measured volocities (EN + CC + LP5) as a single data set, designated by COMP.

While the velocity measurements were similar, the target tracking abilities of the three computer norms were not the same. As expected, the LP5 norm was more successful in the patchy sub-solar region. The streaky clouds in the mid latitudes were difficult for LP5 because the light and the dark patches were

too large and too diffuse to provide a sharp correlation peak. The useful image information in mid latitudes resided in the edges of features, so the CC norm was more successful there. The EN norm was useful almost everywhere and seems the best compromise technique given the varied structure of clouds on Venus.

The best success in target tracking on Venus was obtained by staying away from the limb to avoid foreshortening, and by staying at least 40 degrees in phase angle away from the terminator. As one moves closer to the terminator in the images, the first noticeable effect is a loss of contrast. Features are harder to follow because as the scene brightness diminishes, the digitization level for any intensity becomes a larger fraction of the scene dynamic range. The net effect is to lose both spatial and photometric resolution as neighboring pixels are quantized into the same gray level in the camera, producing a very contoured image. Near the terminator itself, no cloud detail is apparent, only contours of uniform gray. Generally, if the McIDAS operator would follow a cloud feature easily in the enhanced or filtered image, the computer could track it in the raw image. Where the operator had trouble, so did the computer. A practical limit of 230° longitude was established to define the bound of the "difficult" tracking region on the planet. Figure 9 shows this region to include about 40% of the visible disk of Venus.

A loss of 40% of the observable area of the planet is substantial. We plan to pursue cloud motions in that region in some fashion, possibly in higher resolution images, since the velocities in the morning terminator part of the planet could have bearing on definition of the drive mechanism for the zonal winds.

The bias catching trap, mentioned earlier, did catch something during the analysis which is of significant value. While the v-component (meridional) averages of SP, EN, CC and LP5 show no significant differences, the u-component (zonal) velocities determined by SP consistently average 5-10 m/s larger than the computer determined velocities. Moreover, the RMS scatter in the measured u-component is 2-3 times the RMS scatter in the v-component for all four norms. One place to look for an explanation is in the image navigation, and another is the McIDAS operation. Those possibilities are examined next.

C. Vector Data Set Selection

The vectors generated from the 13 minute time interval between the second and the third pictures in the sequence had unacceptably large scatter in the measurements, with some vectors ranging as high as 60-70 m/s from a target mean, which generally was determined from an average of about 15 computer measurements (6 for the SP target means). From Table IV this result is expected. Consequently only the 5 longest time intervals were used, reducing the sample to 887 vectors. The individual target means were then recalculated on the basis of the remaining 5 time intervals.

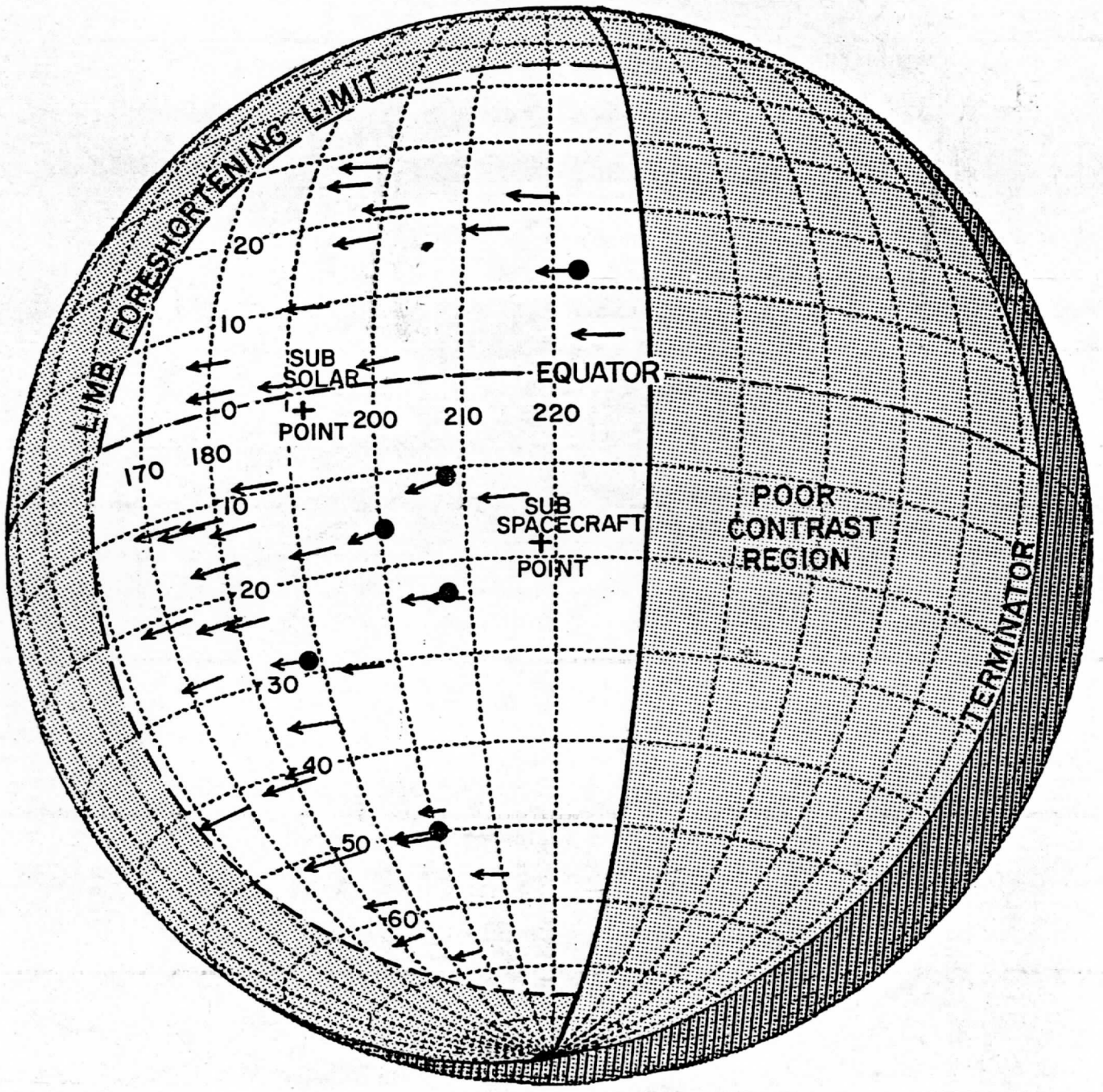

Figure 5. Appearance of Venus in the measured images 2 1/2 days after encounter. Crosshatched portion is the portion not illuminated by the sun. Shaded areas are regions containing no measurements due to poor contrast or foreshortening. Each arrow represents one cloud target, with the solid dots identifying the location of the six "wierd" targets. Note the bias introduced by the fact that cloud targets above 30 degrees latitude lie at the leftmost longitudes.

TABLE V

Mean Measured Velocities and RMS Deviations

	NORM	NUMBER OF VECTORS	u		v	
			MEAN OF ALL VECTORS	RMS DEV. FROM TARGET MEANS	MEAN OF ALL VECTORS	RMS DEV. FROM TARGET MEANS
46 TARGETS 5 TIME INTERVALS	SP	381	-103.89	16.55	-3.75	6.60
	COMP	506	- 91.20	14.00	-1.53	8.54
15 m/s CUTOFF	SP	256	-101.14	7.37	-3.40	4.72
	COMP	364	- 91.36	5.93	-0.06	4.96

TABLE VI

Velocity Correction from Image Misalignment Test
(All vectors, SP and COMP)

IMAGE PAIR	TIME INTERVAL	VELOCITY CORRECTION (RMS)		
		2 Pixel Estimate from Table IV	Actual Δu	Actual Δv
T_1-T_2	102 min	4.9 m/s	1.72 m/s	.44 m/s
T_2-T_3	13 min	32.0 m/s	22.4	1.62
T_3-T_4	91 min	5.5 m/s	1.56	.39
T_1-T_3	115 min	4.4 m/s	3.85	.41
T_1-T_4	206 min	2.4 m/s	1.99	.32
T_2-T_4	104 min	4.8 m/s	1.52	.26

TABLE VII

Summary of Cloud Motion Vector Selection

	VECTORS REMAINING
Initial Data Set (47 targets)	1007
13 Minute Time Interval Rejected	887
15 m/s Edit to Sharpen Distributions	620

A large RMS scatter still remained in the measurements (Table V). It was decided to discard about 1/3 of the most deviant measurements to sharpen the distribution. Care had to be taken to avoid throwing away any maxima and minima in the velocities as functions of latitude or longitude. We could not simply calculate an average over all latitudes and longitudes and throw away the fastest and slowest vectors. Instead, the mean velocity in u and v for each separate cloud target was used, so that the deviation of a vector from its own target mean was the criterion for rejection. Provided targets were not substantially accelerating, such a selection technique would preseve latitudinal and longitudinal structure of the cloud motion field, as well as isolate targets with motion anomalously different from the majority. The 6 "slow" targets seen in the COMP measurements are anomalously different in this sense. They are therefore deserving of more study.

The fact that the scatter in the u component is 2-3 times the scatter in v requires explanation. This cannot be explained in terms of a systematic bias in the measuring process because of the matrix transforms and planet tilt, which linearly combine x and y image directions in nearly equal proportions to generate u and v. A single McIDAS operator (Krauss) made all target selections and measurements. The use of a single person to make the measurements was advantageous from the standpoint of consistency, but introduces a greater risk of bias. Any tracking bias would, however, have to occur before the matrix transform from line-element to latitude-longitude coordinates. We feel that it would be impossible to intuitively grasp the necessary time and geometry relations necessary to bias over 1000 measurements made with vastly different techniques over a variety of surface orientations in different places on Venus and still obtain consistent velocity profile patterns independent of time interval or tracking method. Thus, neither the different scatter in u & v nor the velocity profile shape seem related to operator bias.

Next, we examined the navigation procedure more carefully, looking for an underestimate of image misalignment, roundoff, or truncation errors. Each of the remaining 5 time intervals was separately examined. In each case the u component scatter was 2-3 times that in v. A program was written to take the average calculated latitude and longitude of the displacement vector in picture A, and use the navigation model for picture A to convert to line-element coordinates in picture A. The identical line-element coordinates in picture B were then taken and converted to latitude and longitude using the navigation model for picture B. This gave an independent quantitative estimate of image misalignment in terms of velocities instead of pixels. Table VI shows the RMS correction factors obtained, which are consistent with the v component scatter and the estimate in Table IV and nowhere near large enough to explain the u component scatter.

The Δu correction due to misalignment, roundoff, and truncation is around 1 pixel, slightly less that predicted. The v alignment is considerably better than expected. We do not know why! This correction is for systematic error in alignment, but random error in roundoff and truncation. Grid placement on the planet could vary by ~1 pixel between pictures and would impart a systematic rotation to the vectors. It is reasonable to say that we do

not fully understand what goes on at resolution below 1 pixel, but for this data set can still safely claim 5-10 m/s as our upper limit on systematic error in alignment and measuring, corresponding to ~2 pixels total misalignment and random error over the time intervals considered (see Table IV).

We conclude that the larger scatter in u is real and is probably due to actual time variations in cloud structure and vertical shear effects. The significant fact to keep in mind is that all evidence indicates measurement errors no larger than 5-10 m/s RMS while the "structure/shear" modifications are in the 10-20 m/s range. There is reason to believe, therefore, that second order effects in the cloud motions on Venus are measureable. We will return to this in the discussion in Section IV.

Cutoffs in u and v ranging from 5 m/s to 40 m/s from the individual target means were used to select vectors for plotting and least squares analysis. A 15 m/s cutoff was chosen as representative. Larger cutoffs left more scatter in the data, hiding its functional form, while smaller cutoffs threw away many more points without uncovering any added characteristics of the profiles. The 15 m/s cutoff threw out 30% of the most deviant measurements, leaving 620 vectors which formed our "cleanest" and hopefully unbiased data set. All analysis from here on is based on the 620 vector sample (Table VII).

IV. ANALYSIS OF CLOUD MOTION MEASUREMENTS

We present here the measurements of the motion of the small scale UV markings or cloud features. It should be possible now, in light of the previous discussion, to estimate the validity of the measurements and also to estimate the significance of the deviations and scatter in the measurements. We report in addition on observations of vertical wind shear and its organization. The facts are then summarized in Section V, and possibilities for further investigations using the Mariner 10 image data are examined.

A. Zonal Motions

Figure 6 shows the 15 m/s edited zonal velocities which were measured. Both SP and COMP velocities are shown, with the results presented both as separate target means, including RMS errors, and as scatter plots showing all 256 or 364 vectors, respectively, in the edited samples (see Table V and related discussions concerning vector selection). The SP measurements (Figures 6a and 6b) appear to have a 50 degree latitude velocity maximum. The COMP measurements (Figure 6c and 6d) are in better agreement with a maximum at 40 degrees latitude. Both SP and COMP data sets have approximately a -92 m/s minimum zonal velocity at the equator. A dashed line shows nearly constant angular momentum assuming -92 m/s equatorial zonal velocity and a linearly increasing decrement of angular momentum so the velocity at 45° is closer to 125 m/s than the 140 m/s if angular momentum were perfectly conserved. Least squares fits using second order polynomials were made to the measurements to determine a velocity minimum in the profile and assess the degree of symmetry about the equator. The polynomial fits were limited to latitudes less than 45 degrees. The results are presented in Table VIII and shown in Figure 6 as solid lines. At high latitudes, the measurements lie near a line of constant angular velocity, also shown dashed.

Figure 6c shows solid circles corresponding to the anomalous six "slow cloud targets" having lower velocities than their neighbors. They appear to be scattered randomly over the planet (See Figure 5) and are significantly different from neighboring cloud targets in that they do not show acceleration in the zonal direction (Figure 7c). The six targets lie close to a line of constant angular velocity, shown dotted in Figure 6c. The least squares fit between $\pm$ 45 degrees latitude without those slow targets is shown in Figures 6c and d as well as a separate least squares fit to the six slow targets. Visual inspection of the slow cloud targets in the TV images shows nothing distinctive about them with regard to shape, brightness, or position.

What is most surprising is that the low velocity cloud targets show up in the COMP measurements but not in the SP. This may be an example of how the precision of the computer measurements is affected by formation and dissipation at leading and trailing edges of clouds passing through a local pressure change or region of subsidence. The computer could thus be detecting an organized large scale wave phenomenon, as the constant angular velocity would seem to indicate. The McIDAS operator, tracking a center of brightness or

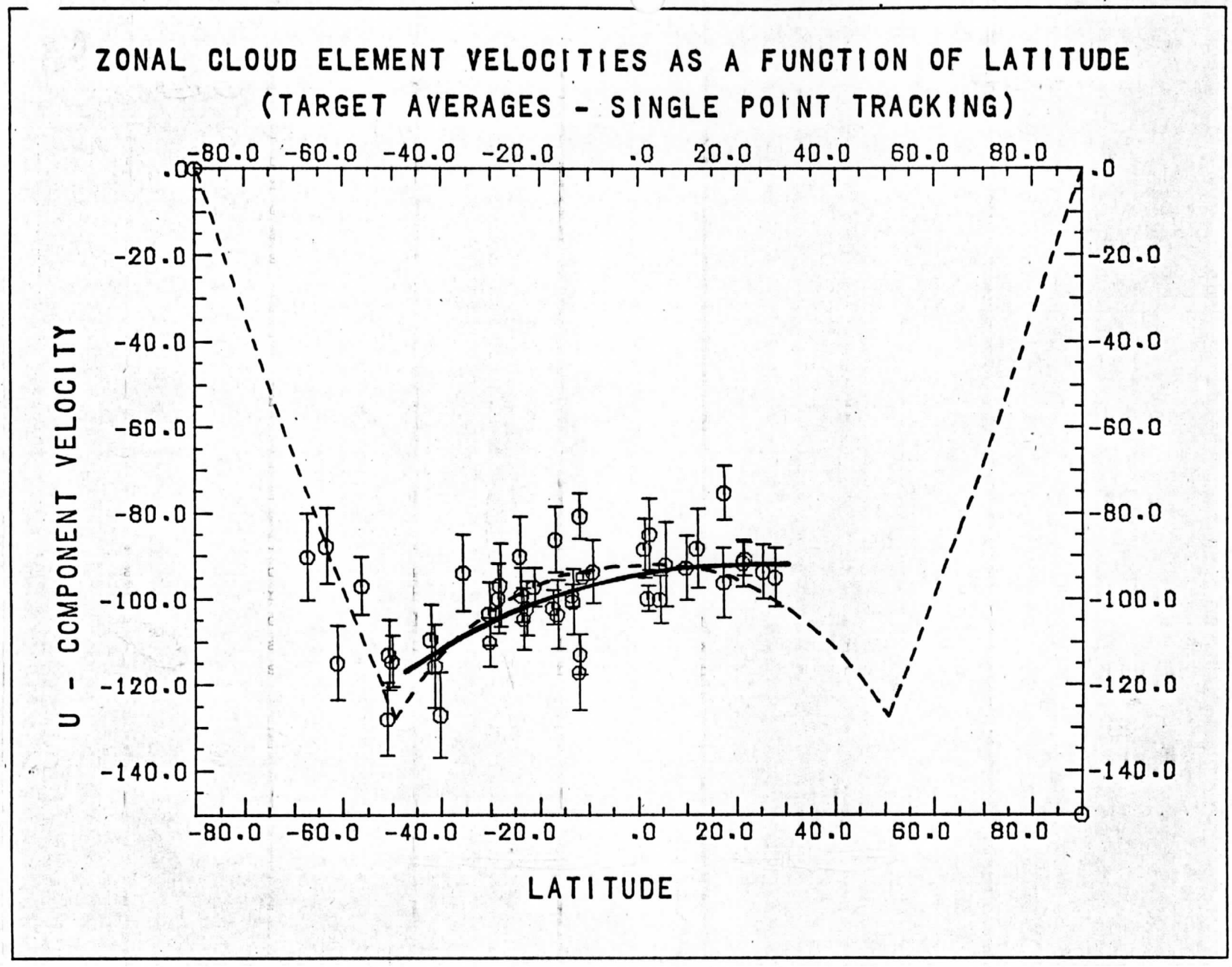

Figure 6a. Single Point Tracking using 15 m/s cutoff to edit data. Target averages are shown with RMS Errors. The dashed line is a model with a velocity maximum at 50° latitude, with nearly constant angular momentum at lower latitudes and constant angular velocity at higher latitudes, chosen to simulate a vortex as in Suomi, 1975. Solid line is least squares second order polynomial fit to data points within 45° of the equator.

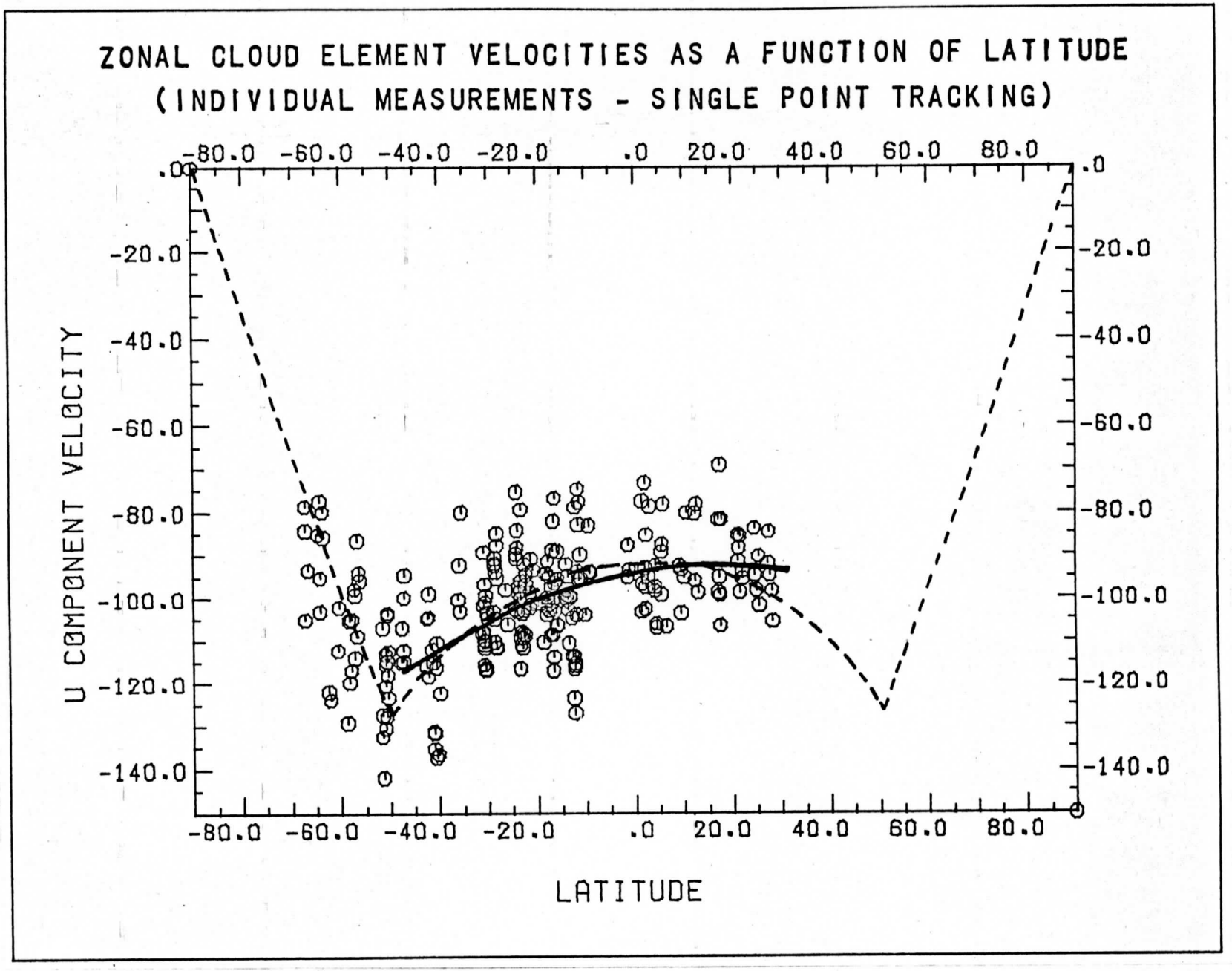

Figure 6b. Single Point Tracking. Scatter plot of 15 m/s edited vectors without target averaging. Dashed and solid lines same as in 6a.

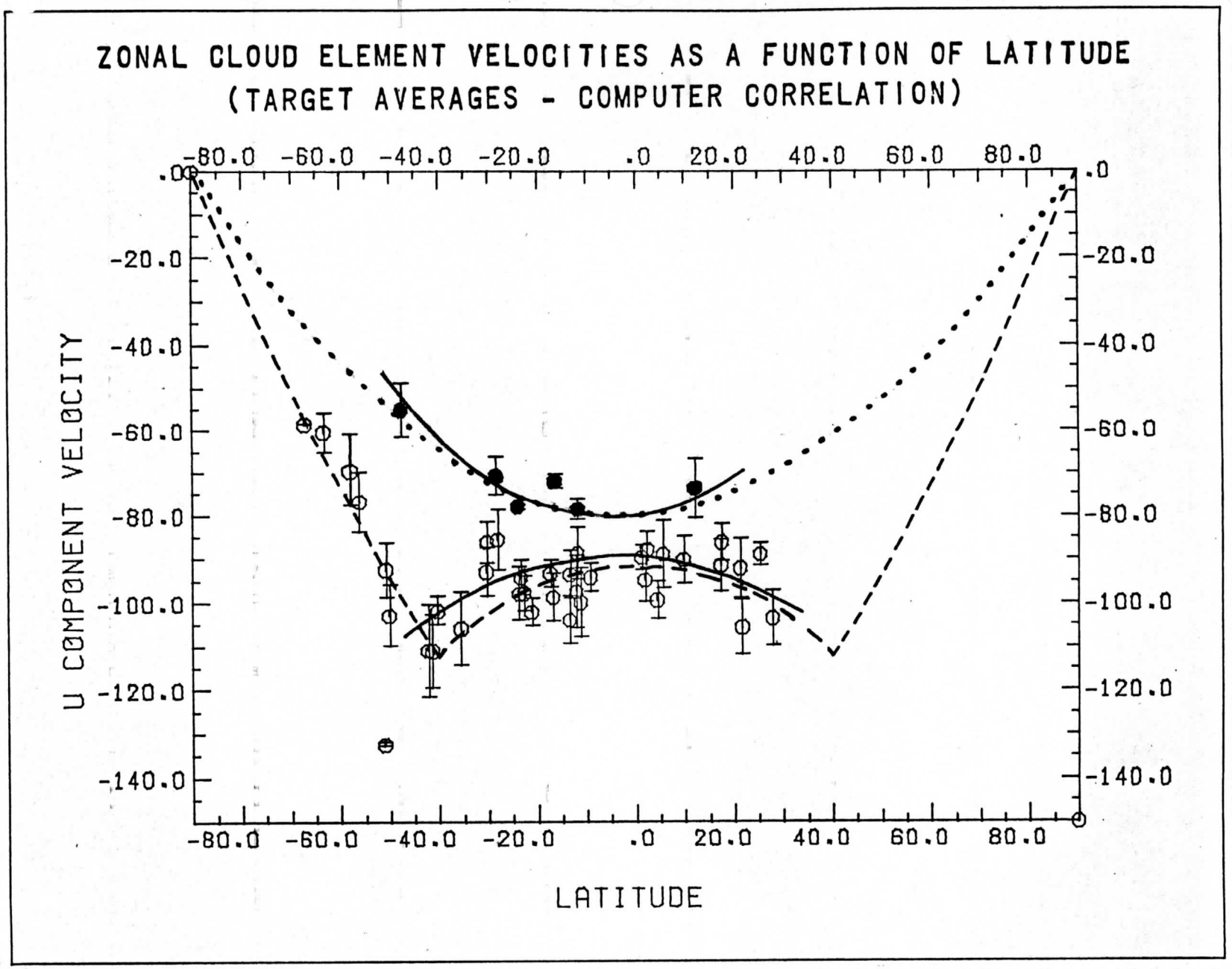

Figure 6c. Computer Measured Vectors. Target averages with RMS Errors indicated. Dashed line is a model having velocity maximum at 40° latitude, with nearly constant angular momentum equatorward and constant angular velocity poleward. The higher velocity solid line is a least squares second order polynomial fit to data points within 45° of the equator. The six targets, lying on the dotted line representing constant angular velocity, are fitted with their own second order polynomial, shown as the lower velocity solid line.

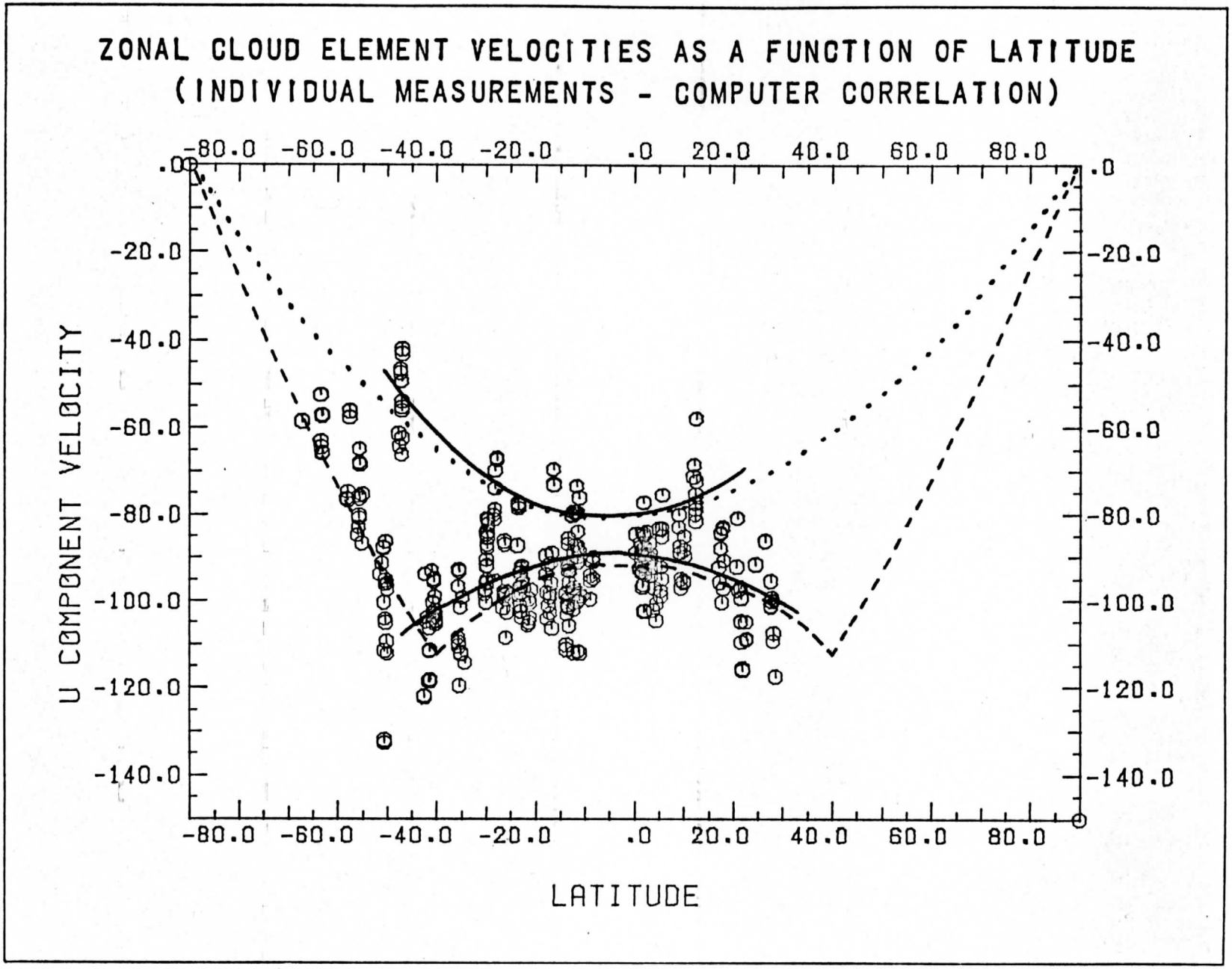

Figure 6d. Computer Measured Vectors. Scatter plot of 15 m/s edited vectors without target averaging. Dashed and solid lines same as in 6c.

TABLE VIII

Summary of Least Squares Fits for Measured Zonal Velocities

VELOCITY MEASUREMENT SET	DISPLAYED IN FIGURE	ZONAL VELOCITY MINIMUM AT LATITUDE	
SP Target Averages	6a	-91.3 m/s	+16°
SP all measurements	6b	-92.1	+12
COMP Target averages	6c	-88.9	-3
COMP all measurements	6d	-89.7	-4
COMP Averages (w/o slow targets)	curve not displayed	-92.3	+3
COMP All (w/o slow targets)	curve not displayed	-92.2	+3

a shape in a time sequence of several frames, is less likely to be affected by edge phenomena. The computer is forced to compare only two data grids and has no other reference frame, such as time continuity.

The differing results of the two measuring techniques, give a potential means of isolating points of constant phase related to wave phenomena, even though a wave may not be structurally coherent or contrasty enough to be seen in the Mariner images. Alternatively, if we are not seeing a wave, the differing results may permit isolating variations in altitude due to shear or changes in cloud structure related to local processes. The further analysis of both higher and lower resolution images (with large numbers of measurements in order to get good statistics) is indicated to identify the exact causes of the observed velocity differences and develop the means to use this technique to advantage. We must understand exactly what is changing and distinguish how the varied measuring techniques respond to such changes.

B. Meridional Motion

The general increase in zonal velocity from the equator to the mid latitudes on Venus is consistent with the simple assumption of conservation of angular momentum, provided some frictional dissipation is allowed. One can say that the zonal velocity profile thereby implies meridional motion. Moreover, the spiral streaks and vortex structure evident in the Mariner 10 images are by themselves strongly indicative of convergent motion toward the poles. Consequently, meridional motion is to be expected. What is surprising is how small it apparently is.

The meridional cloud motions show a correlation with latitude. The velocity tends to be zero near the equator and increases approximately 1.2 m/s in the poleward direction in each hemisphere for every 10 degrees in latitude away from the equator. Figure 7 shows the v-components of the edited measurements, both as target averages (7a and 7c) where the error bars represent RMS deviations in each distinct target average, and as scatter plots (7b and 7d) of all separate measurements. The data points within 45 degrees of the equator were fitted with a least squares straight line, shown solid in each plot. Results are summarized in Table IX.

A comparison with Table VIII shows that the zero crossing in all four plots in Figure 7 occurs at roughly the same latitude as the corresponding minimum zonal velocity in Figure 11. The SP and COMP data sets consistently differ by 20 degrees in where they put the "dynamic equator."

Three targets in 7a and 7c are shown as solid circles. These three should be considered biased since they coincide with the circumequatorial belts. The belts exhibit a southward motion quite anomalous from the other cloud features in that they move much faster (-24 ± 6 m/s) and are organized nearly along lines of constant latitude. They show a brightness maximum about every 12 degrees of latitude, though a filmy structure can be barely discerned between the maxima. The circumequatorial belts are seen only near the equator, only moving south, and only in the period 2-3 days after encounter. Figure 8 shows a scatter plot of SP measurements of the belts made over two 90 minute time intervals. From tables III and IV we would expect 10-18 m/s RMS scatter.

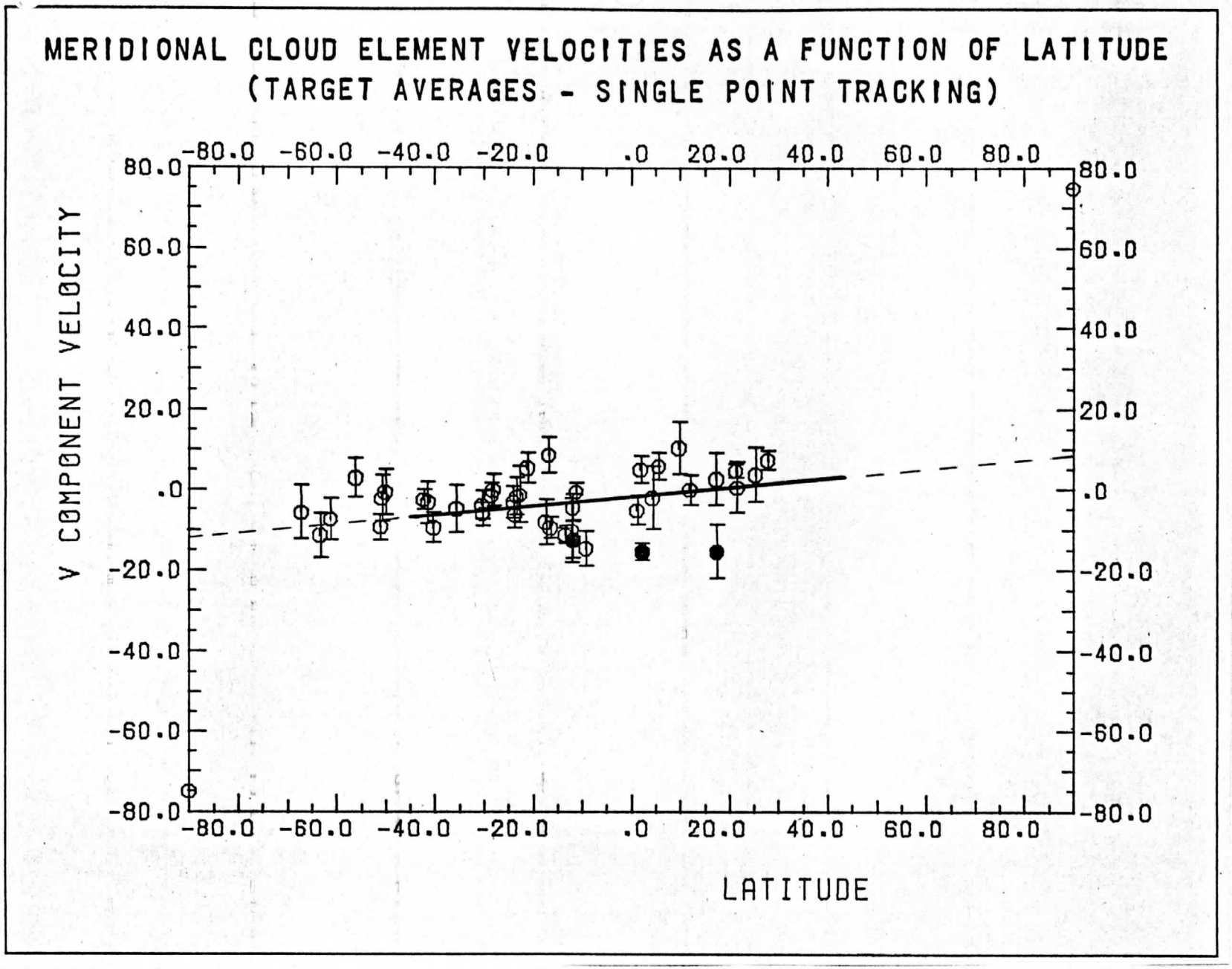

Figure 7a. Single point tracking using 15 m/s cutoff to edit data. Target averages are shown with rms errors. The solid dots are targets coinciding with the circumequatorial belts. The straight line is a least squares fit to the data point.

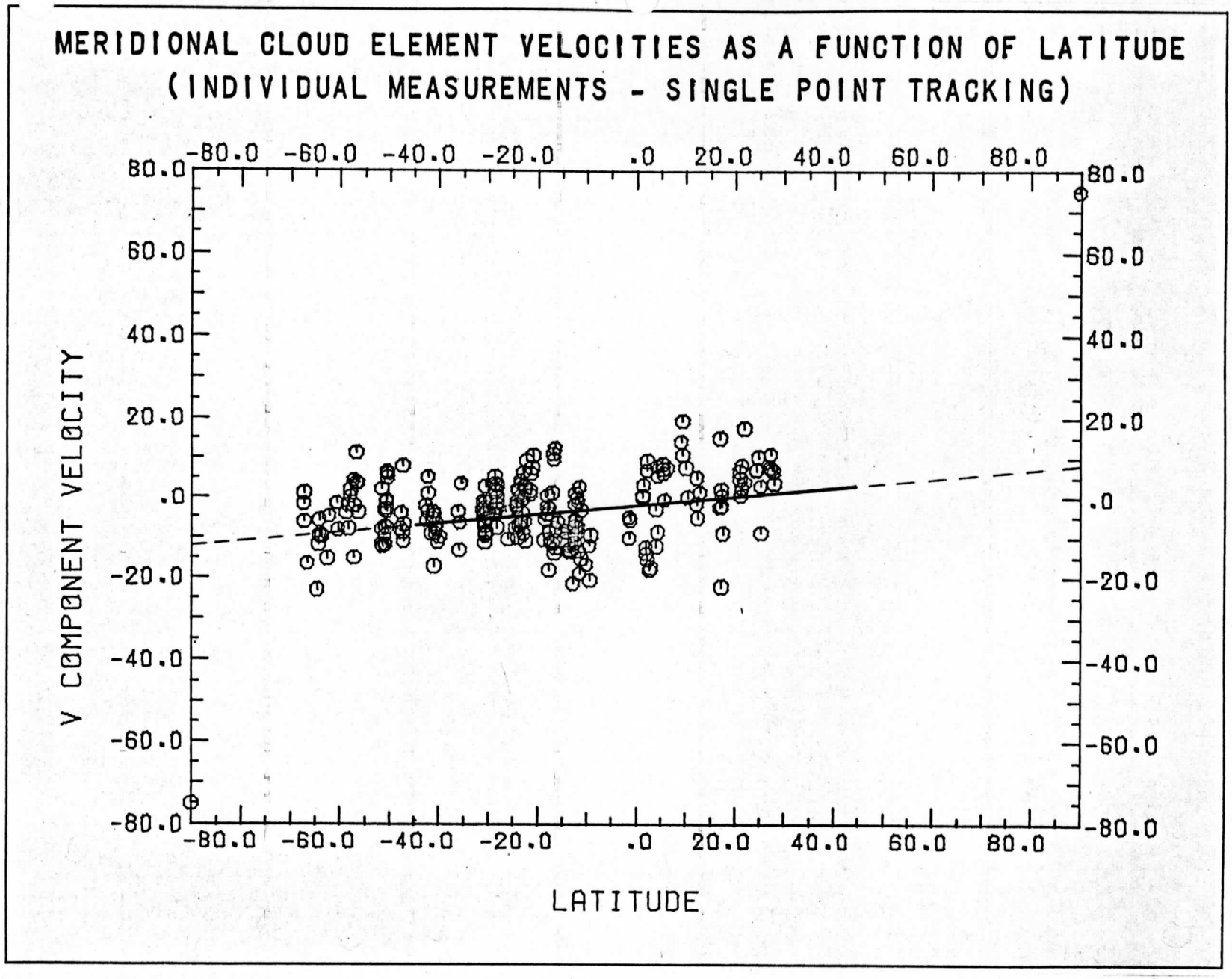

Figure 7b. Single Point Tracking. Scatter plot of 15 m/s edited measurements used to generate target averages in Figure 7a. Linear least squares fit to data points is shown.

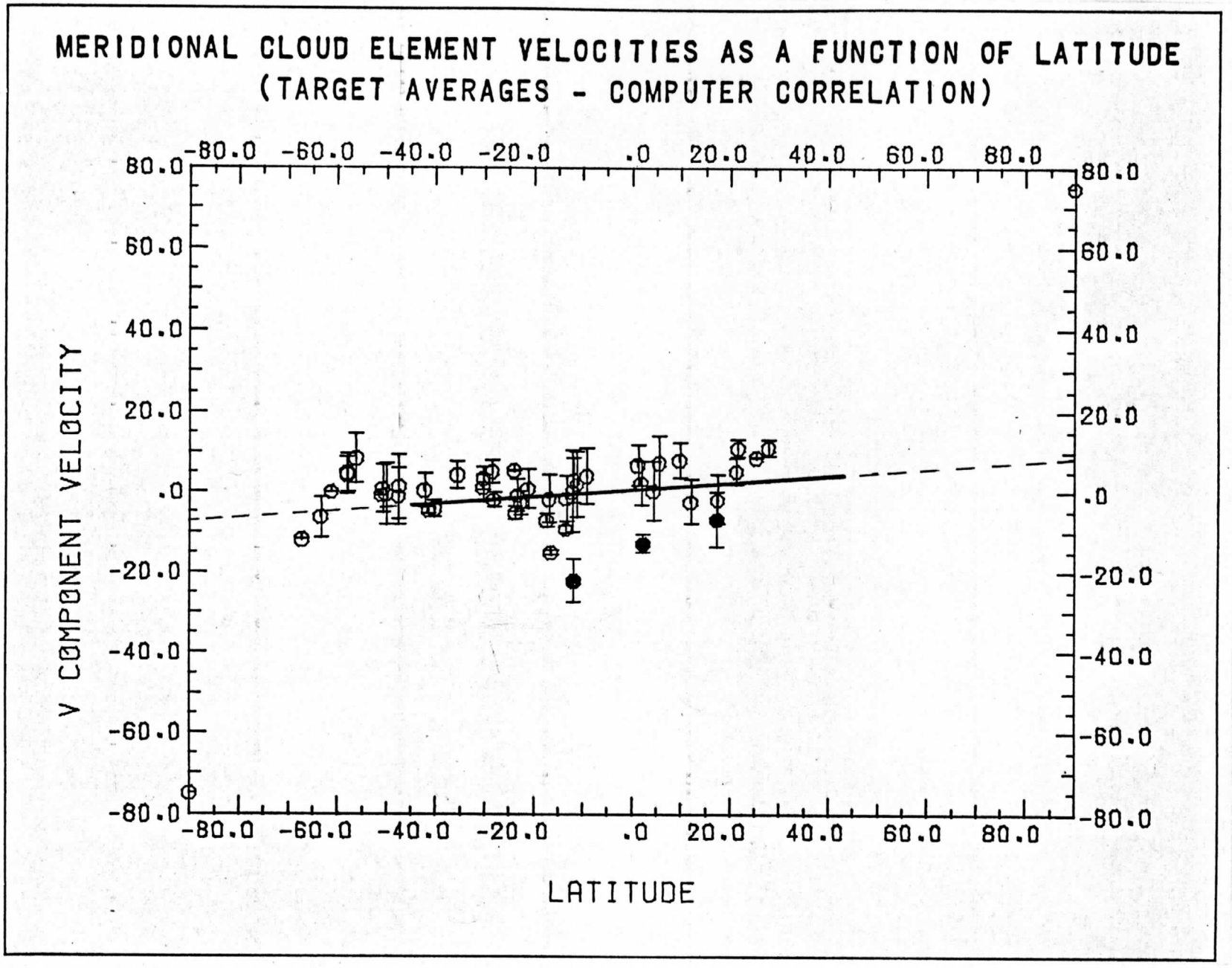

Figure 7c. Computer Measured Vectors. Target averages and rms error are generated from 15 m/s edited data shown in Figure 7d. Solid dots show cloud targets coinciding with circumequatorial belts. Linear least squares fit is also shown.

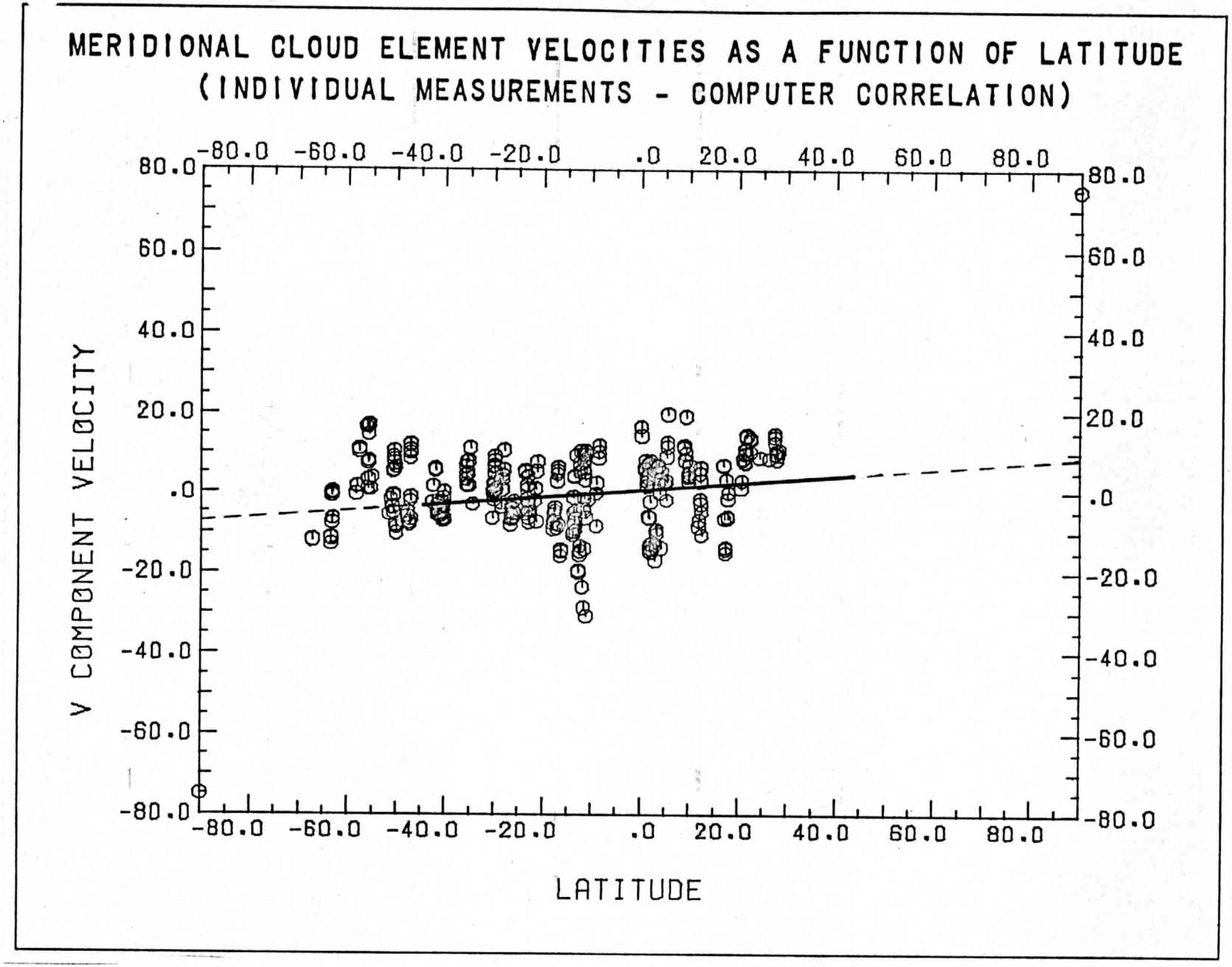

Figure 7d. Computer measured vectors and least squares fit to scatter plot.

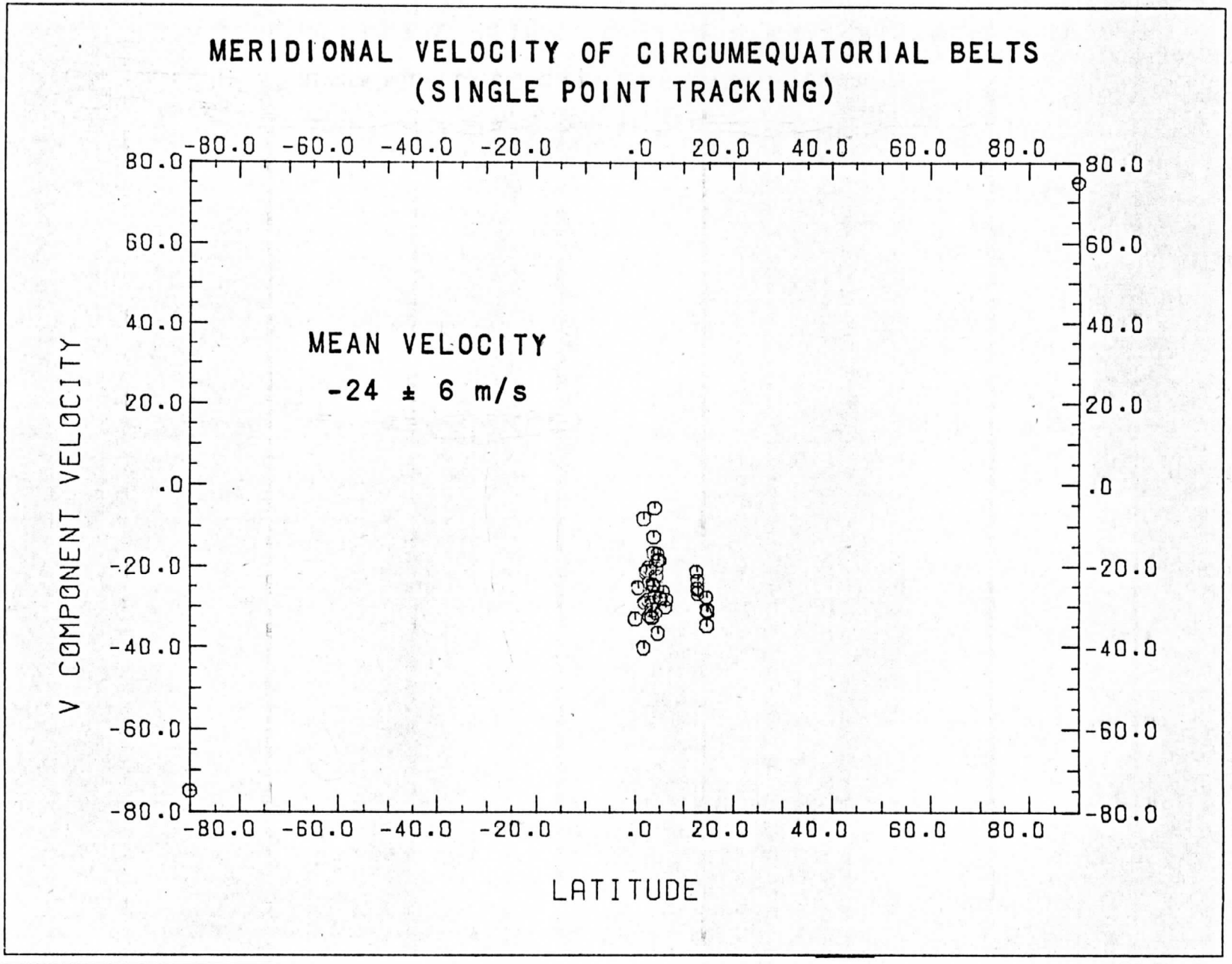

Figure 8. Meridional component of circumequatorial belts as function of longitude. Motion is toward the equator at~20 m/s, as all measurements were made between 0 and 20 degrees north latitude. Belt maxima are about 12 degrees apart in latitude.

TABLE IX

MERIDIONAL MOTION - LEAST SQUARES LINEAR FITS

	Slope	Zero at Latitude
SP Target Averages	.117 m/s/deg.	+17 deg.
SP all Vectors	.133	+12
COMP Target Averages	.103	-7
COMP all Vectors	.102	-8

Returning to Figure 7 one could argue that the northern hemisphere points bias the fitted slopes to somewhat larger values. The southern hemisphere points still exhibit some slope by themselves, however. There is, therefore, a small meridional motion present, and it is definitely not zero.

Note that there is more variance in the measurements at low latitudes (near the subsolar convective region) than in mid latitudes. This may well be due to local "turbulent" fluctuations. Note also that there is far less scatter, and also smaller RMS errors in target means in Figure 7a compared with 6a. We feel that 7a shows what we might reasonably expect to obtain, given the error analysis in Section III. The same scatter and error bar size ought to be present in Figure 6a. Instead, the scatter about the least squares line and the RMS deviations (error bars) for each individual target are considerably larger. Thus, while measurement error and local turbulence might account for some of the scatter in Figure 6a, another phenomenon must also be present. The existence of clouds at different heights moving at different zonal velocitites (vertical wind shear) was strongly suspect at this point, and the results of a search for vertical shear are discussed later.

C. Zonal Velocity Gradient

A correlation is observed between the u-component of the UV cloud motions and longitude such that the lower latitude clouds have a higher velocity. There apparently is a widespread component of zonal acceleration in the direction of motion. One must be careful in interpreting this however, because there is a strong bias in the measurements. Another compelling reason for caution is that models developed to explain the drive for the zonal wind will be influenced by the extent of the measured acceleration effect, its magnitude, and its fluctuation with time. To claim too much at this point could be detrimental to development of a realistic model. Thus, although we feel confident of the measurements of the zonal and meridional wind field to the accuracy stated, the zonal velocity gradient measurements should be treated as a more qualitative observation.

The bias in the correlation plots of Figure 9 can be explained in terms of Figure 5. Notice that because of the tilt of the planet axis with respect to the spacecraft orbit, and because of the lighting conditions at this time, a larger region of observable planet (and hence most of the cloud targets) lies between -20 and -50 degrees latitude and at a lower mean longitude. The mean zonal velocities at these middle latitudes tend to be 10-15 m/s higher

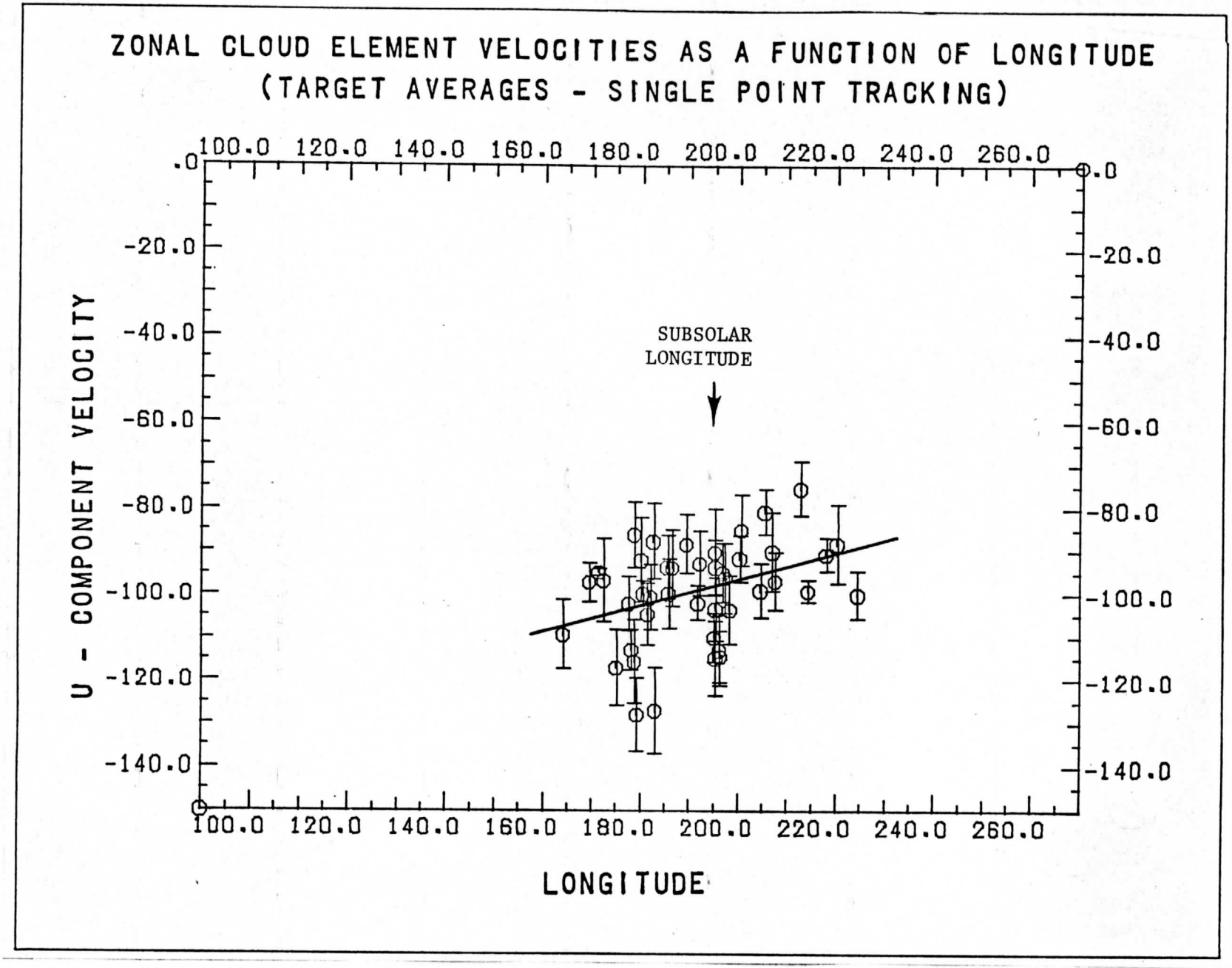

Figure 9a. Zonal wind component of SP measured cloud target averages, with RMS scatter for each target shown as error bars. Slanted line is least squares fit, which may be slanted too much due to the target selection bias mentioned in text. Only latitudes below 45 degrees are included here.

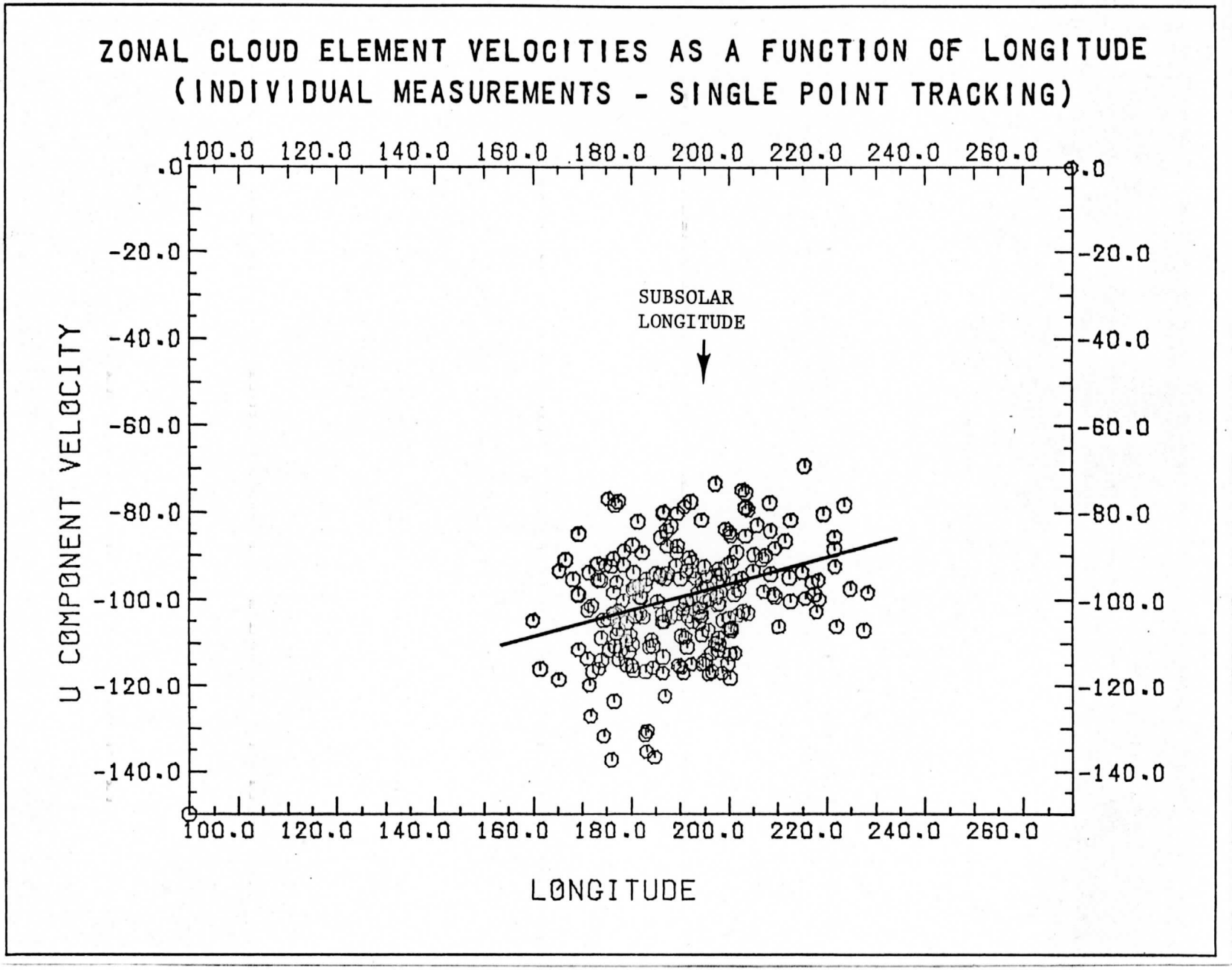

Figure 9b. Scatter plot of individual SP measurements used to generate target averages in Figure 9a.

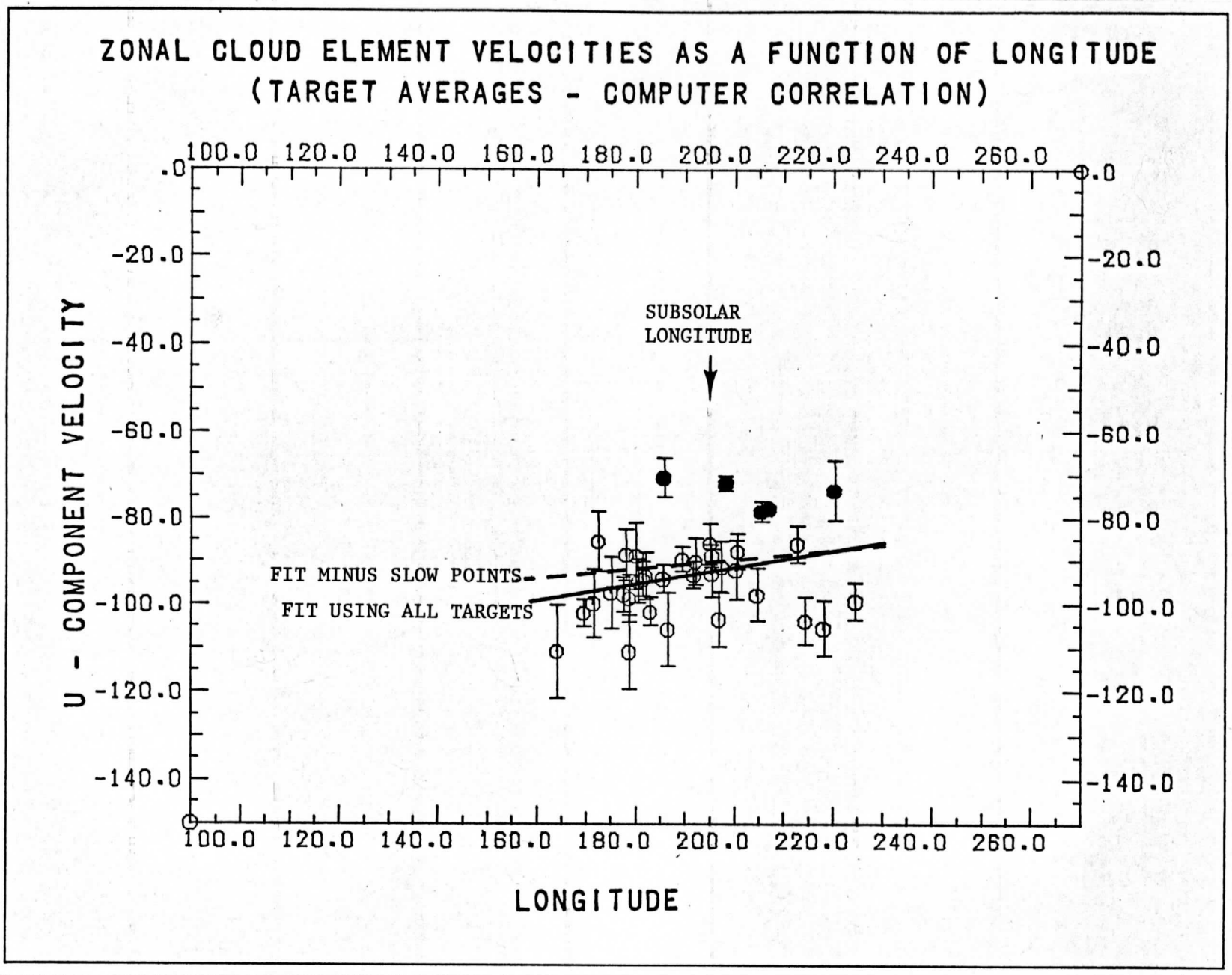

Figure 9c. Computer correlation measurements of zonal wind shown as target averages. Five of the six slow targets are shown as solid dots. A sixth is at a latitude higher than 45°. Least squares fits are shown with and without slow targets.

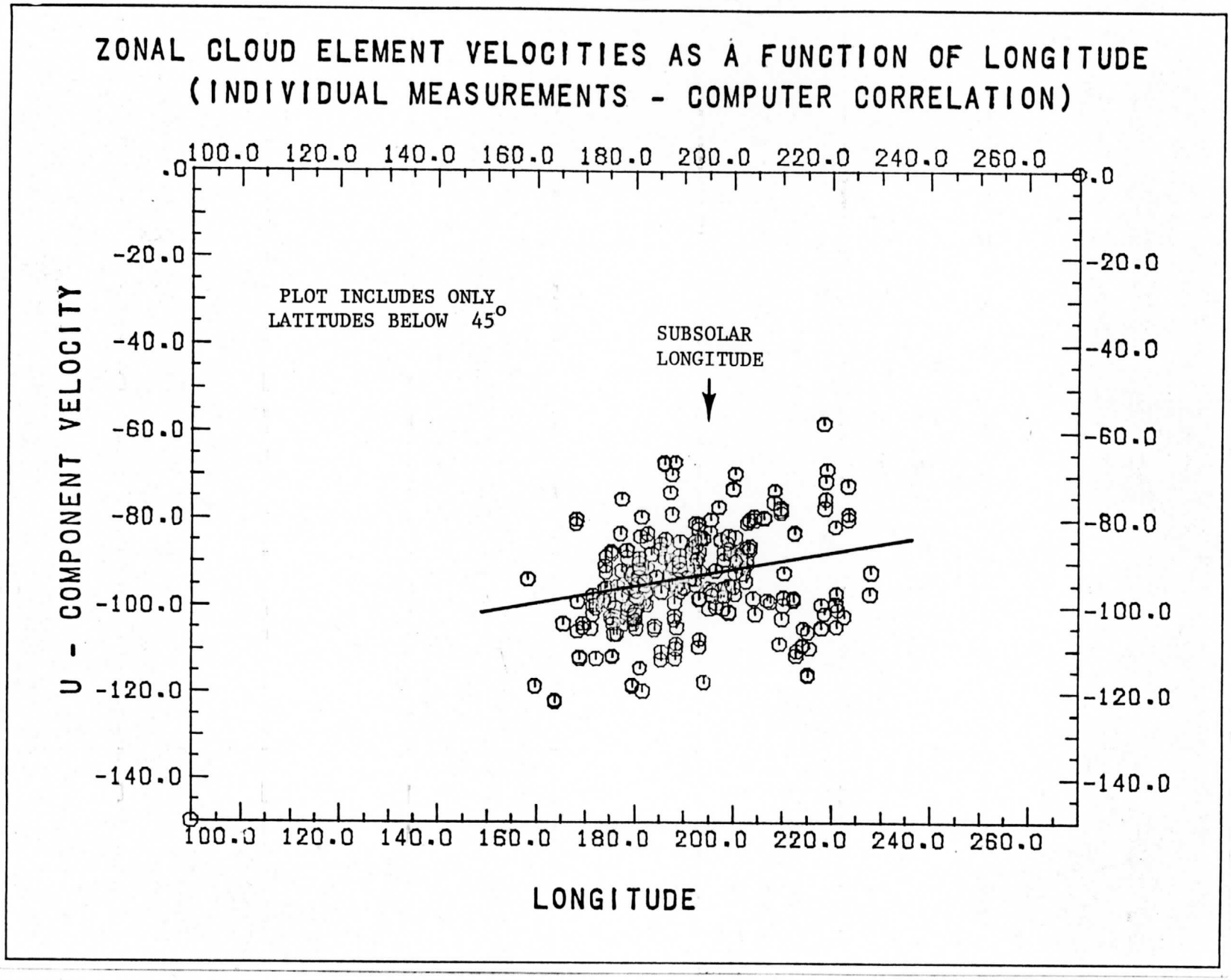

Figure 9d. Scatter plot of measurements used to generate target averages in Figure 9c.

than at the equator, and they would consequently tend to tilt the scatter polts. The data was therefore subdivided into 15 degrees latitude intervals in an attempt to investigate the extent of the bias. Every 15 interval at all latitudes, even poleward of -45 degrees, showed a linear least squares acceleration of 5 to 20 m/s over a latitude range of 220 to 160 degrees. The difficulty, of course, is that when one subdivides into finer and finer data sets the statistics become so poor that the least squares fits don't mean as much. Thus, we claim only that there is a latitudinally widespread zonal velocity gradient present, probably greater than 1-2 m/s over each 10 degrees of longitude. This makes it roughly the same size as the observed meridional velocity gradient. The zonal gradient is not solely limited to the subsolar convective zone, although since all measurements were in regions of solar heating, zonal acceleration could still be sun related. Most important is the fact that, in conjunction with the observed meridional velocity profile, the zonal velocity gradient indicates a widespread divergence centered on the subsolar region.

We must also again note the five "slow" targets discussed earlier and also shown in Figure 9c (the sixth target lies at 47° latitude). These show no indication of participating in any zonal acceleration. This is consistent with the interpretation that they move at constant angular velocity apart from the general fluid flow, and therefore may be wave related or, if not as organized as presently appears, possibly lie at a different altitude relative to the faster targets.

Finally, it should be mentioned that a 5-10 m/s zonal velocity change could account for some of the dispersion in the zonal wind profile. This would add a fourth possible cause for measurement scatter in addition to large scale waves, vertical shear and local turbulent fluctuations.

D. Variation of Meridional Motion with Longitude

There is no observed variation in the v-component with longitude. This effect would be important, since if it existed, it would support the hypothesis of kinetic energy being generated in large amounts in the subsolar convective zone. None of the correlation plots in any and all previously mentioned subdivisions of the data showed more than a total slope of 1-2 m/s. We also see no indication of horizontal wind shear across the spiral streaks, so they cannot be jets. We conclude there is no measureable variation of v with longitude. Any variation which exists is less than 20% of the magnitude of the meridional velocity gradient, and far below the noise level of our measurements.

E. Investigation of Vertical Shear

A detailed search for vertical shear was made in the four 15 km/pixel images to see if this would afford an explanation of why the zonal velocity measurements, shown in Figure 6, had anomalously large scatter compared to both the expected scatter from error analysis and comparison with the measured meridional motions in Figure 7. No convincing evidence was found in the 1 1/2 hour or longer time intervals, but in the 13 minute time interval it was possible to see a few cases where darker blotches evolved in a pattern. The dark spots tended to shrink from the zonally upwind direction and grow zonally

a)

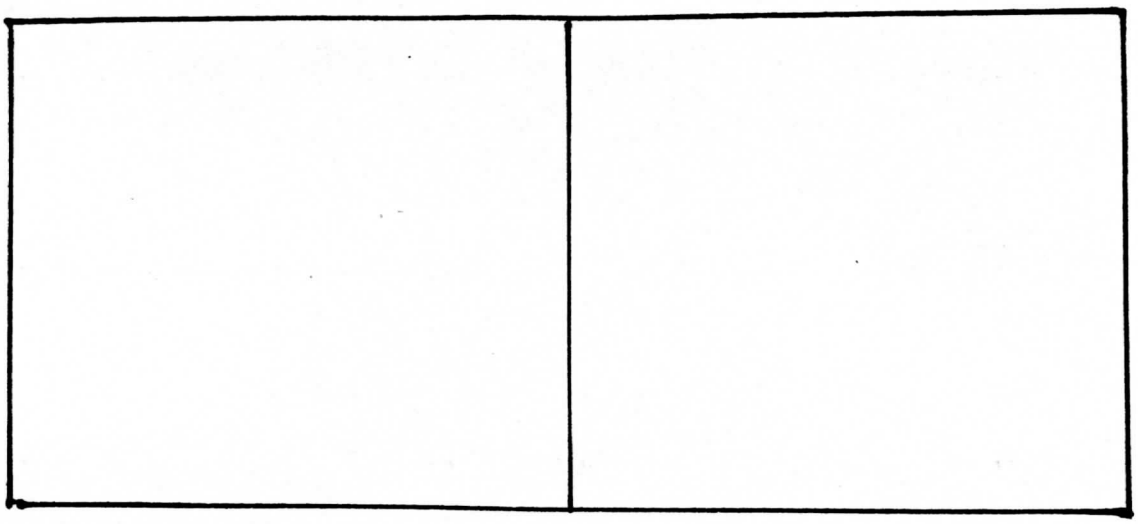

b)

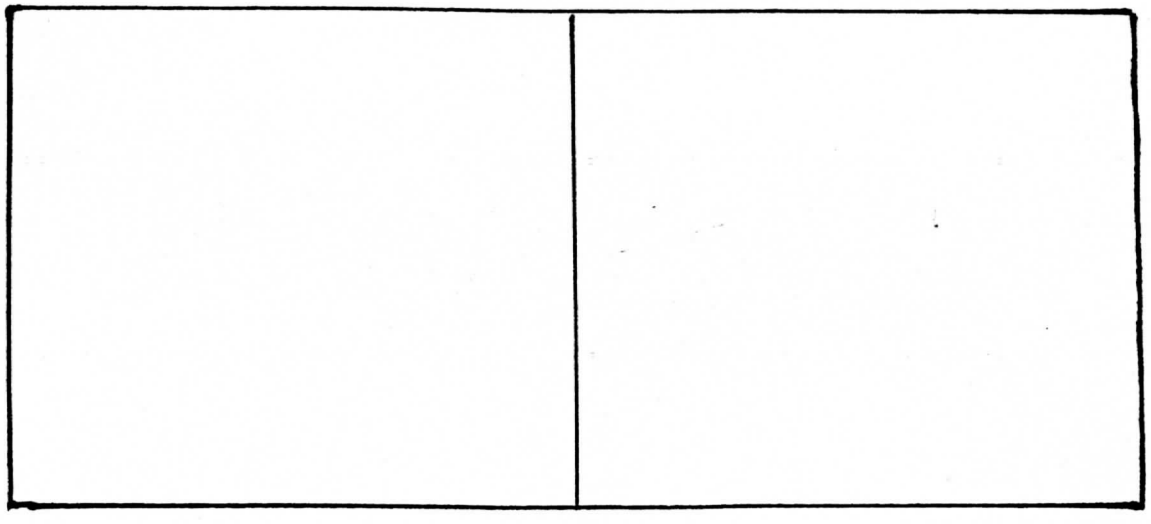

Figure 10. Two examples of vertical shear are shown above in stereo pairs of Mariner 10 pictures made 13 minutes apart. The arrows point to places where bright clouds are covering or uncovering dark patches or other bright clouds at a lower altitude. The upper and faster moving clouds have more parallax and appear closer to the observer in a stereo pair.

downwind as if they were obscured by the lighter features. The changes were barely discriminable in the short time interval, corresponding to relative motions of only a pixel or two, a relative velocity of 15-30 m/s. Once identified in the short time interval, the same features could be seen in the longer time intervals as a change in cloud shape or brightness. Figure 10 illustrates several such features in time sequence.

The darker areas were being obscured by lighter clouds which one can therefore assume to be higher in altitude. Bright patches merged with each other and changed shape and brightness, but showed no such distinct growth pattern. The obscuring bright clouds are partially transparent, since they vary in brightness depending on their background. The higher bright clouds move in the retrograde zonal direction, the same direction as the dark features they obscure, only they move faster. Assuming that the scatter in Figure 7 is due to measurement uncertainty and/or turbulence, and subtracting that from the scatter in Figure 6, one can estimate a shear of 10-30 m/s in the u-component. It must be kept in mind that many of the most deviant u-component measurements were thrown away in the 15 m/s editing process. Consequently the limits of the measured shear may be closer to 0-40 m/s, considering individual cases.

Attempts to measure the shear directly using SP and COMP techniques proved fruitless. The cloud targets could not be tracked well using any technique. They gave widely scattered velocities, although the targets appearing faster to the eye tended to cluster more toward higher velocities. It is likely that instead of two separate velocity fields at two different altitudes, we are observing a continuum of velocities and cloud features over a range of altitudes.

A look at possible causes for the u-component scatter yields the following results:

1. Turbulence - can account for only 1/2 of the scatter in u, and then only if we assume it accounts for all the scatter in v. More likely, some of the v scatter is also due to measurement errors, as our error analysis indicates. Thus, turbulence cannot completely explain the scatter in u.

2. Large Scale Waves - can account for all the scatter if properly organized. Certainly the six wierd cloud targets must be organized by a wave, if anything. They cannot represent mass flow. The chief difficulty with this hypothesis is the fact that except for those six targets, the u-component scatter is, in general, not highly organized, but appears random in character.

3. Longitudinal Acceleration - is simply too small to yield a 15 m/s RMS scatter. At best, the acceleration term amounts to approximately 10 m/s after a cloud has moved 60-80 degrees in longitude. The acceleration ought to be considerably less for any given cloud target in only 3 1/2 hours.

4. Vertical Shear - is the right order of magnitude and is consistent with all the evidence. Shear plus partially transparent clouds could give a mixture of edge velocities, brightness center velocities, and phase velocities whose scatter would vary up to the maximum velocity difference of the shear.

V. CONCLUSION

In this last section, we first summarize the quantitative results of our measurements item by item for easy reference. Then we compare our measurements with those of other experimenters. Finally we give our interpretation of what the measurements mean and indicate where further study could give fruitful results in determining the general circulation regime and dynamical phenomena associated with cloud structure and motions.

A. Summary of Measurements

It is useful to summarize the quantitative results of the measurements before we continue. Remember that all these measurements were made in a 3 1/2 hour period at one point in time, 48 hours after Venus encounter. Considering all the preceding discussion of wave phenomena in sections I and IV, it would be unwise to assume that the velocities themselves are representative of the steady state. Rather, one should consider the structure and organization of the motion fields as the more pertinent information to emerge from these data.

(1) Zonal Flow

a. The mean zonal velocity of small scale cloud elements at the equator is -92 ± 7 m/s, increasing toward higher latitudes with a tendency to conserve angular momentum about the poles.

b. Near 45 degrees latitude, the meridional profile of the zonal wind peaks at a value of -120 ± 10 m/s.

c. Poleward of the zonal velocity maximum is a region of solid rotation with a constant angular velocity of approximately -2.4×10^{-5} r/s.

(2) Meridional Flow

a. A small meridional flow with a mean velocity gradient of 0.12 m/s/deg. is observed, moving from equator to pole in each hemisphere. Scatter in the measurements is too great to determine if the acceleration is constant or varies slightly with latitude.

(3) Longitudinal Velocity Gradient

a. Acceleration of the zonal wind was observed to be present over the entire 60-70° range of longitudes measured, centered on the sub-solar point.

b. Acceleration of the zonal wind was observed to be present over the entire +30° to -60° range of latitudes measured.

c. The magnitude of the zonal velocity gradient is approximately .15 m/s/deg. but could not be precisely measured because of a bias introduced by the viewing geometry.

(4) Vertical Shear

a. Vertical wind shear is present, primarily in the u-component cloud motions, and is observed directly in a few cases and indirectly as velocity measurement scatter with a range generally between 10-30 m/s and an RMS value of about 15 m/s.

b. The shear is at least partially organized in the vertical, since in those cases which can be clearly recognized, the light clouds move faster and both obscure and uncover darker areas, indicating that the zonal wind increases with height. The u-component scatter is slightly more pronounced on the high velocity side of the velocity profiles.

(5) Large Scale Wave Phenomena

a. The circumequatorial belts move south across the equator at -24 ± 6 m/s. Rather than a meridional mass flow or a vertical wind shear, their periodic organization and limited appearance in time argue for interpretation as a wave phenomenon. Insufficient structural detail prevented measurement of the zonal motion of the belts.

b. An 80 m/s (5.5 day period) equatorial velocity appears in a small 6 target subset of the COMP measurements of the u-component. The measurements are organized in such a way as to indicate motion at a constant angular velocity of -1.4×10^{-5} r/s. This velocity is considerably slower than the ~100 m/s (4.4 day period) seen in the large scale "Y" or "Ψ" features in the Mariner 10 data and that of Caldwell (1972). Our -92 m/s cloud velocity at the equator corresponds to a 4.8 day period.

B. Comparison With Other Experiments

Venus has been observed for many years by Earth-based observatories. The motion of the large scale features (the "Y" and "Ψ") have been thoroughly analyzed. Results were reported by Smith (1967), Dollfus (1968), and Boyer & Guerin (1969). There seems to be general agreement that the speed of the large UV features is about 90 to 110 m/s, corresponding to a rotation period of 4 to 5 days. The wide variation of the measured periods indicates, however, that the markings may vary in speed or shape from time to time. More recent work reported by Caldwell (1972) from Planetary Patrol observations gives 4.41 days as the rotation period of the "Y" and suggest variations in velocity and cloud altitude as a possible reason for the discrepancy between the earlier observations.

Scott and Reese (1972) point out that there is a bimodal distribution of measured rotation periods and that a shorter period of 4.06 days, although most dominant, can be explained on the basis of a commensurability between the 1 day period of Earth and the assumed 4 day period of the Venus clouds, whenever all the observations are made from a single observatory. This lends more credence to the 4.59 day period they mention, the 4.41 days of Caldwell, and the 4.7 days of Smith. If, indeed, the large scale features are coupled to a fluctuation in altitude or velocity or some other parameter which varies along with the intensity of the "Y", or are coupled to a wave which triggers convection or alters the cloud optical properties or shape of the "Y", a slight variation about a 4.5 day mean measured period is not unreasonable. A period of 4.6 $\pm$ 0.2 days would fit most of the observations, including ours. A distinction must be made, however, between motion of large scale, telescopically observed features, which could be wave related, and motion of small scale cloud elements, which are more likely to correspond to true mass motion.

Particular attention should be given to results of measurements performed by Sidi (1975) using a stereoscopic comparator technique on Mariner 10 hard copy images. The Sidi measurements cover a similar time interval to ours and overlap with ours by 50%, although none of the frames used are exactly the same. One would thus expect the measured velocities to be the same in both cases, and they are indeed quite similar.

Sidi finds increasing zonal velocity at higher latitudes, tending toward conservation of angular momentum about the poles. The mean equatorial velocity is -82 m/s east of the subsolar point and -82 to -110 m/s toward the west. A transition longitude passing through the subsolar point sharply divides the accelerated from the unaccelerated zonal flow. The magnitude of the acceleration Sidi found is 0.48 m/s/deg., compared with our ~0.15 m/s/deg. averaged across the disk with no sharp transition longitude observed. It should be noted that Figure 9, especially 9c and 9d, could be in agreement with Sidi.

Sidi also finds an "equatorial belt" moving 5 m/s slower than the zonal flow, with meridional velocity toward the equator (probably the "circumequatorial belt" mentioned here and in Murray, et.al. (1974), although the terminology used by Sidi is somewhat confusing), and a perfectly spherical appearing polar region (with no bumps or hollows) therefore implying solid body rotation. Meridional velocities are small, <10 m/s everywhere, and generally moving from equator to poles with no obvious organization. We have noted a tendency for the meridional velocities to increase at higher latitudes, but in all other respects, Sidi's observations agree reasonably well with ours.

Boyer (1973) measured the velocity of the "Y" and "Ψ" features in Earth-based photos of Venus and obtained faster velocities near the evening terminator. The "morning" average zonal velocity was -83 m/s while the "evening" average zonal velocity was -122 m/s. It should be noted that Boyer's velocities are again for larger scale features and thus not directly comparable with the measurements of Sidi and our own, both of which rely on small details in the clouds. On the other hand, there exist velocity

measurements of Traub and Carleton (1975) based on spectroscopic Doppler shifts which yield similar gradients: -73 m/s in the "morning" and -111 m/s in the "afternoon". The zonal variation in velocity thus appears to be very real, and also apparently sun-locked and visible at all scale sizes on Venus from global scale to molecular.

The question of meridional motion is somewhat more confused. If we believe with Traub and Carleton that there is at least occasionally a substantial CO_2 flow toward the equator, the situation becomes much more complex than indicated by our measurements. Traub and Carleton allude, in fact, to the possibility of multiple cloud layers and vertical wind shear. Everyone who has seen the circumequatorial belts in the Mariner 10 images agrees they can move toward the equator, and there is no proof that they represent only wave motion and not mass motion. The higher resolution Mariner 10 pictures may permit resolving some of the confusion by giving us a better look at vertical structure in the UV clouds.

C. Conclusions

In light of the foregoing discussion, it is evident that one should be extremely cautious in believing too literally in any number representing a velocity or period. Rather, our measurements should be considered as giving greater insight into the structure and organization of the upper atmosphere dynamics. It is on this point we ought to place the emphasis.

1. The zonal flow on Venus above 60 km altitude, is organized like a vortex, as first explained by Suomi (1975). There is a slow meridional flow from equator to pole in each hemisphere and a tendency for the zonal flow to conserve angular momentum about the poles, but with a slight frictional loss. The result is that we find differential rotation of the upper atmosphere at low latitudes and solid rotation at high latitudes, with a transition region near 45° latitude.

   That this is mass motion and not a wave is evident from the velocity profiles and the correlation with spectroscopic Doppler shifts in CO_2 absorption lines. We can also infer from the amount of angular momentum present that this vortex could be perturbed, but is likely to be structurally stable over periods of days or weeks. As a result, the upper level global energy transport is most like a modified Hadley cell, and we would expect from the evidence of the Venera probes and the Mariner 5 & 10 radio occultation results to find considerable vertical dynamic structure on Venus below 60 km altitude.

2. Evidence of zonal velocity perturbations is strong. The zonal flow is faster toward the evening terminator, according to most recent observations, and shows up in both small scale and large scale features. Whether this acceleration is due to a solar tide, a global scale wave, Reynolds stresses, or some other phenomenon is unexplained. We can be reasonably sure that it occurs in a wide band at least 20° each side of the equator, and may extend

to even higher latitudes. It is hard to escape the fact that the sun strongly influences the upper atmosphere dynamics, and probably in a very direct way, as opposed to indirectly by merely supplying energy. On the other hand, there seem to be no large horizontal pressure gradient forces generating jets or large meridional flow. The emphasis is more on a steady or periodic influence of the sun in the zonal and vertical dimensions only.

3. Some evidence of vertical shear in the zonal flow is evident, with higher clouds travelling faster and obscuring lower features, both light and dark. Error analysis reveals that this u-component shear probably appears as a major component of the scatter in the zonal cloud velocity measurements. Coupled with the low meridional velocities, this vertical shear is evidence for a global dynamic balance similar to geostrophic flow on Earth. One must find another inertial force, however, for the coriolis force on Venus is too small to balance a meridional pressure gradient of even a few millibars.

4. The picture of waves on Venus is very confused. We mentioned in the introduction that the small lapse rate of temperature above 60 km tends to give the atmosphere great vertical stability. This inhibits convection, and also provides a strong restoring force to damp out vertical perturbations. These conditions are very conducive to wave motion, and we must therefore pay a good deal of attention to wave motions as a possible means of transport of energy and momentum. This complicates the dynamic picture considerably, since no unambiguously clear interpretation of the dynamics can be made without proof that waves are not present. Unfortunately, all the proof is in the other direction. We see evidence of waves all over the place.

   The "Y" features are wavelike in that they are coherent in time over periods of 5-10 revolutions in the presence of a differentially rotating mass field. The spiral streaks are wavelike in that they move with the mass field but are at least semi-periodic along lines of constant latitude, especially near the equator. The circumequatorial belts are wavelike, being periodic in the meridional direction and appearing only at certain times and moving in certain directions. The bowlike waves appear in pairs and only at certain times. The bright polar band "nutates" with a 4-5 day period. There are periodic variations in the intensity of CO_2 absorption in the upper atmosphere. The one consolation in all of this is that the vortex motion of the mass field seems unaffected to first order. Venus looks in the Mariner 10 pictures like it usually does from Earth.

There are bright aspects to consider too, however. It appears that we can measure second order effects (~10 m/s) in the velocity field. Moreover, because Venus appears so inhomogeneous in the UV images of Mariner 10, there is a wealth of detail to study in a quantitative way. We can extend the velocity measurements over several more days, paying particular attention

to variations and eddy components. We can study the obvious inhomogeneities and vertical structure and shear present in the closeup high resolution data. Moreover, we can use the measured velocity fields to provide boundary conditions for theoretical models, thereby limiting the range of "reasonable" conditions which have to be considered.

It is overwhelmingly clear, from this first look at the Mariner 10 data, that we have an exceedingly complex and variably structured data set. On the other hand, the many pictures, taken over almost the entire range of time and space scales on which the atmosphere is evolving, permit a glimpse into practically all the dynamic interactions short of climatological change. The Pioneer Venus orbiter will give us a long time base in a couple years, while the atmospheric probes should give insight into the vertical structure and deep layers. The prospects for finding out more about the atmosphere of Venus have never looked brighter. There is much interesting work ahead.

ACKNOWLEDGEMENTS

We gratefully acknowledge the help of the staff at the Jet Propulsion Lab for their aid in obtaining and processing the image data tapes and the care and attention to the myriad small details which have made our work easier. In particular we wish to thank Ed Danielson, Bob Toombs, and Ken Klassen for their contributions as imaging team representatives and also Jim Soha and Don Lynn of the Image Processing Lab for their help in data preparation.

The McIDAS system at the Space Science and Engineering Center was built with ideas from many sources, but its power and versatility is the result of the creative combination of talents of four people: Terry Schwalenberg, hardware design and construction; John Benson, systems programming; Dennis Phillips, navigation and correlation algorithms; and Eric Smith, applications programming. Image alignment was done by Gary Chatters. Some of the plotting routines were written by Bruce Knaack. Special mention should be given to Sanjay Limaye for the excellent job he has done in the tedious task of reseau measuring, and for his aid in helping to navigate the images. Finally, we wish to thank Nancy Kitzman for her usual excellent care and attention to detail in typing of the final manuscript.

This research was supported by JPL Contract #953034.

BIBLIOGRAPHY

Barker, Edwin S.; 1975: "Comparison of Simultaneous CO_2 and H_2O Observations of Venus," J. Atmos. Sci., 32, 1071-1075.

Boyer, C.; 1973: "The 4-day Rotation of the Upper Atmosphere of Venus," Planet Space Sci., 21, 1559-1561.

Boyer C. and Guerin, P.; 1969: "Etude de la Rotation Rétrograde, en 4 Jours, de la Couche Exterieure Nuageuse de Vénus," Icarus, 11, 338-355.

Caldwell, John; 1972: "Retrograde Rotation of the Upper Atmosphere of Venus," Icarus, 17, 608-616.

Coffeen, David L.; 1971: "Venus Cloud Contrasts," Planetary Atmospheres, Sagan, et.al., Eds., Reidel, 84-90.

Deveaux C.; Herman, M.; and Lenoble, J.; 1975: "Interpretation of the Photometric Measurements of Venus by Mariner 10," J. Atmos. Sci., 32, 1177-1189.

Dollfus, A.; 1968: "Synthesis on the Ultraviolet Survey of Clouds in Venus' Atmosphere," The Atmospheres of Venus and Mars, J. Brandt and M. McElroy, Eds., Gordon and Breach, 133-144.

Hansen, J.E.; and Hovenier, J.W.; 1974: "Interpretation of the Polarization of Venus," J. Atmos. Sci., 31, 1137-1160.

Hapke, Bruce; 1975: "Mariner 10 Photometry," The Atmosphere of Venus, NASA SP-382, 69-76.

Howard, H.T., et.al.; 1974: "Venus: Mass, Gravity Field, Atmosphere, and Ionosphere as Measured by the Mariner 10 Dual Frequency Radio System," Science, 183, 1297-1301.

Lacis, A.A.; 1975: "Cloud Structure and Heating Rates in the Atmosphere of Venus," J. Atmos. Sci., 32, 1107-1124.

Marov, M. Ya.; 1972: "Venus: A Perspective at the Beginning of Planetary Exploration," Icarus, 16, 415-461.

Murray, Bruce C., et.al.; 1974: "Venus: Atmospheric Motion and Structure from Mariner 10 Pictures," Science, 183, 1307-1315.

O'Leary, Brian; 1975: "Venus: Vertical Structure of Stratospheric Hazes From Mariner 10 Pictures," J. Atmos. Sci., 32, 1091-1100.

Pollack, James B., et.al.; 1975: "A Determination of the Composition of the Venus Clouds from Aircraft Observations in the Near Infrared," J. Atmos. Sci., 32, 1140-1150.

Prinn, Ronald G.; 1975: "Venus: Chemical and Dynamical Processes in the Stratosphere and Mesosphere," J. Atmos. Sci., 32, 1237-1247.

Sidi, C.; 1976: "Stereoscopic Observations of Winds on Venus," Preprint, submitted to Icarus.

Soha, J., et.al.; 1975: "IPL Processing of the Mariner 10 Images of Mercury," J. Geophys. Res., 80, 2394- .

Scott, A.H. and Reese, E.J.; 1972: "Venus: Atmospheric Rotation," Icarus, 17, 589-601.

Smith, B.A.; 1967: "Rotation of Venus: Continuing Contradictions," Science, 158, 114-116.

Suomi, Verner; 1975: "Cloud Motions on Venus," The Atmosphere of Venus, NASA SP-382, 42-58.

Traub, W.A. and Carleton, N.P.; 1975: "Spectroscopic Observations of Winds on Venus," J. Atmos. Sci., 32, 1045-1059.

Travis, L.D.; 1975: "On the Origin of Ultraviolet Contrasts on Venus," J. Atmos. Sci., 32, 1190-1200.

Young, A. T.; 1973: "Are the Clouds of Venus Sulfuric Acid?," Icarus, 18, 564-582.

Young, Andrew T.; 1975: "The Clouds of Venus," J. Atmos. Sci., 32, 1125-1132.

Navigation of Mariner 10 Images of Venus

Dennis Phillips and Sanjay Limaye

Abstract

In order to make quantitative use of spacecraft images such as those obtained from Mariner 10 flyby mission to Venus it is necessary to obtain a navigation transform which enables one to determine the planet coordinates of a feature from its image coordinates. The problem of obtaining the required navigation for images of Venus is complicated by the lack of any landmarks, as are available in the cases of the Earth, Moon, Mercury and Mars.

A procedure is described herein to obtain the navigation transform using a least squares solution to the bright limb of the planet and a knowledge of the spacecraft position relative to the planet. The procedure requires that a "sufficient" portion of the bright limb be present in the image and that the attitude of the spacecraft camera be specified.

The quality of the navigation is judged by the consistency among several consecutive frames. The scheme is easily applicable to snapshots of other planets as will be available, for example from the proposed Mariner missions to Saturn, Jupiter and Uranus.

Introduction

In order to determine the absolute position on a planet of a point seen in a spacecraft image of that planet, it is necessary to obtain a navigation transform. The problem is made more difficult for images of Venus as they do not show any "landmarks" which are stationary relative to the planet. The error in the relative position of points is dependent on the accuracy and precision of the navigation transform. The precision of the navigation transform is limited by the spatial resolution of the imaging system and any smear in the images caused by the relative motion of the spacecraft with respect to the planet. A good navigation transform is a pre-requisite for obtaining displacement of mobile features in the images, and accurate velocity measurements additionally necessitate a certain minimal time interval between the image pairs selected for such measurements. Table 1 indicates the tracking error introduced for a given accuracy of the navigation transform for various time intervals.

A navigation transform is obtained by determining the transformation matrix which will transform an image coordinate vector into its counterpart in planet centered polar coordinates. Frequently this is done by selecting and measuring a few landmarkes in image coordinates whose planet coordinates are known (Smith and Phillips, 1972). Due to the lack of landmarks in images of Venus the image coordinate vector has to be defined in terms of other parameters. This procedure is described in the following sections.

Table I

TRACKING ERROR FOR VARIOUS GROUND RESOLUTIONS AND TIME INTERVALS IN M/SEC

TIME	RESOLUTION					
	10 KM	20 KM	30 KM	40 KM	50 KM	60 KM
10 MIN	16.7	33.3	50.0	66.7	83.3	100.0 M/SEC
20	8.3	16.7	25.0	33.3	41.7	50.0
30	5.6	11.1	16.7	22.2	27.8	33.3
40	4.2	8.3	12.5	16.7	20.8	25.0
60	2.8	5.6	8.3	11.1	13.9	16.9
90	1.9	3.7	5.6	7.4	9.3	11.1
120	1.4	2.8	4.2	5.6	7.4	8.3

The Navigation Transform:

The first step necessary to obtaining an image navigation transform is the identification of an image coordinate vector whose planet coordinate counterpart is known. The extensive cloud cover on Venus evolves with time and it is necessary to look for other "natural" points to describe the image coordinate vector. It seems that this is likely to be the case for images of Jupiter and Saturn too. One natural candidate is the sub-spacecraft point which is easily identifiable in whole disc pictures of a spherical object. From a knowledge of the spacecraft orbit the planet coordinates of the sub-spacecraft point on the planet surface is generally known with reasonable accuracy.

A second point is needed in order to determine how the image is rotated around the ray joining the spacecraft to the planet's center. How this point is to be chosen is not immediately clear. However, information about the imaging system, its position relative to the spacecraft and the trajectory of the spacecraft relative to the planet generally contains enough information to compute the image coordinate position of a second reference point. For example, Mariner 10 which is a three axis gyro-stablized spacecraft has two sensors, a Canopus sensor and a sun-sensor to determine the orientation of the spacecraft in its orbit. Thus from the known celestial positions of either of the stars the sub-star reference point on the planet is known and its image coordinates relative to the first reference point namely the sub-spacecraft point can be computed. This requires knowledge of the spacecraft design. Attitudes of spin-scan cameras need be determined in a similar way also.

The necessity to use the sub-spacecraft point as one of the reference points means that its position be known by some means, in the specific image. Perhaps the most reliable way to obtain the image coordinates of the sub-spacecraft point for a spherical object is to use the bright limb as the reference circle and determine its center of curvature. This problem is made slightly easier if the radius of curvature in the planet image is independently known. A successful planet center determination requires that the individual image have a substantial amount of the planet limb. Thus, this navigation scheme can only be used for whole or substantial limb containing images and a modification of this technique need be developed for other images. The navigation problem can be divided into two kinds:

(i) navigation of whole disc or images with a substantial amount of bright limb present, and,

(ii) navigation of images containing little or no limb, e.g. mosaic frames.

Under special circumstances the second class of frames can be navigated by using a modified version of the technique used for the whole disc or "enough limb" images. This technique will be described in a follow-up paper. The whole disc or "enough-limb" frame navigation will now be described in detail.

a. Determination of the sub-spacecraft point

As mentioned earlier this is frequently a case of determining the radius of curvature and the center of curvature for a given arc. In the more general case an ellipse needs to be determined such that it will pass through the points defining the arc. Numerically this involves minimizing the sum:

$$S(x_c,y_c,a,b) = \sum_i \left[\frac{(x_c-x_i)^2}{a^2} + \frac{(y_c-y_i)^2}{b^2} - 1\right]^2$$

In general the line scan direction will be at an angle Θ with the axes of the ellipse defining arc, so that the coordinates (x_i,y_i) of the points on the arc and (x_c,y_c) of the center of the ellipse in angular space are defined in terms of:

$$\begin{pmatrix} x \\ y \end{pmatrix} = \begin{pmatrix} \cos\Theta & \sin\Theta \\ -\sin\Theta & \cos\Theta \end{pmatrix} \begin{pmatrix} l_i * \text{RDPLIN} \\ e_i * \text{RDPELE} \end{pmatrix}$$

As such there are five unknowns in Equation (1) namely the two numbers giving the ellipse center (x_c,y_c) or equivalently l_c and e_c, the semi-major and semi-minor axes a and b, and the inclination angle Θ between the line scan direction and the semi-major axis of the ellipse (the relative camera roll angle). The number of unknowns can be reduced to four if the eccentricity of the ellipse (in other words that of the axisymmetric spheroid) is known a priori such that either of the two axes of the ellipse can be expressed in terms of the other.

The problem is further simplified if the object is known to be spherical. In fact, when the eccentricity, e, of the ellipse is too small to be measured within the resolution of the sampling, including the variables (a,b,e) gives us an over determined problem with associated difficulties. In the case of Venus, from ground-based radar observations, the oblateness has been known to be quite small. Howard, et.al. (1974) report that the fractional differences in the principal moments of inertia of Venus are no larger than 10^{-4}. However in the Mariner 10 images of Venus one does not see the solid surface of the planet but only its cloud cover. Diagnostic studies of the pole-equator thermal contrast at the cloud-top level, Limaye (1975), place an upper limit of a maximum of 14 km in the cloud-top height difference between the equator and the poles for an assumed temperature lapse rate of about 5°K/km at the 80 km altitude. The actual difference in altitude levels of cloud-tops seen in the Mariner 10 images are likely to be smaller, as is the temperature contrast used in arriving at the above figure. Barker and Perry (1975) report that there may be about 3% more carbon dioxide gas above the cloud-tops in the polar latitudes compared to the equatorial latitudes, as indicated by increased absorption in spectroscopic observations. In view of this it may be concluded with reasonable assurance that the cloud-top figure may be considered to be a sphere. The radius of this sphere is as yet left as an unknown.

For the particular case of Venus the expression to be minimized reduces to:

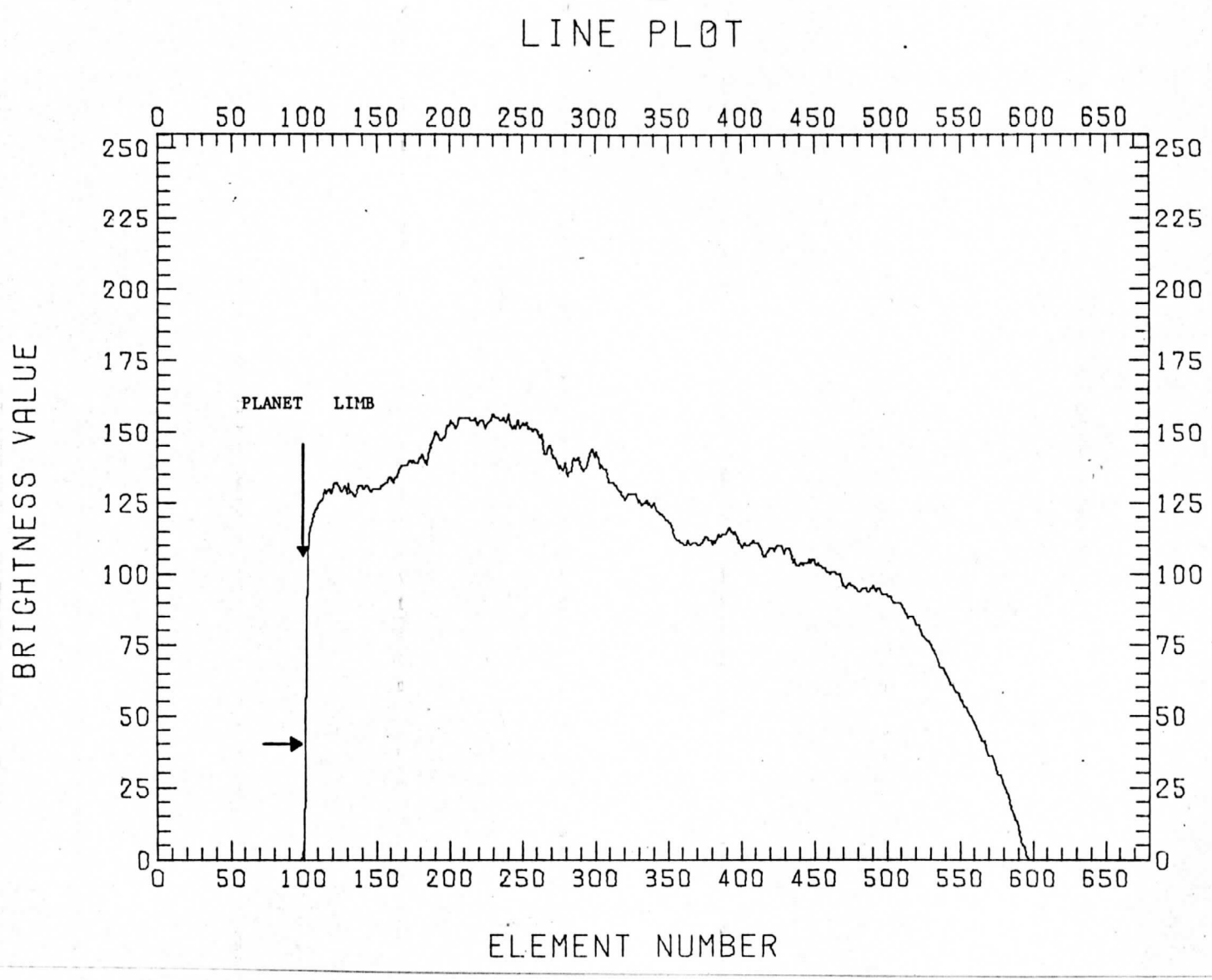

Figure 1. Brightness variation along a scan line. The slope of this curve at any point gives the combined scale height of the gas and scattering aerosol mixture. O'Leary (1975) has determined that the unit slant optical depth generally corresponds to a 40 DN in a FICORed image and occurs at about 6131 km from planet center.

$$S = \sum_i [(x_c - x_i)^2 + (y_c - y_i)^2 - a^2]^2$$

since for a circle a ≡ b and e = 0.
The three unknowns x_c, y_c and a are determined by the constraints:

$$\frac{\partial S}{\partial a} = \sum_i \frac{\partial}{\partial a} [(x_c - x_i)^2 + (y_c - y_i)^2 - a^2]^2 = 0$$

if a is not independently known.

$$\frac{\partial S}{\partial x_c} = \sum_i \frac{\partial}{\partial x_c} [(x_c - x_i)^2 + (y_c - y_i)^2 - a^2]^2 = 0$$

and,

$$\frac{\partial S}{\partial y_c} = \sum_i \frac{\partial}{\partial y_c} [(x_c - x_i)^2 + (y_c - y_i)^2 - a^2]^2 = 0.$$

In practice the solution is obtained by iteration using the Newton-Raphson scheme.

b. Limb Determination and the Radius of the Cloud-top Figure of Venus

For a planet with a thick atmosphere such as Venus the scans across the limb show a gradual rather than a sharp increase in brightness due to atmospheric scattering (see Figure 1). The points defining the limb in the image have to be chosen with care since they determine the location of the sub-spacecraft point from high resolution limb scans from Mariner 10. O'Leary (1975) has determined that the slant optical depth of unity occurs in the atmosphere of Venus at the 4 mb level or at about 6131 km from the planet center. We have adopted this result to determine the limb location and the radius at the cloud-top level for navigational purposes. The slant optical depth is determined by the relation:

$$I_{\tau_{s=1}} / I_{\tau_{s=\infty}} = (1 - e^{-1}) = 0.63.$$

The corresponding level for the limb scan of Figure 1 is indicated therein. Experience with Mariner 10 UV images has shown that frequently the $\tau_{s=1}$ position or the limb position in a given line scan ocurrs at the pixel with digital brightness number closest to 40 for a typical exposure (~78.3 milliseconds). A one resolution element error in a single limb location is not a serious error as it causes a smaller error in the sub-spacecraft point if more than four limb points are used.

c. The Reference Vector

The Mariner 10 cameras were mounted on a scan platform which had only two degrees of freedom - the clock and cone directions. Its orientation relative to the sun-sensor and Canopus sensors was thus fixed if small errors such as scan platform backlash are ignored. A direct consequence of this is that all the scan lines point towards the sun within the combined 3 axis attitude error limits ($<\pm 0.4$ degree). Thus, both the sub-solar and the sub-spacecraft points are, within the attitude error limits, on the same scan line. It is obvious that the extent of parallelism of the vidicon scan lines with the line passing through the sub-solar and sub-spacecraft points is governed by the ratio of the separation of the two points to the small roll error.

Once the scan line number of the sub-solar point is known, its sample element number is easily determined knowing the angular separation of the sub-solar point relative to the sub-spacecraft point and the average angular size of a sample element in the scan direction.

Thus the two reference points defining the reference vector are now known, both in the image coordinates and the planet coordinates and the transformation matrix can be determined as two successive rotation operations - the first one brings the sub-spacecraft point to coincide with its image coordinate and the next one brings the sun onto the same scan line.

The Transforms:

a. The transformation T such that:

$(l,e) = T(\lambda,\phi)$

$(\lambda,\phi) = T^{-1}(l,e)$ is required.

Let us first state the properties of a Euclidean transformation in a finite dimensional Cartesian coordinate system. A Euclidean transformation preserves both the distances between points and angles between intersecting rays. All Euclidean transformations can be characterized as

$$X_v = RX_s + b$$

where R is a rotational matrix and b is a displacement vector. Let us assign the subscript s to vectors in our satellite centered coordinate system and the subscript v to vectors in our Venus centered coordinate system.

II. Coordinate Systems

Let our spacecraft-centered coordinate system (Figure 2) be defined as follows:

The x axis points from the focal point of the image camera through the center point of the vidicon frame. Our y axis originates at the same point, is perpendicular to the x axis and is parallel to the scan lines going from

Figure 2. The Venus centered coordinate system.

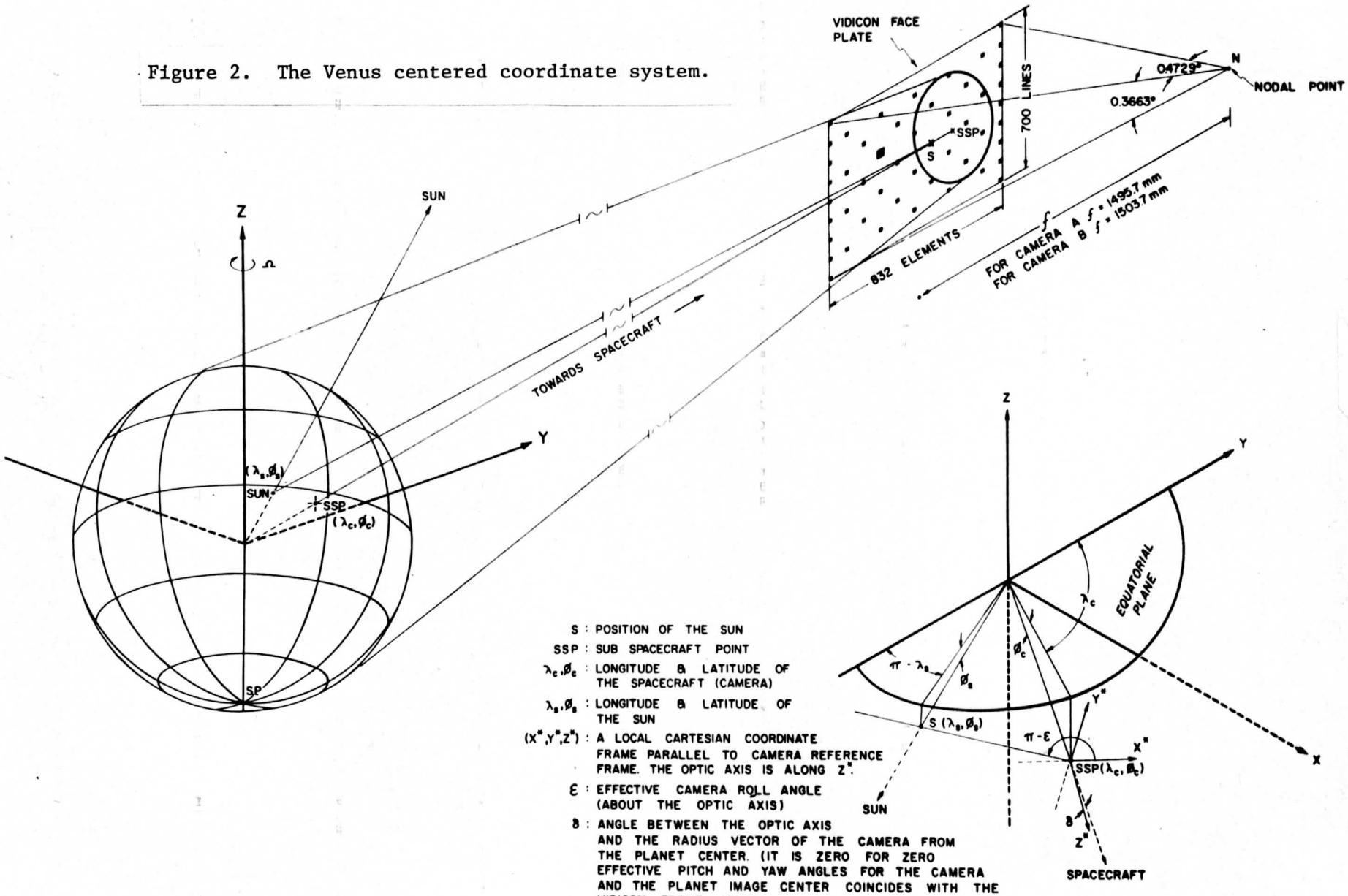

the right to left direction. The z axis completes a right handed orthogonal coordinate system.

Our Venus centered coordinate system (Figure 2) has its z axis coinciding with the spin axis of Venus and its x axis pointing towards (0°, 0°) of a latitude and longitude coordinate system tied to the planet's surface. The y axis makes the coordinate system right handed.

III. Parameter Base for Transformations

Let us start with the following parameters:

(e_c, l_c) - the displacement of picture coordinates of the center of the planet Venus from the nominal picture center.

(λ_c, ϕ_t) - (Figure 2) the longitude and latitude of the spacecraft's sub-satellite point.

(λ_s, ϕ_s) - (Figure 2) the longitude and latitude of the subsolar point.

h - the altitude of the satellite.

a - Venus radius

From this set of parameters we will derive the rotational matrix R and the displacement vector T.

IV. Derivation of R and b

Let us consider the equation again $X_v = RX_s + b$, where it is understood that "b" and any subscripted "X" are vectors. When we are at the center of the satellite frame $X_s = 0$ and $X_v = b$. Hence b is the vector from the center of Venus to the satellite.

Hence

$$(b) = \begin{pmatrix} (a+h)\cos\phi_c \cos\lambda_c \\ (a+h)\cos\phi_c \sin\lambda_c \\ (a+h)\sin\phi_c \end{pmatrix}.$$

Now we can restrict our attention to finding the rotational matrix R. Consider the action of R on the vector X_v^s pointing towards the subsatellite points

$$X_s^s = \begin{pmatrix} \cos(l_c * \text{RDPLIN}) * \cos(e_c * \text{RDPELE}) \\ \cos(l_c * \text{RDPLIN}) * \sin(e_c * \text{RDPELE}) \\ \sin(l_c * \text{RDPLIN}) \end{pmatrix}$$

Now $X_v = hRX_s^s + b$,

and $X_v = ba/(a+h)$,

hence, $RX_s^s = X_v - b = -b/(a+h)$.

If we determine how R rotates one more linearly independent vector, we can determine R.

Consider the vector from the center of Venus to the subsolar point:

$$X_v^{ss} = \begin{pmatrix} a\cos\phi_s \cos\lambda_s \\ a\cos\phi_s \sin\lambda_s \\ a\sin\phi_s \end{pmatrix} .$$

Let us find the angle γ between the vector from the spacecraft to the center of Venus and the vector from the spacecraft to the subsolar point.

$$\gamma = -[\arccos b \cdot (X_v^{ss}-b)/(||b||*||X_v^{ss}-b||)].$$

Let us now find the vector X_s^{ss} pointing from the spacecraft to the subsolar point in the satellite coordinate system.

$$X_s^{ss} = (||X_s^{ss}-b||)*\begin{pmatrix} \cos(1_c*RDPLIN)*\cos(e_c*RDPELE+\gamma) \\ \cos(1_c*RDPLIN)*\sin(e_c*RDPELE+\gamma) \\ \sin(1_c*RDPLIN). \end{pmatrix}$$

Hence, $X_v^{ss} = RX_s^{ss} + b$

and $RX_s^{ss} = b-X_v^{ss}$.

Finally $RX_s^{ss}/||X_s^{ss}|| = (b-X_v^{ss})/||b-X_v^{ss}||$.

This gives us our second linearly independent vector and, hence, R is determined.

V. Derivation of T and T^{-1}

Let us now discuss how R and b can be used to find the transformations T and T^{-1}.

A. Finding T or the transformation from Venus coordinates to Picture Image Coordinates:

Let us start with a longitude-latitude pair (λ,ϕ) of Venus coordinates.

Then

$$X_v = \begin{pmatrix} a\cos\lambda\cos\phi \\ a\sin\lambda\cos\phi \\ a\sin\phi \end{pmatrix} .$$

$$X_v = R\,X_s + b$$

$$e = \text{ATAN}\,(X_s^2/X_s^1)/\text{RDPELE}$$

$$1 = \text{ATAN}\,(X_s^3/\text{SORT}((X_s^1)^2 + (X_s^2)^2))/\text{RDPLIN}$$

B. Finding T^{-1} or the transformation from image coordinates.

Let us start with a given (e,1) pair. Set

$$X_s = \begin{pmatrix} \cos(e*\text{RDPELE})*\cos(1*\text{RDPLIN}) \\ \sin(e*\text{RDPELE})*\cos(1*\text{RDPLIN}) \\ \sin(1*\text{RDPLIN}) \end{pmatrix}$$

Set $X_p = Rx_s$.

Now the extended ray from the satellite to the planet Venus, i.e. $b - t\,X_p$ for $t \geq 0$, intersects the planet surface if and only if the following quadratic has a real positive root.

$$(b^1 - tX_p^1)^2 + (b^2 - tX_p^2)^2 + (b^3 - tX_p^3)^2 = a^2.$$

If the quadratic has real positive roots, we select the smallest root t_1 and set

$$X_v = b - t_1 X_p.$$

Then $\lambda = \text{ATAN}(X_v^2/X_v^1)$

and $\phi = \text{ATAN}(X_v^3/\text{SQRT}((X_v^1)^2 + (X_v^2)^2))$

This completes the transformation T^{-1}.

Quality Control of the Navigation

As mentioned earlier no landmark measurements are directly available from the images as is possible in terrestrial and lunar cases, or for images of Mars and Mercury. Lacking a clearcut comparison between computed coordinates and true coordinates, one is forced to judge the accuracy of the navigation by internal consistency. On McIDAS it is possible to load a sequence of images with the same load point on the analog disc for the sub-spacecraft point. If the first step in the navigation, the calculation of the center of the image, is accurate then on looping through the sequence the successive images should look aligned. Any misalignment can be attributed to an error in the location of the sub-spacecraft point, which can then be recomputed.

Aside from the mislocation of the sub-spacecraft point the navigational errors arise mainly due to:

(i) roll, pitch, and yaw error

(ii) remaining geometric distortions in the vidicon image.

Of these, the corrections for roll pitch and yaw errors can be estimated from camera pointing information. The errors introduced by geometric distortions are difficult if not impossible to obtain without measuring location of nearby reseaus and determining local image geometry. However, these errors are generally (in GEOMED images only) comparable to the resolution of the vidicon and can be ignored.

Summary

A technique has been described herein to navigate planetary images obtained from spacecraft with vidicon type cameras. At present this has been used for Mariner 10 images of Venus having a substantial portion of the bright limb. Use of pattern recognition techniques and some idea of the atmospheric (cloud) motions will allow this technique to be used for higher ground resolution mosaic images also. Work is now in progress along these lines.

Acknowledgements:

The authors thank Messrs. Robert Krauss and Eric Smith of the University of Wisconsin Space Science and Engineering Center for their help in the implementation of the navigation scheme on McIDAS, and Mr. K. Klaasen and Mr. G. E. Danielson of the Jet Propulsion Laboratory for their assistance with the SEDR output.

This research was supported by JPL Contract 953034 and by NASA Grant No. NGR-50-002-189.

REFERENCES

Barker, E.S. and M.A. Perry, 1975: Semi Periodic Variations in CO_2 Abundance on Venus, ICARUS, (25), 282-295.

Howard, H.T., G.L. Tyler, G. Fjeldbo, A.J. Kliore, G.S. Levy, D.L. Brunn, R. Dickinson, R.E. Edelson, W.L. Martin, R.B. Postal, B. Seidel, T.T. Sesplauleis, Z.Z. Zygielbaum, P.B. Esposito, J.D. Anderson, I.I. Shapiro, and R.D. Rosenberg, 1974: Venus: Mass, Gravity Field, Atmosphere, and Ionosphere as Measured by the Mariner 10 Dual Frequency Radio System. Science, (183), 1297-1306.

Limaye S.S. 1975: Pole-Equator Temperature Contrast on Venus and its Implications. Space Science and Engineering Center, University of Wisconsin, Madison, Report to NASA.

O'Leary, B., 1975: Venus: Vertical Structure of Stratospheric Hazes from Mariner 10 Pictures, Journ. Atmos. Sci. (32), 1091-1100.

Smith, E.A., and D.R. Phillips, 1972: Automated Cloud Tracking Using Precisely Aligned Digital ATS Pictures. IEEE Trans. on Computers, (C-21), 715-729.

New Measurements of UV Cloud Motions on Venus

Robert J. Krauss

ABSTRACT

Preliminary results of three additional sets of measurements of the velocity of small scale UV cloud features in the Mariner 10 pictures of Venus support findings based on the first measured data set reported by Suomi (1975) and Krauss (1976). The global velocity field consists of a small meridional component towards the poles, increasing linearly with distance from the equator, and a zonal component which is a minimum at the equator and increases toward a maximum near 45° latitude. The differential rotation at low latitudes tends to conserve angular momentum about the poles. Because of the poorer resolution, the solid rotation region above 45° latitude could not be measured in the new data sets. Two new features were observed, however. A small amount of horizontal eddy transport of momentum toward the poles is present in all data sets. In addition, the zonal velocity, zonal velocity gradient with longitude, and the meridional velocity gradient with latitude all show correlated trends suggesting the likelihood of a global velocity field which fluctuates about a mean. However, both the eddy transport and the velocity fluctuations are at least an order of magnitude less than the mean flow. The trend of the zonal velocity gradient indicates that zonal velocities occasionally decelerate toward the evening terminator, throwing doubt on sun-locked mechanisms as drives for the zonal wind.

INTRODUCTION

We present here the preliminary results of additional cloud motion measurements in Mariner 10 UV images of Venus. A previous detailed analysis of four UV images (Krauss, 1976) produced several key observations:

1. The upper atmosphere wind field is organized in a vortex structure with a small meridional flow from equator to poles, and in addition, a zonal flow an order of magnitude greater. The flow pattern causes the atmosphere to rotate differentially at low latitudes (tending to conserve angular momentum about the poles) and to rotate with constant angular velocity at latitudes above 45 degrees, where the atmosphere must converge and sink.

2. The zonal flow accelerates in the sub-solar region. There is a u-component velocity gradient along lines of constant latitude which is about the same size as the v-component velocity gradient along lines of constant longitude. The meridional velocity gradient does not measurably change with latitude.

3. Vertical wind shear is observed in the zonal flow, with higher clouds moving faster. This shear is most likely responsible for a large proportion of measurement scatter visible on the high velocity side of zonal wind profiles.

4. Many kinds of wave phenomena are present in the images, and they complicate analysis of the motion field because waves could carry energy and momentum in addition to that carried by the mass field. The vortex structure in the upper atmosphere appears to be stable and to represent Venus as we usually see it from Earth, but the measured velocity field is likely to be perturbed by several phenomena and thus, at any given time, represents only a single observation and not a mean state of the atmosphere.

In order to better define what the "mean state" is for the Mariner 10 data, we chose to extend the velocity field measurements from the first four pictures (at the start of day 39) into day 40. The main intent was to find out if there were short time variations in the global velocity field. There were really several reasons for picking day 40, however. First, the UV features on Venus show a slight change in character in the period from 2 to 4 days after encounter (closest approach to Venus occurred at $36^{d}\ 17^{h}\ 01^{m}$ GMT). There appears to be an increase in convective activity and generation of brighter clouds near the equator. In addition, the curvature of the spiral streaks increases. A second reason was that if the assumed 4 1/2 day period of the "Y" feature was reflected in the motion field, a time interval of 24-36 hours from the first set of measurements seemed optimal. Too short a time would make changes hard to detect. Too long a time (i.e. 1/2 wavelength or more) would introduce ambiguities in phase. A third reason was that day 40, at ~3 1/2 days past encounter, contained additional interesting features. Both the circumequatorial belts and the bowlike waves were visible. These could be studied in conjunction with the motion field. A fourth consideration was more practical in nature. The 25 km/pixel resolution on day 40 permitted

TABLE I

Data Set Image Identification

DATA SET	FDS NUMBER	GMT DAY	SHUTTER TIME (HHMMSS)GMT
I	62693	39	020656
	62839		034908
	62857		040144
	62987		053244
II	64747	40	020444
	64897		034944
	65023		051756
	65179		070708
III	65343	40	090156
	65473		103256
	65623		121756
	65787		141244
IV	65923	40	154756
	66067		172844
	66223		191756
	66380		210750

TABLE II

ERROR BUDGET ESTIMATE FOR DAY 40

Geometric Rectification	1 pixel
Navigation Model Fit	1½ pixel
Latitude-Longitude Grid	1½ pixel
Roundoff and Truncation	½ pixel
RMS TOTAL	2½ pixel

ERROR BUDGET ESTIMATE FOR DAY 39

Geometric Rectification	1 pixel
Navigation Model Fit	1 pixel
Latitude-Longitude Grid	1 pixel
Roundoff and Truncation	½ pixel
RMS TOTAL	2 pixel

tracking cloud features under 500 km in size. If later images had been used, only larger scale features could have been tracked. Consequently, direct comparison of the velocity profiles with day 39 would have been more subject to question, because the characteristics of the cloud targets used for tracking would have been somewhat different.

Table I identifies the pictures used. The earlier data set from day 39 (Krauss, 1976) is numbered set "I". The data from day 40 is divided into three sets (II, III, and IV) to better identify any trends. In this paper, we report only on preliminary comparison of the COMP or computer measured (cross correlation) velocities from the two days. Single point tracking and target averaging (as for day 39) will be done at a later time.

IMAGE PROCESSING AND ERROR ANALYSIS

The new images in sets II, III, and IV, were processed through the FICOR and GEOM programs at the Jet Propulsion Laboratory and navigated at the University of Wisconsin in exactly the same way as data set I. Extensive error analysis was not repeated, as there seemed no reason to believe that any new sources of error would exist. The previous day's analysis had shown that the true navigation and measurement error was slightly more than half that which was estimated, and had shown that vertical wind shear and changes in cloud shape were the most likely reasons for most of the observed measurement scatter. Without contrary evidence, there was no reason to expect anything different in other data sets, and that indeed appears to be the case here. Except for a larger scatter in the measurements, proportional to the reduced resolution, nothing unusual was seen in the measurements from day 40. Consequently, the present limited analysis appears adequate to determine the trends we seek.

We estimate the limit of useful resolution will probably be reached at 35-40 km/pixel for the velocity measurement techniques used here. At that point, the measurement scatter due to degraded resolution dominates all the structure now visible in the velocity profiles, and one is limited to following only the larger albedo features. Edges and shapes of smaller features are not visible. One can better compare such low resolution measurements with Earth based observations, but the fine structure of the wind field is likely to be lost, and is best observed at resolutions of 10-20 km/pixel, with appropriate time resolution to detect velocity increments of 5 m/s or less.

The wind field measurements are shown in Figures 1, 2, and 3. The order of presentation is: a) data set I - Target averages for 15/15 edit; b) data set I - All data points for day 39; c) data sets II, III, and IV - All data points for day 40; d) data set II alone; e) data set III alone; f) data set IV alone. The data sets for day 40 have fewer cloud targets than day 39 because the lower ground (cloud) resolution made selection and tracking more difficult. Thus, the total of all three data sets is a more reliable indicator of the day's mean velocity field. Note too, the absence of measurements at latitudes above 45° and also the low number of measurements in the northern hemisphere, especially in data set IV. As cloud targets get

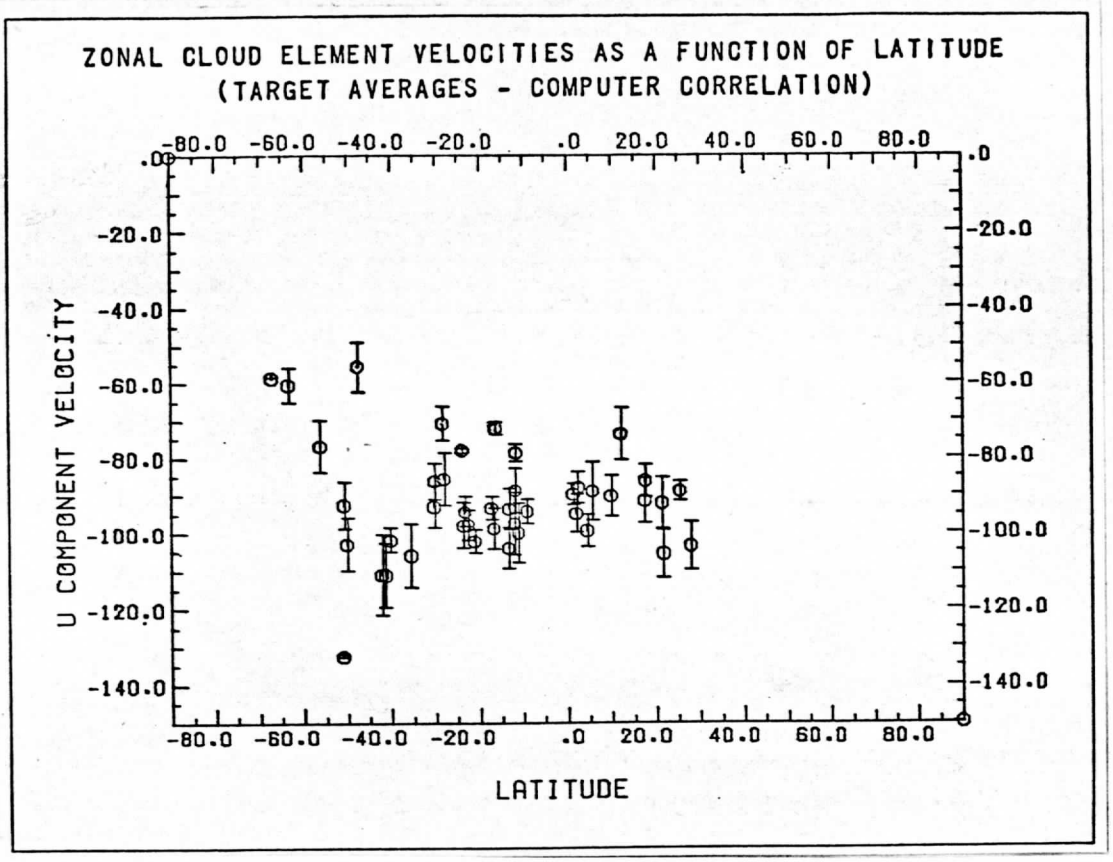

Figure 1a. Target averages for 15 m/s edited measurements -- data set I. The editing and averaging process removes single widely divergent measurements and gives a "cleaner" view of the underlying structure.

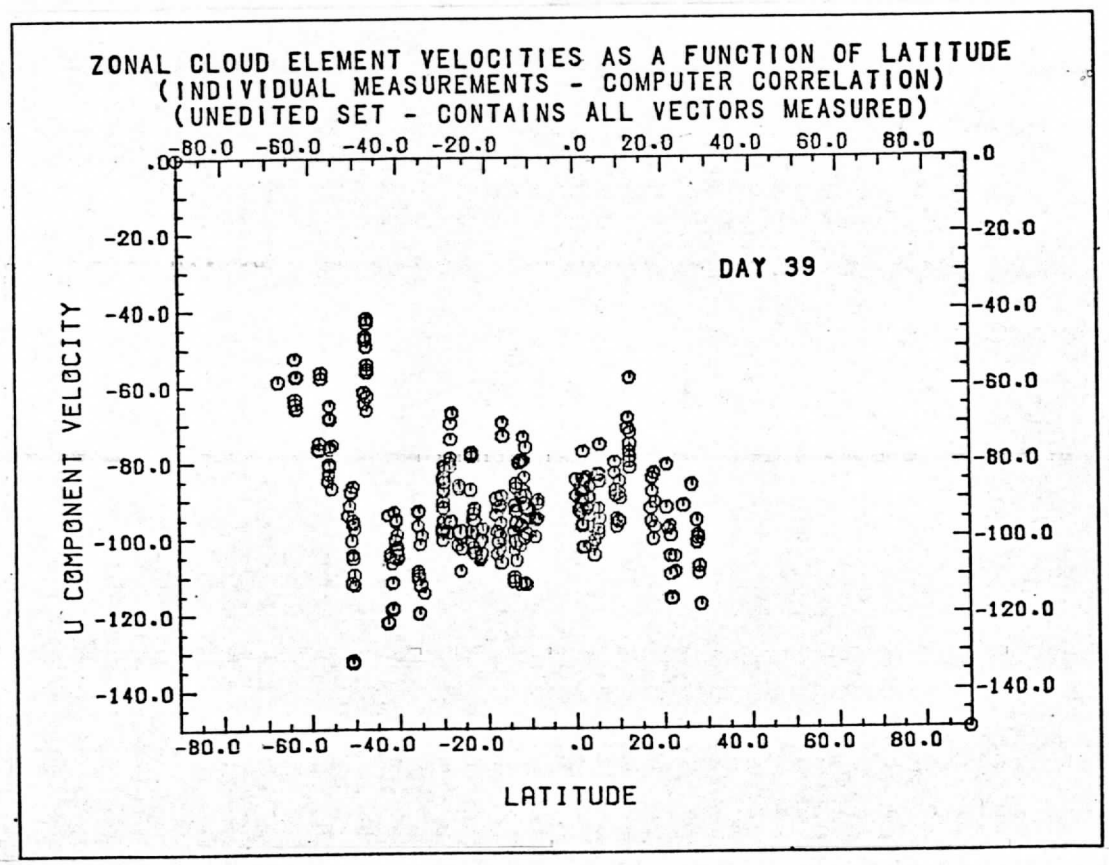

Figure 1b. Unedited measurements for data set I (day 39). Compare with Figures 1 c-f.

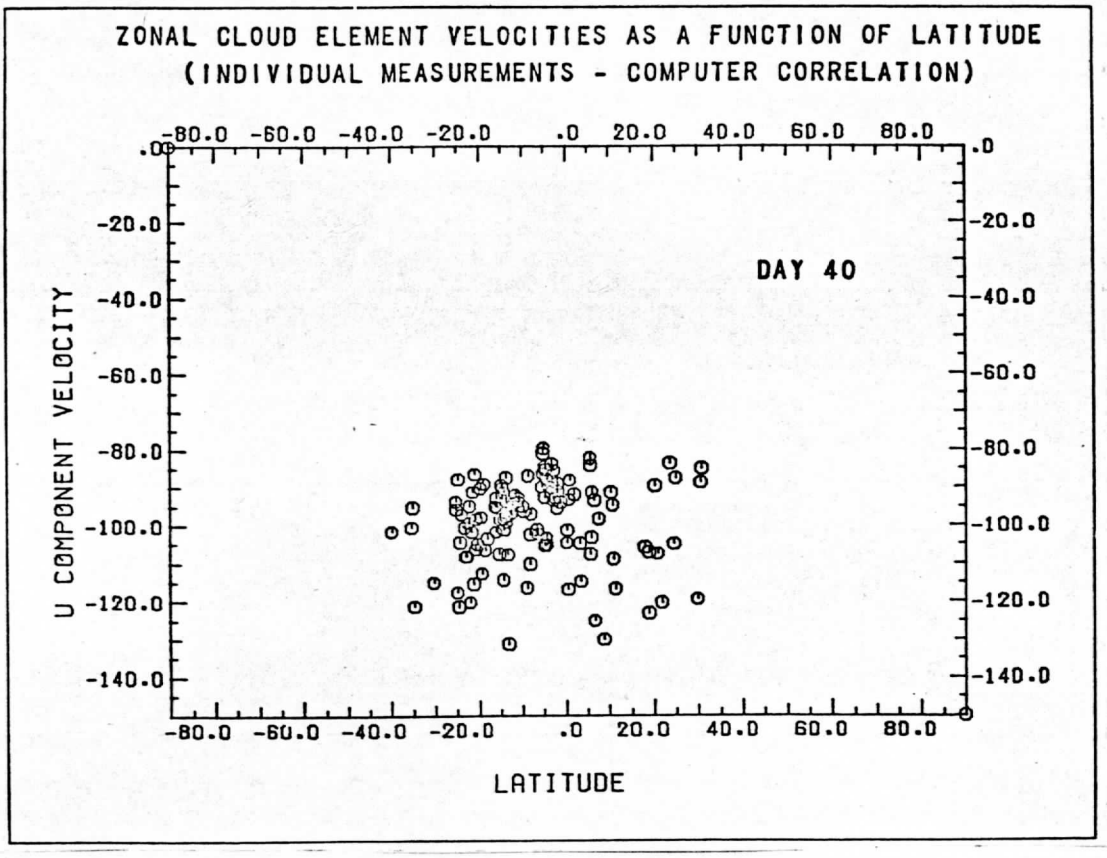

Figure 1c. Unedited measurements for day 40 (sets II, III, and IV, combined).

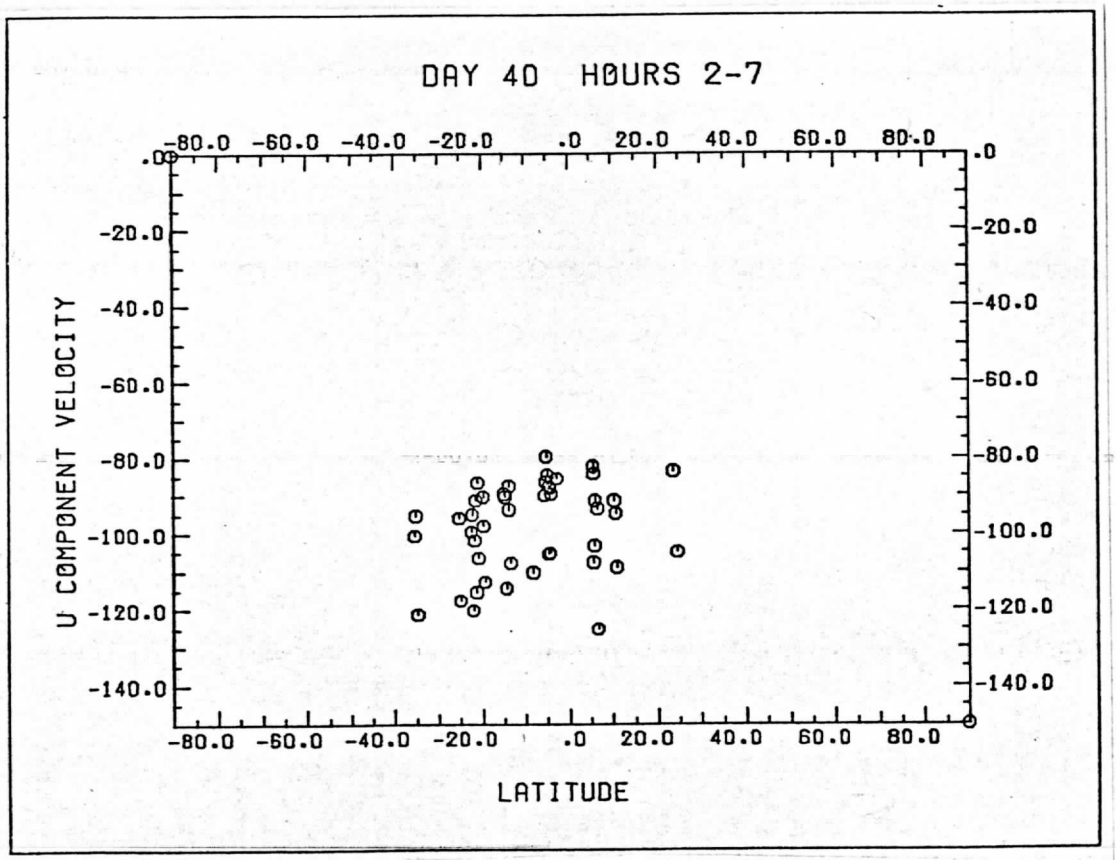

Figure 1d. Unedited measurements for set II.

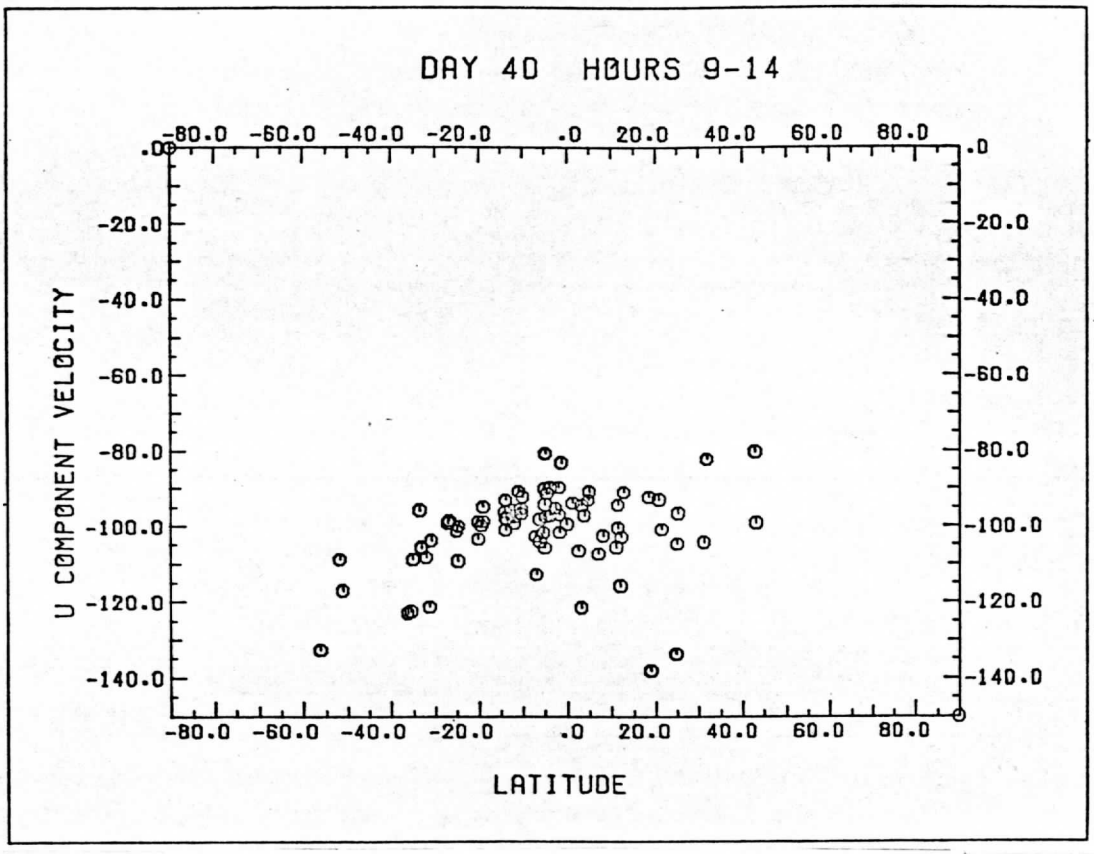

Figure 1e. Unedited measurements for set III.

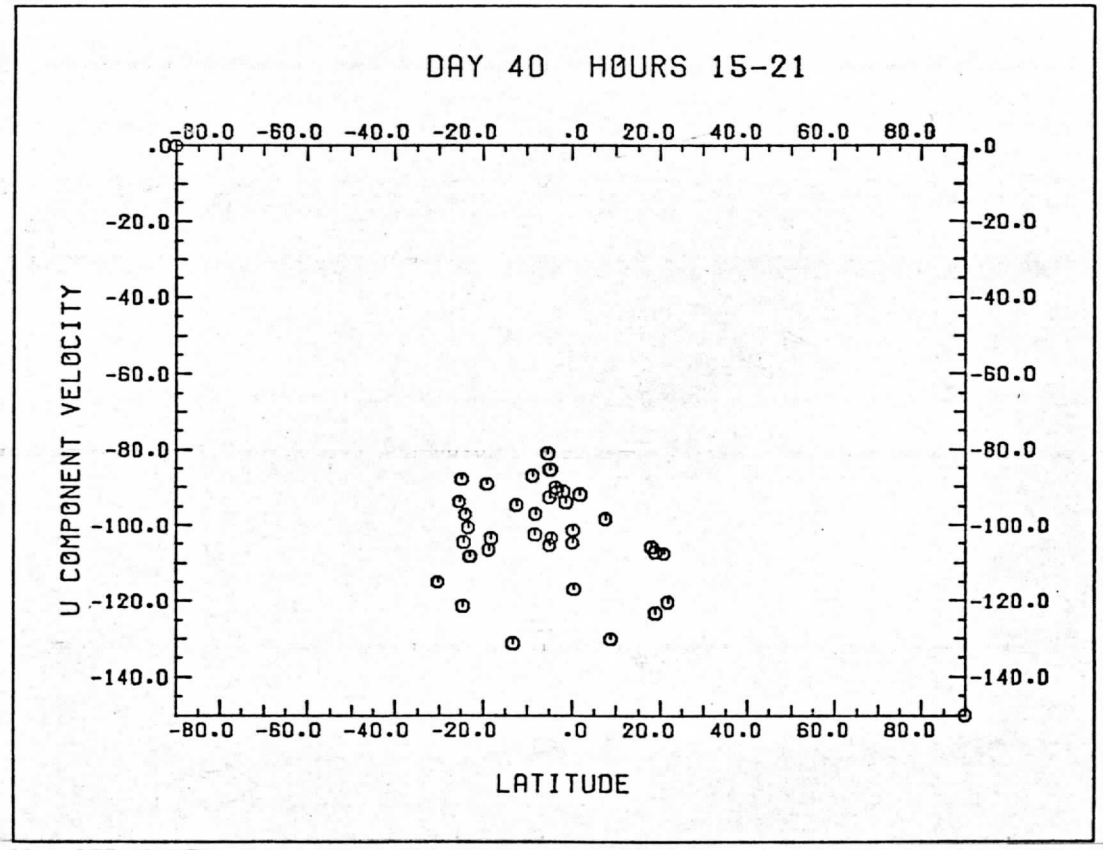

Figure 1f. Unedited measurements for set IV.

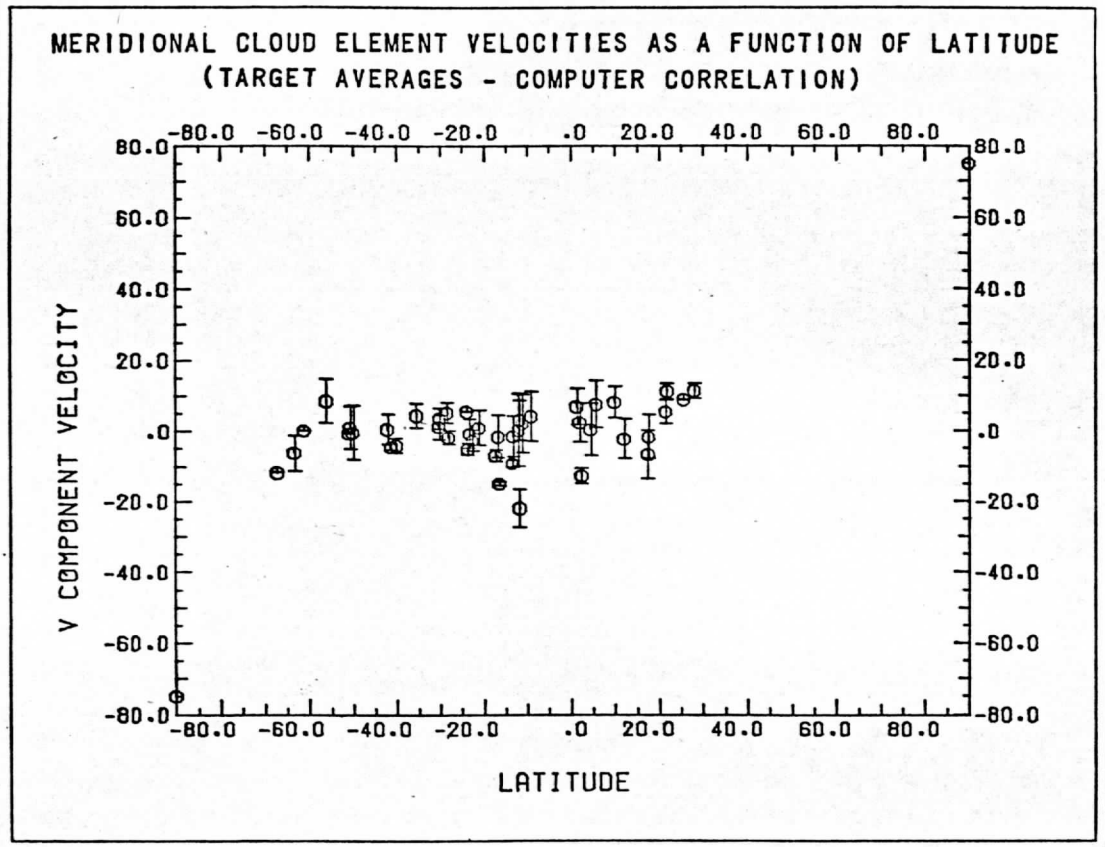

Figure 2a. Target averages for 15 m/s edited measurements -- data set I.

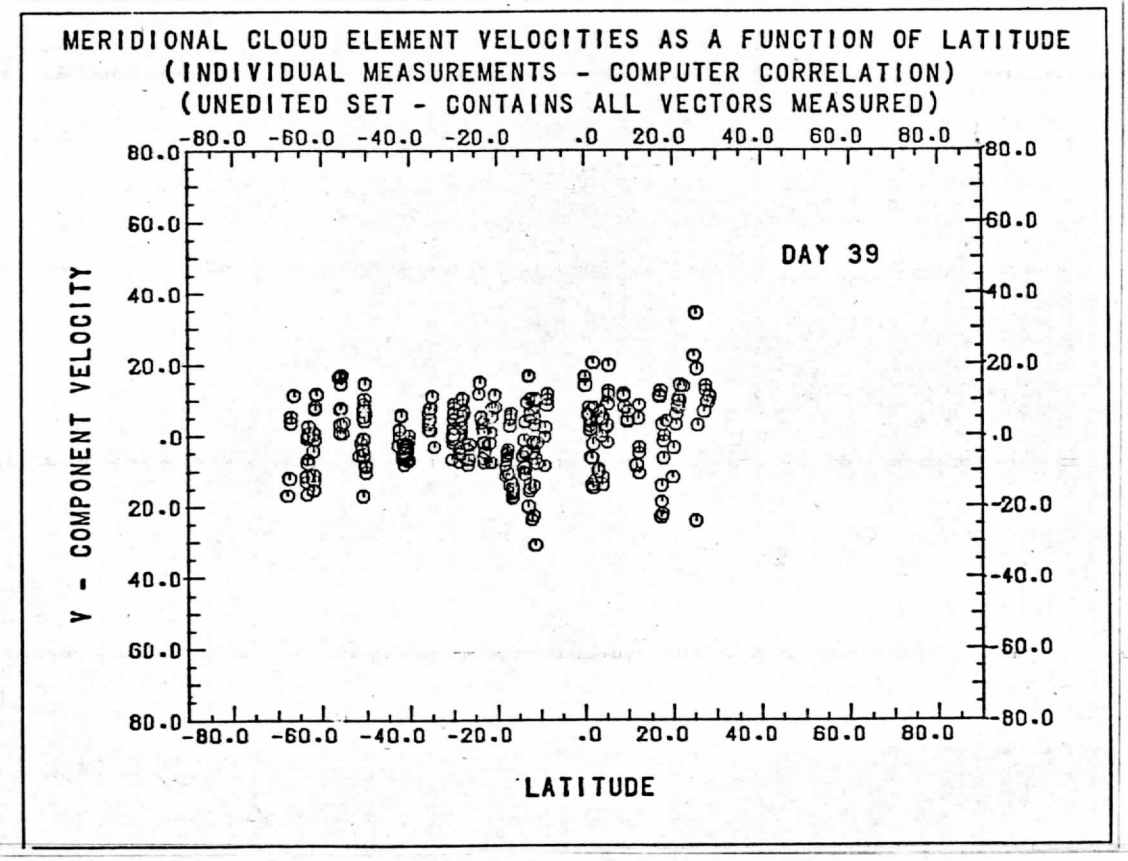

Figure 2b. Unedited measurements for day 39 (data set I). Compare with Figure 2c and with Figures 2 d-f.

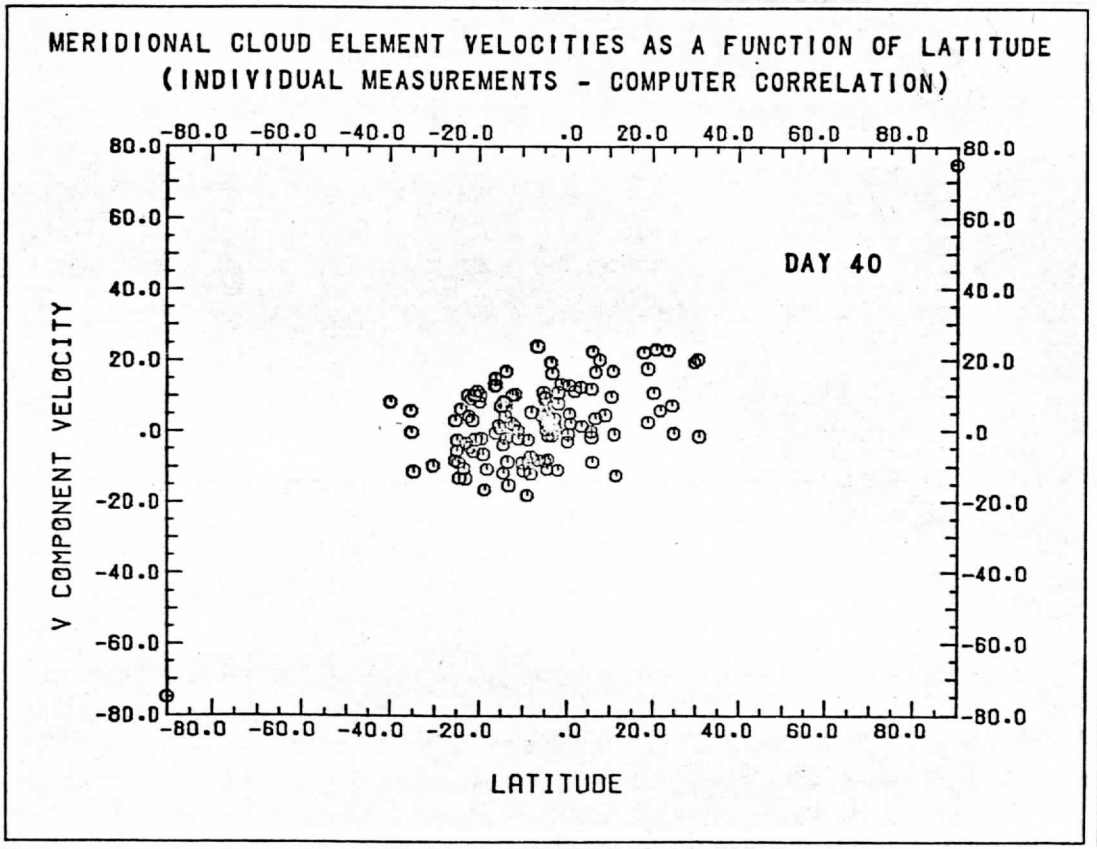

Figure 2c. Unedited measurements for day 40 (data sets II, III, IV, combined).

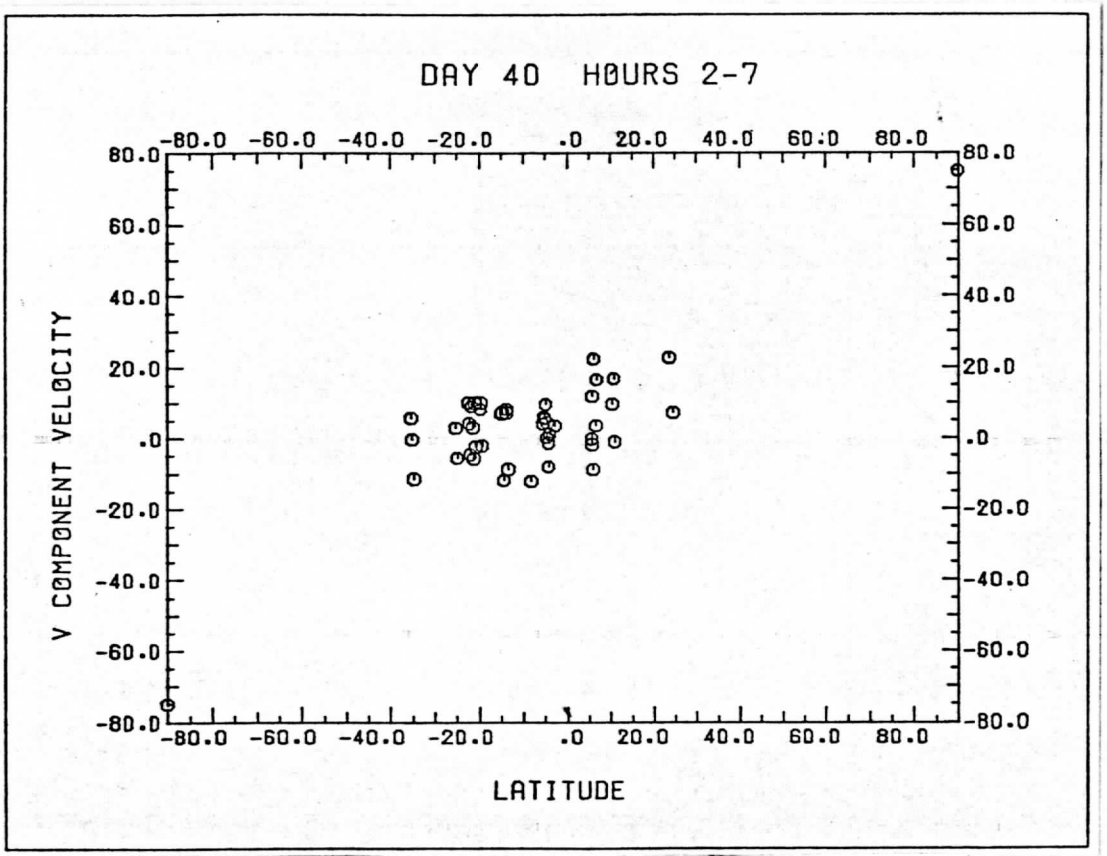

Figure 2d. Unedited measurements for data set II.

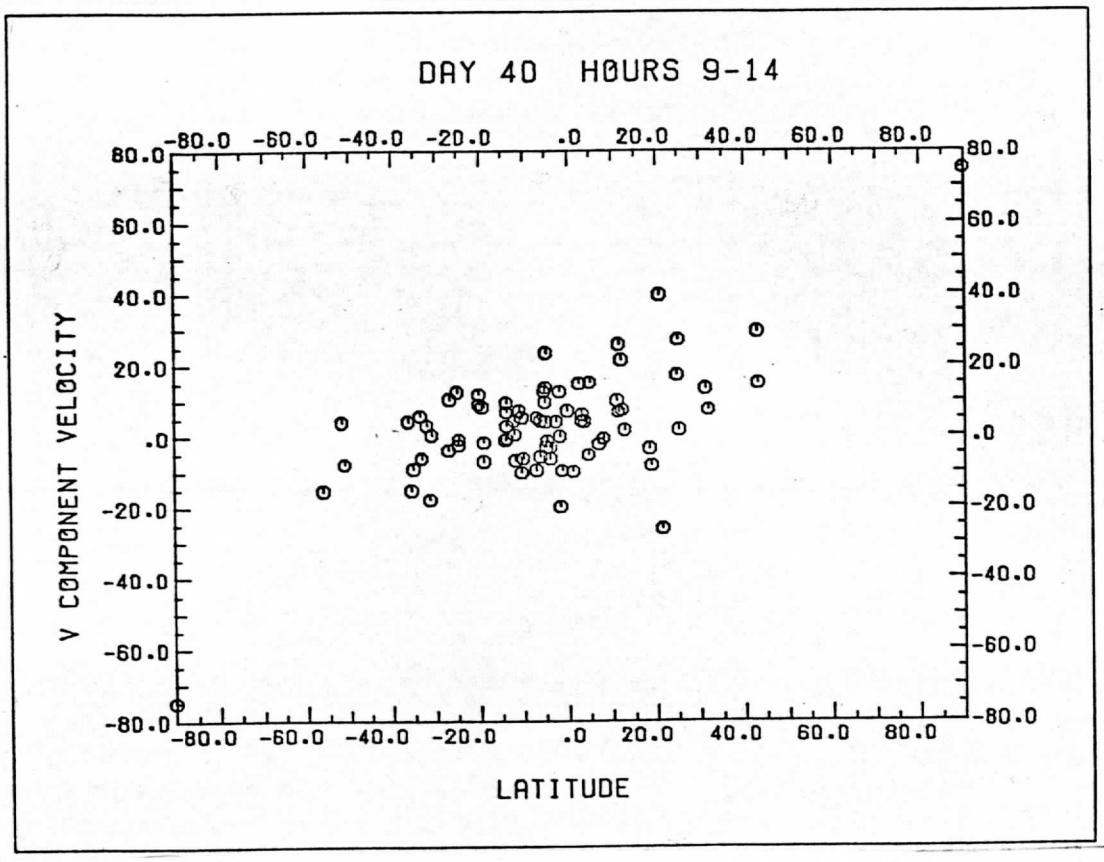

Figure 2e. Unedited measurements for data set III. Note how the slope of the distribution changes from Figure 2d to Figure 2f.

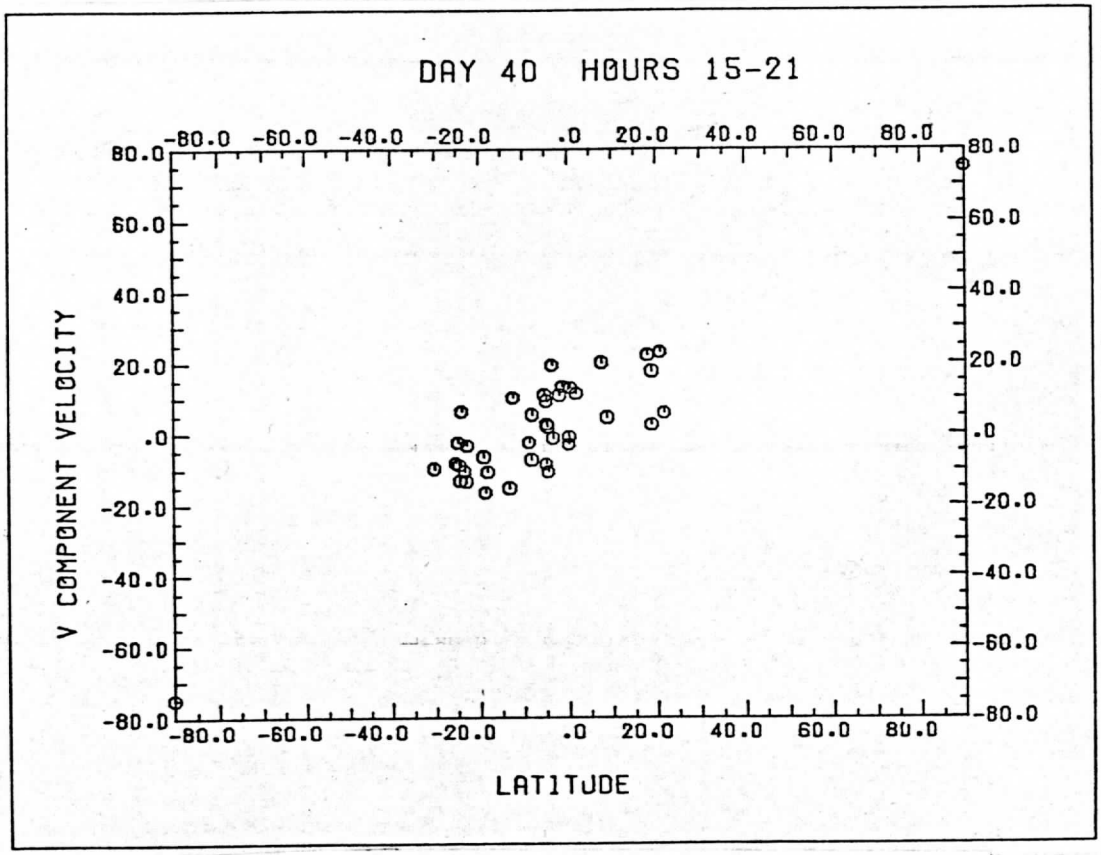

Figure 2f. Unedited measurements for data set IV.

harder to find and track, there is a higher proportion of correlation failures by the computer and the scatter in the remaining good measurements increases. With greater care and effort, we may eventually double the number of acceptable vectors obtained from day 40.

MEASUREMENTS OF CLOUD MOTION

Figure 1 contains plots of u-component (zonal) velocities versus latitude. In data set I (Figure 1a) there were enough high resolution details in the clouds to get velocities above 45° latitude and show the sharp dropoff at constant angular velocity as one approaches the pole. The velocity maximum at 45° is clearly defined, as is the small subset of six targets appearing to move at constant angular velocity (along the dotted line) at low and mid latitudes. The majority of targets in the low and mid latitudes show a velocity profile which gradually increases as one moves away from the equator. This indicates a tendency to conserve angular momentum about the poles and this differential motion is also present in data sets II, III, and IV, as well. Note that there is no group of slow, constant angular velocity points as in set I. Scatter in the measurements is somewhat greater on day 40 in the proportion one would expect from the poorer resolution in the image.

The meridional velocity gradient is seen in Figure 2, appearing as a slope to the distribution in the plots. Note that there is a definite increase in slope from day 39 to day 40 (Figures 2b and 2c) and that throughout day 40, the slope continues to increase (Figures 2d, 2e, 2f). Data set IV (Figure 2f) does not have enough good measurements at high latitudes. This lack of successful image correlations at high latitudes is due primarily to poorer resolution, which makes finding and tracking small cloud targets more difficult and more subject to correlation failures. Coupled with the increased measurement scatter, the result of the poor resolution in Figure 2f is a slope of the points in the plot which is probably twice as large as it should be. This degradation of data can be partially offset by a greater effort to get better measurements from the data, but we believe that as resolution gets worse, it will be necessary to choose larger and larger albedo features to track, since small cloud features such as edges and minor convective elements will no longer be visible.

The longitudinal velocity gradient of the zonal winds shows a definite drop from day 39 to day 40. Indeed, the gradient on day 40 appears to be nonexistent (Figure 3c). Lower or equal velocities at the evening terminator cannot be explained in terms of a target selection bias due to viewing geometry (as the higher velocities on day 39 could be explained), so we conclude that the reduction in slope is real. That this is an actual physical trend we are observing, and not a statistical deviation, is evident from Figures 2d, 2e, and 2f, which show that the longitudinal gradient does not merely disappear on day 40, but is undergoing a change in sign. As discussed in Krauss (1976), other experimenters have also seen higher velocities at the evening terminator. This is the first observation of <u>lower</u> zonal velocities at the evening terminator, and has profound

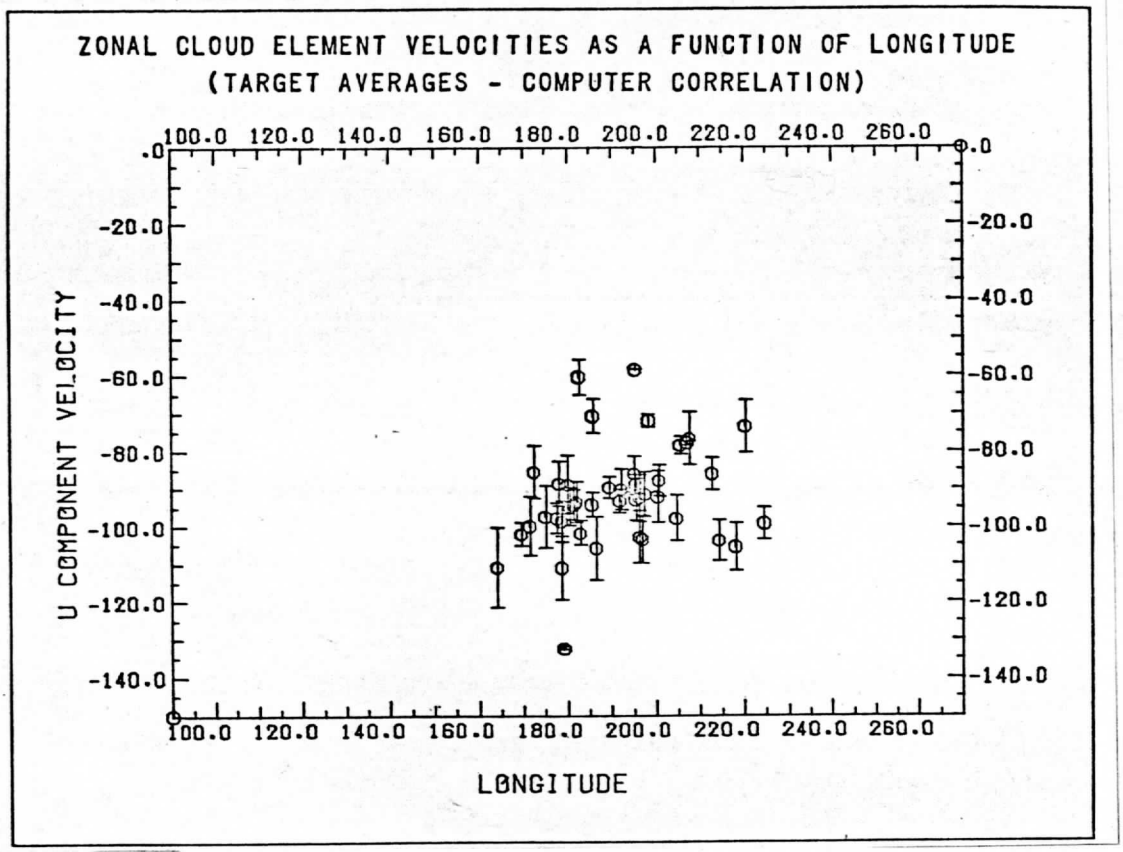

Figure 3a. Target averages for 15 m/s edited measurements -- data set I.

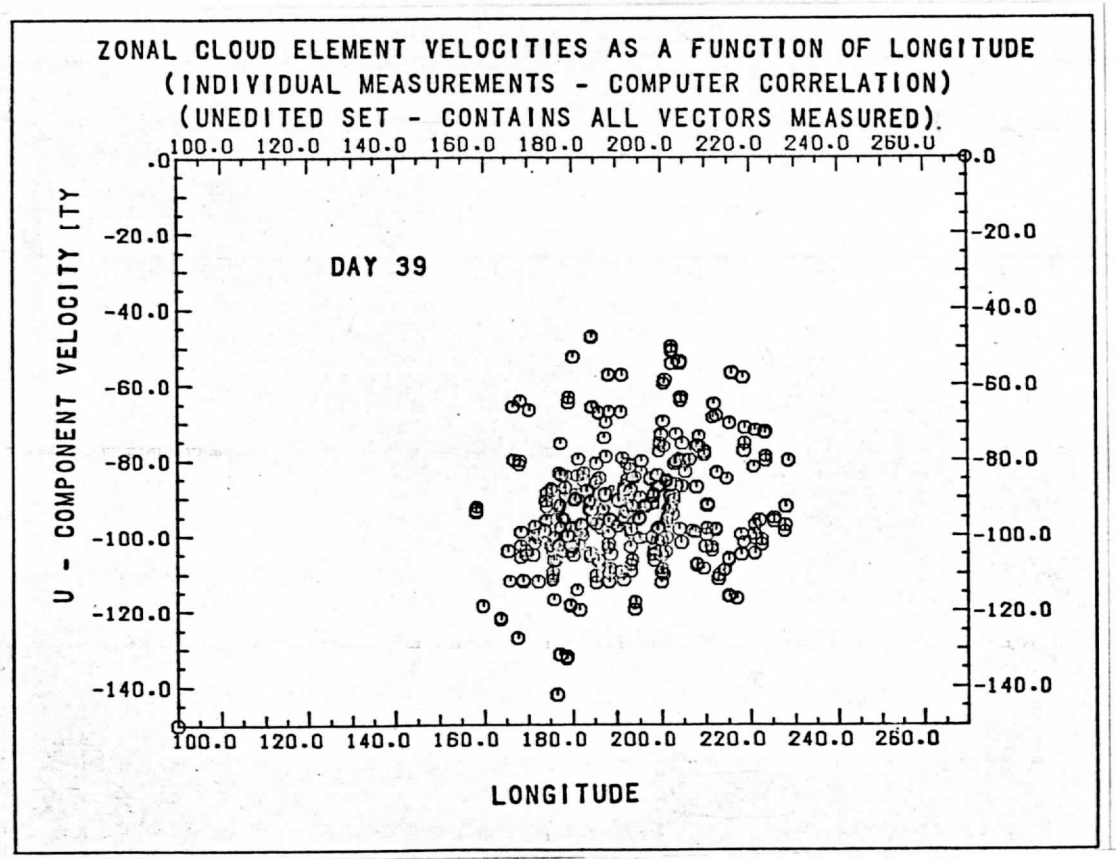

Figure 3b. Unedited measurements for day 39 (data set I). Compare with Figure 3c and Figures 3 d-f.

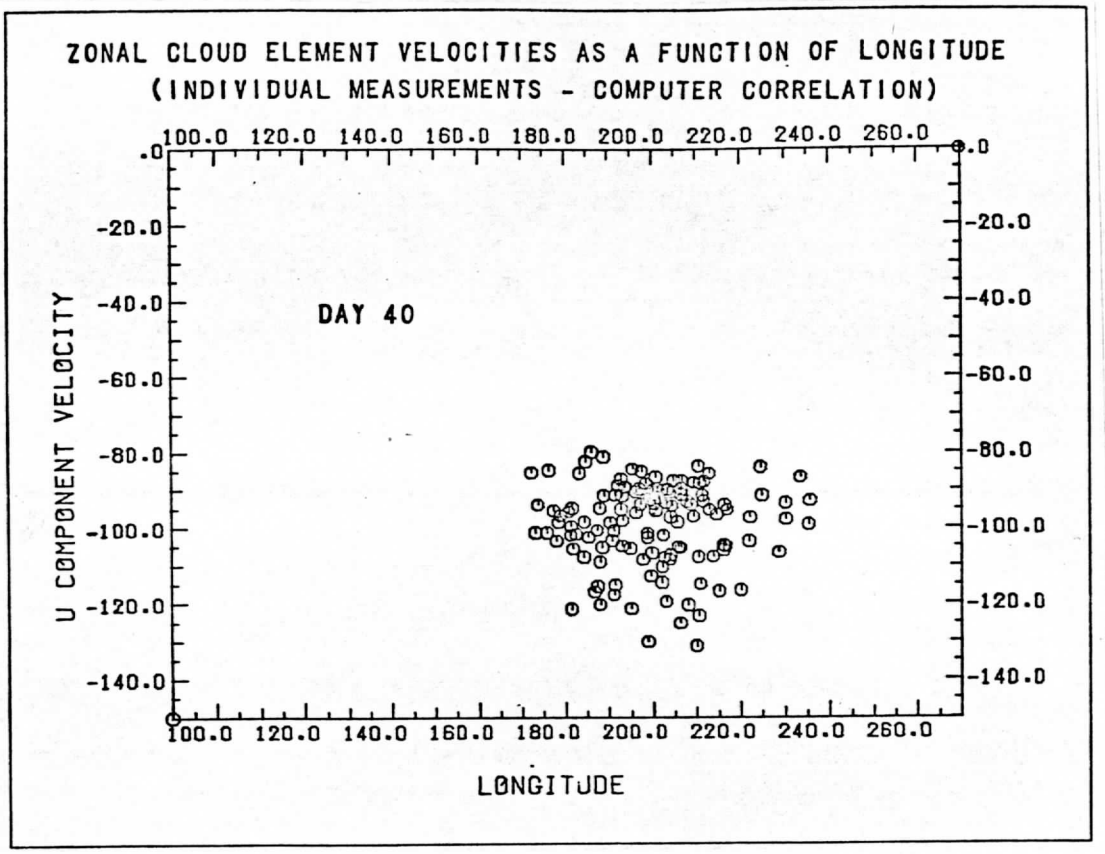

Figure 3c. Unedited measurements for day 40 (data sets II, III, IV, combined).

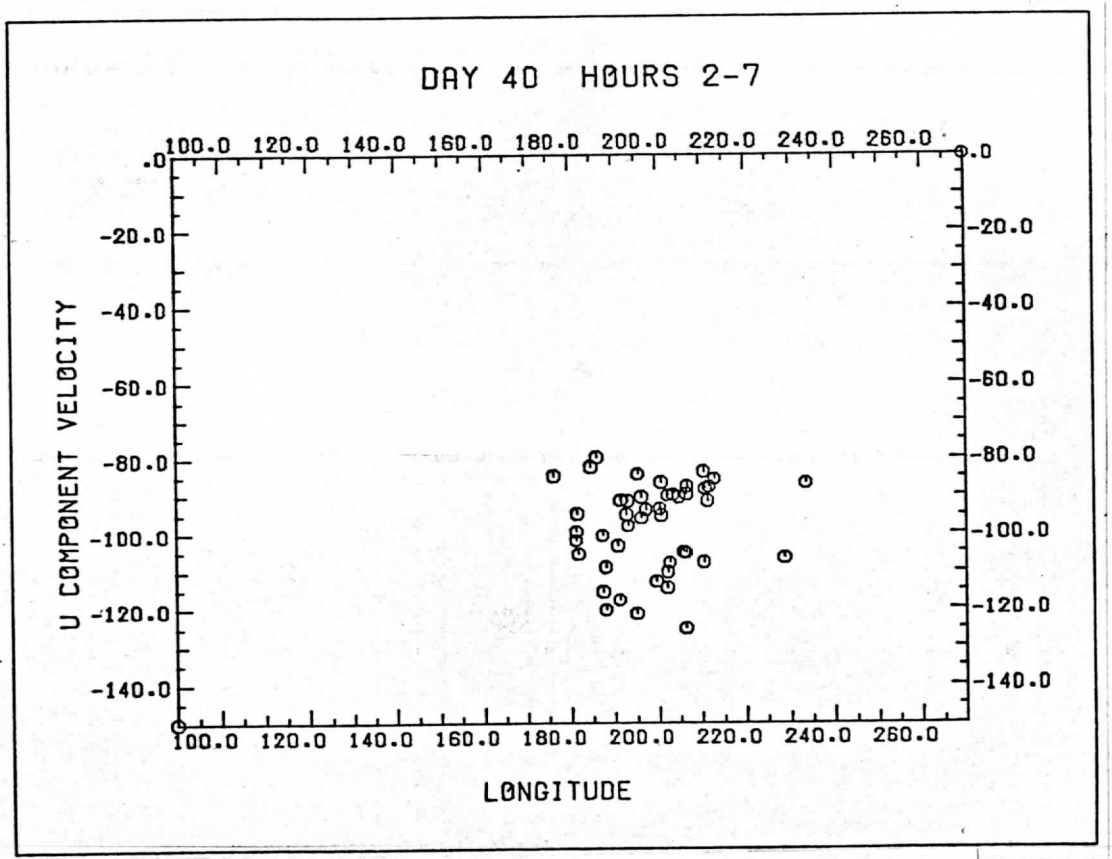

Figure 3d. Unedited measurements for data set II.

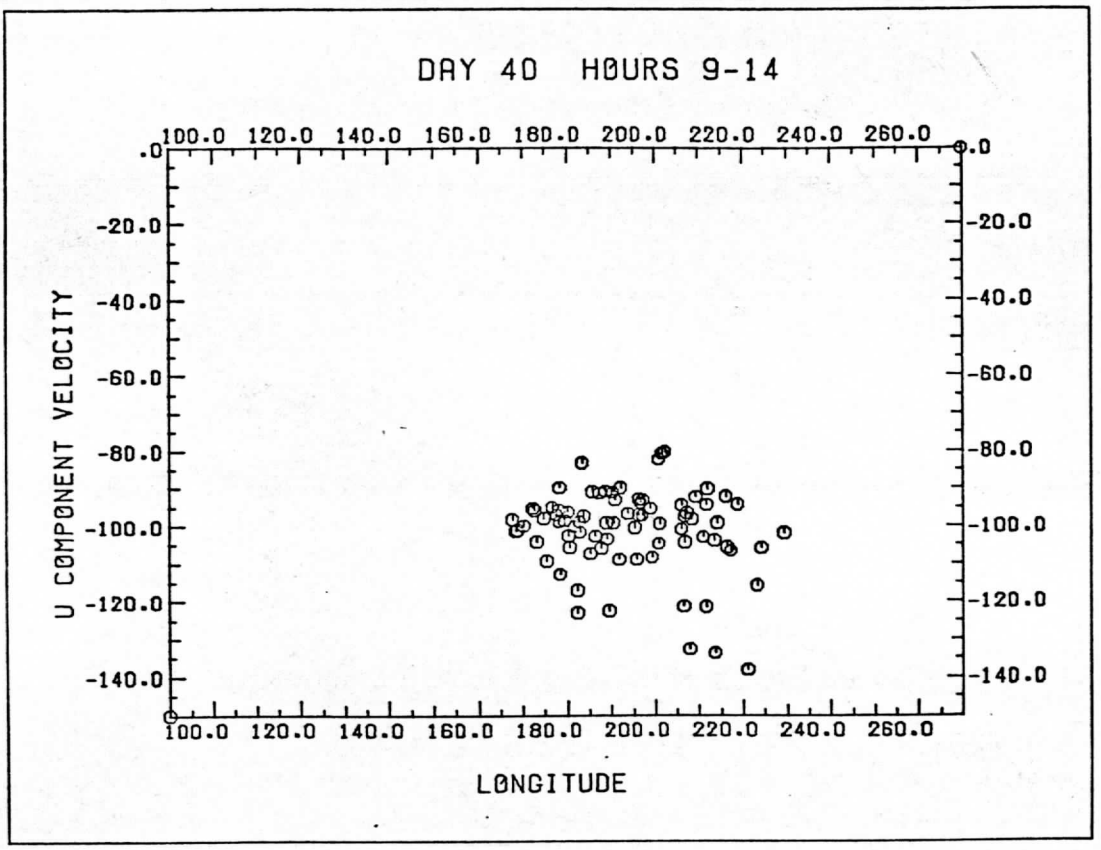

Figure 3e. Unedited measurements for data set III. Note how the slope of the distribution changes from Figure 3d to Figure 3f.

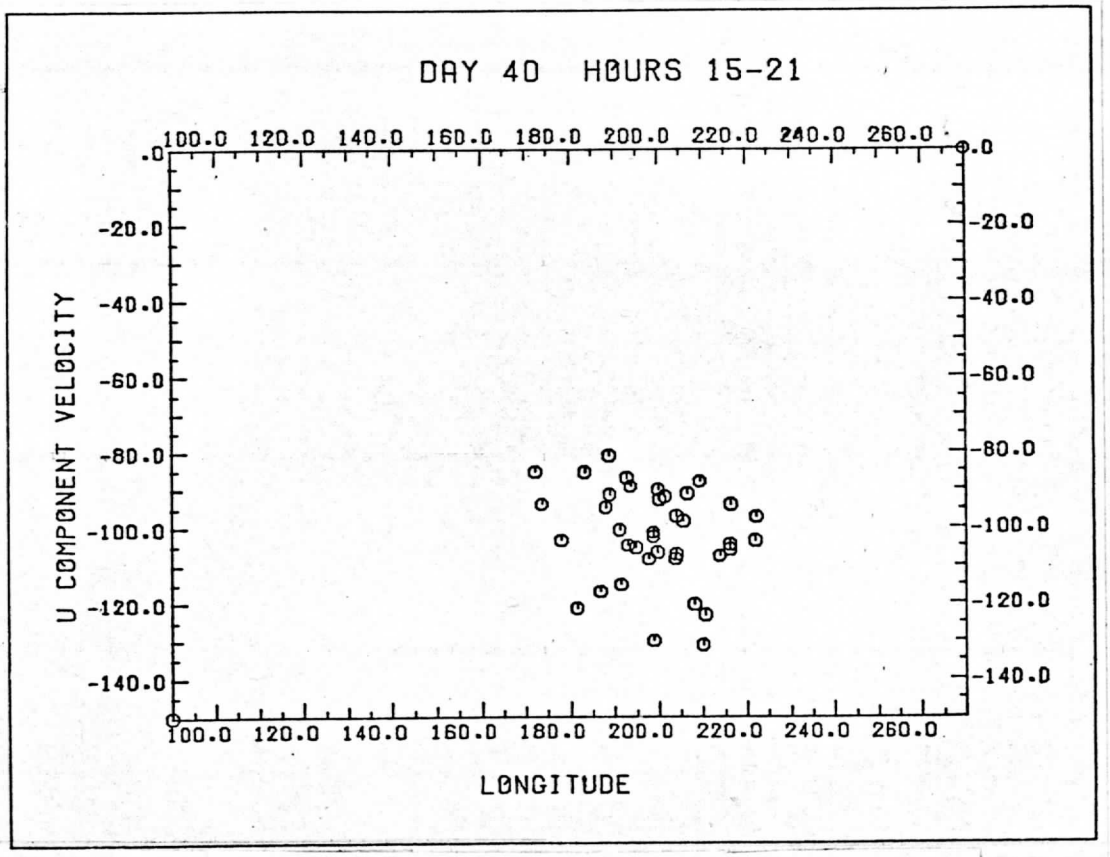

Figure 3f. Unedited measurements for data set IV.

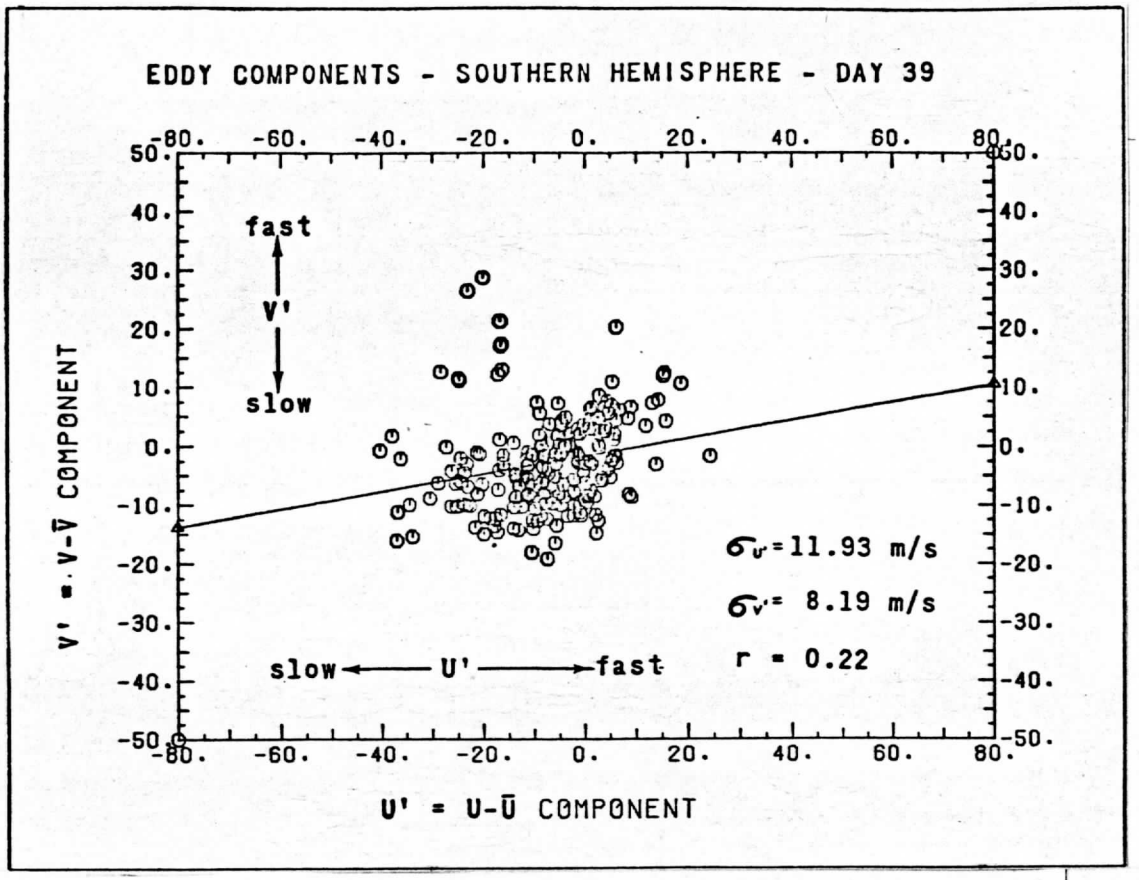

Figure 4a. Eddy transport in southern hemisphere (day 39).

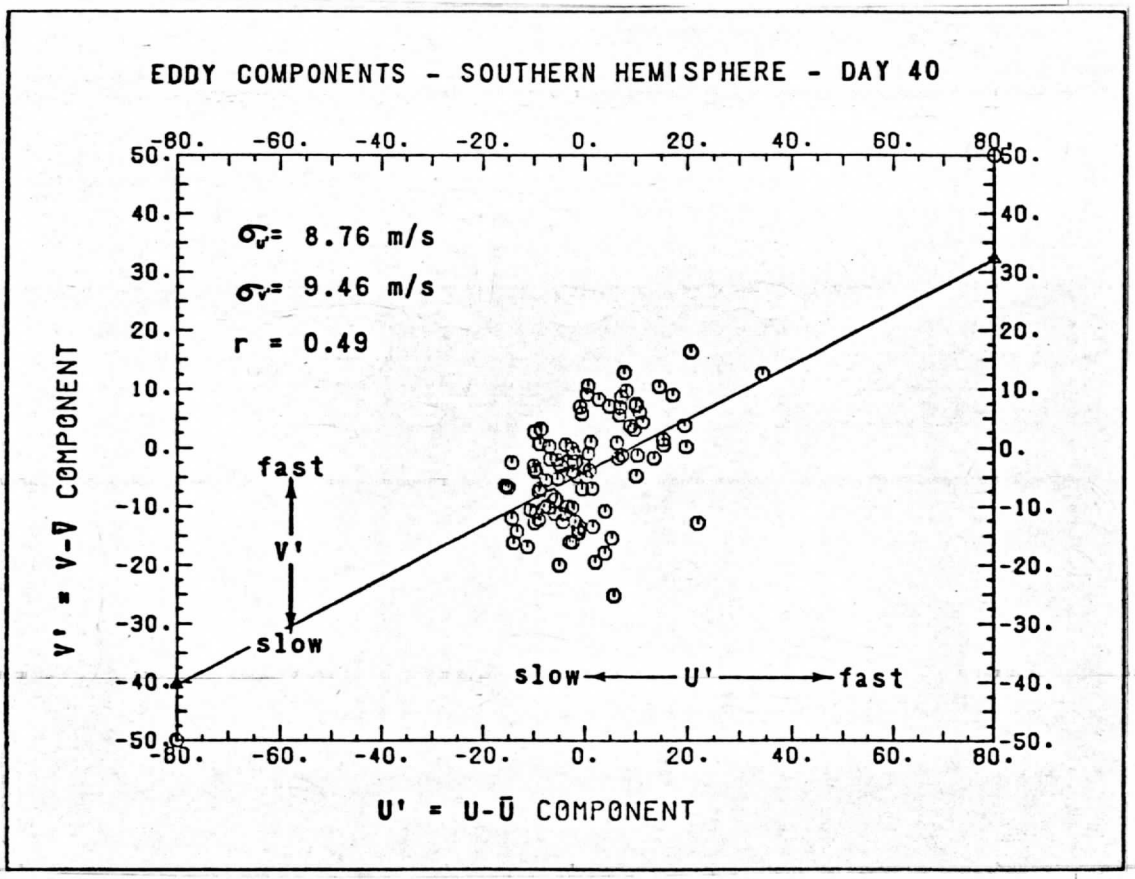

Figure 4b. Eddy transport in southern hemisphere (day 40).

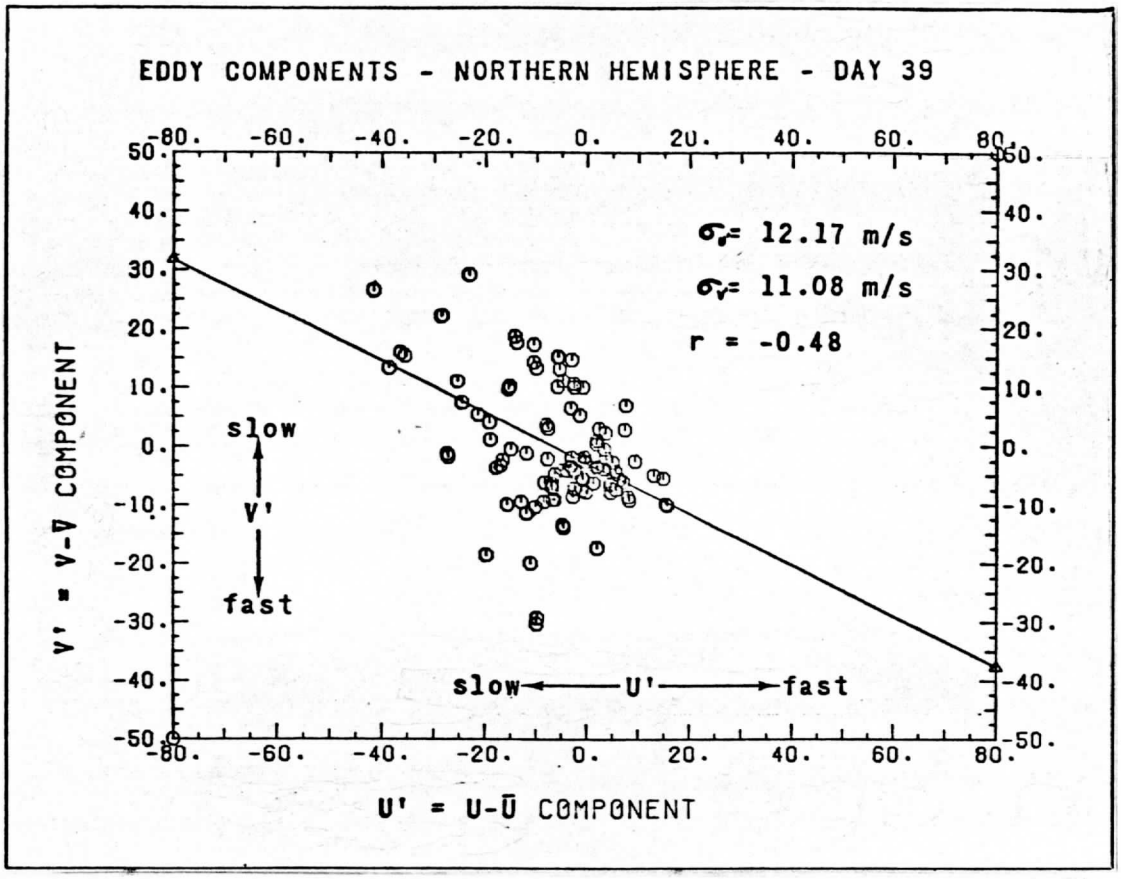

Figure 5a. Eddy transport in northern hemisphere (day 39).

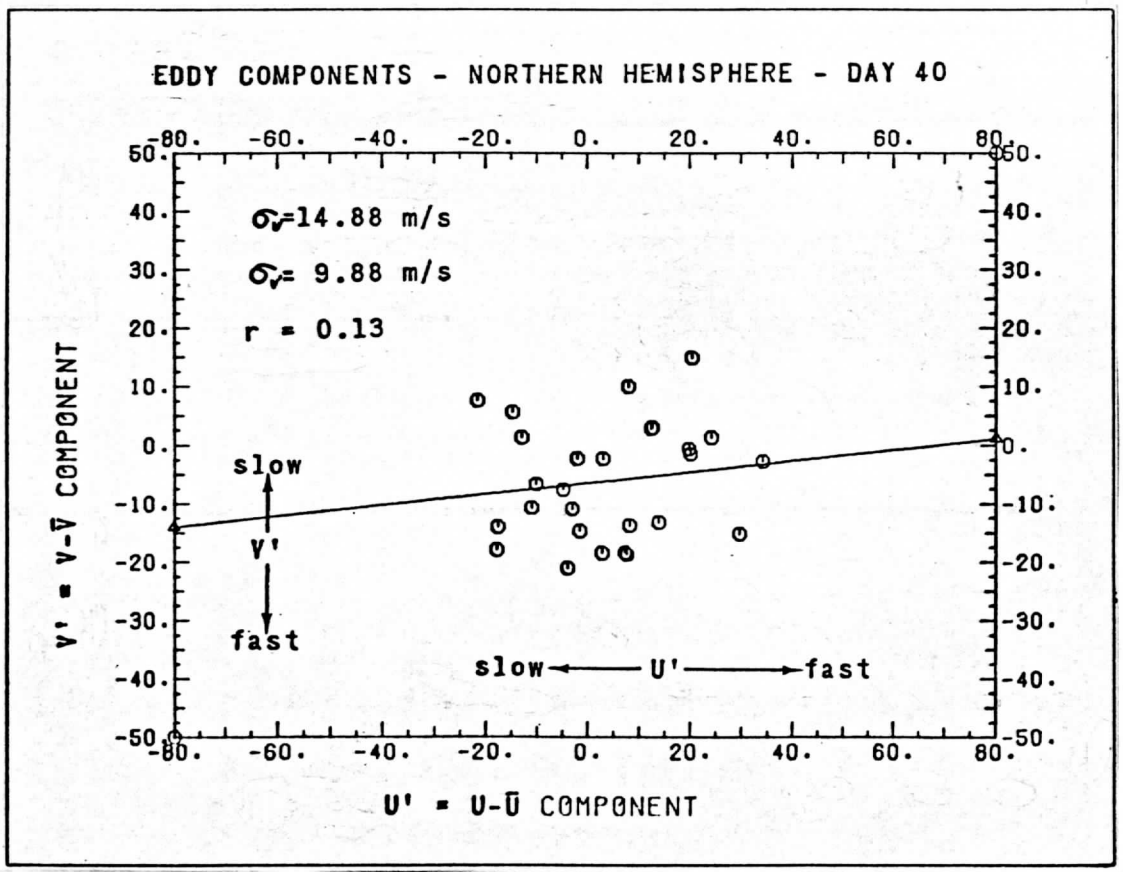

Figure 5b. Eddy transport in northern hemisphere (day 40). This is the only correlation plot indicating equatorward momentum transport. Correlation is low, however, and measurements too few for confidence.

implications for explanations of the drive for the zonal winds. Solar tides and Reynolds stress theories require a sun-locked zonal velocity field. If velocities at the terminator are occasionally lower, the drive for the zonal winds cannot be sun-locked.

No change of the meridional velocities with longitude was observed in any data set. Least squares fits showed no slope to within 2 m/s over the entire longitude range measured.

EDDY MOTIONS

It is possible, using the measured u and v profiles, to investigate the transport of zonal momentum along a meridian. One computes a mean $\bar{u}$ and $\bar{v}$ as a function of latitude and subtracts it from the u and v components of each measured velocity vector. What is left must be the residual components u' and v', respectively. If there is no organization to the residual flow, u' and v' will be randomly scattered around the origin. One could then assume that the scatter is due to measurement uncertainty, random cloud motions, convection, etc. The displacement of the center of mass of the distribution and the increase in $\sigma_{u'}$ over σ_u and $\sigma_{v'}$ over σ_v are measures of how accurately $\bar{u}$ and $\bar{v}$ were chosen as a function of latitude, so the $\bar{u}$ and $\bar{v}$ choice need not be perfect, merely reasonable enough to keep the scatter from growing significantly.

If one finds a non-zero correlation in the scatter plots, however, that means that the faster u' are associated with the faster v' (poleward zonal momentum transport) or the slower u' are associated with the faster v' (equatorial zonal momentum transport). Figures 4 and 5 show the results of such an analysis. In the southern hemisphere (Figure 4), the correlation coefficient, r, is 0.22 on day 39 and 0.49 on day 40. In the northern hemisphere (Figure 5), v and r must change sign, but we still find a correlation of -0.48 on day 39. Day 40 shows a very slight equatorward momentum transport, but it should be remarked that there are only a few points in the plot, widely scattered, and we really ought to have better statistics. One would not change $\sigma_{u'}$ and $\sigma_{v'}$ very much by tilting the least squares fit to a negative correlation in Figure 5b. On the whole then, momentum transport seems to be toward the poles in the plots.

The total momentum transport is given by the sum of the mean flow transport and the eddy transport:

$$\overline{uv} = \bar{u}\,\bar{v} + u'v'r$$

$$= 93 \text{ m/s} \cdot 6 \text{ m/s} + 5 \text{ m/s} \cdot 3 \text{ m/s} \cdot 0.4$$

where we have substituted representative mean values for the quantities in the equation. Even if u' and v' are estimated wrong by several hundred percent, it is clear that the eddy transport toward the poles is still considerably smaller than transport by the mean flow.

INTERPRETATION OF THE MEASUREMENTS

Figures 6, 7, and 8 show the results of least squares fits to determine the mean zonal velocity with latitude (2nd order polynomial fit) and the slopes or velocity gradients (straight line fits). There is change, and the change is organized.

The zonal velocity at the equator has increased in 24 hours by nearly 5 m/s and were that rate of increase to be maintained over any great length of time, one would have the upper atmosphere rotating twice as fast after 2 weeks. Moreover, one would have to assume that 2 weeks before encounter, the upper atmosphere was standing still. Clearly, such a rate of change cannot be constant in time. There is a tendency for that rate of change to drop off toward the end of day 40, leaving some doubt that we would be able to measure much over 100 m/s at any later time. Thus, the evidence indicates that the zonal velocity probably fluctuates about some mean value, although we cannot say how regular such fluctuations are or exactly what the mean value is. Looking at prior observations including those of other experimenters, one would tend to place the mean zonal velocity at the equator around 90-95 m/s (See again, the discussion in Krauss, 1976).

Note now, in Figure 8, how the zonal velocity varies with longitude. The trend from a negative to a positive gradient is clearly defined. The gradients in Figure 8 are negatively correlated with the velocities in Figure 6. The diminishing rate of increase in zonal velocity on day 40 (change of slope in Figure 6) is in agreement with the change in sign of the zonal velocity gradient (Figure 8). Clearly, large zonal gradients of 0.2 m/s/deg. cannot be maintained around the planet or one would have a substantial velocity discontinuity after 4 days. The diminishing gradient on day 40, however, argues against a sun-locked or solar tide theory of acceleration. Apparently, larger velocities observed at the evening terminator are only present some of the time and not all of the time. As a result, one is now led toward a wave travelling around the planet as a more reasonable explanation of vertical momentum transport. The zonal velocity gradient leads the zonal velocities by about 180°.

In Figure 7, the meridional velocity gradient is strongly correlated with the increase in zonal velocity. The last point on day 40 (data set IV) is too high, as previously explained, but the meridional velocity definitely fluctuates like the zonal velocity, that is, we see a positive correlation of speeds. The same continuity argument we used for Figures 6 and 8 can now be used again here. If one extrapolates back to encounter, the meridional gradient indicates that flow toward the equator would have existed. That would destroy the vortex interpretation of our measured velocity profiles. On the other end, extrapolation to higher velocities toward the end of the mission would give a 20-30 m/s meridional flow on day 45. This is such a severe change, it is likely to affect the energy balance and cloud structure of the planet. It is unlikely that such a trend would continue for very long. We cannot see any indications of gross departure from the steady state in the later pictures. A more reasonable interpretation is that the meridional flow also fluctuates between bounds like the zonal flow. With such a strong correlation in the u and v components, it is tempting to assume the flows are also dynamically coupled.

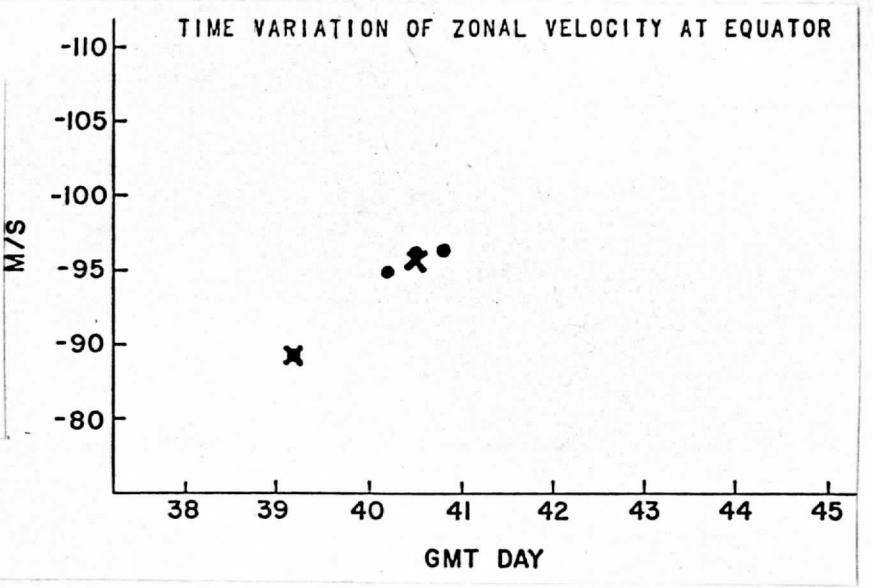

Figure 6. Zonal velocity of the upper atmosphere of Venus at the equator increases by about 5 m/s from day 39 to day 41. The velocity is determined by the minimum in a second order polynomial least squares fit to all cloud motion measurements between +45° and -45° latitude.

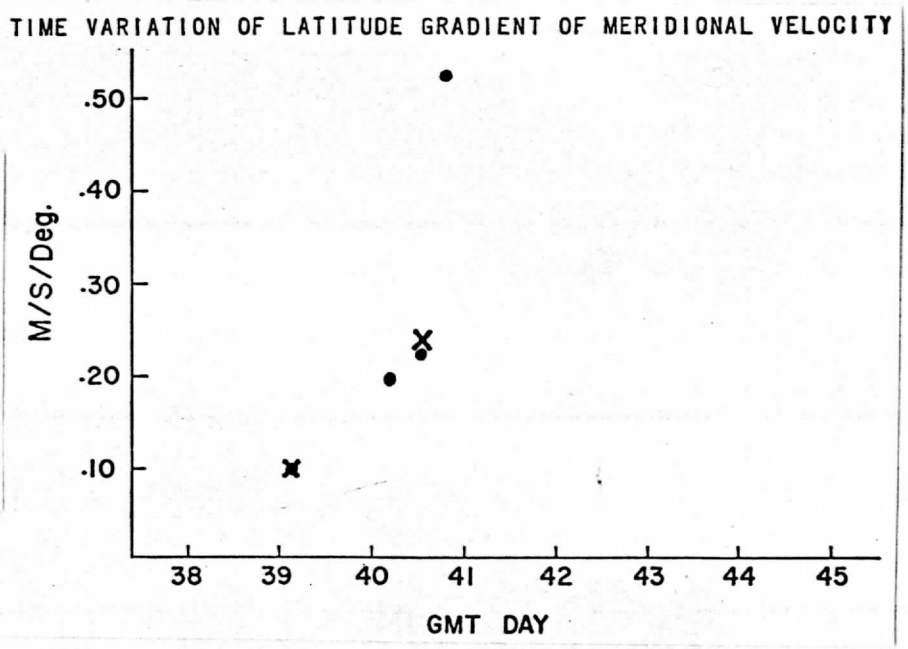

Figure 7. The meridional velocity, which is directed away from the equator in each hemisphere, tends to accelerate as it approaches higher latitudes. The rate of increase is substantially higher on day 40 than on day 39.

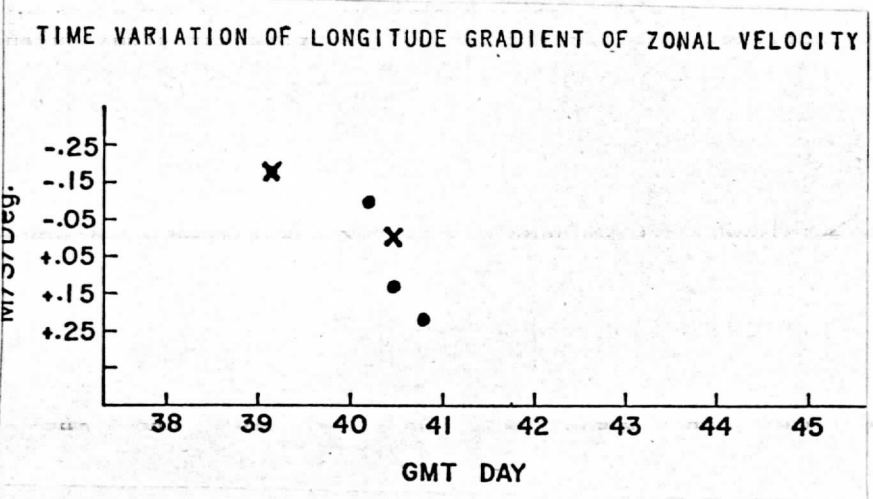

Figure 8. The zonal velocity may increase in time from day 39 to day 41, but it shows a negative gradient with respect to longitude on day 39 (faster speed at the evening terminator), and changes to a positive gradient through day 40 (slower speeds at the evening terminator). Note that there is a high degree of correlation of changes shown in Figures 6, 7, and 8.

Suppose the dynamic coupling is due to a large scale wave. The eddy component transport indicates that there is some kind of global scale organization in the deviations from the mean flow. This same organizational structure could be visible in the correlation of trends in the horizontal velocity measurements and velocity gradients, although there is no evidence that they are related. We can, however, speculate how a global scale wave might transport momentum upward by assuming that the measured divergence at the start of day 39 is coupled to rising motion near the equator. In the simplest case, this involves using only the equation of continuity. Then vertical motion, $+w'$, is correlated with increasing zonal velocity, $+u'$.

Now we make another "reasonable" assumption not yet supported by any evidence. Suppose, considering how the correlated velocities fluctuate, that we have relative convergence at some later time. We are assuming that u' and v' will thus both decrease together in time. Then, by continuity, we should have sinking motion near the equator. In actuality, because the vortex flow is dominant, we merely have reduced rising motion. The result is the same, however, for then $-w'$ is coupled to $-u'$. The product in both cases ($+w' \cdot +u'$ and $-w' \cdot -u'$) is positive, so, following the same argument as before for the eddy transport due to u'v', we can say that zonal momentum is transported upward near the equator.

Now, identifying what kind of wave or combination of waves couples u, v, and w in the proper phase relationship and with the proper period will take further study. The simplest picture would have the upper atmosphere vortex spinning like a global scale taffy pull with a single pressure bulge centered on the equator and moving around the planet with a period close to that of the 4 day UV cloud motions.

Clearly, the next most important step is to extend the velocity field measurements to earlier and later times to determine the period and amplitude of the velocity fluctuations and to see if the correlation in the measurements is maintained. We cannot go beyond day 40 because the time resolution of the Mariner 10 data was cut to 8-12 hours and is not suitable for small scale motion measurements. Consequently, it would appear that we must concentrate on day 38, and possibly 37 (as close as our existing navigation scheme will permit before it breaks down). Another area of study will be an intensive look at the characteristics of other wavelike features on Venus -- the bowlike waves, circumequatorial belts, etc. -- and at vertical structure of the UV clouds. We must determine what influences the velocity fields, where, when, and how much. This task will also require detailed analysis of the higher resolution Mariner 10 imagery.

ACKNOWLEDGEMENTS

The author wishes to thank V. E. Suomi for suggesting the search for eddy transport and Sanjay Limaye for navigating the images. The manuscript was typed by Rosanne Koehler.

This research was supported by NASA Grant #NGR-50-002-189 and JPL Contract #953034.

BIBLIOGRAPHY

Krauss, Robert J.; 1976: "UV Cloud Motions on Venus From Mariner 10 Images," SSEC Report on Atmospheric Dynamics of the Planets, Vol. 1.

Suomi, Verner; 1975: "Cloud Motions on Venus," in The Atmosphere of Venus, NASA SP-382, p. 42-58.

A NORMALIZED VIEW OF VENUS

Sanjay Limaye, Verner Suomi

ABSTRACT:

It is now known that Venus has a fairly thick and massive atmosphere, the 10 mb level occurring at a height of about 80 km above the surface. Mariner 10 television observations indicate that the single scattering albedo for Venus is about 0.920 in the ultra-violet region of the spectrum, and like all thick planetary atmospheres should, the cloud cover of Venus behaves almost like a Lambertian reflector. Based on this knowledge, a few Mariner 10 images have been "normalized" to a standard scattering geometry both using Lambert's law of diffuse reflection and also an exact solution by Chandrasekhar (1950) involving his H-functions.

As expected, a cosine corrected brightness is an overestimate for large zenith angles, otherwise the visual appearance is similar to the solution using H-functions.

The most striking feature of the normalized images is the bright polar ring or cap beyond about 50° latitude circle and a sharper brightness frequency distribution.

INTRODUCTION:

This paper deals with "normalization", of several Mariner 10 UV images of Venus based on the assumption of diffuse reflection by the cloudy atmosphere such that every point on the planet is viewed in the image with the same scattering geometry. This facilitates a comparison of the absolute brightness of the UV features in various regions of the sunlit planet. The terrestrial experience is that in a normalized image the general rule of thumb that brighter clouds are optically thicker can be quantified (Martin, et.al., 1975). The question of the ultra-violet contrasts in the atmosphere of Venus is still unsettled and it may be premature to postulate a general yardstick between the brightness of UV features and their optical and/or geometric thickness. Nevertheless, the sun and viewing angle normalized images show up some interesting characteristics, and as described later, these are being used for UV feature tracking.

It was pointed out by Huggins (1867) that optically thick planetary atmospheres would behave roughly like Lambertian reflectors. This was confirmed by observations of Mars from Mariner 9 (Leovy, et.al., 1972) even though the Martian atmosphere is thin compared to that of Venus.

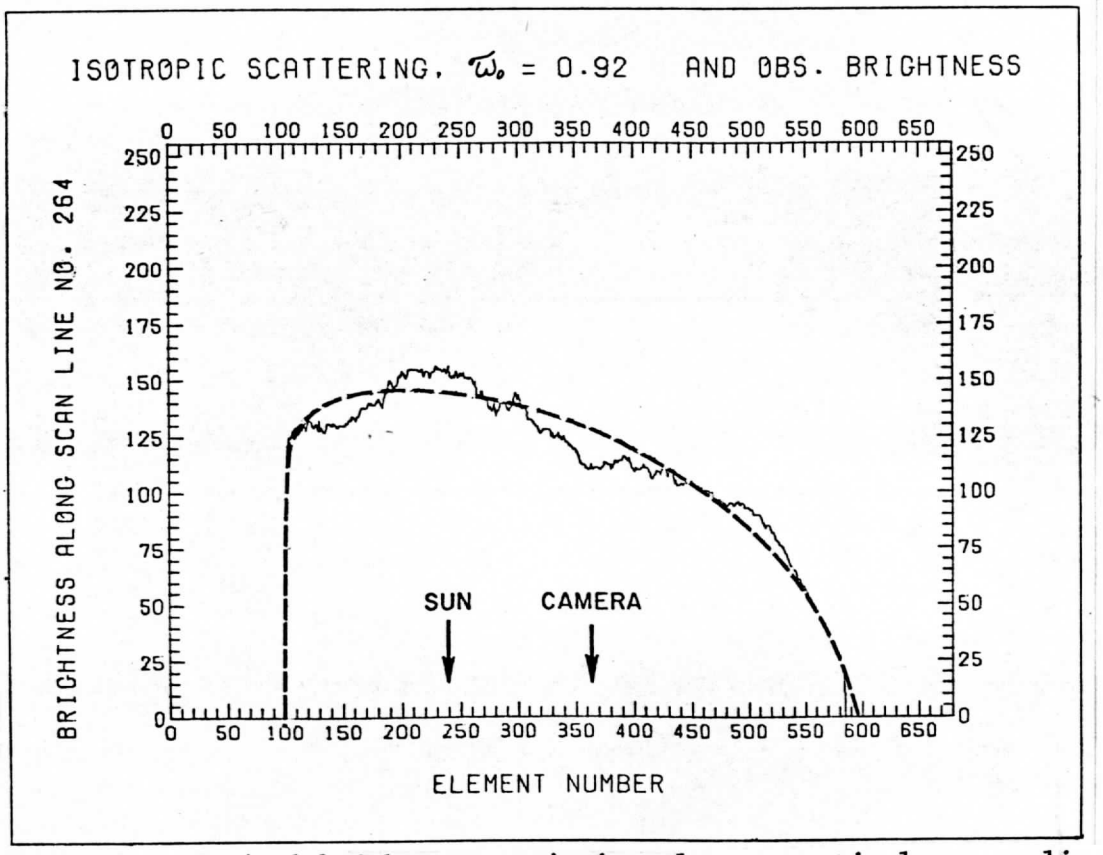

Figure 1a Typical brightness variation along a particular scan line. This scan passes through both the sub-solar point (indicated by SUN) and the sub-spacecraft point (indicated by CAMERA) on the planet. The dashed line is the H-function solution.

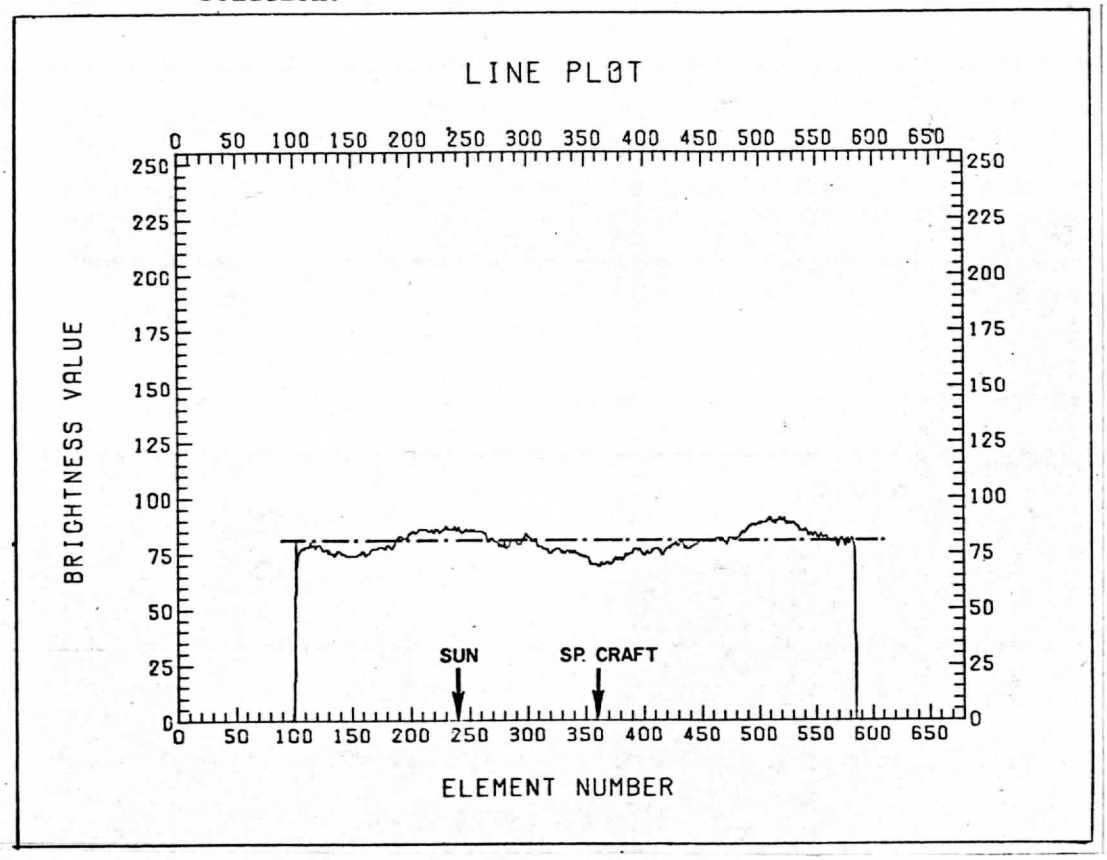

Figure 1b Variation along the same scan line as in Figure 1a, but after brightness normalization.

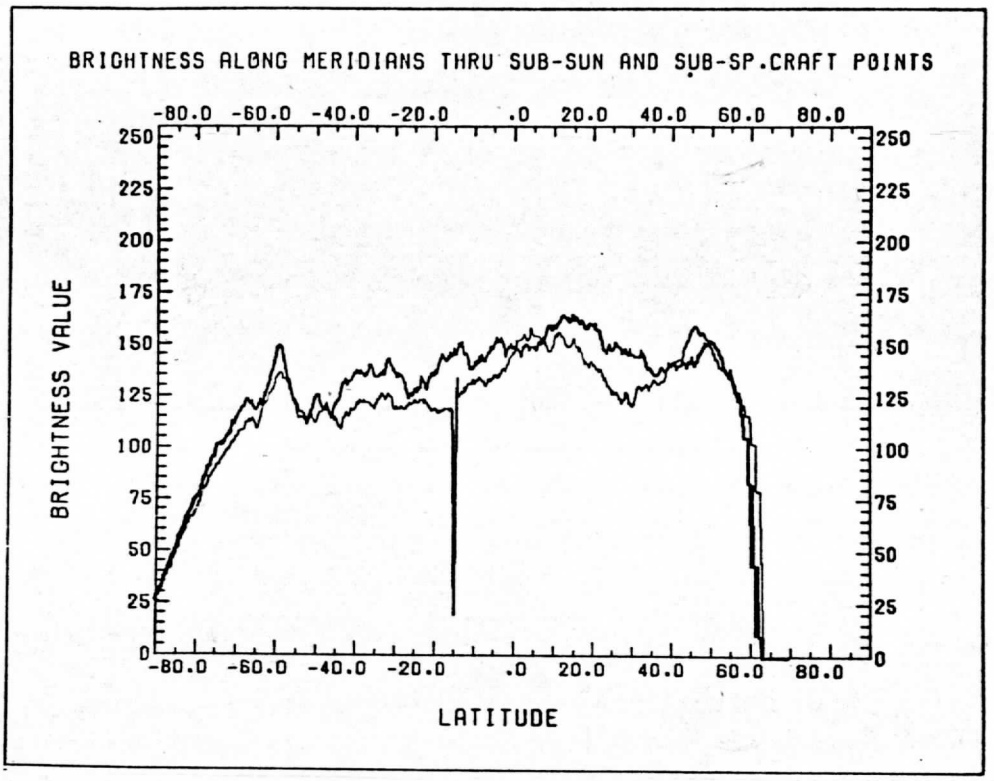

Figure 1c Brightness variation along two meridians, illustrating relative contrasts. The dip in the one trace at -15° latitude is a reseau mark in the image.

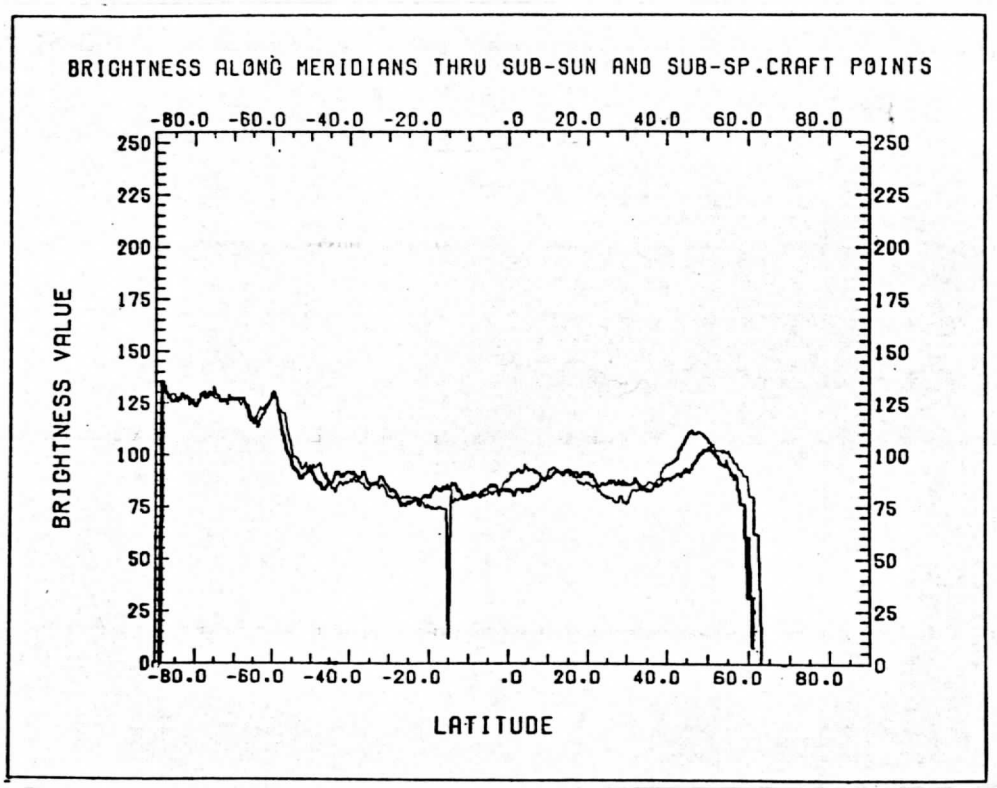

Figure 1d In the normalized images, the variation from one meridian to another is minimized and the bright polar regions stand out much more clearly.

Horak (1950) reported that the visual and photographic curves for Venus can be represented by known laws of diffuse reflection for phase angles less than 130° with isotropic scattering and a single scattering albedo $\tilde{\omega}_o = 0.950$. While not of particular importance here, it is interesting to note that the limb darkening in yellow light can also be represented fairly well by isotropic scattering again with $\tilde{\omega}_o = 0.950$ and that the polarization of the atmosphere of Venus is not due to Rayleigh scattering (Horak, 1950).

Hapke (1975) has found similar results from observations of the planetary limb from Mariner 10. In particular, a single scattering albedo $\tilde{\omega}_o$ between 0.910 and 0.930 plus isotropic scattering agrees very well with the observations, better than results from Mie scattering or Raleigh scattering.

Using a mean single scattering albedo of 0.925 in the law of diffuse reflection, it is possible to normalize a Mariner 10 Venus image to a standard sun-planet-camera geometry for every point on the planet so that the brightness variations in a normalized image represent actual physical characteristics of the features alone and are not due to different solar and spacecraft (camera) zenith angles.

2. Image Normalization

As Figure 1a shows, the intensity along a particular image scan line is similar to the cosine response characteristic of a Lambertian surface. The scan line shown in Figure 1 passes through both the sub-solar and the sub-spacecraft point for the particular image (FDS #64897). The departures from the curve are the Venusian features. It should be mentioned here that the image was corrected for geometric distortion as well as for photometric deviations at the Image Processing Laboratory (IPL) of Jet Propulsion Lab.

Mariner 10 images of Venus show a large number of atmospheric features in the ultra-violet, though the contrast is generally fairly small. In particular, one sees a few recurrent bow like features which seem to move at approximately the same speed as other features without drastically changing their shape or size. As will be seen in the "raw" sequence in Figure 3, there are certain features which show a marked change in their overall brightness as they move across the planet. Since the solar and camera zenith angles vary substantially for a certain feature as it moves across the planet disc, it is not immediately clear whether the observed changes in the overall brightness of a feature are real and whether they depict physical changes in the feature or whether they are simply due to a change in illumination and viewing angles. The normalization of a sequence of Mariner 10 Venus images would ensure that any changes in the

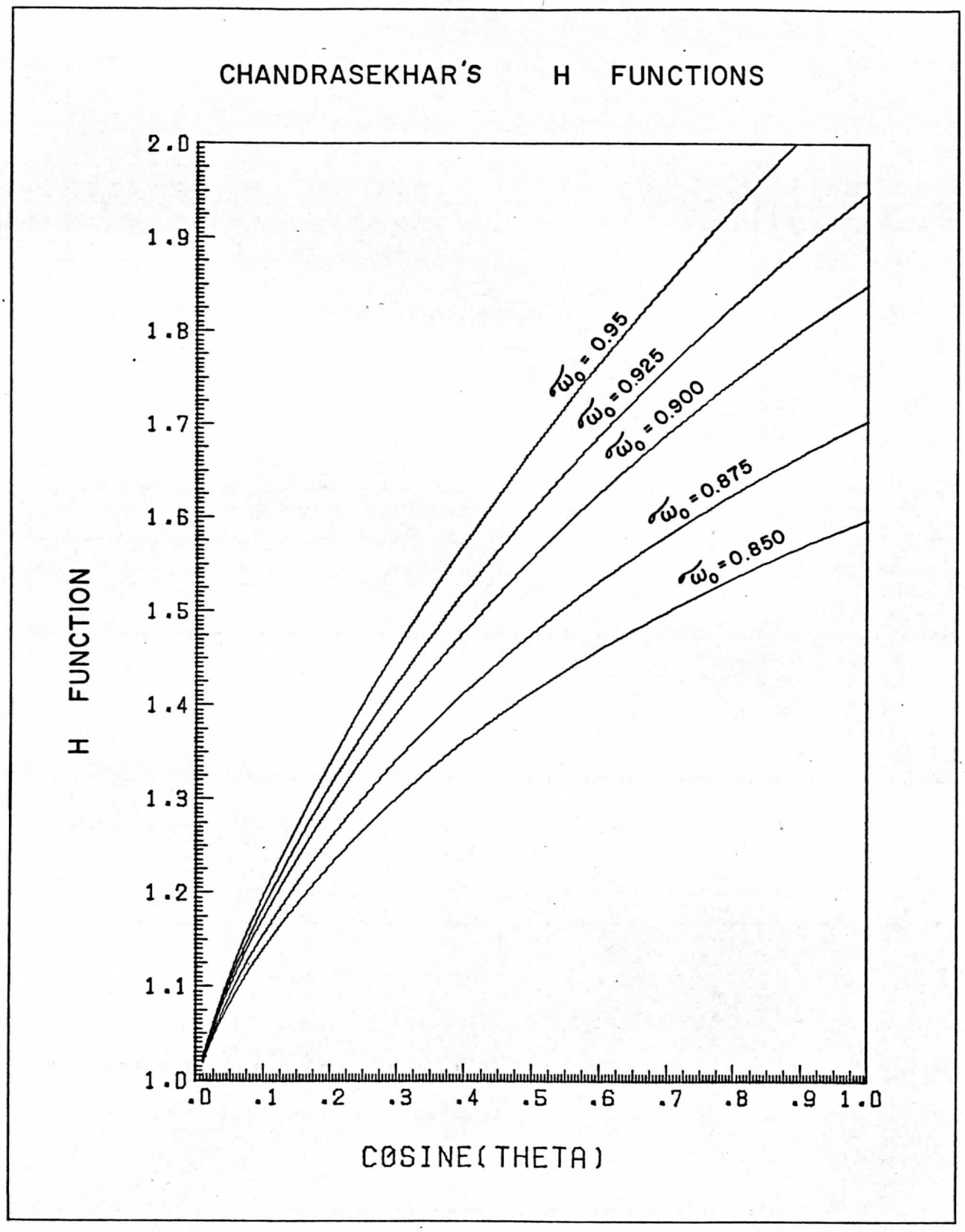

Figure 2 H function values for $\tilde{\omega}_o$ = 0.95, 0.925, 0.9, 0.875 as a function of cosine of angle (from Chandrasekhar, 1950).

brightness of a feature as it moved across the planet would be due to actual physical changes in the feature and not be due to changing scattering geometry. Thus, standardizing every point on the planet to the same sun/camera geometry enables us to gain information about the properties of the features themselves.

3. Normalization Procedure

Chandrasekhar (1950) has obtained the exact solution for the case of diffuse reflection from a plane parallel atmosphere as follows:

$$I(o,\mu) = \frac{\tilde{\omega}_o F}{4\pi} \left(\frac{\mu_o}{\mu_o+\mu}\right) H(\mu)\ H(\mu_o) \qquad (1)$$

Where I is the emergent intensity, πF is the flux incident on the planet, $\mu_o = \cos\zeta$ is the cosine of the solar zenith angle, and $\mu = \cos\eta$ is the zenith angle of the camera. The isotropic scattering phase function $P(\cos\Theta) = \tilde{\omega}_o$ has been used, where in $\tilde{\omega}_o$ is the single scattering albedo. $H(\mu)$ and $H(\mu_o)$ are Chandrasekhar H-functions, and tabulated values are available (Chandrasekhar, 1950). Figure 2 shows the values of the $H(\mu)$ for various values of the single scattering albedo $\tilde{\omega}_o$.

For normalizing an image, we introduce an arbitrary scaling constant $X(\lambda,\phi)$ to describe the light and dark features seen on the planet in Equation (1):

$$I_{OBS} = \frac{\tilde{\omega}_o F}{4\pi} \left[\left(\frac{\mu_o}{\mu_o+\mu}\right) H(\mu)\ H(\mu_o)\right] X(\lambda,\phi). \qquad (2)$$

So that $\frac{F}{4\pi} X(\lambda,\phi)$ is the normalized brightness for the point (λ,ϕ) on the planet, given by:

$$I^* = \frac{F}{4\pi} X(\lambda,\phi) = I_{OBS} \frac{(\mu_o+\mu)}{\tilde{\omega}_o \mu_o\ H(\mu)\ H(\mu_o)}. \qquad (3)$$

One then needs to know the single scattering albedo $\tilde{\omega}_o$, and the two zenith angles ζ and η for the sun and spacecraft in order to obtain the normalized brightness for every point.

To be able to compute $\mu_o = \cos\zeta$ and $\mu = \cos\eta$ the image has to be navigated first (i.e. to obtain a transform between the image plane coordinates of a point P (ℓ,e) where ℓ is the scan line number and e the sample element number in that scan line to the absolute position P (λ,ϕ) in latitude and longitude on the planet):

$$T(\ell,e,\lambda,\phi)\ P(\ell,\ e) = P(\lambda,\phi).$$

The coordinate transformation function $T(\ell,e,\lambda,\phi)$ can be obtained from a knowledge of the spacecraft orbit parameters and the location of the sub-solar point and the sub-spacecraft point with the crucial constraint that the sub-solar point and the sub-spacecraft point lie on the same image scan line. A more detailed description of image navigation is given by Phillips and Limaye (1976).

The navigation scheme enables us to compute the latitude and longitude (λ,ϕ) corresponding to a line-element point (ℓ,e) and its Cartesian co-ordinate (x,y,z) as:

$$x = R\cos\phi\cos\lambda$$
$$y = R\cos\phi\sin\lambda$$
$$z = R\sin\phi$$

Similarly the Cartesian coordinates of the sub-solar point(s) and the sub-spacecraft point (sat.) are:

$$x_s = R\cos\phi_s\cos\lambda_s$$

$$y_s = R\cos\phi_s\sin\lambda_s$$

$$z_s = R\sin\phi_s, \text{ and}$$

$$x_c = R_{sat.}\cos\phi_c\cos\lambda_c$$

$$y_c = R_{sat.}\cos\phi_c\sin\lambda_c$$

$$z_c = R_{sat.}\sin\phi_c.$$

The three components of a vector from the point (ℓ,e) on the planet to the spacecraft are then:

$$x_v = x_c - x$$

$$y_v = y_c - y$$

$$z_v = z_c - z.$$

The solar zenith angle for that point (ℓ,e) is then given by:

$$\cos\zeta = (xx_s + yy_s + zz_s)/\{x^2 + y^2 + z^2\}^{1/2}\{x_s^2 + y_s^2 + z_s^2\}^{1/2} \qquad (4)$$

and the spacecraft zenith angle by:

$$\cos\eta = (xx_v + yy_v + zz_v)/\{x^2 + y^2 + z^2\}^{1/2}\{x_v^2 + y_v^2 + z_v^2\}^{1/2}. \qquad (5)$$

The H functions for these zenith angles are then computed by a four point Lagrangian interpolation scheme from the tabulated values given by Chandrasekhar (1950).

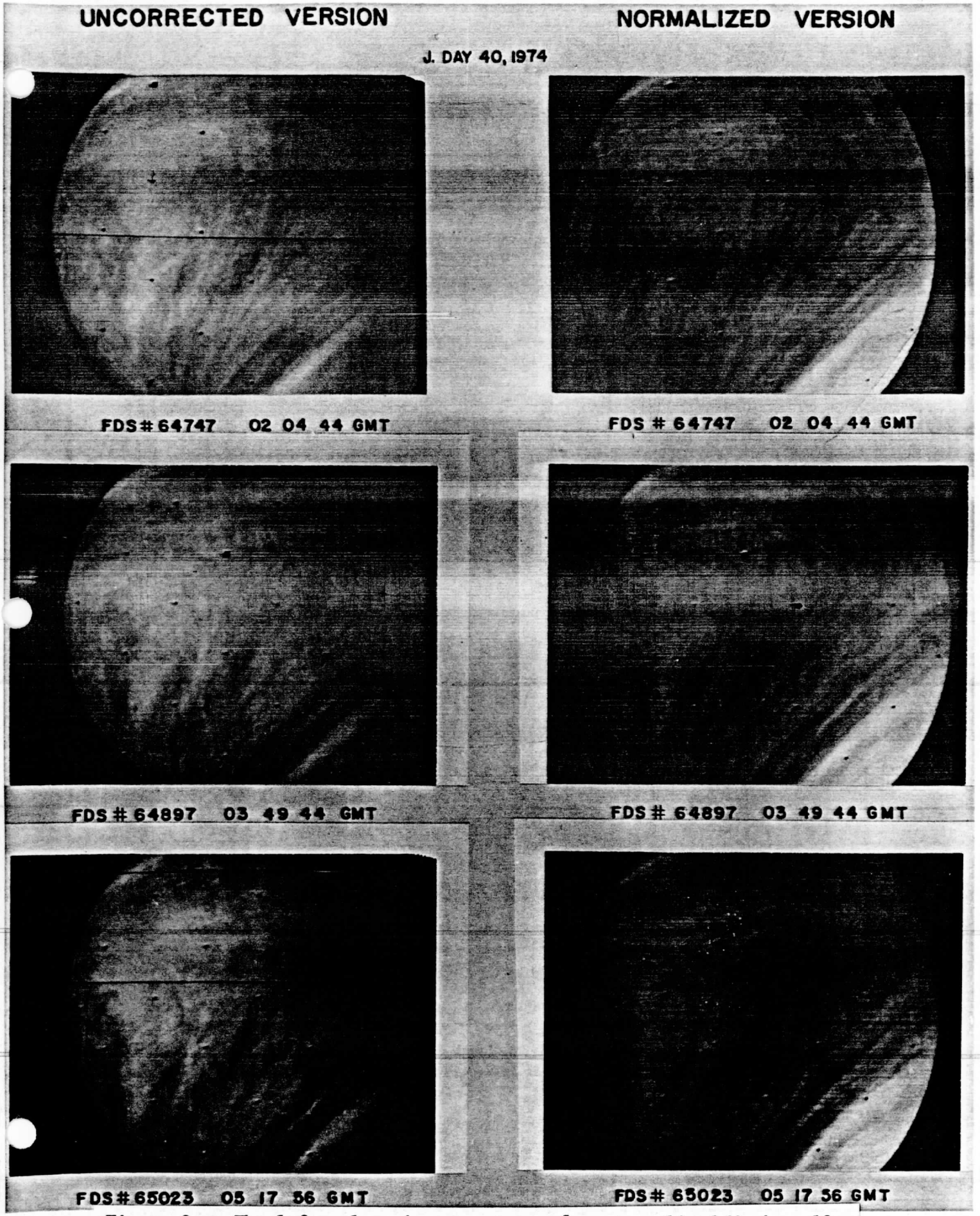

Figure 3 The left column is a sequence of un-normalized Mariner 10 UV images of Venus. In the right column are corresponding normalized versions. The exposure times are mentioned for

UNCORRECTED VERSION

NORMALIZED VERSION

J. DAY 40, 1974

FDS # 65179 07 07 08 GMT

FDS # 65179 07 07 08 GMT

FDS # 65343 09 01 56 GMT

FDS # 65343 09 01 56 GMT

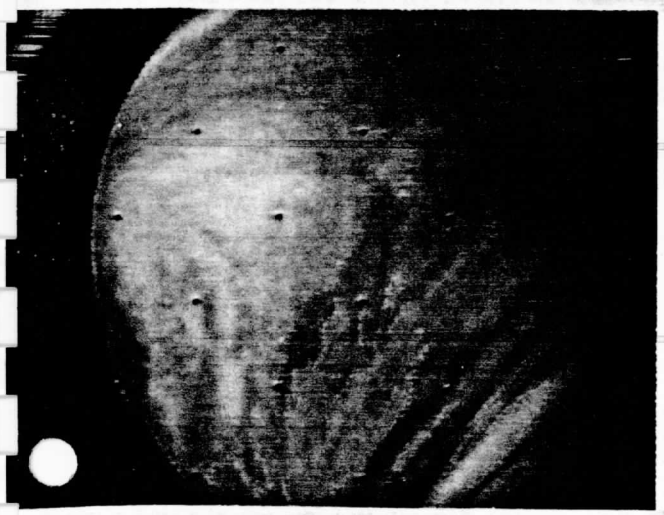

FDS # 65473 10 32 56 GMT

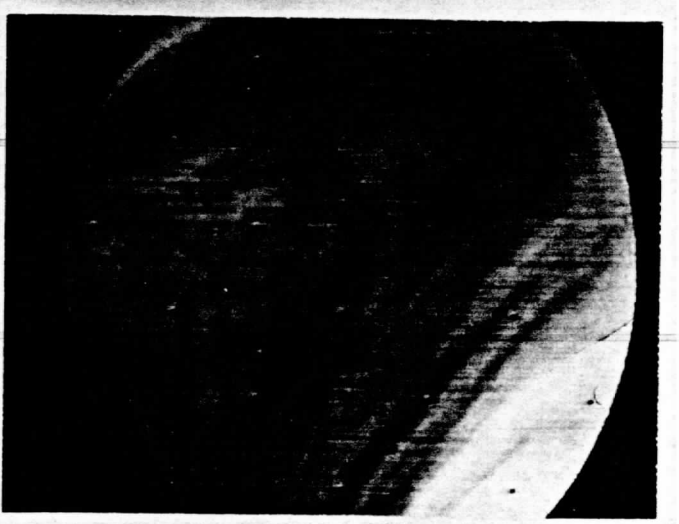

FDS # 65473 10 32 56 GMT

UNCORRECTED VERSION

NORMALIZED VERSION

J. DAY 40, 1974

FDS# 65623 12 17 56 GMT

FDS# 65623 12 17 56 GMT

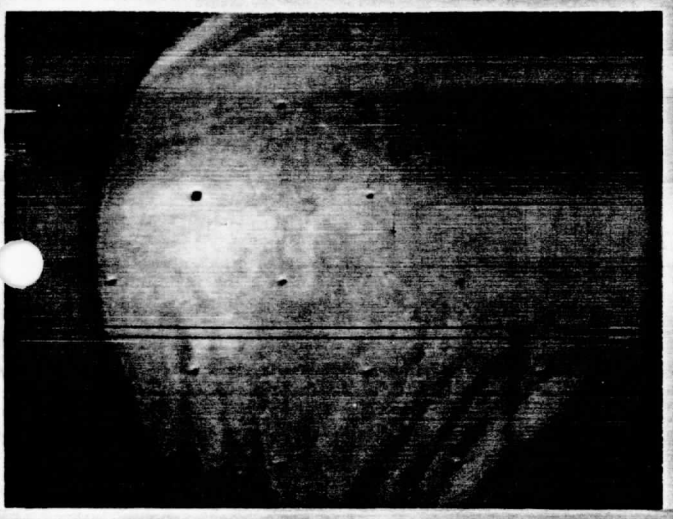

FDS# 65787 14 12 44 GMT

FDS# 65787 14 12 44 GMT

FDS# 65923 15 47 56 GMT

FDS# 65923 15 47 56 GMT

UNCORRECTED VERSION

NORMALIZED VERSION

J. DAY 40,1974

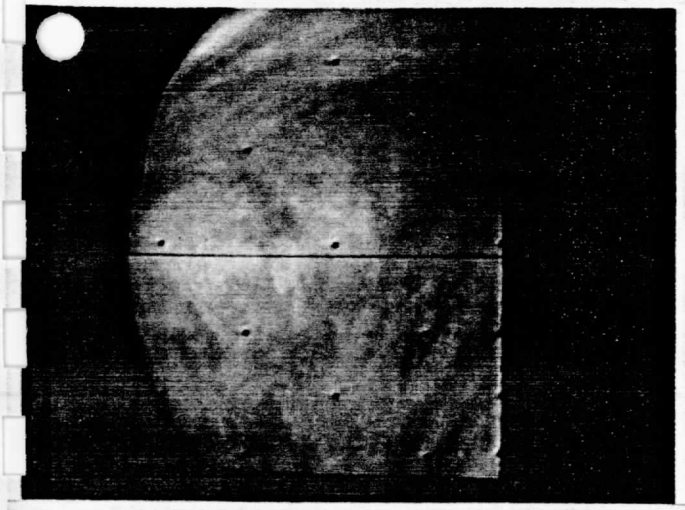

FDS# 66067 17 28 44 GMT

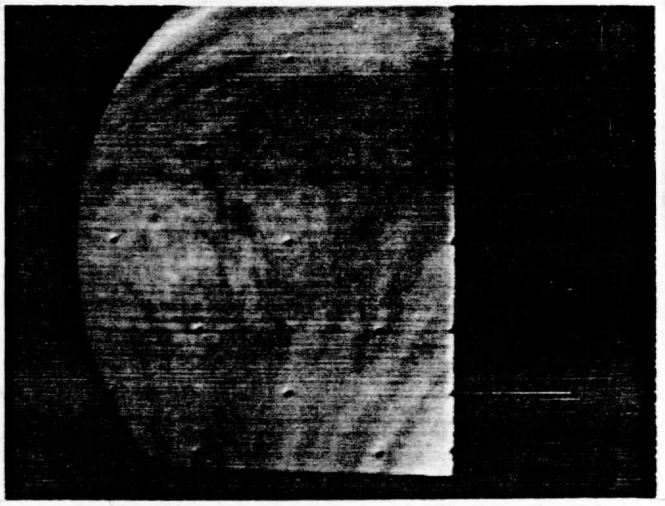

FDS# 66067 17 28 44 GMT

FDS# 66223 19 17 56 GMT

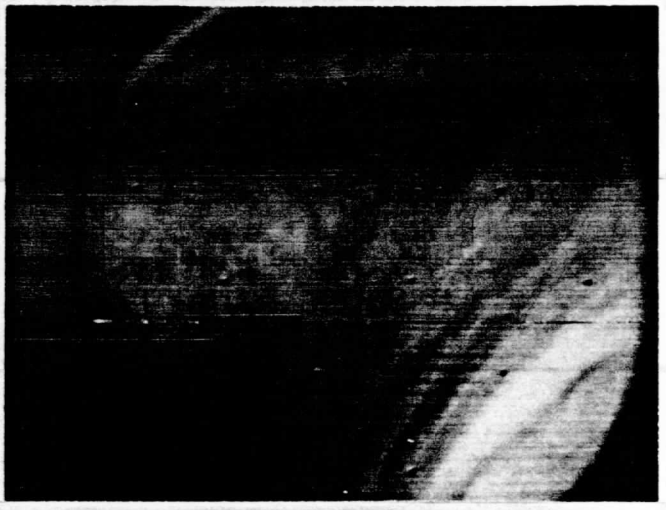

FDS# 66223 19 17 56 GMT

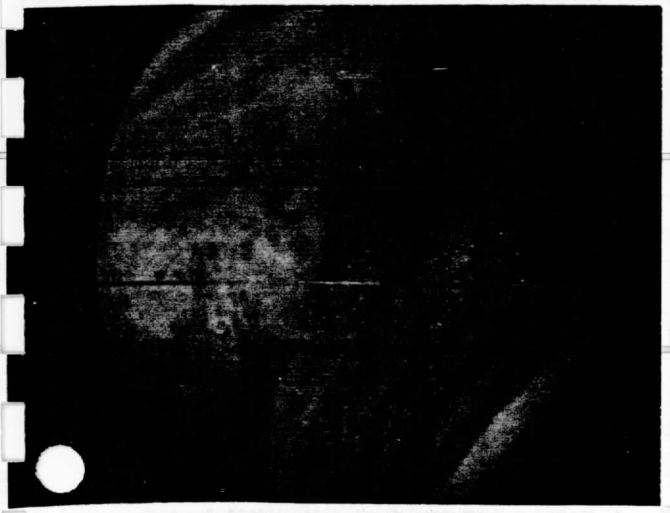

FDS# 66380 21 07 50 GMT

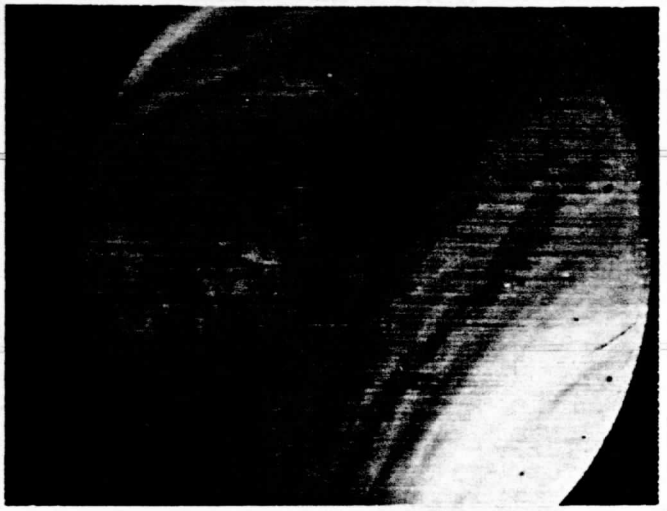

FDS# 66380 21 07 50 GMT

a)

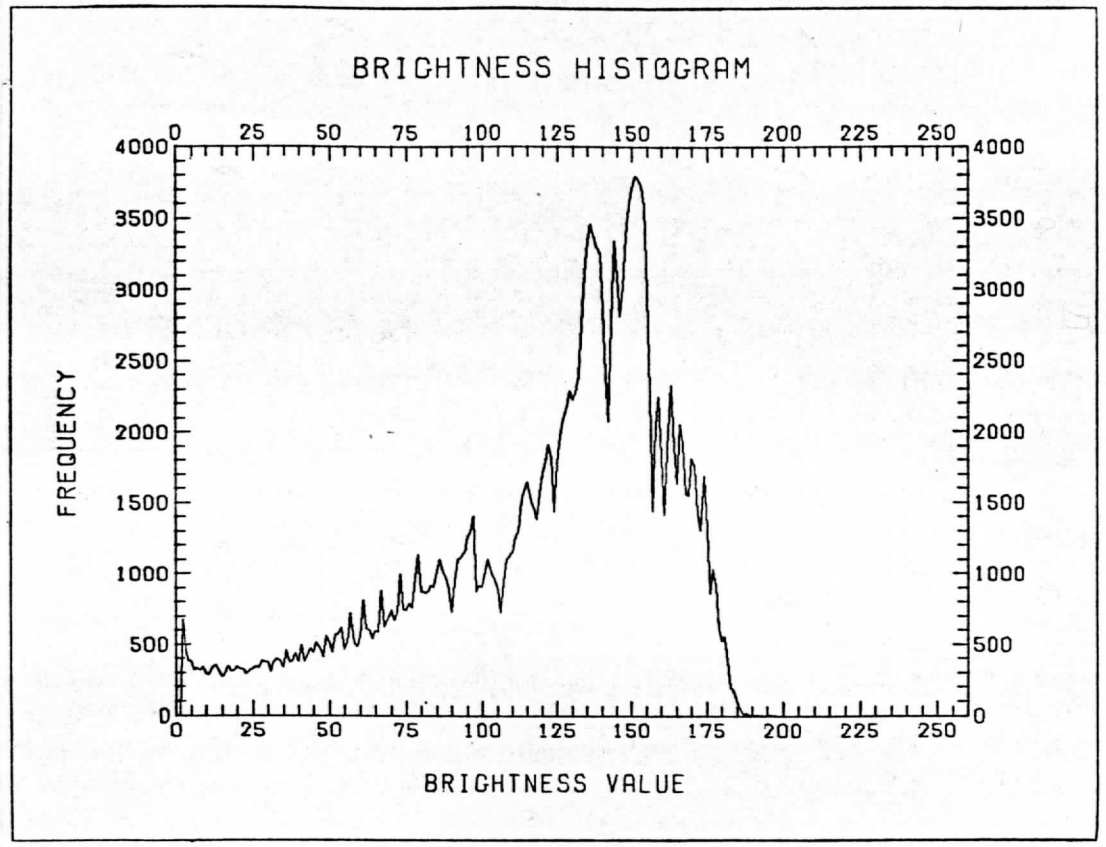

Figure 4 Brightness digital number histograms for a un-normalized image (a) and its normalized version (b). The second smaller peak in the normalized version is due to the enhanced brightness in the polar region.

b)

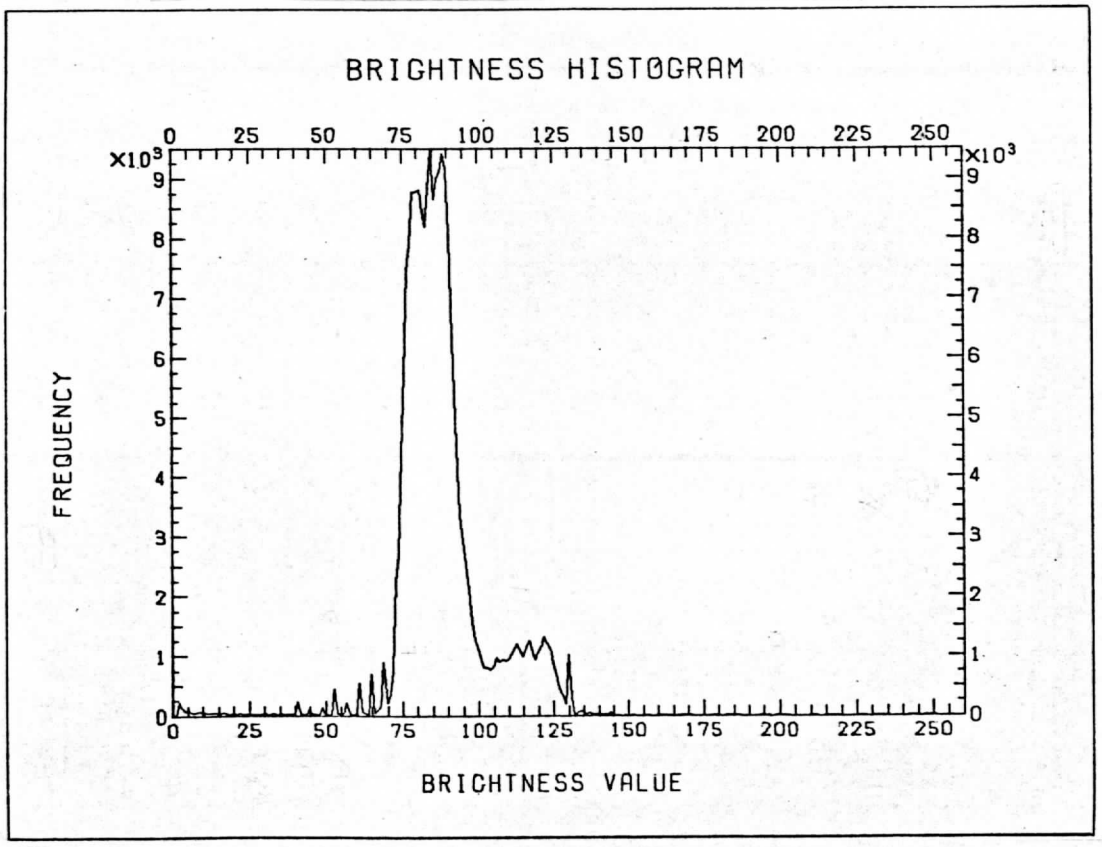

4. Discussion

Figure 3 (left) shows a "raw" photometrically and geometrically correct image. At the right is a corresponding normalized version. These images, and others not shown, have been normalized to the same maximum brightness level 255, so that brightness variations in the normalized sequence are indicative of actual changes in the scattering properites of the features.

Figure 4 shows a comparison of brightness frequency histograms for the original and normalized versions of a typical Mariner 10 UV image. The normalized version shows a bi-modal distribution, the lower peak corresponding to higher brightness values is due to the brighter polar region. The median polar region brightness is about 50% higher than the equatorial value.

(a) Mean Brightness and RMS Deviation:

It is known that the contrast in the UV images of Venus is scale dependent (Hapke, 1975). On a global scale when the phase angle is small, the contrast of the whole disc depends on the distribution of bright and dark features which move across the disc at speeds between 80 and 130 m/s (Suomi, 1975). Any large spatial dependence of bright and dark features in the upper atmosphere should thus show up in a time series of pictures monitored for contrast. Figure 5 shows variation of contrast c, the ratio of RMS brightness number deviation σ and the mean brightness number $\bar{B}$ for eleven UV images on Julian Day 40. The solar zenith angle at the sub-spacecraft point decreased from 29.12° in the beginning of the sequence to 28.16° at the end of the sequence. Two images were partial images. The average value of c for the remaining nine images in the sequence is 0.332 and the maximum deviation in this sequence is less than 1%. It can thus be concluded that given the performance reliability of the MVM-73 vidicons the planet did not show any large change in the spatial distribution of bright and dark features over periods of about a day. As seen in Figure 6 the average brightness of the visible disc also did not change greatly within the accuracy limits of the vidicon.

The dashed lines in figures 5 and 6 show variation of c and $\bar{B}$ for normalized versions of the images. The striking fact here is the much lower value of c for the normalized versions.

The reduced value of c is due to the removal of the monotonic decrease in observed brightness due to increasing solar and vidicon zenith angles as is evidenced in Figure 1. The way the normalization is done enhances the contrast when the normalizing factor is greater than unity and reduces the contrast when it is smaller than unity (Equation 2).

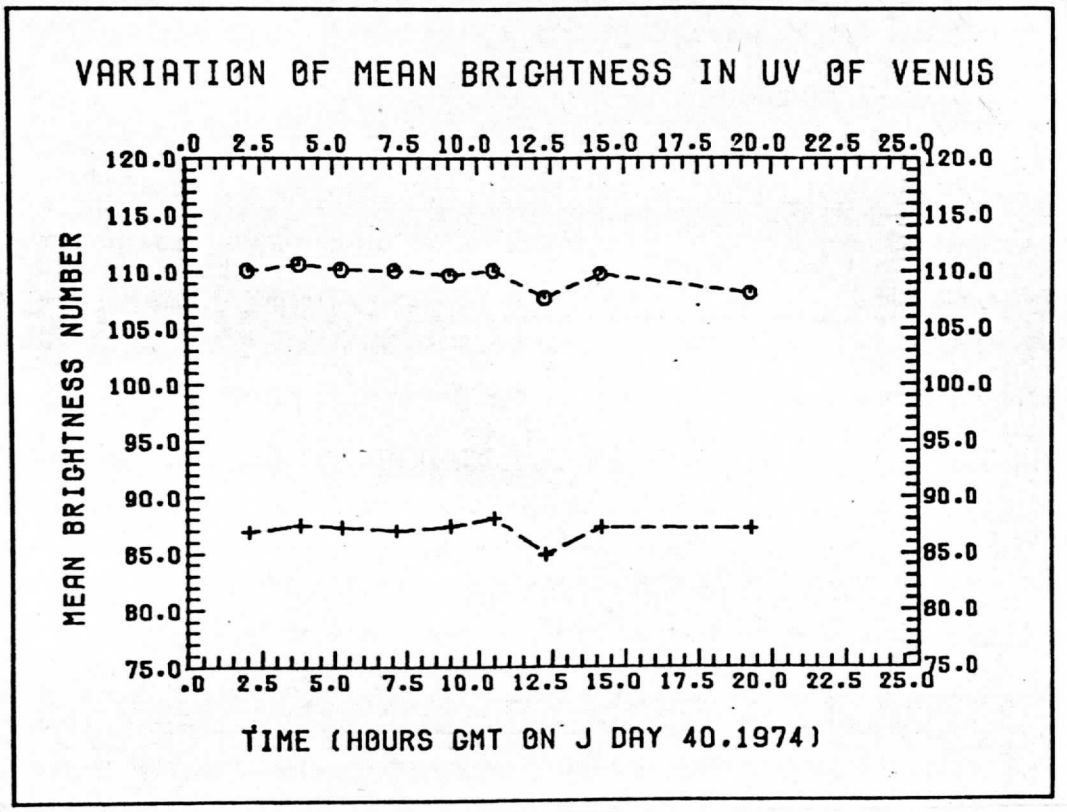

Figure 5 Variation of the ratio of the standard deviation of the brightness digital number σ and the average brightness digital number $\bar{B}$. Solid line - un-normalized version, dashed line - normalized version.

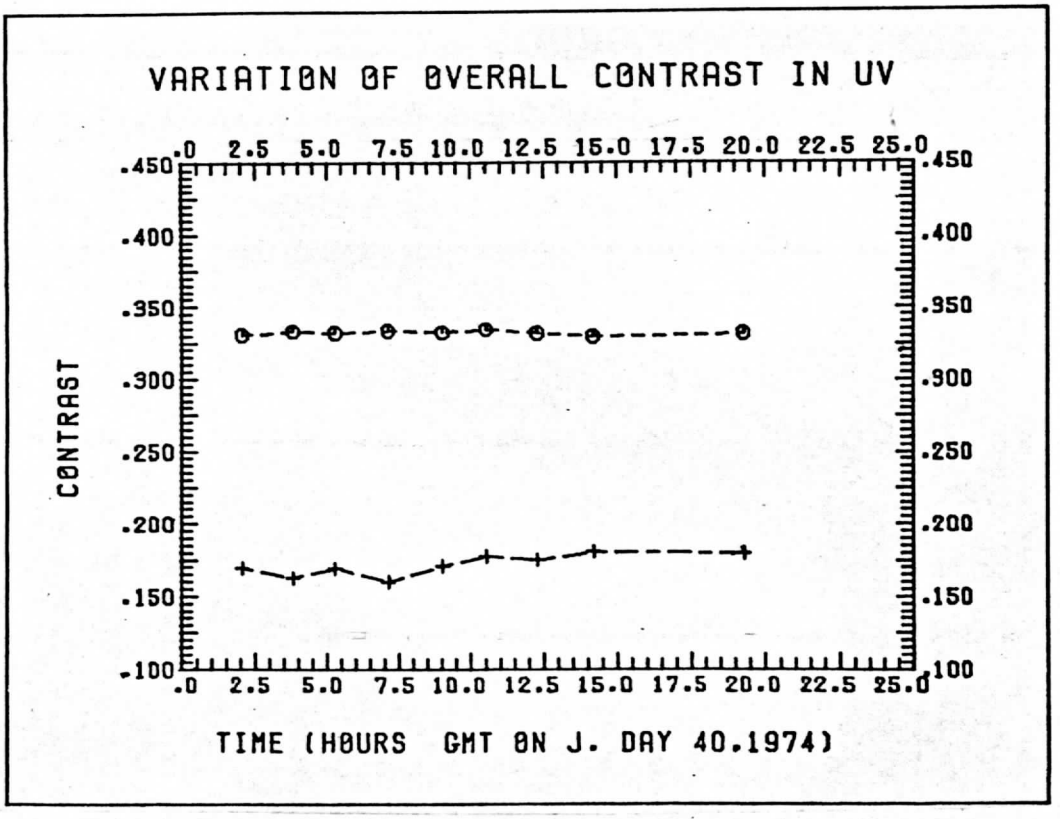

Figure 6 Variation of the average brightness digital number for images in the sequence. Solid line is for the un-normalized version and dashed line for the normalized version.

(b) The Bright Polar Region:

The edge of the south polar cloud is uniformly around 52° latitude. One can also see an indication of a similar bright polar cloud in the northern hemisphere at about the same latitude. Unfortunately, the flyby trajectory of Mariner 10 was unsuitable for imaging the north polar region so that no conclusion about the north polar cloud can be drawn. Dolfuss (1974) has examined earth based photographs of Venus over a long period and reports a variability in the appearance of the polar clouds. They seem to appear and disappear periodically, and all four cases - (i) both the polar clouds (ii) northern polar cloud only (iii) southern polar cloud only and (iv) no polar cloud, have been observed. From the observation of the bright patch in the northern hemisphere, it is probable that Venus had both polar clouds at the time of Mariner 10 encounter.

The high contrast between the polar cap and the sub-polar region is indicative of different atmospheric scattering conditions in those regions. The increase in the brightness of the polar cloud can be seen Figure 1d which is plot of brightness along a meridian. At present, there is no conclusive evidence regarding the constituents in the bright polar cap responsible for scattering ultra-violet light, and this enhanced brightness is a puzzle.

There is possibility that the thermal structure may reflect the existence of the polar caps. The infrared radiometer on-board the Mariner 10 made one swath across the planet in the northern hemisphere, and in the 45μ band the departure from the linear limb darkening law is maximum at the longitude of closest approach to the northern polar ring (Chase, et.al., 1974). The deviation from the linear limb darkening law decreases sharply as the radiometer field-of-view moves away from the suspected position of the polar ring (see Figure 7, reproduced from Chase et.al., Science, (183), 29 March 1974). It is quite possible that the associated higher brightness temperature is related to the existance of the northern polar ring. The southern polar ring counterpart seems to be a permanent feature of the UV images during the duration of Mariner 10 coverage.

Calculations by Ingersoll and Orton (1974) about the sun-associated function indicate that at least on the night side, the brightness temperature at about 50° latitude is approximately 7°K lower than at the equator. There are indications from the symmetry of their diagrams that this may be the case on the day-side also. It is possible that this brightness temperature corresponds to the "cloud top" temperatures and that such cloud tops are seen as UV features in the UV images. As the above authors point out, it is difficult to resolve the observed brightness temperature variations into horizontal and vertical components from available data. It is known that at least in the lower latitudes, the atmosphere is very stable with a sub-adiabatic lapse rate of 4-5°K/KM. (Howard et.al., 1974), so that lower cloud tops in polar regions with a comparable meridional temperature decrease could give rise to brightness temperatures in polar regions only a few degrees lower than in the equatorial regions.

It is possible then that this polar region of enhanced brightness has a lower "cloud top" than its equatorial counterpart with only a small

75%

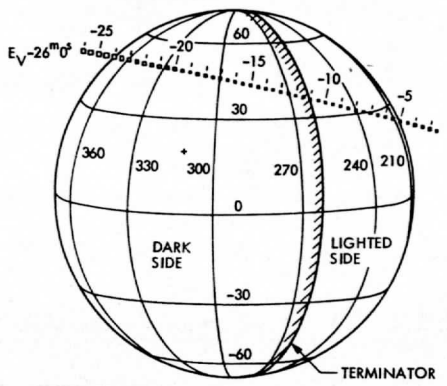

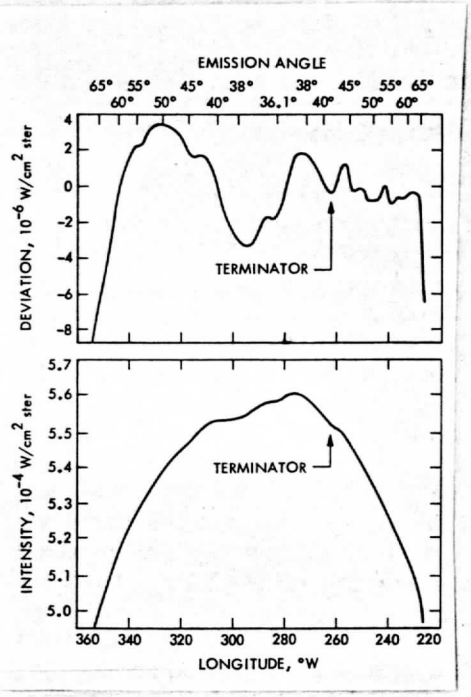

Figure 7

On left hand side the swath of the radiometers field of view across the disk of Venus is shown. The times indicated by the trace are given in minutes before the closest approach of Mariner 10.

On the right (bottom) the 45 μm intensity observed in the single swath across the disk of Venus and (top) the deviation from the linear limb law ($I_{45}(\mu) = I_{45}(0)\ (0.76 + 0.24\mu)$) is shown as a function of latitude. A large deviation from the limb darkening is seen at the point of closest approach to the suspected position of the northern polar cap.

This figure has been reproduced from Chase et.al. 1974.

decrease in its brightness temperature. If this is the case then perhaps there is more carbon dioxide gas above the polar cloud tops than over the rest of the planet and spectroscopic observations of carbon dioxide line strengths with sufficient spatial resolution should be able to detect it.

From ground based spectroscopic measurements Young, et.al. (1973) find that while the correlation between the carbon dioxide abundance over the cloud tops and dark and light UV markings is not obvious, there is an indication that there is more carbon dioxide above the brighter areas. If this is true this lends support to the hypothesis that the cloud tops in the polar regions are lower than in the equatorial regions and the brightness temperature in those regions is lower due to a north-south horizontal temperature gradient - large enough to offset the higher cloud top temperature due to lower cloud top heights. The enhanced polar brightness could be due to increased scattering in the UV.

At this point it is interesting to note that the zonal component of the motion of UV features as revealed by Mariner 10 images shows a maximum somewhere between 45° and 50° latitude in the southern hemisphere (Suomi, 1975). Poleward of that the zonal component is smaller and must vanish at the pole. The latitudinal shear of such a profile is quite large and it is possible that shear instability causes an increase in the vertical component of vorticity which leads to large scale "cloudiness" in the polar regions, with cloud tops occuring much lower in altitude due to a meridional temperature gradient.

Under this hypothesis then, the upper atmospheric dynamics and the large scale polar-equatorial brightness difference are very closely related. The cloud tops in latitudes higher than about 50° are hypothesized to occur at lower altitudes to explain their enhanced brightness by increased scattering in the atmosphere overlying them. In order to be consistent with only a weak meridional gradient of sun-associated brightness temperature, there has to be a compensating isobaric or isohypsic meridional temperature gradient, assuming non-isothermal, sub-adiabatic lapse rates in that part of the atmosphere. Needless to say, under steady state conditions the meridional heat transport must be such as to be able to maintain the required meridional thermal contrasts. Future observations particularly from the Pioneer Venus Orbiter and multiprobe missions would be valuable indeed.

Lastly, it is possible to place an upper limit on the possible altitude difference between the equatorial and polar cloud tops if one assumes a certain meridional temperature variation. For example, it can be shown that for a cosine decrease of temperature with latitude, the maximum equator to pole temperature contrast that can be maintained through global radiative balance is about 70°K. For an average lapse rate of about 5°K/km above 65 km altitude everywhere, and noting that the surface polar temperature seems to be at least as high, if not higher, than the equatorial temperature from microwave measurements (Sinclair, et.al., 1971), the polar cloud tops can therefore only be a maximum of about 14 km lower than the equatorial cloud tops. However, the actual temperature difference is probably much smaller as well as the cloud top altitude difference.

5. Summary & Recommendations

A sequence of Mariner 10 Venus images have been normalized according to an exact solution obtained by Chandrasekhar (1950) for the problem of diffuse reflection from a semi-infinite plane parallel atmosphere. The isotropic scattering phase function with single scattering albedo of 0.920 was used for normalization. A sequence of images normalized in this fashion helps identify physical changes in the UV features seen in the image sequence by isolating them from effects of varying scattering geometry.

The south polar cap stands out as the brightest part of the image with no significant contrast. The sub-solar region is relatively dark. The high brightness of the polar cap is suggestive of significantly different atmospheric conditions.

It is strongly recommended that at least one of the atmospheric probes from the next Pioneer mission to Venus be launched so as to probe the atmosphere in the polar cap region. Temperature profiles obtained through radio occultations from the Venus orbiter would give valuable information about the 3-D thermal contrasts in the atmosphere.

Maps of carbon dioxide abundances with a high enough spatial resolution might prove to be valuable in understanding the UV contrasts on Venus, in particular the pole-equator differences. Thermal infrared maps will also be useful in finding an answer to this riddle.

Acknowledgements

The authors express thanks to the people at the Image Processing Lab (at JPL, Pasadena, Cal.) for providing photometrically corrected pictures. We are thankful to Dr. J. H. Joseph and Mr. Fred Mosher, both at the Dept. of Meteorology at the University of Wisconsin, Madison, and to Mr. Robert Krauss for valuable suggestions and discussions. Lastly, we appreciate the programming help of Messrs. Eric Smith, Dennis Phillips, and Ralph DeDecker.

This research was supported by JPL Contract #953034 and by NASA Grant #NGR-50-002-189.

REFERENCES

Chandrasekhar, S., 1950: Radiation Transfer Theory, Clarendon Press, Oxford, 381 pp.

Chase, S. C., E. D. Miner, D. Morrison, G. Munch, and G. Neugebauer, 1974: Preliminary Infrared Radiometry of Venus from Mariner 10, Science, (183), 1292-1293.

Dollfuss, A., 1974: Paper presented by the Howard Conference on Venus, Goddard Inst. of Sp. Studies, New York.

Hapke, B., 1975: Photometry of Venus from Mariner 10. To be published in Journ. Atmos. Sci.

Horak, H. G., 1950: Diffuse Reflection by Planetary Atmospheres, Astrophys. Journ., (112), 445-463.

Howard, H. T., G. L. Tyler, G. Fjeldbo, A. J. Kliore, G. S. Levy, D. L. Brunn, R. Dickinson, R. E. Edelson, W. L. Martin, R. B. Postal, B. Seidel, T. T. Sesplauleis, D. L. Shirley, C. T. Stelzried, D. N. Sweetnam, Z. I. Zygielbaum, P. B. Esposito, J. D. Anderson, I. I. Shapiro, and R. D. Reasenberg, 1974: Venus: Mars, Gravity Field, Atmosphere, and Ionosphere as Measured by the Mariner 10 Dual Frequency Radio System. Science, (183), 1297-1306.

Huggins, W. (1867): On the Spectrum of Mars, with some remarks on the Colour of that Planet. Month. Notice. Roy. Astron. Soc. (27), 178-181.

Ingersoll, A. P. and G. S. Orton, 1974: Lateral Inhomogeneities in the Venus Atmosphere: Analysis of Thermal Infrared Maps, ICARUS, (21), 121-128.

Leovy, C. B., G. A. Briggs, A. T. Young, B. A. Smith, J. B. Pollack, E. N. Shipley, and R. L. Wildey, 1972: The Martian Atmosphere: Mariner 9 Television Experiment Progress Report, ICARUS, (17), 373-393.

Martin, D. W., J. Stout and D. N. Sikdar, 1975: GATE Area Rainfall Estimation from Satellite Images. (See Appendix B by F. Mosher: Brightness Normalization of Satellite Images). A report on NOAA Grant 04-5-158-47.

Phillips, D. and S. S. Limaye, 1976: Navigation of Mariner 10 Images of Venus, Space Science and Engineering Center, University of Wisconsin, Madison, Annual Report.

Sinclair, A.E.C., J.P. Basart, D. Buhl and W.A. Gale (1972): Precision Interferometric Observations of Venus at 11.1 cm Wavelength. Astrophys. J., (175), 555-572.

Suomi, V. E., 1974: Mariner 10 Observations of Cloud Motions. Presented at the Conference on the Atmosphere of Venus, Goddard Institute for Space Studies, 15-17 October, 1974. Also NASA Report SP-382 (1975).

Young, L. G., A. T. Young, J. W. Young, and J. T. Bergstralh, 1973: The Planet Venus: A New Periodic Spectrum Variable, Astrophys. Journ., (181), L5-L8.

A SHEAR MODEL FOR SPIRAL STREAKS IN THE VENUS CLOUDS

Robert J. Krauss

ABSTRACT

Large spiral streak features are seen in Mariner 10 UV images of the upper level clouds on Venus. Measurements of the cloud velocities in and around the streaks indicates that the spiral streaks are unlikely to be either streamlines or jets in the atmosphere, since they have a comparatively small meridional velocity component. A hypothesis is developed that the shape of the streaks is caused by horizontal shear in the measured velocity field. This approach can be inverted to infer the global velocity field from the curvature of the streaks. Such an analysis reveals that a global scale wave with a 4 1/2 day period is likely to be superimposed on the predominant mean flow at high altitudes. The shear hypothesis also provides a means of correlating large scale cloud features and albedo changes on Venus with the global atmospheric flow patterns that have been measured. On the basis of the correlations, one can speculate what the upper level general circulation of Venus might be like.

INTRODUCTION

The bright spiral streaks in the Mariner 10 UV images are one of the most conspicuous features of the global cloud patterns on Venus. The appearance of the streaks changes superficially from day to day as the upper atmosphere rotates through the 8 day sequence of Mariner pictures. We can see variations in streak brightness, variations in streak width, and irregularities and blobs along the edges of the streaks. Several features of the spiral streaks are important, however, in that they do not change substantially over the 8 days: a) The streaks originate near the equator and spiral around the planet some 200-300 degrees in longitude before merging into a bright polar ring near 50 degrees latitude; b) More often than not, the streaks are coherent across the equator and a corresponding bright streak is also present in the other hemisphere; c) The streaks always diverge from the equator in a "V" pattern, with the arms of the "V" pointing in the direction of the retrograde mean zonal flow; d) The streaks do not change very fast in time, appearing to be virtually fixed on the rotating sphere, similar in character to the stripes on a barber pole, creating the illusion of motion without exhibiting true motion themselves.

The large scale organization and the temporal and spatial stability of the spiral streaks indicates some relation to the global scale motion field and to the general circulation of the upper atmosphere which also appears to exhibit large scale organization and stability in time over periods of days or weeks. The streaks may thus be of potentially greater significance in determining the large scale mass motion field than, say, the circumequatorial belts, which would be difficult to interpret in any other way than as a periodic wave phenomenon. Murray, et.al. (1974) offered several tentative explanations for the origin of the spiral

streaks. If the zonal motion is caused by periodic solar heating from above, then the streaks are likely to be wavelike disturbances caused by some interaction of the zonal flow with the subsolar convective zone. With no meridional flow, the streaks would have to be entirely wavelike. If meridional flow exists, the wavelike character would be strongest in the equatorial regions of maximum solar heating, but the streaks (at higher latitudes at least) are more likely to be streamlines in the fluid flow field. A third possibility was proposed which maximizes solar heating effects to the point where we have not only wavelike interactions and streamlines, but also large heat induced pressure gradients centered at the subsolar point. These pressure gradients generate large scale horizontal jets due to the cross-isobar flow. Both of the latter views require a subsequent moderate to strong meridional flow.

Detailed measurement of the small scale cloud motions (Suomi, 1975; and Krauss, 1976a&b) has shown very small meridional motions, well under 10 m/s everywhere. The only exception is the circumequatorial belts, which have a $\sim$ 20 m/s southward component. If the spiral streaks were either jets or streamlines, their angle to the equator as seen in the Mariner pictures, would require meridional velocities of 30-50 m/s. This is not observed. Moreover, a jet ought to exhibit horizontal shear at its edges. We have seen no velocity changes across the spiral streaks. The motion field is everywhere locally uniform, except for a 10-15 m/s measurement scatter due most likely to convection, turbulence, or vertical shear. Thus, the only remaining hypothesis is that the spiral streaks are wavelike in origin.

Now, the wave hypothesis is believable near the equator. Interaction of the mean zonal flow with the subsolar convection zone is bound to generate vertical oscillations in the atmosphere, especially in the presence of the very stable temperature lapse rate observed at 60-70 km altitude. Cloud streets or billow patterns might possibly remain even after a number of days and one or two revolutions around the planet. The cloud features need only to be preserved for several days after being formed by wave induced processes. In view of the unknown nature of the UV contrasts, persistence of some features for several days is a reasonable assumption.

Two characteristics of the spiral streaks require some added explanation before we attribute them exclusively to waves, however. The first unexplained characteristic is that the spiral streaks appear everywhere to move with the mean zonal and meridional flow. No organization whatsoever is observed anywhere along a spiral streak to indicate it has a propagation velocity relative to surrounding cloud features. To explain the streaks as waves thus requires combining origins and phase velocities in such a way as to produce a periodic standing wave train which remains fixed, not with respect to its source, but with respect to its medium. This seems highly unrealistic. The second unexplained characteristic of the streaks is that, in the mid-latitudes at least, the streaks are distorted by the increasing angular velocity of the mean zonal flow at higher latitudes. The "streak wave" thus moves with the mass field, tends to locally conserve angular momentum, and exhibits horizontal shear. If the spiral streaks are indeed waves, they are, in many respects, very unwavelike in character.

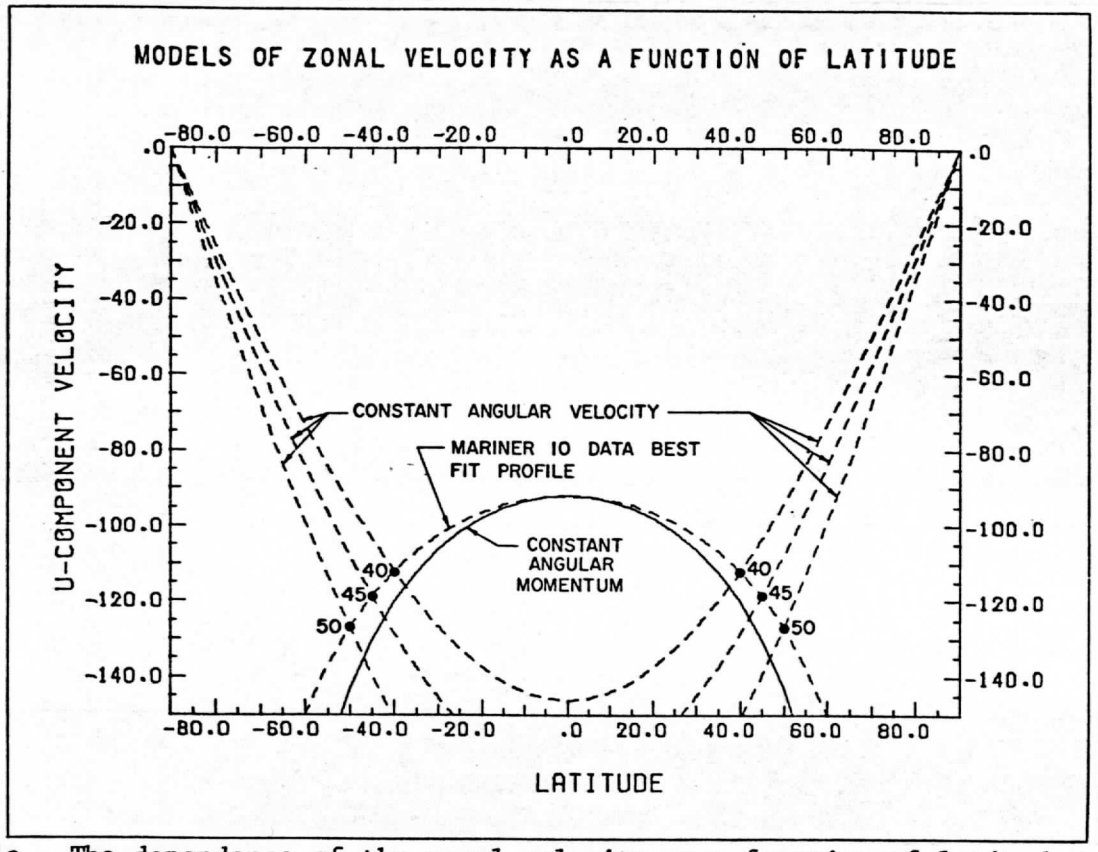

Figure 1a. The dependence of the zonal velocity as a function of latitude can be modeled by a profile of nearly constant angular momentum at low latitudes and a constant angular velocity at high latitudes. The transition between the two regimes seems to vary between 40 and 50 degrees (illustrated by solid dots). Of the three transition latitudes shown, 45 degrees was chosen for the streak model as a good average value.

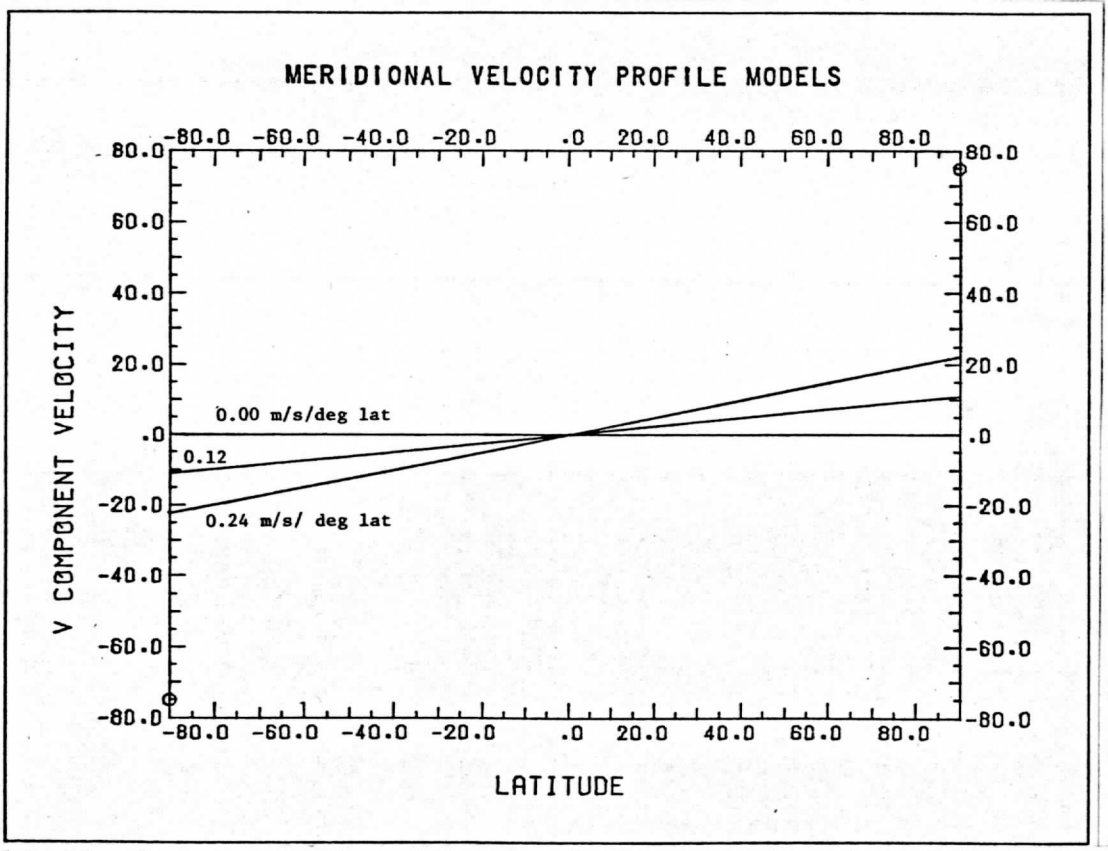

Figure 1b. The dependence of meridional velocity as a function of latitude is modeled by a constant velocity gradient. Scatter in the data prevents meaningful use of anything other than a linear approximation. The range of gradients shown here was used to generate the seven streak families shown in Figure 3.

The next obvious question is "Do we need a wave at all?" If the streaks tend to distort like the mass field at higher latitudes, maybe they also move with the mass field at lower latitudes where the distortion due to shear is too small to detect by direct velocity measurement. If that is the case, the streaks may have their origin in a wave, perhaps caused by an interaction of the mean zonal flow with the subsolar convective region. The waves generate and feed bright cloud material into the streaks, but the shape of the streaks would be due entirely to their being carried along with mass motion of the surrounding atmosphere. Since we have a measured global velocity field, it is easy to test the shear hypothesis by looking at the effects of horizontal shear in the zonal and meridional velocity fields as a function of latitude.

THE SHEAR MODEL

To test this hypothesis, we constructed a computer model using a zonal velocity profile with a -92 m/s equatorial velocity and a 120 m/s zonal maximum velocity at 45 degrees latitude (Figure 1a). The velocity profile was derived from our measurements of the Venus cloud motion in Mariner 10 images on day 39 (Krauss 1976a). Various meridional velocity gradients (Figure 1b) were used to generate a family of trajectories. Figure 2 illustrates schematically how a single mass element might spiral toward the pole under the combined influence of the u (zonal) and v (meridional) motion vectors. Note the shallow angle of the trajectory with respect to the equator, requiring several trips around the planet to reach higher latitudes. The v component of the measured velocity profiles is too small for the trajectories to have the same large angle relative to the equator as we see for the spiral streaks.

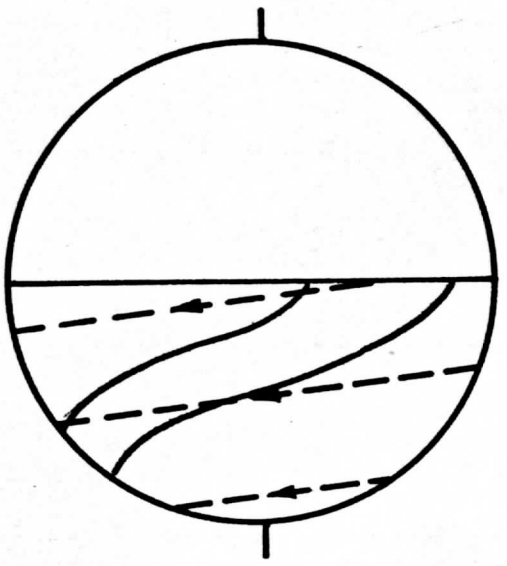

Figure 2. The dashed lines schematically illustrate the slow departure from the equator taken by a mass parcel under the influence of the velocity field defined by Figures 1a and 1b. Note that the spiral streaks, depicted by the solid lines, have a much larger angle with respect to the equator.

SPIRAL STREAK LINE MODEL

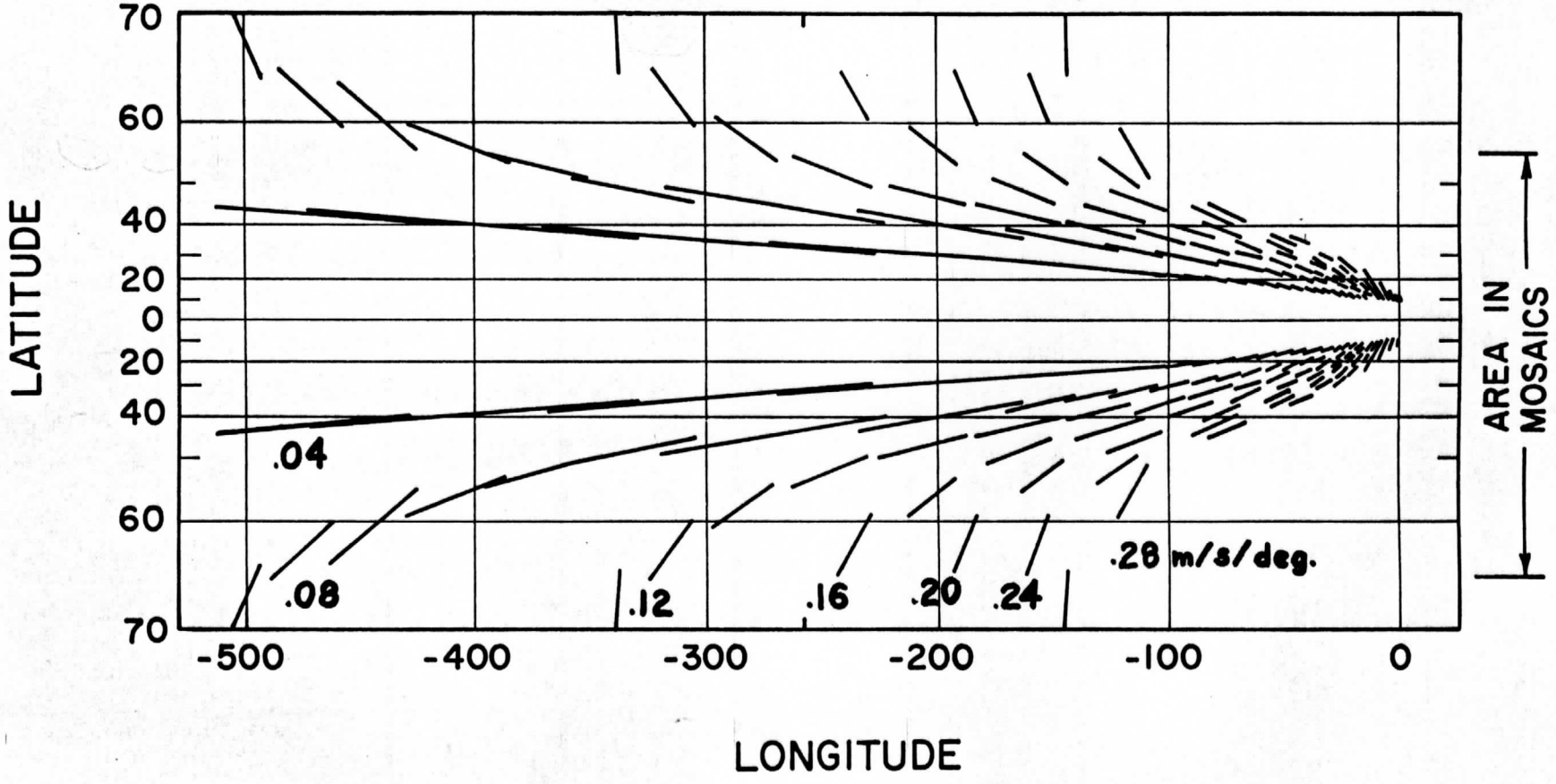

Figure 3. The seven streak families generated by differential rotation in a spherical shell are shown here. The velocity profiles used are defined in Figure 1. The longitude scale shows displacement from the point of origin (longitude zero) in a coordinate system moving with the mean equatorial flow of -92 m/s.

A poleward moving mass element would tend to distort, however. This effect can be approximated by considering two mass elements starting on the same meridian, but 100 km apart. Initially, a line connecting two such mass elements would be parallel to the meridian. As the effect of horizontal shear builds up, the line between the elements would both stretch and tilt. Figure 3 is a mercator plot of seven sets of such stretched and tilted lines corresponding to trajectory pairs for the meridional velocity gradients of 0.04, 0.08, 0.12, 0.16, 0.20, 0.24, and 0.28 m/s/deg as illustrated in Figure 1b.

The best analogy to what is illustrated in Figure 3 is the case of an observer in a boat floating down a stream. The observer throws a dye marker overboard and continues to watch the development of the resulting dye plume as he floats downstream with the mean flow. The spiral streak angle best fitting the streaks observed in the Mariner 10 images on day 39 corresponds to the 0.12 m/s/deg meridional velocity gradient in Figure 3. This compares nicely with our measured velocity gradients of 0.11 to 0.14 m/s/deg, so the streak model seems to be consistent with the data. Note, in addition, that the shape of the streaks in the model is not dependent on the magnitude of u, the zonal wind. The model is a function of $\partial u/\partial y$ and $\partial v/\partial y$ only. We cannot therefore directly predict divergence or infer vertical motion from the shape of the streaks, but because of the need to conserve angular momentum on a global scale, $\partial u/\partial y$ should be stable to 10-20%. We see no large storms or other dynamic features which could significantly perturb the mean zonal flow. As a result, the strong dependence of the model on $\partial v/\partial y$ makes the spiral streak angles extremely sensitive indicators of the magnitude of the meridional flow.

In the first movie made of the Venus flyby images (Danielson, 1975), one can see an oscillation or nutation of the bright polar ring. The period is about 4 days. A shift in latitude of the ring can also be seen in an early Mercator projection of the data (Murray, et. al., 1974, Figure 11). Belton, et. al. (1976) have generated an improved set of Mercator projections covering a full 7 day period and consisting of both high pass filtered and photometrically corrected versions of the data. We examined spiral streak angles in the high pass filtered mosaic to see if there existed a correlation of meridional velocity (inferred from the streak line tilt in the model) with the latitude shift of the polar band. Figure 4a is a copy of the Belton, et. al. mosaic. Figure 4b shows the streaks with the inferred value of the meridional velocity gradient needed to produce the observed tilt angle. The dashed line is the low latitude edge of the polar ring. A correlation is indeed present. The meridional velocities are higher when the polar ring is at higher latitudes. This appears to occur about every 4 1/2 days.

Belton, et. al. (1976) note that the darker regions of the photometrically corrected mosaic (Figure 5a) form the often observed dark "Y" feature, and that the coherence of this feature in time, and in the presence of the larger mid-latitude shear in our measured zonal wind profile (where higher latitudes have considerably higher angular velocity) argues for the association of the "Y" with a global scale wave.

The meridional velocity gradient inferred from the spiral streak model also shows a correlation with the dark "Y" feature. This is most evident

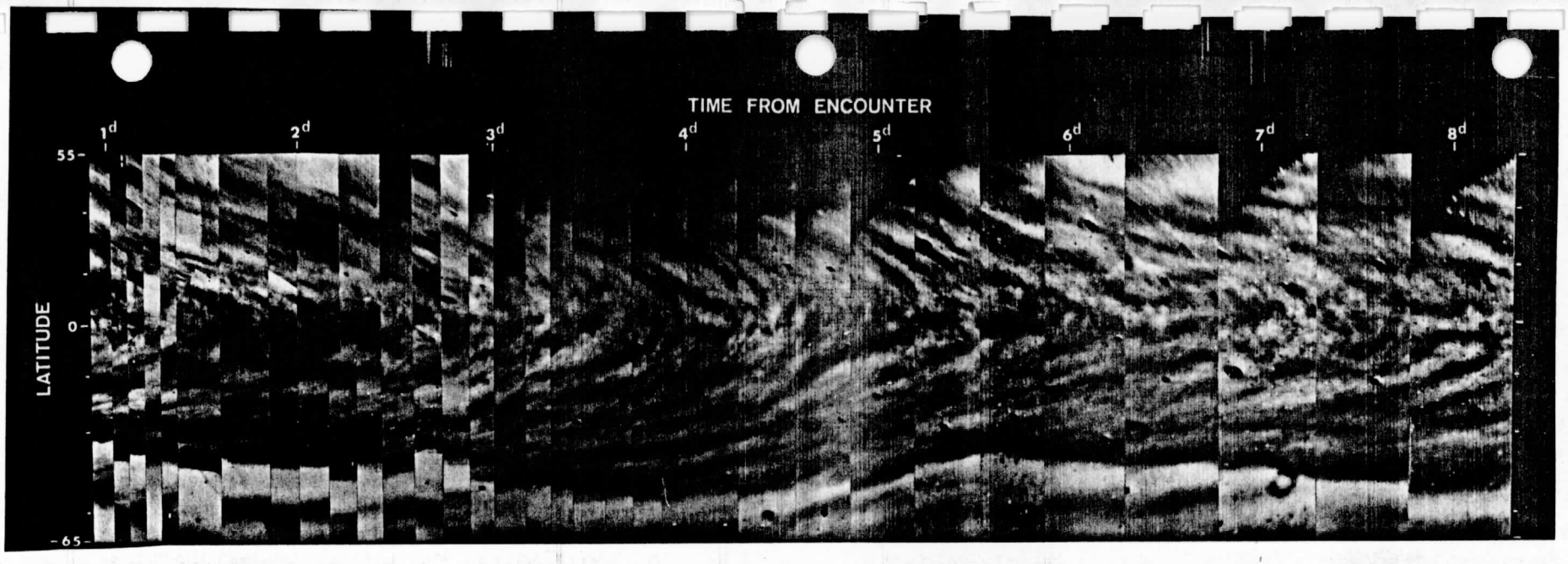

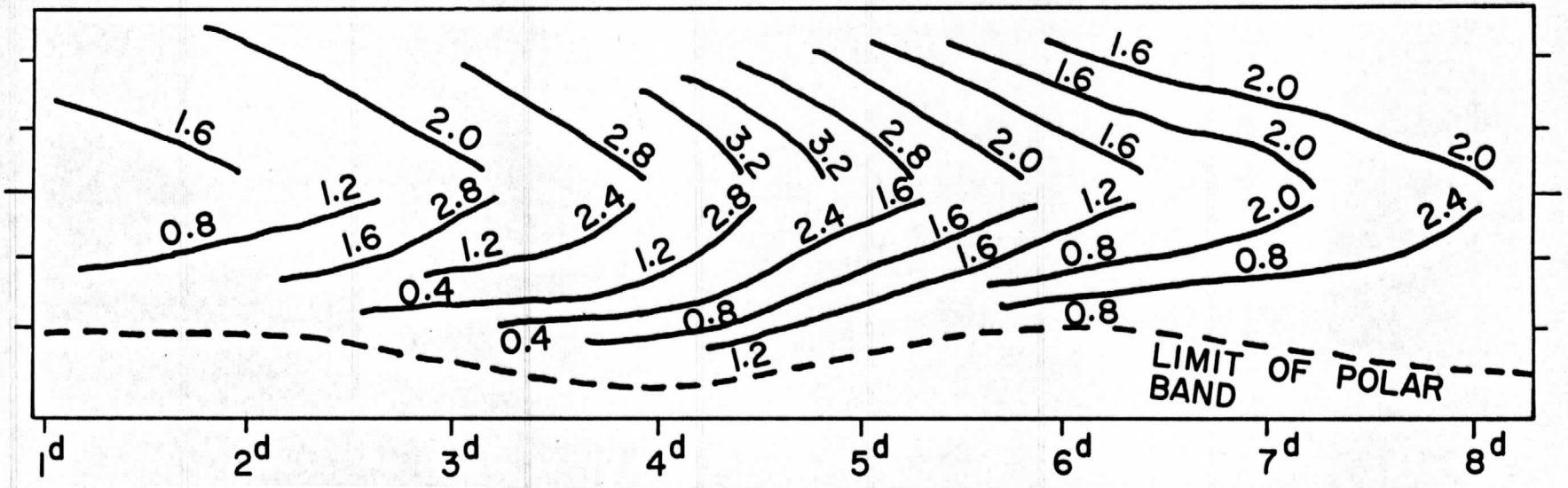

Figure 4. Mercator projection mosaic of high pass filtered pictures of Venus centered on the Mariner 10 spacecraft subpoint as a function of time. The vertical coordinate represents image data on a meridian passing through the subpoint, and is plotted as a function of days past Venus encounter along the horizontal axis. Figure 4b shows streak line curvature expressed in units of m/s/ten degrees as inferred from the shear model and Figure 4a.

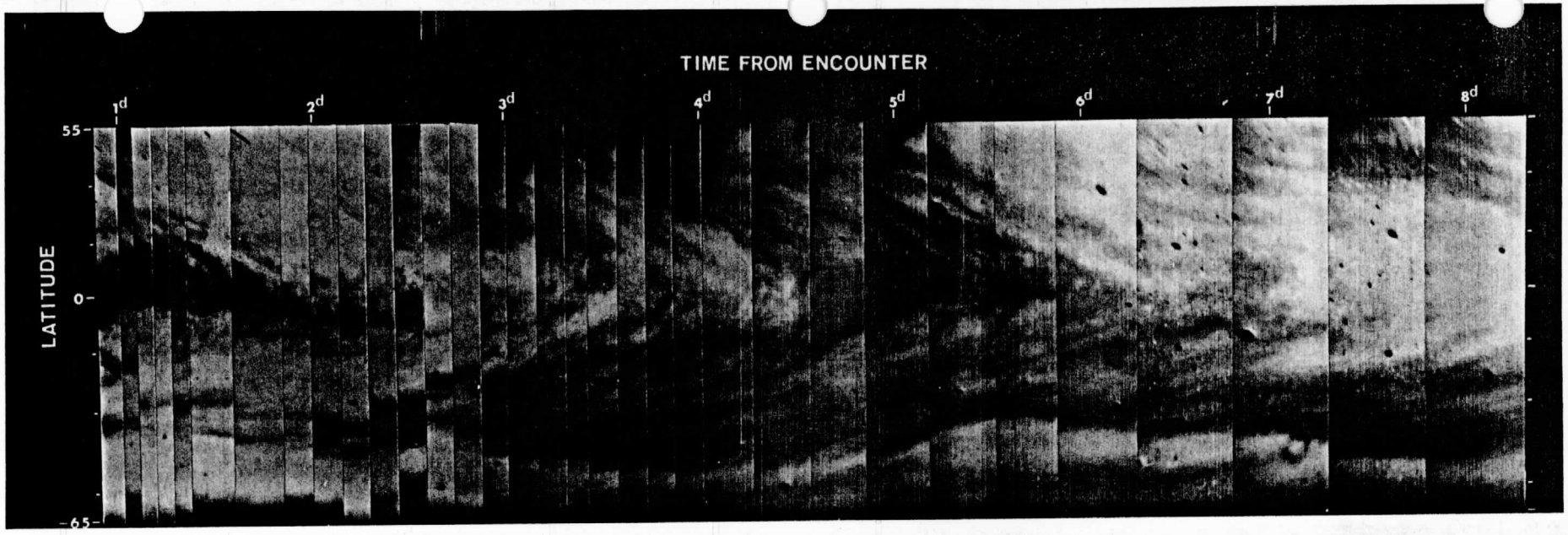

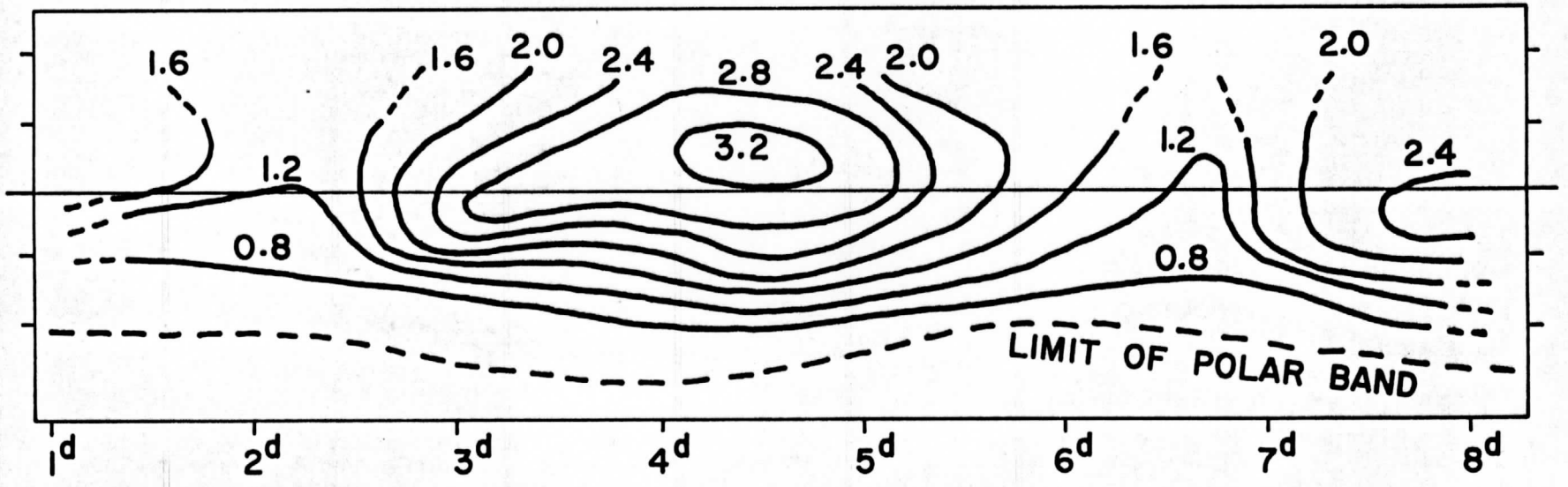

Figure 5. Same mosaic as Figure 4, except the images have been photometrically corrected. While Figure 4a is filtered to enhance small scale details in the clouds, Figure 5a preserves the albedo information. Figure 5b shows contours of the meridional velocity gradient as inferred by means of the model from the curvature of the streaks in Figure 4.

in Figure 5b where we have contoured the meridional velocity gradients inferred from the shape of the spiral streaks in Figure 4, and compare the contours with the photometrically corrected mercator mosaic (Figure 5a).

The brightest clouds in the equatorial regions occur when both the zonal and the meridional velocities are increasing, divergence is measured, and the polar ring moves toward higher latitudes. The darkest clouds at the equator form the leg or base of the "Y" feature, which narrows to a thin wisp near 2 days and again near 6 days after encounter. As the base of the "Y" is narrowing, the bright polar ring is moving toward the equator, and as the base of the "Y" disappears, the bright clouds begin to dominate the equatorial regions and velocities again begin to increase in both the u and v directions.

Note that there is a periodic 4 1/2 day undulation symmetric about the equator, with the dark leg of the "Y" appearing in the northern hemisphere, followed by the bright region between the arms of the "Y" appearing in the southern hemisphere. The contours in Figure 5b, however, show a systematic offset toward the northern hemisphere, indicating that the streak curvature is less there, and that the meridional flow is therefore stronger in the northern hemisphere than in the southern hemisphere.

VELOCITY FIELD ANALYSIS

With the streak model as developed, we can use the observed periodicity in the streaks to analyze the measured cloud motions. We have measured widespread zonal acceleration in low and mid latitudes on day 39 (Krauss, 1976a & b). Coupled with meridional flow toward the poles, this is direct evidence of divergence superimposed on the mean zonal flow. On day 40, we observe a divergent pattern early in the day, but it changes to an indeterminate pattern later in the day. The longitudinal gradient of the zonal velocity reverses sign while the meridional flow toward the poles continues to increase. The mean zonal velocity on day 40 is about 5 m/s higher than on day 39. Figures 6, 7, and 8 summarize the results of the velocity measurements made so far. We will be extending the measurements to earlier and later times in the future.

Now, the Mariner 10 flyby images show Venus as it usually appears in the great majority of ground based observations. It is reasonable to assume that this constitutes the nominal or "steady state" condition. That being the case, it would be unlikely for the trends we observe in Figures 6 and 7 from day 39 to day 40 to continue for any great length of time. Too much momentum would have to be transferred, and a substantial change would occur in the character of the global circulation. It is much more likely that we are observing oscillations or perturbations on the steady state, since these can be conservative and thus not seriously affect the mean flow. Indeed, from the 4 1/2 day periodicity evident in Figure 5b, such an interpretation of the trends in Figures 6, 7, and 8 appears to be a reasonable possibility.

One can, in fact, carry this interpretation one step further by using the rate of change of u and v in time, plus the 4 1/2 day period, to infer an amplitude for the oscillations. The dashed lines in Figures 6, 7, and 8

Figure 6. Mean value of zonal velocity measured at equator. Solid dots represent the separate 4 picture data sets, while crosses are averages for a given day. The dashed line is a 4 1/2 day period sine wave with an amplitude chosen to best fit the trend of the velocity measurements.

Figure 7. Meridional velocity gradient measured in the four data sets. Each data set is shown as a solid dot, and each day's average by a cross. The last point in day 40 is spuriously high because not enough points were measured at high latitudes and the least squares fit was influenced too much by measurement scatter. The average of all three data sets on day 40 is more meaningful. The sine curve amplitude is again defined by the slope of the data and an arbitrarily chosen 4 1/2 day period. Note that the phase is the same as in Figure 6.

Figure 8. The zonal velocity gradient shows a similar trend toward a 4 1/2 day cycle. Note that the velocity gradient here changes sign, indicating a tendency for the zonal wind to slow down. The "acceleration" shown here is 180° out of phase with the zonal velocity in Figure 6.

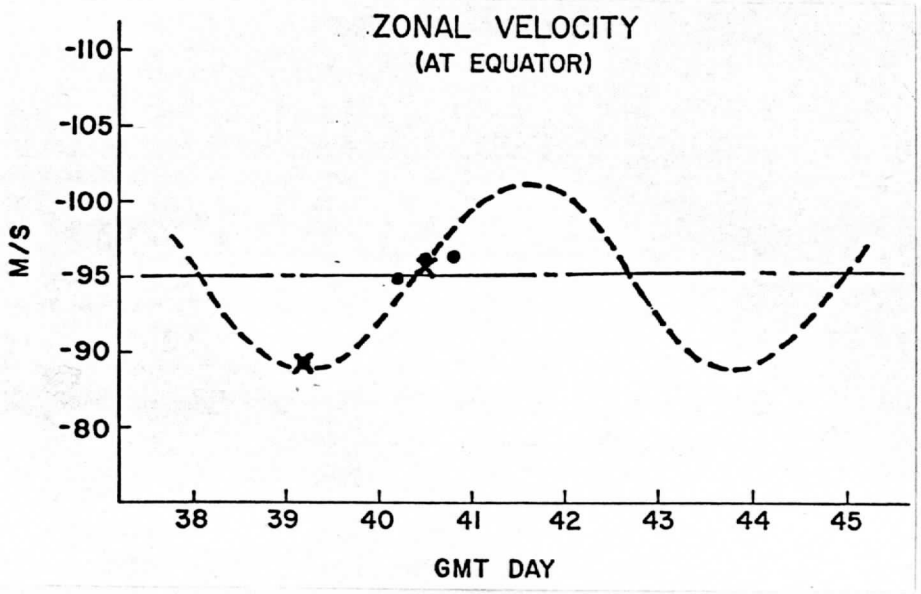
ZONAL VELOCITY
(AT EQUATOR)
-110
-105
-100
-95
-90
-80
M/S
38
39
40
41
42
43
44
45
GMT DAY

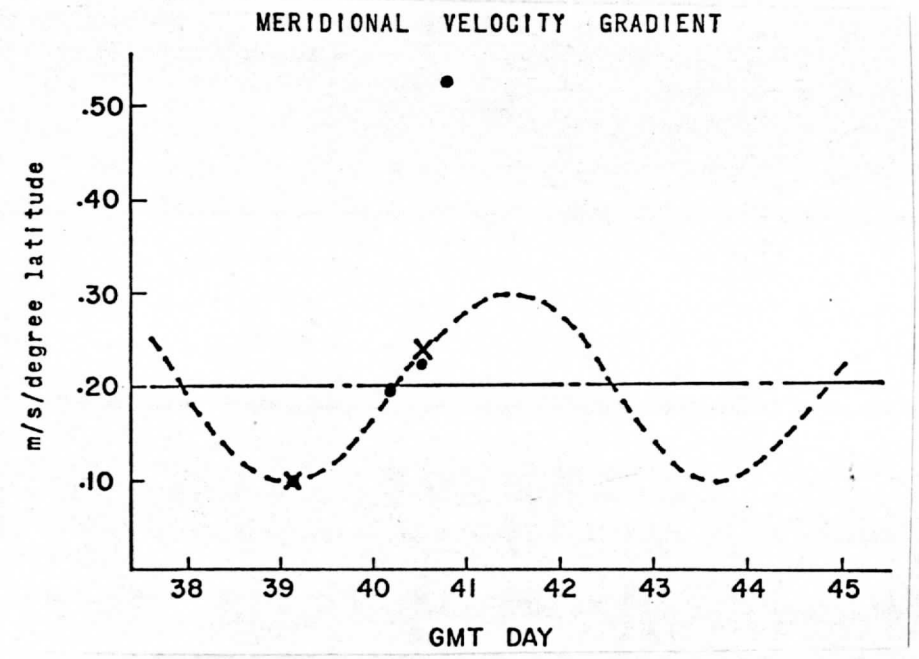
MERIDIONAL VELOCITY GRADIENT
.50
.40
.30
.20
.10
m/s/degree latitude
38
39
40
41
42
43
44
45
GMT DAY

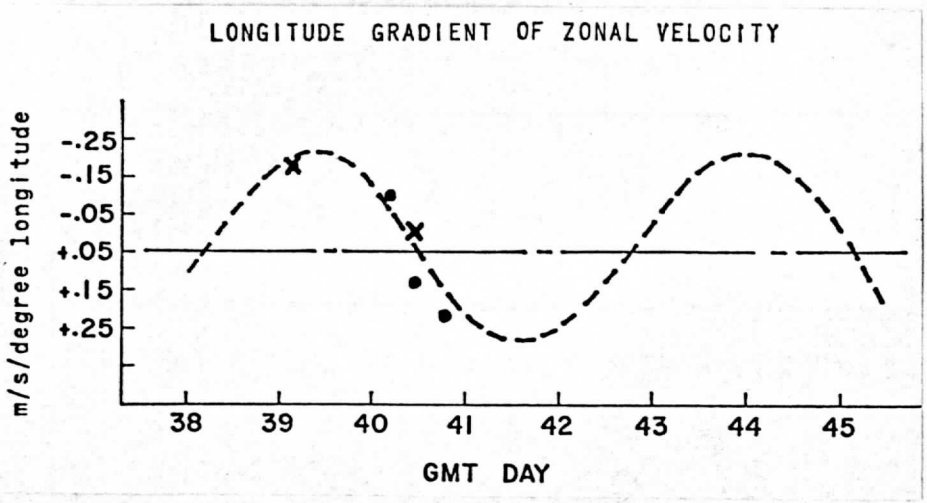
LONGITUDE GRADIENT OF ZONAL VELOCITY
-.25
-.15
-.05
+.05
+.15
+.25
m/s/degree longitude
38
39
40
41
42
43
44
45
GMT DAY

illustrate how the trends can be interpreted in terms of sinusoidal fluctuations with a 4 1/2 day period. Knowing the period from large scale albedo fluctuations and spiral streak curvature, and the slope of the sine curve from the actual velocity measurements, the amplitude of the oscillations can be easily inferred as well as the mean or equilibrium state.

The negative correlation of the zonal velocity (Figure 6) and the zonal velocity gradient (Figure 8) translates into an almost exact 180 degree phase difference. This is somewhat reminiscent of simple harmonic motion (the "restoring force" or velocity gradient is a maximum at maximum "displacement" or zonal velocity) and provides further support for the wave interpretation of the velocity fluctuations. Note too that the amplitude of the waves in Figures 6, 7, and 8 corresponds well with the magnitude of the eddy fluctuations determined on days 39 and 40 (Krauss, 1976b). While one cannot say that the eddy terms and the periodic fluctuations inferred from the streak model are one and the same, it is worthy of note that they are of the same size. The eddy terms, as measured, also tell us that there is some small amount of momentum transport toward the poles at the same time the mean velocities are fluctuating.

FURTHER SPECULATION

When Mike Belton first cut out the center portions of the disk of Venus out of a series of Mariner pictures and pasted them together on a sheet of paper (Murray, et. al., 1974, Figure 11), the entire MVM imaging team thought the result very profound, though at the time nobody could explain why. The importance of that pseudo-mercator projection is only now being appreciated. The correlation of the cloud albedo, spiral streak angles, polar ring motion, and the measured cloud velocities, all with an apparent 4 1/2 day period, is by far the most striking feature of our streak line analysis. It would certainly appear that large scale waves are affecting cloud formation and the velocity field. The evidence is preponderant, but nevertheless circumstantial, for no cause-effect relationship can be established as of yet. Indeed, one ought to be very careful of believing too strongly in a 4 1/2 day wave.

To make this more clear, and perhaps put things in better perspective, several points should be made. First, it must be kept in mind that the upper atmosphere of Venus rotates differentially. There is no "4-day rotation", although the term has become very commonly used and tends to affect how we think about the clouds. To substitute "4 1/2 day rotation" at this point would be equally misleading. Secondly, the hemispheric vortices are still the dominant dynamic structure of the general circulation. The wavelike phenomena we see in the changes of streak curvature, as well as the measured eddy components (Krauss, 1976b), are perturbations on the steady state, demonstrably over an order of magnitude less intense. Finally, only 8 days of Mariner 10 observation are a poor statistical sample. While the appearance of Venus in those 8 days is its most common, one must remember that spectroscopic evidence (Barker and Perry, 1975) gives periods of fluctuations of 6 and >9 days in addition to 4 1/2 days. The 4 1/2 day wave may merely be the most common fluctuation seen, or the most dominant, or perhaps only a superposition of several other waves with entirely different periods. The

fact that the "Y" feature occasionally disappears in ground based observations lends credence to this possibility.

Nevertheless, it is instructive to speculate further, for in so doing, we may be able to find a pattern into which the disparate pieces of the Venus puzzle will fit. Two additional pieces of evidence should be mentioned. First is the fact that we see vertical shear in some of the images, with the higher velocity clouds at the higher altitudes, obscuring lower features. This shear contributes substantially to the measurement scatter in the u-component. The second piece of evidence which will prove useful is that we see wavelike phenomena of different scale sizes at several different altitudes. What this implies is that there exists a rather tenuous balance of pressure, temperature and albedo at 60-70 km such that "something" influencing the optical properties of the atmosphere is significantly affected by local physical conditions. The observation of waves in addition to convection, differential motion, eddies, vertical shear, etc. leaves little doubt that the UV markings we are observing are embedded in a fluid flow field and are not something unknown masquerading as a familiar phenomenon. Consequently, though the atmospheric chemistry and cloud physics are different on Venus, the presence of familiar processes allows us to draw on our Earth-based dynamical experience. The general circulation of Venus must still obey the equations of motion.

A. The Mean General Circulation

The only explanation of the streaks consistent with the evidence is the hypothesis that the streaks are indicators of relative shear, i.e. trajectories in a thin spherical shell which is rotating differentially. On the basis of this hypothesis we can draw some further conclusions. The shape and curvature of the streaks does not locally change or show sinuous fluctuations of any kind. Whatever shears are operating, they are uniform with longitude and change in a monotonic way with latitude. Thus, although the formation of the streak material may initially be due to interaction of the zonal flow with a sun-locked disturbance, and the bow-like waves may be similarily generated, neither a persistent high pressure anomaly nor a solar thermal tide can be the predominant dynamic feature because each would cause a change in curvature of the streaks when solar heating is turned off at night. Every 48 hours, the acceleration would change and the spiral streaks would show wiggles. The sun-locked effect can at most be a small perturbation on what must in general be a very uniform horizontal flow field. The Hadley cell, modified by the zonal flow is such a uniform flow field.

If a modified Hadley cell is the dominant dynamic feature then the convection cells are superficial. The shallow 200 km wide cells at low latitudes with 20:1 ratio of width to height are likely to be the result of solar heating, since they are visible where solar input is a maximum and do not appear near the morning terminator nor at latitudes above 30°. The divergence measured in the velocity field covers an even larger region, from equator to polar ring. One can interpret this as a generalized upwelling at low and mid latitudes with superimposed local heating in a layer about 10 km deep. There is no evidence of deep or very strong local convection. Meridional flow in both hemispheres is measured away from the equator, but is very slow. The

divergent region is not strong enough to overcome or significantly modulate velocities in the predominantly balanced zonal flow. We see only a small acceleration term in the zonal direction, equal to the meridional acceleration.

The zonal motion profile varies with latitude like a vortex. This conforms with the need for a Hadley cell to show convergence and sinking motion at the poles in addition to divergence at the equator. The motion field tends to conserve angular momentum except for a small loss attributable to friction. At 45° latitude we observe turbulent eddies approximately 200 km in diameter, strongly indicative of barotropic instability. The eddy curvature (see Murray, et. al., 1974, Figure 7) shows higher velocity on the poleward side, in the bright polar ring. The zonal velocity profile at 45° latitude obeys the approximate relation $\partial u/\partial y \gtrsim 2\Omega\sin\phi$, which is the theoretical threshhold for dynamic instabilities to form. We can thus infer that the bright polar band is a region of turbulent stirring and of higher eddy viscosity and is likely to be a transition zone to a region of less horizontal shear and more constant vorticity, because the atmosphere cannot support the laminar flow and conserve angular momentum at the same time. Beyond the 45° point we observe uniform angular velocity. Such an organization is exactly that of the inner portion of a vortex, which rotates at constant angular velocity as mass is drawn out of the horizontal plane and into vertical motion. It is hard to avoid concluding that the atmosphere of Venus similarly sinks at the poles.

Three pieces of evidence can support a sinking of the atmosphere of Venus at high latitudes. First, there is more CO_2 generally seen at the poles (L. D. G. Young, et. al., 1975), implying a lowering of the reflecting layer or cloud haze. Second, the poles are slightly colder in effective temperature most of the time, except when a "hot" spot ~5-10°K warmer than its surroundings appears (Murray, Wildey and Westphal, 1963). This hot spot could be the eye of the polar vortex, either made transparent by loss of clouds, or warmed by adiabatic compression. Third, radar observations (Sinclair, et. al., 1969) imply that, at the surface of Venus, the poles are probably a few degrees warmer than the equator. Such a reversal of the equator to pole temperature gradient is not possible under strict conditions of radiative balance, but is easily maintained if the atmosphere moves so that the polar regions could be warmed by advection or adiabatic sinking. A horizontal temperature gradient also guarantees that there will be atmospheric motion at the surface of Venus.

The general picture, so far described, is that of a simple Hadley cell modified by the zonal flow to resemble a hemispheric vortex. A single directly driven cell, with heat and momentum sources and sinks coinciding is impossible. On the Earth one needs the equivalent of a subtropical high to maintain geostrophic balance in the low level return flow, and this upsets the pressure gradients needed to perpetuate a pure Hadley circulation. The resulting compensating mechanism is a statistical three cell breakdown in the meridional structure of the general circulation (Lorenz, 1967). Since Venus seems to have a simple direct Hadley cell in its upper atmosphere, it is likely that compensation on Venus occurs in vertical cells which we cannot see. The vertical wind shear profiles from the Russian Venera probes (Kerzhanovich, et. al., 1972; Marov, et. al., 1973) and the turbulent layer seen by Mariner 10 (Howard, et. al., 1974; Woo, 1975) are possible glimpses of such structure.

Whatever else one can say about the vortex, it appears to be stable. The structure of the velocity profiles is much larger than our estimated errors and is well organized. Moreover, the motion field was independently derived from motion of small scale cloud features, yet is strongly correlated with the semi-permanent features such as the polar ring and the arms of the "Y" or spiral streak angles seen in earth based observations. The "Y" and reversed "C" always are oriented in the same direction (O'Leary, 1975). Consequently, the vortex is highly likely to be representative of the usual or mean state on Venus. The dynamical structure of the vortex is stable over at least short time periods, since its destruction would require redistribution of a large angular momentum. Over the long term, however, changes are likely. The bright polar rings, for example, occasionally disappear singly or in pairs (Dollfus, 1975). Venus thus appears to have a "change of climate" now and then in its upper atmosphere even though its axis is not significantly tilted.

B. Vertical Momentum Transport

If the vortex structure and modified Hadley cell are the usual conditions in the upper atmosphere on Venus, we must ask what drives the zonal winds. What maintains the zonal flow so uniformly in the face of frictional dissipation and cycles planetary angular momentum back up to the top of the atmosphere? Momentum should diffuse from regions of high velocity to regions of low velocity. To bring momentum upward at low latitudes from the slow moving surface into the 100 m/s flow requires a very efficient pump.

One such mechanism proposed was the "moving flame" model of Schubert and Whitehead (1969) and Schubert and Young (1970), and further developed by Gierasch (1970) and Malkus (1970). Periodic solar heating results in Reynolds stresses and tilted convection cells which move momentum upward in a vertical plane at constant latitude. The effect should be strongest at the equator where maximum heating occurs, and weaker acceleration should be visible at higher latitudes. In fact, we see no significant lessening of zonal acceleration at higher latitudes and the zonal velocities are higher there than at the equator. The spiral streaks are also too tilted at high latitudes to be directly related to a time lag due to solar heating. In addition, the mottled appearance of the subsolar convective zone shows no indication of large scale organized cells and associated cloud rolls or streets expected to be seen with a moving flame mechanism. Indeed, the only place where such periodicity is evident is in the streaks at the morning terminator after 48 hours of radiative cooling.

The existence of a thermal tide is also a possibility for transporting momentum upward, but suffers from two problems. First, the analysis of Ingersoll and Orton (1974) shows a two peak temperature fluctuation around the circumference of Venus with cold regions at the evening terminator and the morning terminator. This double peak could reflect the limited data analyzed (if, say, a single peak travelling around the planet were observed at several different phases). The point to emphasize here is that Ingersoll and Orton see no single stationary temperature maximum. A solar thermal tide would be consistently warm at the evening terminator, with one single wave around the planet. Secondly, the changing convergence and divergence as the atmosphere cools and sinks on the night side and warms and rises on the

day side might be consistent with the measured velocity profiles, but ought to give the same spiral streak curvature at all longitudes. Instead we see global scale longitudinally fluctuating curvature of the streaks coupled with a change in large scale albedo and a shift in latitude of the bright polar ring. The resulting picture is more that of a single wave travelling around the planet with maxima and minima both passing sequentially underneath the sun. Such a wave is also capable of transferring momentum upward in the presence of a mean steady state, and would exist as a perturbation on the vortex flow.

The spiral streak model can help to identify additional features of the motion field. For example, the streaks have north-south asymmetry. The meridional velocity gradient in the northern hemisphere (Figures 4b and 5b) is larger, and the acceleration contours are shifted off the equator. The meridional gradient is only about 1/3 as large at 45 degrees latitude as it is at the equator. Finally, we note that the meridional velocity gradient is likely to be a minimum at 2 days after encounter, while the mean meridional velocity gradient is probably closer to 0.20 m/s/deg (Figure 7). The highest meridional velocities ought to be measured at 4 1/2 days after Venus encounter. The brightest albedo features occur when the meridional velocity is increasing and we see divergence. The darkest feature "Y" occurs when the meridional velocity is decreasing and we see what is probably relative convergence.

Neglecting the question of what the UV clouds really are, we can digress a bit by considering the possible coupling of vertical motion to the wave features. What would we expect to see if rising motion generates bright UV clouds and sinking motion generates darker markings? We find a possible answer for why Young (1975) fails to see a correlation between shading and effective temperature. The bright clouds exist at temperatures of 250 ± 10°K. Depending on their relative altitude, the atmospheric parcels which have risen the farthest will be colder and brighter. Parcels which sink get dark and warm as bright cloud elements disappear from them. A bright region would not get much colder as it rises because there is a "lid" on convection in the stable upper layers. In general, the rising masses would tend to get brighter, colder, and more uniform in temperature as bright cloud elements are generated. The sinking atmospheric masses lose the lower clouds first so one gets to see lower and still warmer regions at a faster rate than the mean gas temperature of the whole mass would rise. Such sinking and partially transparent masses are darker, warmer, and less uniform in temperature with a tendency to show more scatter on the warm side, depending on cloud population as a function of altitude and area.

Such a theory of cloud contrast and formation is adaptable to correlation with CO_2 concentration as well. Large scale vertical motion both intensifies cloud formation by convection and intensifies destruction by subsidence so that one sees a tendency toward brighter clouds when the reflecting layer is rising and darker clouds when the reflecting layer is falling. At CO_2 maxima and minima one would see half bright and half dark and thus no correlation at all! At the poles, clouds have been stirred up and are thick, as well as being radiatively cooled. They could be sinking, but would not dissipate as fast as at the equator, so they would retain a high albedo.

C. Vertical Shear and Dynamic Balance

Pressure forces caused by horizontal temperature gradients can be quite large, even if the pressure differences are only a couple of millibars. There must be a balance condition for the fast zonal flow to keep it moving without deviating significantly from its path as a result of pressure differences induced by solar heating. Without this balance, for example, one would expect to see large jetlike features or streamlines deviating away from the subsolar region. The meridional flow would have to be considerably larger than it is measured to be.

On earth, the balance which keeps the westerlies westerlies and causes the jet stream to meander without moving far out of the temperate zone is called geostrophic balance. It is the equality between the pressure force generated by warmer air toward the equator and the horizontal component of the coriolis force. This balance guarantees that any air parcel moving zonally will tend to remain at constant latitude. If the parcel deviates too far to the north, the horizontal component of the coriolis force turns it back to the south. If it moves too far south, the coriolis force diminishes, but the pressure force pushes the parcel north.

A balanced flow such as this has another property. The equations of motion require that the wind at higher altitudes must move faster. The horizontal temperature gradient is larger at high altitudes on the average than at low altitudes, provided the gas is in vertical hydrostatic balance. This means that the velocity must be greater to balance the increased pressure force due to the larger horizontal temperature gradient at higher altitudes. Since geostrophic balance can only be achieved under conditions where there is a horizontal temperature gradient, the accompanying vertical wind shear is called the "thermal wind."

Venus rotates so slowly that the coriolis forces never amount to much and cannot offset the effect of solar heating. Leovy (1973) has suggested that the zonal flow might be maintained by the horizontal component of the centrifugal force instead. This is called cyclostrophic balance, and for the same reasons as above, we must also have a thermal wind present. In other words, if the zonal wind on Venus is constrained by dynamic balances to move in the mean along lines of constant latitude, the simple requirement that the fluid also obey the hydrostatic equation necessitates the presence of a vertical wind shear.

It is instructive to look at the implications which Leovy derives. A 100 m/s zonal wind would require only a modest 3°K vertically averaged temperature bulge at the equator for the pressure gradient to balance the horizontal component of the centrifugal force. This could easily be maintained by solar heating. Simply stated, the zonal winds on Venus continue to move fast at higher altitudes because the equator is just a little warmer. The zonal rotation can be started in the right direction by a slow overturning of the atmosphere, initiated by solar heating. This motion then causes friction with the planetary surface and eventually brings a small amount of planetary angular momentum to the top of the atmosphere. Viscous losses and turbulent momentum transport would prevent this mechanism from working once the rotation of the upper atmosphere picked up speed, however. Leovy

finds it intuitively difficult to maintain an equatorial thermal bulge, even in the very uniform case with no longitudinal variations in solar heating. He suggest Kelvin waves propagating phase westward as a means of independently moving momentum flux upward against viscous and turbulent dissipation to maintain the cyclostrophic balance. Most of the momentum would then be dumped at an altitude where the phase velocity of the wave equals the speed of the upper level winds. Mass could not begin to move poleward until it was sufficiently warmed, and the pressure force became larger than the centrifugal force.

Now we can see changes in the meridional flow, periodic meridional movement of the polar ring, and a change in curvature of the spiral streaks. These are evidence for a meridional component in the 4 1/2 day wave. It follows that the large scale waves on Venus cannot be pure Kelvin waves, because Kelvin waves exhibit no meridional motion. The waves we see do form a potential source of momentum for the upper atmosphere, however, since they have the right size to coincide with our measured region of divergence and they have the right phase velocity to dump momentum in the altitudes where solar energy input is a maximum. That is, we see divergence and zonal acceleration in the same 60-70 km altitude slice. Consequently, it is possible, by maintaining a high zonal velocity near the equator, to keep the upper atmosphere where it will receive maximum solar input until the 3°K temperature bulge is achieved.

The slow meridional motion and vertical wind shear are strong indications that dynamic balance exists, and the planetary waves are a necessary part of maintaining the stability of the vortex by keeping the zonal velocity in balance with the solar heating. Presumably, the long term changes observed in the large scale UV markings on Venus (the disappearance of its polar caps, for instance) are situations where conditions have gotten unbalanced and need time to reestablish the nominal steady state.

SUMMARY

The fact that the spiral streaks on Venus are neither trajectories or jets nor completely wavelike in character has led to an attempt to interpret them as indicators of relative mass motion in a differentially rotating shell. Using the measured velocity field in the upper atmosphere, it is possible to reproduce the streak shape. Once the connection between the velocity gradients and the streak curvature is established, one can use the streaks to infer velocity field fluctuations from the Mariner 10 images. These velocity fluctuations are strongly correlated with the dark "Y" albedo feature and the latitude motion of the bright polar ring, and appear to have a 4 1/2 day cycle. This suggests a global scale wave phenomenon superimposed on the mean steady state. The velocity field measurements to date partially support this interpretation. They indicate trends which are consistent with a wave amplitude approximately 10% of the mean zonal flow. In addition the proper phase relationship exists between velocity and "acceleration," i.e. between zonal velocity and the zonal velocity gradient. Eddy components of the order of magnitude of 10% have also been measured.

The zonal winds on Venus are organized in a vortex structure with an equatorial velocity of -95 m/s, a slight meridional flow with a mean gradient of 0.22 m/s/deg away from the equator, and a tendency to conserve angular momentum while moving to higher latitudes. At 45° latitude, coinciding with the onset of dynamic instability predicted from the measured velocity profile, we observe turbulent eddies and transition to a more viscid regime of solid rotation, corresponding to the central region of a vortex where motion in the vertical becomes a dominant characteristic. This sinking at the poles is supported by Earth based observations of occasional polar hot spots in the effective temperature of the upper atmosphere, increased CO_2 absorption above the polar reflecting layer, and hot poles at the surface of Venus which could be from adiabatic warming due to a sinking atmosphere.

The vortex appears to be a reasonably consistent feature on Venus because the high velocity zonal winds and the shape of the often observed "Y" features are commonly found in Earth based observations of Venus and are closely related to the motion field we measure. Any change to a different circulation regime would require redistributing large quantities of angular momentum and establishing a different kind of dynamic balance.

The large scale dynamic balance appears to be cyclostrophic. We observe a vertical wind shear of 10-15 m/s, with the higher altitude clouds moving faster than the low altitude clouds which form the majority of our measurements in the 60-70 km altitude layer. The -95 m/s mean equatorial velocity is very close to the phase velocity of the 4 1/2 day wave. This wave phenomenon produces observed variation in planetary albedo, and is correlated with both the meridional motion of the bright polar ring and with changes in curvature of the spiral streaks. Such a wave, propagating phase westward, could bring angular momentum up from below to support the zonal winds.

The momentum supplying wave, being correlated with a small change in planetary albedo, can be driven by the sun. Convective cells in the subsolar region are evidence of energy input at the right altitude. The only requirement is that the amplitude of the wave oscillations not be large enough to disrupt the zonal or meridional flow in the vortex, which in the mean must provide the necessary equator to pole energy transport to maintain global radiative equilibrium. If we believe the streak model, which seems so nicely correlated with everything else, the mean meridional velocity gradient is 0.20 m/s/deg and the amplitude of the wave is 0.10 m/s/deg. The strong vertical wind shear and turbulence observed near the equator at 45-50 km altitude by the Venera probes and Mariner radio occultation may form a lower bound for such planetary scale waves in the vertical.

The combination of an upper level vortex, cyclostrophic balance, and a global wave maintaining the zonal momentum supply in equilibrium with solar heating provides a consistent explanation for the stability of the upper atmosphere circulation pattern on Venus. The wave coupled cloud forms, subsolar convection intensity, and the associated albedo changes provide a means to perturb the mean flow (and thus pump in more or less solar energy as needed to drive the global wave) and also provide an adequate supply of feedback mechanisms to stabilize the vortex over periods of days or weeks and maintain the global energy balance. Long term changes, such as the disappearance of the bright polar cloud caps, may relate to more severe dynamic imbalances. Determining the interaction of the varied mechanisms

requires a longer time base study than the 8-day Mariner 10 flyby data provides. It should be possible to measure the relative strengths of the rich array of visible phenomena, however, and thereby determine which physical processes are likely to be important pieces of the dynamic puzzle of Venus.

ACKNOWLEDGEMENTS

The author wishes to thank Sanjay Limaye for numerous informative and educational discussions and Linda Kluck for typing of the final manuscript.

This research was supported by NASA Grant #NGR-50-002-189.

BIBLIOGRAPHY

Barker, E. S. and Perry, M. A.; 1975: "Semi-Periodic Variations in CO_2 Abundance on Venus," Icarus, 25, 282-295.

Belton, Michael J. S.; Smith, Gerald R.; Elliott, Denis A.; Klaasen, Kenneth; and Danielson, G. Edward; 1976: "Space-Time Relationships in the UV Markings on Venus," J. Atmos. Sci. (to be published).

Danielson, Edward; 1975: "Mariner 10 Imaging System," The Atmosphere of Venus, NASA SP-382, 40-41

Dollfus, Audouin; 1975: "Venus: Evolution of the Upper Atmospheric Clouds," J. Atmos. Sci., 32, 1060-1070.

Gierasch, Peter J.; 1970: "The Four-day Rotation in the Stratosphere of Venus: A Study in Radiative Driving," Icarus, 13, 25-33.

Howard, H. T., et. al.; 1974: "Venus: Mass, Gravity Field, Atmosphere, and Ionosphere as Measured by the Mariner 10 Dual Frequency Radio System," Science, 183, 1297-1301.

Ingersoll, A. P. and Orton, G. S.; 1974: "Lateral Inhomogeneities in the Venus Atmosphere: Analysis of Thermal Infrared Maps," Icarus, 21, 121-126.

Krauss, Robert J.; 1976a: "UV Cloud Motions on Venus from Mariner 10 Images," SSEC Annual Report for 1975 on JPL Contract 953034 and NASA Grant NGR50-002-189.

Krauss, Robert J.; 1976b: "New Measurements of UV Cloud Motions on Venus," SSEC Annual Report for 1975 on JPL Contract 953034 and NASA Grant NGR50-002-189.

Leovy, Conway B.; 1973: "Rotation of the Upper Atmosphere of Venus," J. Atmos. Sci., 30, 1218-1220.

Lorenz, Edward N.,; 1967: "The Nature and Theory of the General Circulation of the Atmosphere," World Meteorological Organization.

Malkus, Willem V. R.; 1970: "Hadley-Halley Circulation on Venus," J. Atmos. Sci., 27, 529-535.

Marov, M. Ya; Avduevsky, V. S.; Kerzhanovich, V. V.; Rozhdestuensky, M. K.; Borodin, N. F.; Ryabov, O. L.: 1973: "Venera 8: Measurements of Temperature, Pressure and Wind Velocity on the Illuminated Side of Venus," J. Atmos. Sci., 30, 1210-1214.

Murray, Bruce C.; Belton, Michael J. S.; Davies, Merton E.; Gault, Donald; Hopke, Bruce; O'Leary, Brian; Strom, Robert G.; Suomi, Verner; and Trask, Newell; 1974: "Venus: Atmospheric Motion and Structure from Mariner 10 Pictures," Science, 183, 1307-1315

Murray, Bruce C.; Wildey, Robert L.; and Westphal, James A.; 1963: "Venus: A Map of Its Brightness Temperature," Science, 141, 391-392.

O'Leary, Brian; 1975: "Comment on Mariner 10 and Ground Based UV Observations," The Atmosphere of Venus, NASA SP-382, 63-68.

Schubert, G. and Whitehead, J. A.; 1969: "Moving Flame Experiments with Liquid Mercury: Possible Implications for the Venus Atmosphere," Science, 163, 71-72.

Schubert, Gerald and Young, Richard E.; 1970: "The 4-Day Venus Circulation Driven by Periodic Thermal Forcing," J. Atmos. Sci., 27, 523-528.

Sinclair, A. C. E.; Basart, J. P.: Buhl, D.; and Gale, W. A.; 1972: "Precision Interferometric Observations of Venus at 11.1cm Wavelength," Astrophys. J., 175, 555-572.

Suomi, Verner; 1975: "Cloud Motions on Venus," The Atmosphere of Venus, NASA SP-382, 42-58.

Woo, Richard; 1975: "Observations of Turbulence in the Atmosphere of Venus Using Mariner 10 Radio Occultation Measurements," J. Atmos. Sci., 32, 1084-1090.

Young, Andrew T.; 1975: "The Clouds of Venus," J. Atmos. Sci., 32, 1125-1132.

Young, L. G.; Young, A. T.; Young, A. W.; and Bergstrahl, J. T.; 1973: "The Planet Venus: A New Periodic Spectrum Variable," Astrophys. J., 181, L5-L8.

A Dry Adiabatic Diagram for the Atmosphere of Venus and the Vertical Thermal Structure of the Atmosphere

Sanjay S. Limaye and Verner E. Suomi

Abstract

The dry adiabatic lapse rate γ_{ad} for an atmosphere of different mixtures of carbon dioxide and nitrogen (8%, 4%, and 0% nitrogen by mass) is computed as a function of temperature and pressure and an adiabatic diagram depicting the dry adiabatic temperature changes constructed. Following Staley (1970) the real gas expression for the dry adiabatic lapse rate is used, incorporating the tabulated values of the specific heats of nitrogen and carbon dioxide. A four point Lagrangian interpolation scheme as recommended by Hilsenrath et al. (1960) is used to minimize interpolation errors in the specific heats at intermediate pressures and the variation in the acceleration due to gravity with altitude is included in the computation.

The results indicate that the dry adiabatic lapse rate is about $7.98 K \cdot km^{-1}$ at 93 atm pressure and 740K and increases to about $10.25 K \cdot km^{-1}$ at 1.0 atm pressure and $T \doteq 300K$ for 4% nitrogen and 96% carbon dioxide. At a given pressure the dry adiabatic lapse rate is seen to increase with pressure and decrease with increasing amounts of nitrogen for the same pressure and temperature.

Comparison of the temperature profiles obtained from Veneras 4 through 8 and Mariners 5 and 10 against the dry adiabatic diagrams indicate a transition layer at about 3-5 atmospheres level (~38 km altitude) wherein the lapse rate changes from a neutral value to a very stable one, depending on the composition, tempting one to define this as the tropopause level for the atmosphere of Venus. This agrees with the lower level limit for maximum solar energy deposition, suggested by Lacis (1974).

Below this transition layer the atmospheric stability is inconclusive due to experimental errors and uncertainty in the adiabatic temperature changes up to 20% of nitrogen by mass needs to be present in the atmosphere to make the observed profile neutrally stable. Other gasses of lower specific heats will also have a similar effect. However there is independent evidence in terms of vertical shear of the horizontal wind (Venera 7 and Venera 8) and in Mariner 5 and 10 detection of turbulence (Woo et.al. 1974, 1975) which is indicative of an unstable layer below about 38 km.

Introduction

The presence or absence of an adiabatic lapse rate of temperature in planetary atmospheres is an important factor in the atmospheric motions. In the case of the terrestrial atmosphere one usually assumes ideal gas behavior. Thus, the dry adiabatic lapse rate is easily defined as the ratio g/C_p where g is the acceleration due to gravity and C_p is the specific heat of air at constant pressure. It was indicated by Staley (1970) that this definition is not readily applicable for the atmosphere on Venus because

at much higher pressures the atmospheric state is far from ideal. An expression derived for a real gas is needed to specify the dry adiabatic lapse rate of temperature on Venus, once the atmospheric composition is known.

The vertical thermal structure of the Venusian atmosphere has been probed so far by five Russian capsules which have descended in the atmosphere and remotely through the radio occultation technique by the American spacecrafts Mariner 5 and Mariner 10. (Marov et al., 1973; Howard et al., 1974). The atmospheric composition, however, has been estimated from the Russian entry probes Veneras 4, 5, and 6, all of which measured the composition at less than about 10 atmospheres pressure. The atmospheric composition indicated is up to about 97% carbon dioxide and the rest predominantly nitrogen, up to about 8% (Vinogradov et al., 1968; Marov, 1973).

Based on this knowledge of the atmospheric composition, all the temperature profiles have been generally interpreted to be mostly adiabatic. Unfortunately, however, the "standard", i.e. the value of the adiabatic lapse rate itself has not been reported in almost all the previous publications.

It is interesting to note that on a slightly more careful scrutiny of the temperature profiles to date, superadiabatic regions are suspected (Fjeldbo et al., 1971; Avduevsky et al., 1968; Ainsworth et al., 1974). Indeed, the experimental conditions involved may cause the measurement errors to be greater than those measured in the laboratory, yet the doubts of a superadiabatic region in the lower atmosphere cannot be completely eliminated as a reinterpretation of the Venera 8 profile also indicates (Ainsworth and Herman, 1974).

This paper describes the attempt to specify the magnitude of the dry adiabatic lapse rate in the Venusian atmosphere more accurately.

In the following sections, the considerations which went into the construction of the adiabatic diagram based on a real gas definition of γ_{ad} are described. It should be pointed out here that except for the case of 100% carbon dioxide, the dry adiabatic lapse rate calculation for a mixture of carbon dioxide and nitrogen is based on a simplistic approach that the molecular interactions at the high temperatures and pressures in the lower atmosphere of Venus are negligible in terms of their influence on the dry adiabatic temperature changes. We then compare the measured (T,p) profiles for the atmosphere of Venus against these values of the dry adiabatic lapse rate to infer about the static stability.

Construction of the Adiabatic Diagram

Staley (1970) has pointed out that the ideal gas definition $\gamma_{ad} = g/C_p$ is not applicable in the case of Venus because of large deviations of the atmosphere from idealness. As a result, the specific heat at constant pressure cannot be taken to be constant. Fig. 1 shows the variation of the specific heat of carbon dioxide at constant pressure under the conditions found in the atmosphere of Venus. The critical parameters for carbon

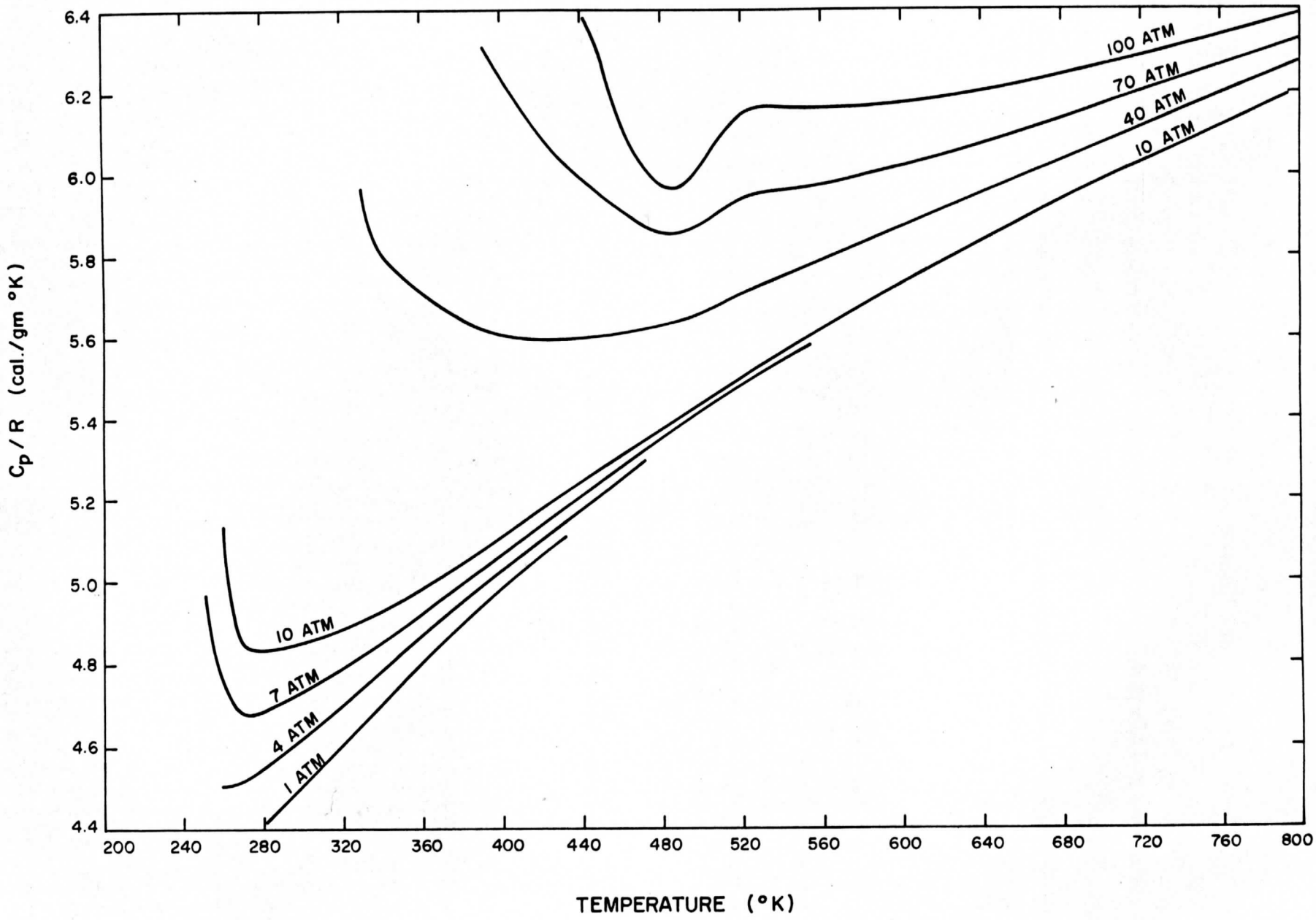

Figure 1. Variation of specific heat C_p of carbon dioxide at constant pressure at various temperatures and pressures. The tabulated values of C_p have been taken from Hilsenrath et al. (1960).

dioxide and nitrogen are given in Table 1 (from Handbook of Physics and Chemistry, Pergamon Press, 1962).

TABLE 1

Critical Temperature and Pressure for Nitrogen and Carbon Dioxide

	PRESSURE	TEMPERATURE
Nitrogen	34 atm	126.3K
Carbon Dioxide	75.27 atm	304K

It is seen that the critical pressure level for carbon dioxide and nitrogen occurs in the lower Venusian atmosphere.

For a real gas, the dry adiabatic lapse rate can be shown to be (Staley, 1970):

$$\gamma_{ad} = -\frac{dT}{dz} = -\frac{T(\partial p/\partial T)_\alpha}{(\partial p/\partial \alpha)_T}\left(\frac{g}{C_p}\right) = \frac{T(\partial p/\partial T)_\rho}{(\partial p/\partial \alpha)_T}\left(\frac{g}{C_p}\right) \qquad (1)$$

where α: specific volume

ρ: density $= \frac{1}{\alpha}$

g: acceleration due to gravity.

The hydrostatic assumption is made in arriving at the above expression. There seems to be only one source of tabulated values of thermodynamic variables for carbon dioxide and nitrogen (Hilsenrath, 1960). The tabulated values which have been used in the present work have been arrived at from a compilation of all available measurements and interpolation. The deviation of the tabulated values from direct measurements is generally less than 2% for specific heats of carbon dioxide and nitrogen and about 0.5% for their tabulated valued for density/compressibility.

The expression for ∂_{ad} can be transformed into a form involving the compressibility factor Z, through the use of the virial equation of state:

$$\frac{\alpha p}{RT} = 1 + \frac{B(T)}{\alpha} + \frac{C(T)}{\alpha^2} + \ldots = Z \qquad (2)$$

where B(T) and C(T) ... are the virial coefficients. The aforementioned source contains tabulated values of Z(p,T) and C_p(p,T). Following Staley (1970):

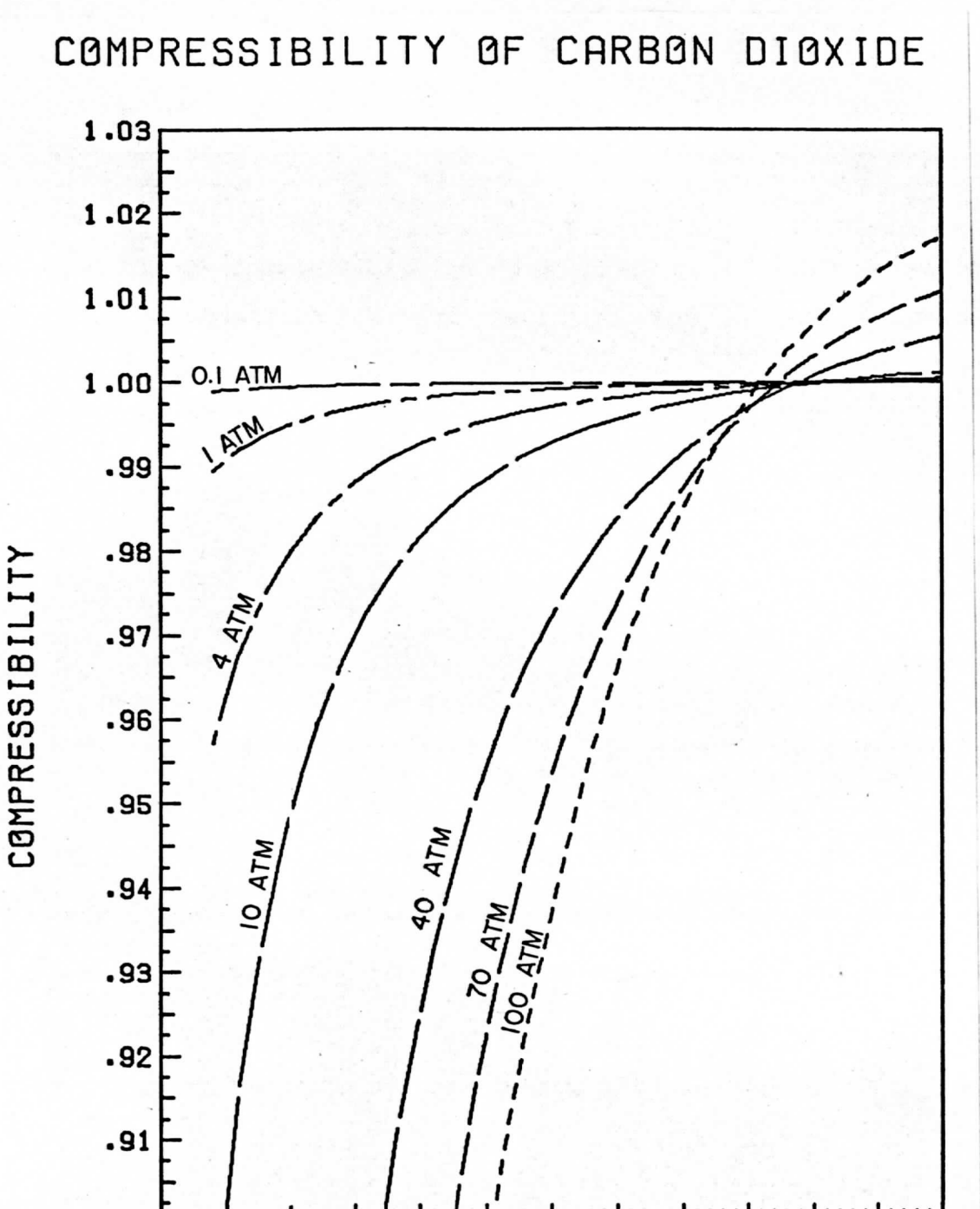

Figure 2. Compressibility factors for carbon dioxide (values from Hilsenrath, 1960).

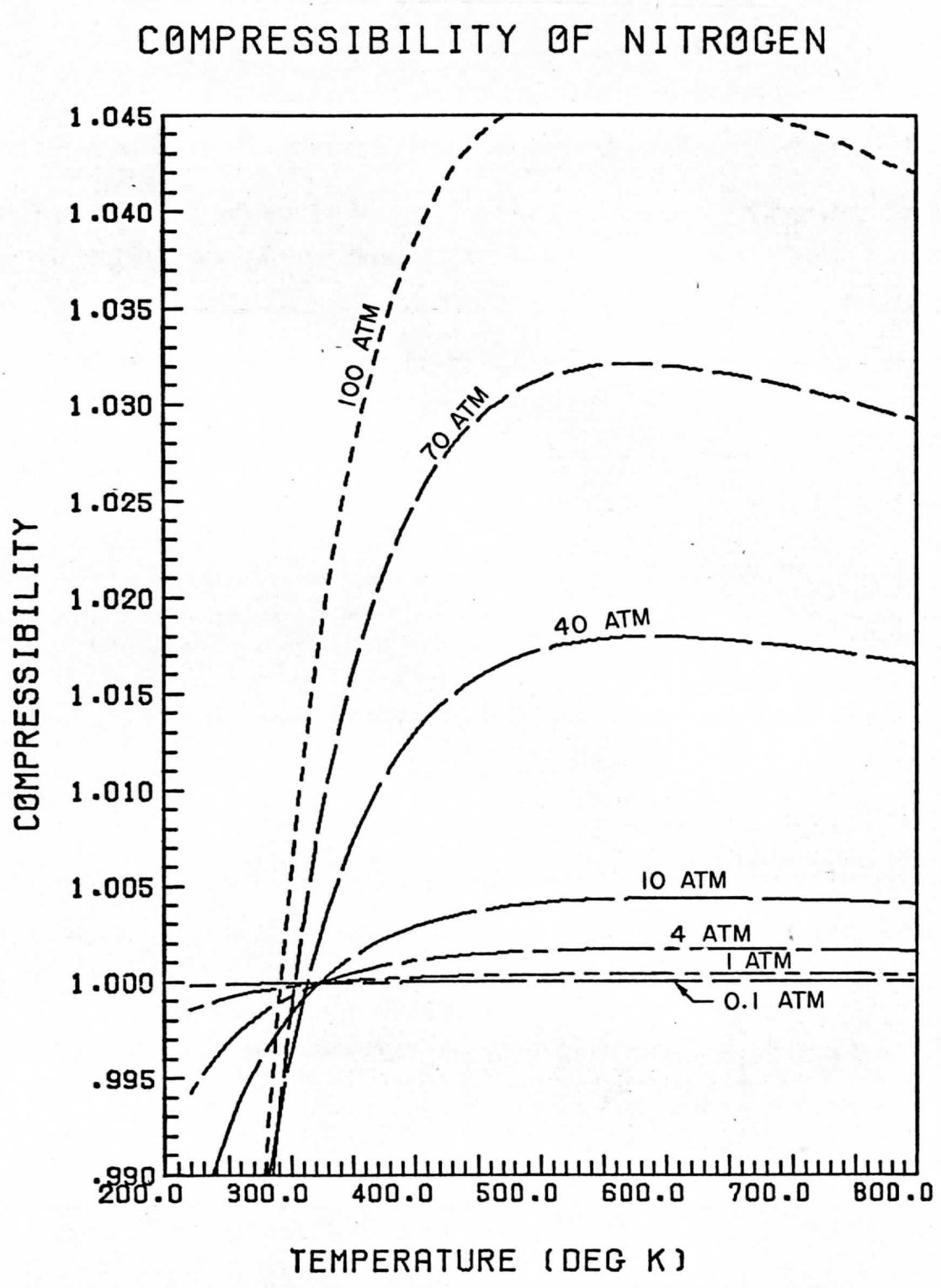

Figure 3. Same as Figure 2, but for nitrogen.

$$T(\partial p/\partial T)_\rho = \frac{p[\frac{\partial}{\partial T}(TZ)_p]}{Z - p(\partial Z/\partial p)_T} \tag{3}$$

and $$\rho(\frac{\partial p}{\partial \rho})_T = \frac{pZ}{Z - p(\partial Z/\partial p)_T} \tag{4}$$

so that $$\gamma_{ad} = \frac{1}{Z}[\frac{\partial}{\partial T}(ZT)]\frac{g}{C_p} \tag{5}$$

or equivalently,

$$\gamma_{ad} = -\frac{T}{\rho}(\frac{\partial}{\partial T})_p \frac{g}{C_p} \tag{6}$$

However, this form offers no advantage over the one involving the compressibility factor for computational purposes since the tabulated values of density and the compressibility factor have been made internally consistent (Hilsenrath, 1960).

The thermodynamic values needed for calculation are tabulated at 0.01 and n.(0.1, 0.4, and 0.7) atmospheres pressure (where n = 1, 10, 100) up to 100 atmospheres and at every 10K interval from generally 200K to 1500K. (See Figs. 2 and 3 for Z(p,T) for carbon dioxide and nitrogen respectively).

The adiabatic diagram was then constructed using the aforementioned definition of γ_{ad} as follows: the value of $\gamma_{ad}(T_o,p_o)$ was first computed at an initial point T_o and p_o. T_o was varied from 1000K to 700K and p_o was fixed at 100 atmospheres. The temperature T at a pressure $p-\Delta p$ is computed using the previous value of the lapse rate. The compressibility factor at this new pressure level and temperature is then computed from the tabulated values by a linear interpolation for temperature and four point Lagrangian interpolation (Conte, 1965) for pressure, in order to minimize the errors introduced by linear interpolation for pressure as suggested by Hilsenrath et al. as follows:

$$f(p) = \sum_{k=0}^{n} L_k(p) f_k \tag{7}$$

where L_k are the polynomials:

$$L_k(p) = \prod_{\substack{j=0 \\ j\neq k}}^{n} (p - p_j) \Big/ \prod_{\substack{j=0 \\ j\neq k}}^{n} (p_k - p) \quad j,k=0,1,2,\ldots,n$$

TABLE 2

CONSTANTS USED IN CALCULATIONS

Ratio of Mass of Sun to Mass of Venus (Howard, et.al. 1974) = 408,523.9±1.2

Equivalently, product of gravitational constant mass of sun = 324,858.6±1.0 km^3 sec^{-2}

Radius of Venus = 6053.0 km

ALTITUDE	ACCELERATION DUE TO GRAVITY
0 km	885.14 cm sec^{-2}
10	882.2
20	879.3
30	876.4
40	873.5
50	870.4
60	867.9
70	865.0
80	862.0

Thus L_k is a polynomial of degree n. The first four terms are retained for interpolating C_p and Z values as a function of pressure. p_is are the values of pressure for which the values of specific heat and the compressibility factor have been tabulated. The pressure decrement was initially taken to be one atmosphere up to one atmosphere, 0.1 atmosphere up to 0.1 atmosphere pressure and further reduced to 0.01 atmosphere from then on.

The lapse rate is then computed from a finite difference form of (5) with a temperature step of 10K.

The hypsometric height of every pressure level was also computed along the way through the use of the hypsometric equation:

$$\Delta Z = \frac{R\overline{T}}{g} \ln \frac{p_1}{p_2} \tag{8}$$

a. Variation in Acceleration Due to Gravity

The adiabatic change in temperature from a pressure of 100 atmospheres to 10 atmospheres is about 250K, for a temperature of 750K at 100 atmospheres the altitude at 10 atmospheres computed hysometrically is approximately 28 km, and about 50 km for one atmosphere. It is obvious then that the variation in the gravitational acceleration with altitude is about 3%. Thus the adiabatic change over a large pressure drop could be significantly in error. For this reason, the gravitational acceleration g was computed at every step during the upward marching calculations. The relevant factors used in arriving at the surface value of g (=885.14 $cm \cdot sec^{-2}$) are listed in Table 2 and are based upon the most recent estimate of the ratio of the mass of Venus to the mass of the sun from Mariner 10 orbit parameters (Howard et al., 1974).

b. Computational Stability

In order to check whether the accumulated error due to the finite pressure decrement was significant, the calculations were repeated for half the original step. At the end of 200 such steps (i.e. at one atmosphere level from an initial pressure of 100 atmospheres) the adiabatic change was within 0.5-1% of that arrived at by twice the step-size. Error in the computed adiabatic change in temperature is thus less than those caused by the uncertainty in the tabulated valued of compressibility and the specific heat at constant pressure. Small changes in the 10K step size used in the linear interpolation in T also did not cause any significant changes in the results.

c. Addition of Nitrogen

The exact composition of the atmosphere on Venus is not yet known. All in situ measurements have been made at pressures less than 10 atmospheres, so that the well-mixedness of the lower atmosphere has not yet been firmly established. Nevertheless, measurements indicate that there may be up to

10% nitrogen (Avduevsky et al., 1968). The dry adiabatic lapse rate for a mixture of carbon dioxide and nitrogen for a given proportion of mass was computed in a simplistic manner on the assumption that the two constituents change their temperature in an adiabatic process independent of each other. The lapse rate was computed independently for both carbon dioxide and nitrogen and the adiabatic change for the mixture for a given pressure drop was computed knowing the individual adiabatic change for each of the two and the proportion in which they are mixed. It has been tacitly assumed that the atmospheric composition on Venus is uniform throughout the atmosphere. The resultant adiabatic diagrams for 0%, 4%, 8%, 12%, and 20% nitrogen by mass are shown in Figs. 5, 4, 6, 7, and 8 respectively.

The dry adiabats in these figures have been drawn with skew T-ln p coordinates for temperatures between 700K and 800K at 100 atmospheres. The skew T axis is chosen because it tends to maximize the angle between the dry adiabats and the temperature profile (Hess, 1959). The required transformation is:

$$x = T(p) + 200.0 - \frac{100.0}{\ln 10.0} \ln p \qquad (9)$$

The dry adiabats on these diagrams are lines of constant potential temperature. For reasons mentioned earlier the potential temperature for a real atmosphere cannot be accurately specified through the Poisson equation:

$$\theta = T \left(\frac{p}{p_o}\right)^{R/C_p}$$

Comparison of Measured (T,p) Profiles for the Atmosphere of Venus Against the Dry Adiabatic Diagrams

Temperature profiles from Venera 8 in situ measurement and Mariner 10 entry signal (S-band) data are plotted on the skew-T log (p) diagrams in Figs. 4, 5, 6, 7, & 8. The Venera 8 measurements start at an altitude of 53.7 km above surface or 0.51 kg·cm^2 pressure (Marov et al., 1973). The S-band data from Mariner 10 was reduced assuming a 100% carbon dioxide atmosphere (Howard et al. 1974) and hence its interpretation regarding the static stability for a different atmospheric composition is not possible.

For the 100% carbon dioxide atmosphere the Venera 8 profile is seen to be super-adiabatic up to 37 km or about 5 atm pressure level. The S-band signal on Mariner 10 did not penetrate deeper than 40 km and thus no information about the deep atmospheric profile is available.

The existence of a layer with a neutral lapse rate at about 1 atm level reported by Howard et al. (1974) is confirmed. Above this level the Mariner 10 profile is highly stable as evidenced by the sharp increase in potential temperature (referred to 100 atm pressure). The great instability of the atmosphere above 3 atm level or about 40 km above the surface was observed in Mariner 5 profile (Fjeldbo et al. 1971) and Venera 8 measurements also.

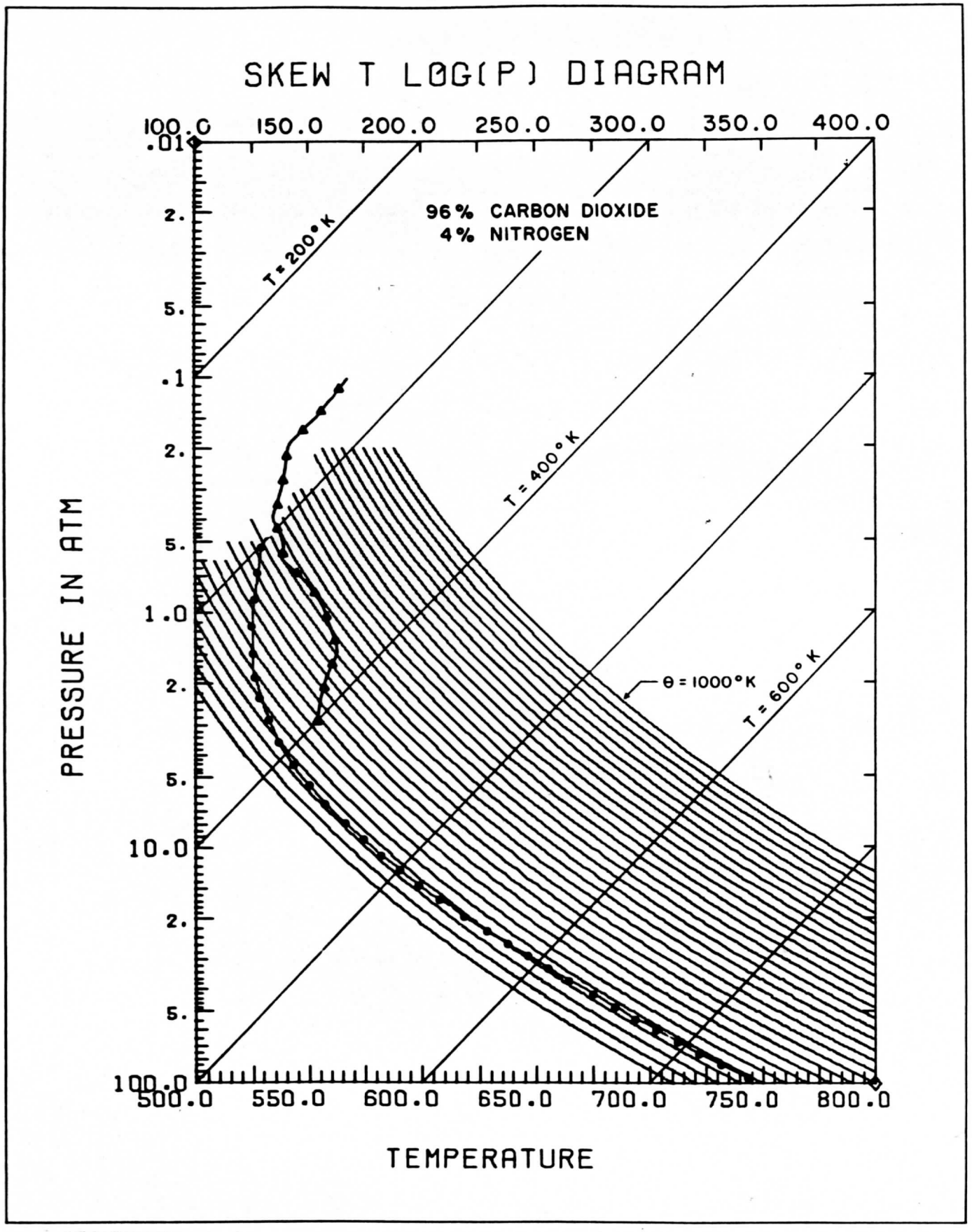

Figure 4. The dry adiabatic diagram for 96% carbon dioxide atmosphere. The dry adiabats are drawn at 10K intervals, between 700K and 1000K. The potential temperature is referred to 100 atm pressure.

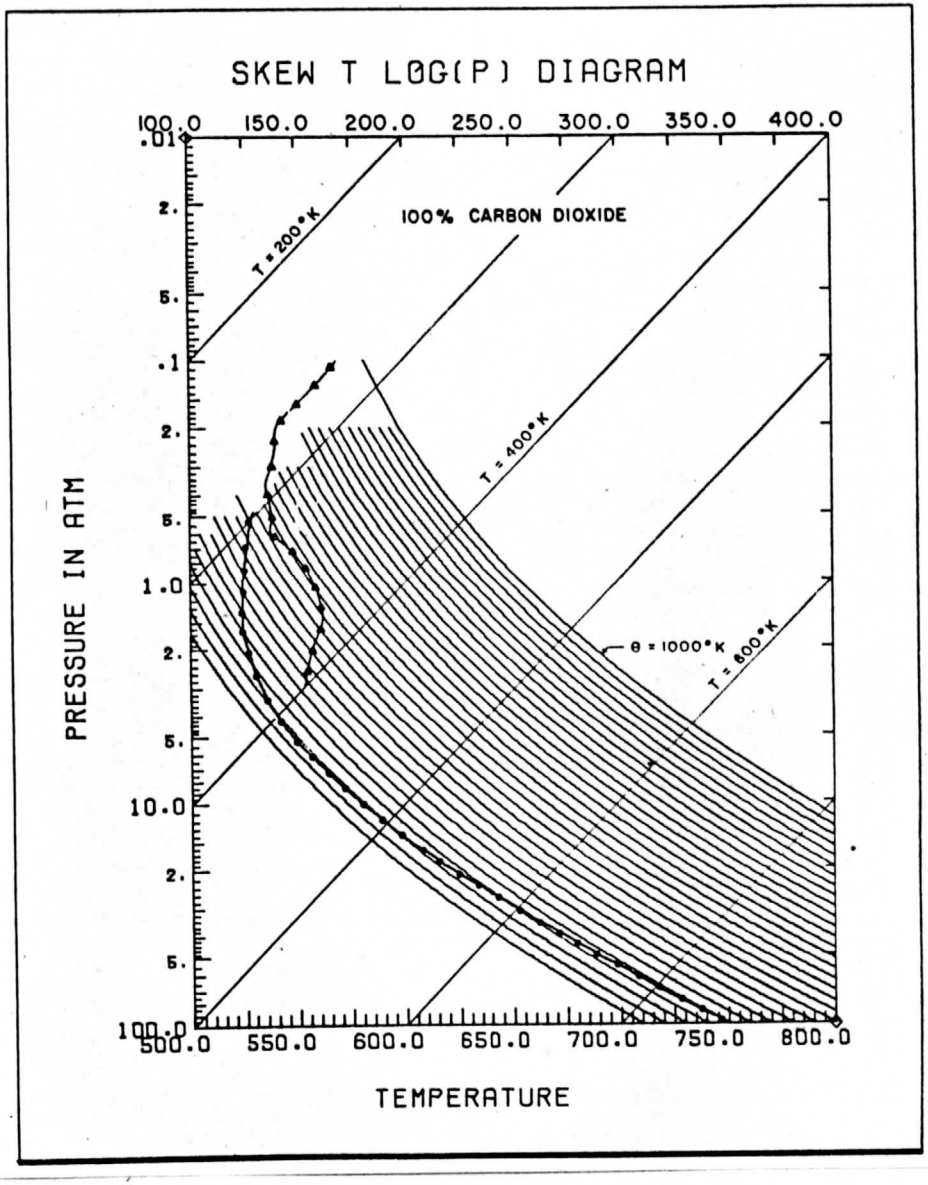

Figure 5. Same as Figure 4, for pure CO_2.

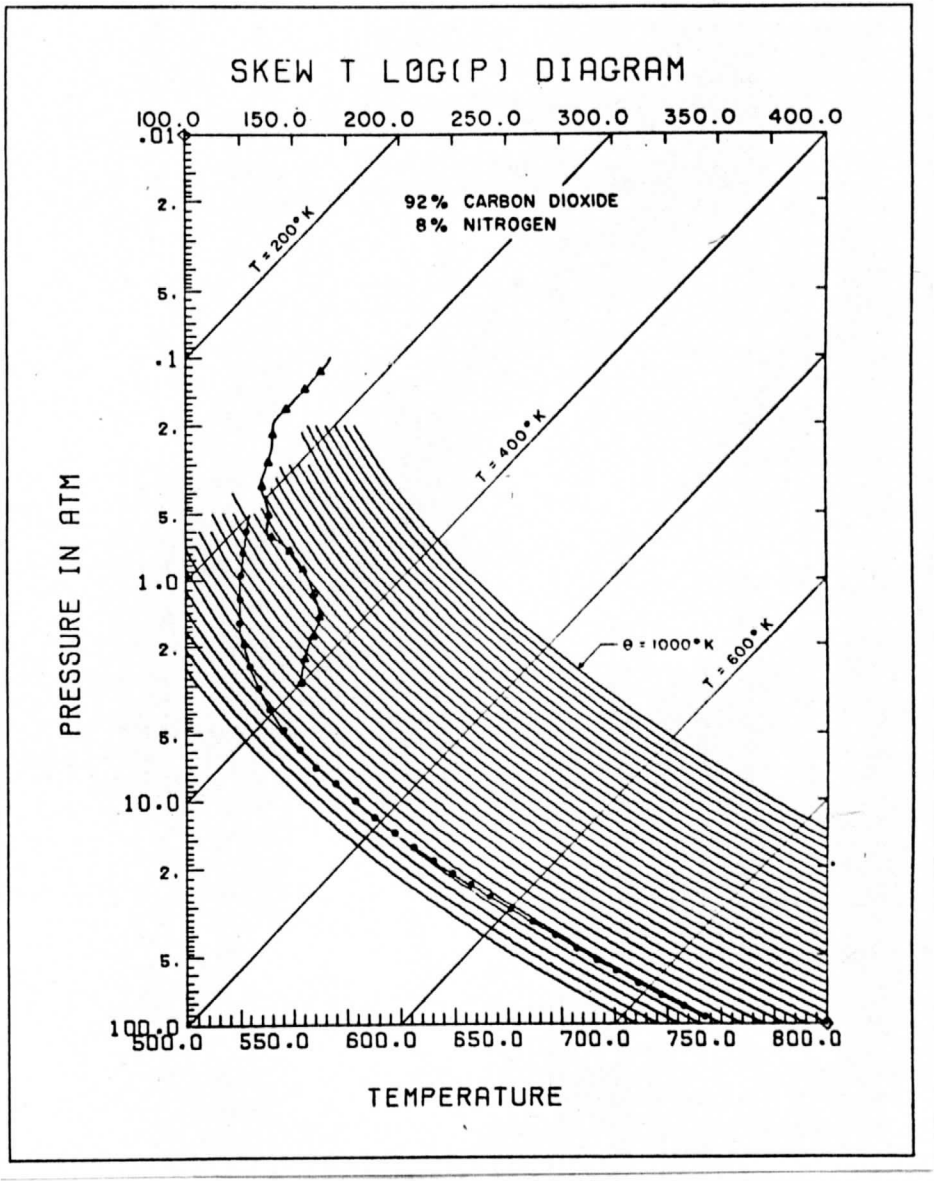

Figure 6. Same as Figure 4, for 8% N_2.

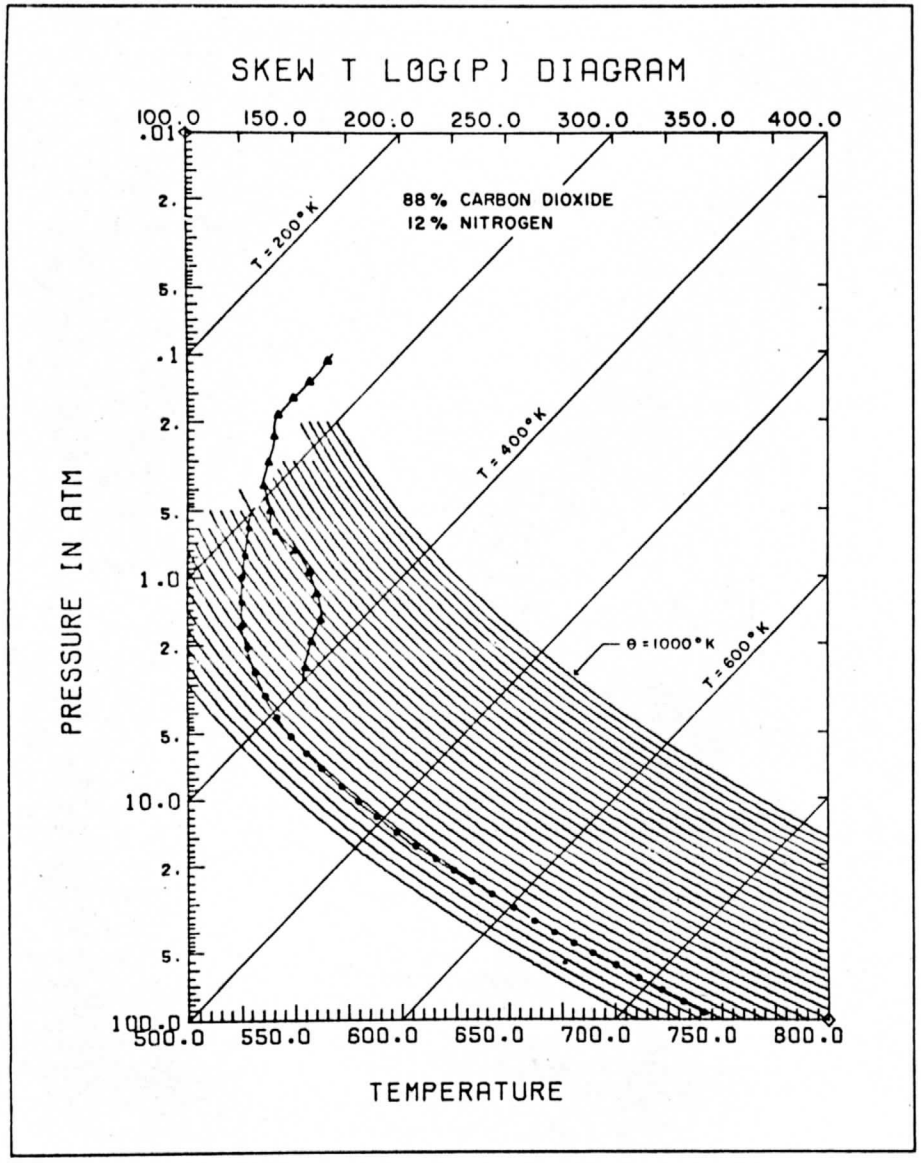

Figure 7. Same as Figure 4, for 12% N_2.

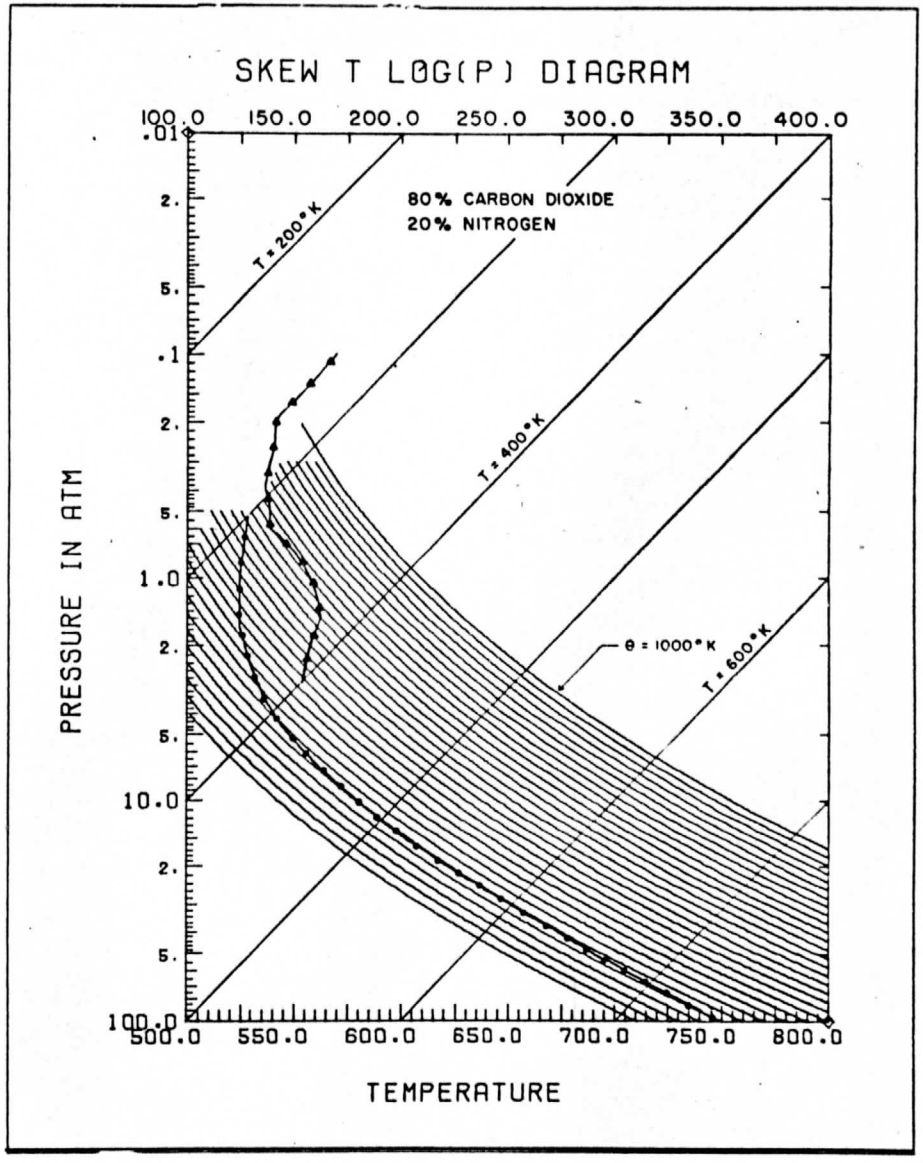

Figure 8. Same as Figure 4, for 20% N_2.

Interpretation of the Venera 8 solar illumination and ground based observations by Lacis (1975) that most of the solar energy is deposited above 40 km for a homogeneous distribution of cloud particles with height and between 50 km and 80 km for a continuous cloud particle distribution, is consistent with the increasing stability observed in both the Venera 8 and Mariner 10 profiles.

It is of interest to note that both the Venera 7 and 8 vertical profiles of horizontal wind show a very large shear between about 38 km and 50 km above the surface and a very small shear between about 18 km and 38 km. Such strong shear is possible in a stable environment, and if it is of a semi-permanent nature, can be maintained only in a stable stratified atmosphere wherein the vertically adjacent layers are decoupled as far as flow in those layers is concerned.

Going back to the earlier measurements of the temperature profiles, one again sees an increase in the static stability in the Venera 4 profile (Avdeuvsky et al., 1968) based on the lapse rate reported by Avdeuvsky et al. (1968) and the adiabatic lapse rates calculated here, after the altitude values of Venera 4 have been corrected for the wrong surface radius assumed by Avdeuvsky et al. (1968), (a discussion of the discrepancy is given by Ash et al., 1968, Science, (1960), 985).

Lastly, no information about the thermal structure is available in the vicinity of 38 km above the surface from either Mariner 5 or Mariner 10 due to loss of signal.

Turning the attention now to the part below the strongly stable layer, there seems a neutrally stable layer a few atmospheres thick, down to about eight atmospheres level. Below this level, however, one sees a largely superadiabatic layer. The immediate question that arises then is whether it is real.

It should be borne in mind here that a very accurate indication of the measurement error for the temperature profiles is unavailable. The accuracy of the Mariner 5 and Mariner 10 radio occultation measurements is limited by the fact that an atmospheric composition must be known beforehand and that the sampling volume is relatively large. Further, the temperature at a certain level above the surface needs to be specified as an initial condition, though it does not seem to affect the derived temperature profile below about 80 km (Howard et al., 1974).

The temperature profile measurements by the Venera probes have different kinds of problems. These are all in situ measurements. The errors in the temperature profiles are due to errors in not only the temperature sensors, but also the altimeter and pressure sensor. Ainsworth and Herman (1974) indicate the many possible interpretations of Venera 8 measurements for constructing a temperature profile.

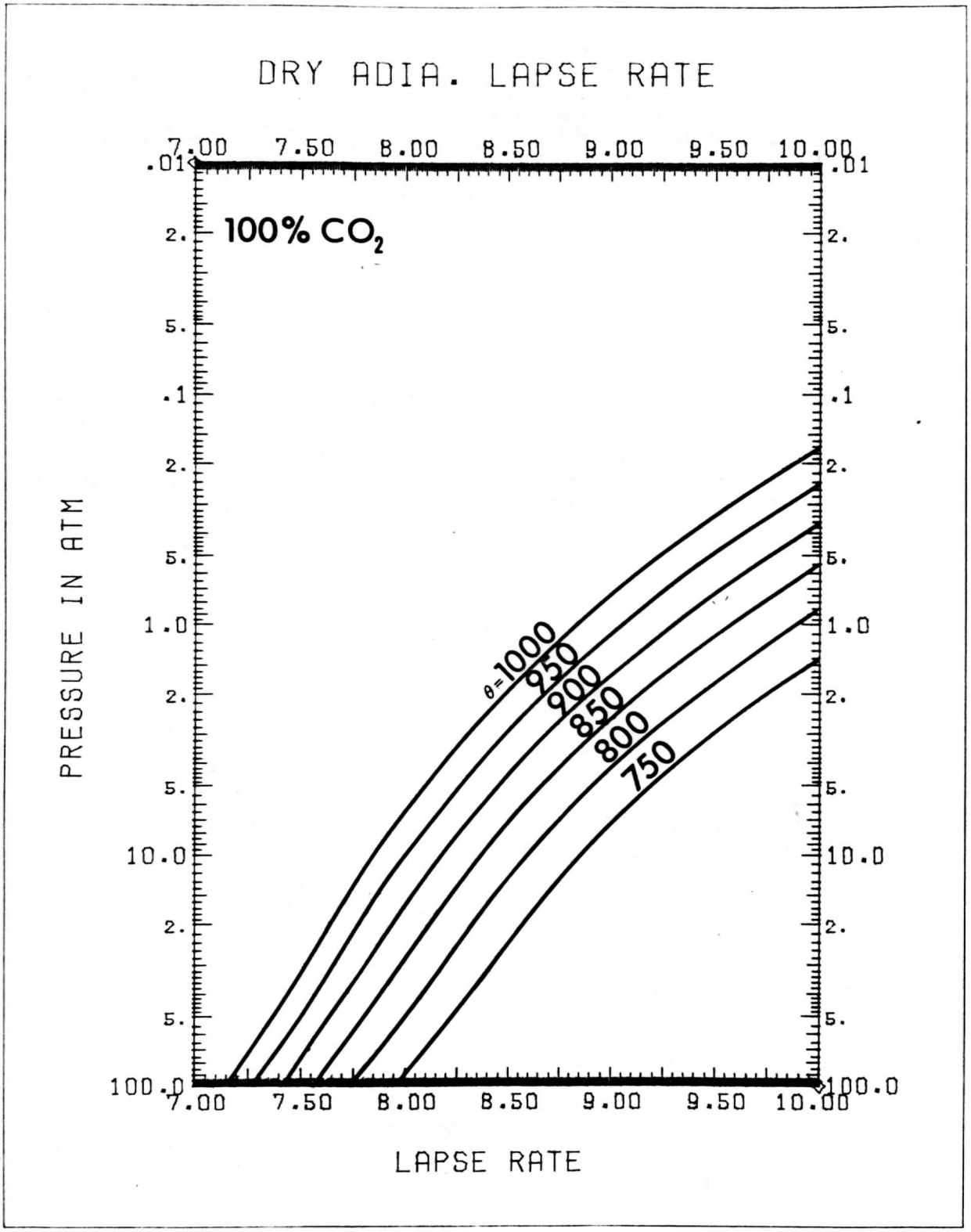

Figure 9. The dry adiabatic lapse rate in 100% CO_2 atmosphere expressed in degrees K/km as a function of atmospheric pressure for constant potential temperature.

a. Is the Lower Atmosphere Statically Unstable?

The RMS error in Venera 8 temperature profiles is ±7K (Marov, 1973). The difference between the surface temperature (at 92.87 ± 1.5 atm) 741 ± 7K and the 10 atm temperature (481 ± 7K) is thus 260 ± 14K. The adiabatic change in temperature between the surface pressure and 10 atm is approximately 244K, for the 100% CO_2 case. As indicated earlier, the tabulated specific heat capacities used in the calculations are within about 1-2% of the measured values so that the uncertainty in the adiabatic change from the surface presure value to the 10 atm level of 244K is about ±5K.

The corresponding values for the 4% nitrogen and 8% nitrogen are ~248 ± 5K and 252 ± 5K. Based on these certainties both in temperature profile and the adiabatic diagram, the possibility of a deep superadiabatic layer below 10 atm level for up to 12% of nitrogen in the atmosphere can neither be confirmed nor eliminated. The only other indirect evidence for existence of unstable layers is the turbulence detected at about the two atmospheres level for Mariner 10 dual band radar (Woo et al., 1974; 1975), discussed later.

The features visible in the Mariner 10 pictures are at about 60 km above the surface or at about 0.3 atmospheres level (Suomi et al., 1974). The level of free sink as determined from the adiabatic diagrams by energy considerations is at a lower level than this, between 0.5 and 2.2 atmospheres for 0 to 8% nitrogen, consistent with the turbulent layer detected from Mariners 5 and 10, as also large shear zones by Veneras 7 and 8 (Marov et al., 1974).

Assuming a deep unstable layer below 10 atmospheres pressure, the state of the atmosphere below 0.3 atmospheres can be visualized as follows. The release of convective instability somewhere in the lower atmosphere causes a parcel to accelerate vertically upwards. At about the 10 atmospheres level, it has attained its maximum buoyancy and speed. Beyond this level, however, the parcel of air starts to lose its buoyancy and there is an increasing restoring force acting on the parcel. The static stability of the atmosphere increases so dramatically that a parcel loses all its buoyancy by the time it reaches approximately the 0.5 atm level for the 100% CO_2 case, 1.4 atm for the 96% CO_2 and 4% nitrogen case, and approximately 2.4 atm level in the 92% CO_2 and 8% nitrogen case. The hypsometric heights in the three cases are respectively 54.2 km, 48.5 km and 44.8 km.

The period of Brunt-Väisälä oscillations in these cases is about 3 minutes. Because the static stability increases very rapidly beyond this point, the period of vertical oscillations decreases rapidly. It is thus conceivable that there is sufficient spatial variation in the instantaneous vertical motion at this level which is detectable as turbulence, as was detected by both Mariner 5 and Mariner 10 missions (Woo et al., 1974, 1975).

The horizontal velocity profile below 40 km altitude deduced from Venera 7 and 8 also warrants some discussion. Both the profiles show a very small shear between about 10 km and 40 km with a large shear region around 10 km. If indeed the lower troposphere is statically unstable, one might expect significant updrafts and downdrafts which would cause

vertical mixing and tend to equalize the linear momentum per unit mass in the vertical, similar to the conditions found in the mature state of a squall line as an empirical model suggests (Lettau, 1974).

Vertical mixing would naturally tend to produce an adiabatic temperature profile. The requirement then, that the instability be of a semi-permanent nature as all available evidence suggests, demands that there be a sustaining mechanism in the form of heating from below and/or cooling in upper layers, up to 40 km.

Thus, while the lower tropospheric velocity profile above 10 km altitude is in agreement with the concept of an unstable atmosphere, it points to other difficulties.

In light of the detection of the turbulence at the expected level, the case for a deep unstable layer on Venus is strengthened. Considering that the to-date temperature profile measurements have been made at different times and different places on the planet, this could be a recurrent feature of Venus as Ainsworth and Herman (1974) also suggest.

b. Visible Evidence of Convection

As mentioned earlier, the top of the clouds or the UV-features on Venus is at about 0.3 atm level (70 km above surface). This is in a very stable region of the atmosphere and the level of free sinking is considerably lower. The strong vertical motions are thus damped out below the level of the cloud tops. The high resolution Mariner 10 UV photographs show small scale polygonal features which are indicators of shallow convection (see Figure 10). The size of these cells is of the order of 10 km (Murray et al., 1974). It is possible that these features are related to the large apparent convective instability in the lower atmosphere.

Summary

A detailed computation of adiabats for the Venusian atmosphere based on the known limits on its composition and the available thermodynamic data for these constituents indicate the following:

1. All available measurements of the temperature profiles for the atmosphere on Venus show a dramatic increase in the static stability between about 3 and 6 atmospheres level, depending on the amount of nitrogen (the limits are for 0% and 8% nitrogen respectively). The in situ measurements have been in the vicinity of the equator of the planet near the morning terminator, and the discussion herein pertains mostly to the tropical regions.

Figure 10. A high resolution image of Venus taken from one of the cameras on the Mariner 10 spacecraft through the ultra-violet filter. The spatial resolution is of the order of 10 km. This image has been stretched in the gray levels to emphasize contrasts.

2. Computations indicate that there is a likelihood of a deep superadiabatic layer below a level of about 5 and 8 atmospheres, depending on the atmospheric composition. This agrees well with the detection of turbulence around 1.5 to 2 atmospheres by Mariner 5, Mariner 10 and the Veneras 4 through 8 measurements.

3. Up to 20% nitrogen by mass needs to be present in the atmosphere to reduce the lower atmosphere to an adiabatic state, according to the results (see Figure 8). Other gases such as argon will have a similar effect.

The accuracy of the adiabatic temperature changes for a given pressure change and a given composition is limited by the accuracy of the specific heat and the compressibility measurements, which for both carbon dioxide and nitrogen are about 2%. The uncertainty in adiabatic temperature changes is thus about 2%.

The computation of dry adiabatic lapse rates for a real gas requires tables of the gas compressibility factors. In some instances the Van der Waal equation of state is a fair approximation to the virial equation of state and in such instances the dry adiabatic lapse rates can be computed readily. Limaye (1975) has computed the Van der Waalian dry adiabatic lapse rate for a 100% carbon dioxide atmosphere and compares the Venera 8 temperature profile with the computed lapse rates. The accuracy of the adiabatic temperature changes based upon Van der Waal equation of state is good only for small pressure changes and thus its applicability in the case of the deep atmosphere of Venus is limited.

In order to really establish or deny the existence of superadiabatic layers on Venus, one needs more accurate knowledge of the atmospheric composition, the thermodynamic properties, and the effects of any minor condensable constituents, whose effect has been ignored in the present work. It should be nice indeed if it were possible to synthesize the Venusian atmosphere in the laboratory and to deduce the thermodynamic properties. Until then, one must wait for more accurate measurements of the temperature profile and also the composition.

The spatial variation of the thermal field in the atmosphere of Venus is not very well known. It is possible that the vertical thermal structure in the polar regions is different from that in the equatorial regions and there may be small but significant day-night differences. It is hoped that the Pioneer Multiprobe mission to Venus and the Pioneer Orbiter mission in 1978 will yield data towards a better definition of the thermal field.

Acknowledgements

The authors thank Dr. M. J. S. Belton for his comments and interest in the present work. This research was supported by JPL Contract #953034 and by NASA Grant #NGR-50-002-189.

References:

Ainsworth, J. E. and J. R. Herman, 1974: An Analysis of the Venera 8 Measurements, NASA/GSFC X-623-74-37, Greenbelt, Maryland.

Ash, M. E., D. B. Campbell, R. B. Dyce, R. P. Ingall, R. Jurgens, G. H. Pettengill, I. I. Shapiro, M. A. Slade, T. W. Thompson, 1968: The Case for the Radar Radius of Venus. Science, (160), 985.

Avduevsky, V. S., M. Y. Marov and M. K. Rozhdestvensky, 1968: Model of the Atmosphere of the Planet Venus Based on Results of Measurements Made by the Soviet Automatic Interplanetary Station Venera 4. J. Atmos. Sci., (25), 537-545.

Avduevsky, V. S., M. Y. Marov, and M. K. Rozhdestvensky, 1970: Preliminary Results of Measurements by Space Probes Venera 5 and Venera 6 in the Atmosphere of Venus, Radio Sci., (5), 333-338.

Avduevsky, V. S., M. Y. Marov, and M. K. Rozhdestvensky, N. F. Borodin, and V. V. Kerzanovich, 1971: Landing of the Automatic Station Venera 7 on the Venus Surface and Preliminary Results of Investigations of the Venus Atmosphere. J. Atmos. Sci., (28), 263-269.

Cess, R. D., 1972: The Thermal Structure within the Stratospheres of Venus and Mars. Icarus, (17), 561-569.

Conte, S. D., 1965: Elementary Numerical Analysis, McGraw Hill Book Company, New York. 278 pp.

Eshelman, V. R., G. Fjeldbo, J. D. Anderson, A. Kliore, R. B. Dyce, 1968: Venus: Lower Atmospheres not Measured. Science, (162), 661-665.

Fjeldbo, G. and A. J. Kliore, and V. R. Eshelman, 1971: The Neutral Atmosphere of Venus as Studied with the Mariner 5 Radio Occultation Experiments. Astron. J. (76), 123-140.

Hess, S. L., 1959: Introduction to Theoretical Meteorology. Holt, Rinehart, and Winston, New York. 362 pp.

Hilsenrath, J., C. W. Becket, W. S. Benedict, L. Farro, H. J. Hoge, J. F. Masi, R. L. Nuttal, Y. S. Toulobian, and H. W. Woolley, 1960: Tables of Thermodynamic and Transport Properties of Air, Argon, Carbon Dioxide, Carbon Monoxide, Hydrogen, Nitrogen, Oxygen and Steam. Pergamon Press, New York.

Howard, H. T., G. L. Tyler, G. Fjeldbo, A. J. Kliore, G. S. Levy, D. L. Brunn, R. Dickinson, R. E. Edelson, W. L. Martin, R. B. Postal, B. Seidel, T. T. Sesplauleis, D. L. Shirley, C. T. Stelzried, D. N. Sweetnam, Z. I. Zygielbaum, P. B. Esposito, J. D. Anderson, I. I. Shapiro, and R. D. Reasenberg, 1974: Venus: Mass, Gravity Field, Atmosphere, and Ionosphere as Measured by the Mariner 10 Dual Frequency Radio System. Science, (183), 1297-1306.

Lacis, 1974: Paper presented at the Conference on the Atmosphere of Venus, Goddard Institute of Space Studies, New York, 15-17 October 1974.

Lettau, H. H., 1974: To be published.

Limaye, S. S. 1975: Dry Adiabatic Lapse Rates using the Van der Waal Equation of State for the Atmosphere of Venus and Examination of the Venera 8 Temperature Profile. Report on Contract #NAS5-21798 Space Science and Engineering Center, University of Wisconsin, Madison.

Marov, M. Y., V. S. Avduevsky, V. V. Kerzhanovich, M. K. Rozhdestvensky, N. F. Borodin, and O. L. Ryabou, 1973: Venera 8 Measurements of Temperature, Pressure, and Wind Velocity on the Illuminated Side of Venus. J. Atmos. Sci. (30), 1210-1214.

Marov, M. Y., 1972: A Perspective in the Beginning of Planetary Exploration, Icarus, (16), 415-461.

Murray, B. C., J. J. S. Belton, G. E. Danielson, M. E. Davies, D. Gault, B. Hapke, B. O'Leary, R. G. Strom, V. Suomi, and N. Trask, 1974: Venus: Atmospheric Motion and Structure for Mariner 10 Pictures, Science (183), 1307-1315.

Murray, B. C., R. L. Wildey, J. A. Westphal, 1963: Venus: A Map of the Brightness Temperature. Science, (17), 391-392.

Woo, R., A. Ishimaru, and W. B. Kendall, 1974: Observations of Small-Scale Turbulence in the Atmosphere of Venus by Mariner 5, J. Atmos. Sci., (31), 1698-1706.

Woo, R., 1974: Paper presented at the Conference on the Atmosphere of Venus, Goddard Institute of Space Studies, New York, 15-17 October 1974.

Woo, R., 1975: Observations of Turbulence in the Atmosphere of Venus Using Mariner 10 Radio Occultation Measurements, J. Atmos. Sci., (32), 1084-1090.